# 情報通信審議会情報通信技術分科会

# 放送システム委員会　報告（案）

（120GHz 帯を使用する放送事業用無線局（FPU）の技術的条件）

Ⅰ　審議事項
　　本委員会は、諮問第２０２３号「放送システムに関する技術的条件」のうち、「放送事業用無線局の高度化のための技術的条件」について検討を行った。

Ⅱ　委員会の構成
　　　別紙１のとおり。
　　なお、検討の促進を図るため、本委員会の下に 120GHz 帯放送事業用無線局検討作業班を設置した。（別紙２）

Ⅲ　審議経過
（１）委員会での検討
　ア　第３４回（平成２５年１月１８日）
　　　委員会の運営方法、審議方針、検討項目及び審議スケジュール等について検討を行った。検討については、120GHz 帯放送事業用無線局検討作業班にて行うこととした。

　イ　第３６回（平成２５年６月１１日）
　　　検討作業班の報告を受け、委員会報告（案）の検討を行った。

　ウ　第３７回（平成２５年７月１６日）
　　　（Ｐ）

（２）検討作業班での検討
　ア　第１回検討作業班（平成２５年３月８日）
　　　作業班の運営方法、今後のスケジュール等について事務局より説明し要求条件について検討を行った。また今後の検討スケジュールを定めた。

　イ　第２回検討作業班（平成２５年５月２０日）
　　　伝送容量や空中線電力など基本的な技術的条件についての検討を行った。いくつかの項目については、次回作業班で検討することとなった。

　ウ　第３回検討作業班（平成２５年６月３日）
　　　共用検討、電波防護指針への適合性及び測定法について検討を行い、作業班報告をとりまとめた。

# Ⅳ 検討概要

## 第 1 章 審議の背景

### 1.1 審議の背景

　近い将来のスーパーハイビジョン（4K、8K[1]）の実用化に向けた放送の規格化や放送機器の開発にかかる取り組みが、放送事業者をはじめ、メーカーなどによって進められている。放送サービスの高度化に関する検討会第3回（平成 25 年 5 月 31 日）では、スーパーハイビジョンのロードマップに関し、以下のように記載されている。

- 2014 年 　（ブラジル(リオデジャネイロ)・ワールドカップの開催年）
  可能な限り早期に、関心を持つ視聴者が 4K を体験できる環境を整備

- 2016 年 　（リオデジャネイロ・オリンピックの開催年）
  可能な限り早期に、関心を持つ視聴者が 8K を体験できる環境を整備

- 2020 年 　（オリンピックの開催年）
  希望する視聴者が、テレビによって、４Ｋ／８Ｋの放送を視聴可能な環境を実現

　これらの放送機器の開発にあたっては、放送スタジオや放送素材の収集のための伝送システムが必要であり、まずこれらの実用化が不可欠となっている。その中でも、放送番組素材の無線伝送を行う FPU（Field Pick-up Unit、テレビジョン放送番組素材伝送用の可搬形無線伝送機器)の開発は、番組制作における機動性や伝送回線の確保のために、喫緊の課題となっている。

　このため、スーパーハイビジョンの情報量（約 24Gbps 程度）を伝送することが出来る帯域を有する 120GHz 帯を使用した放送事業用無線局（FPU）（以下 「120GHz 帯 FPU」という。）の技術的条件について検討を行う。

### 1.2 利用イメージ

　図1に FPU の利用例を示す。FPU の利用は、移動型 FPU 及び固定型 FPU の 2 種類に大別される。

---

[1] 本報告書において、スーパーハイビジョンを４Ｋ、８Ｋと表現する場合があるが、スーパーハイビジョンのITU-R勧告BT.2020に規定されている画素数に対応した略称として以下のとおり使用している。

　　8 Ｋ：7 680×4 320、4 Ｋ：3 840×2 160

移動型 FPU には、①主にマラソン中継などのロードレースに用いられる車載型 FPU と、②主に、報道等に用いられるハンディ型 FPU の２つがある。これらの FPU では、移動伝送を可能とするために、無指向性のアンテナが利用されることが多い。

　固定型 FPU は、様々な番組素材伝送の場面において用いられており、その１つとして、主にイベント時においてケーブル等の敷設が困難な場合に用いられる「短距離仮設型 FPU」があげられる。

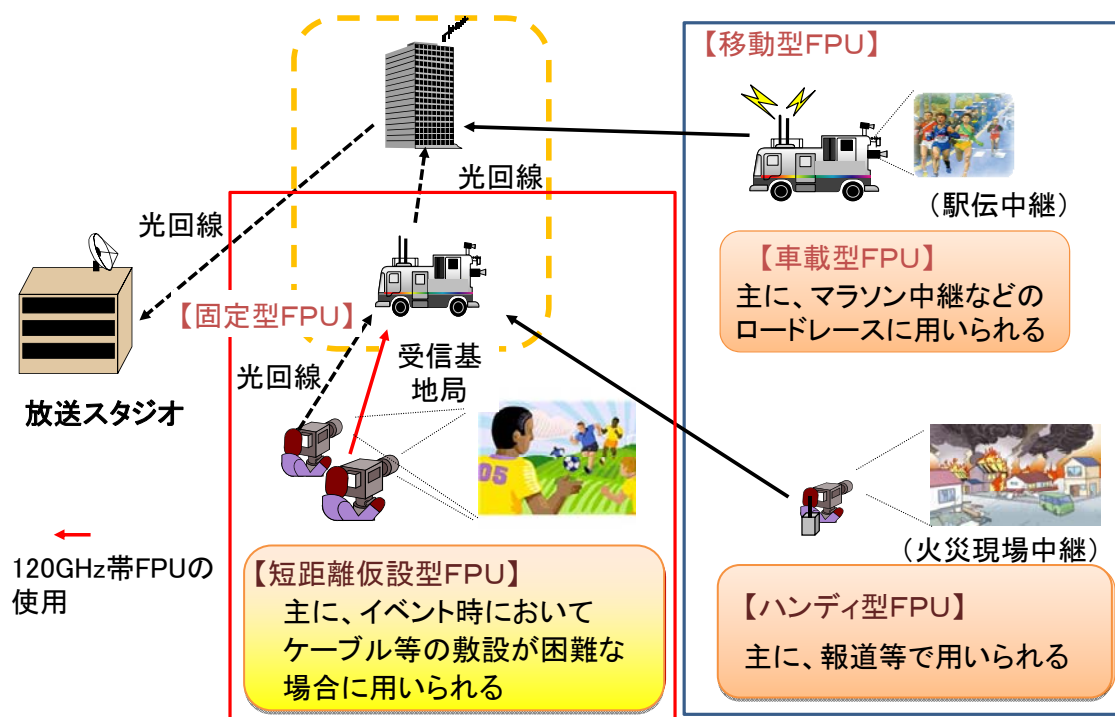　120GHz 帯 FPU においては、空中線利得の高いアンテナを使用して、「短距離仮設型 FPU」としての運用が想定される。



図１　　FPU の使用例

　120GHz 帯 FPU で想定される利用イメージを図２〜4 に示す。

　図2 は、競技場のトラックやホールのステージ等で、120GHz 帯 FPU を仮設して使用する場合である。この利用イメージの場合の伝送距離は 250m 程度である。

　図3は、ゴルフ中継等で、ケーブルの敷設が困難な場合に 120GHz 帯 FPU を仮設して使用する場合である。この利用イメージの場合の伝送距離は 1km 程度である。

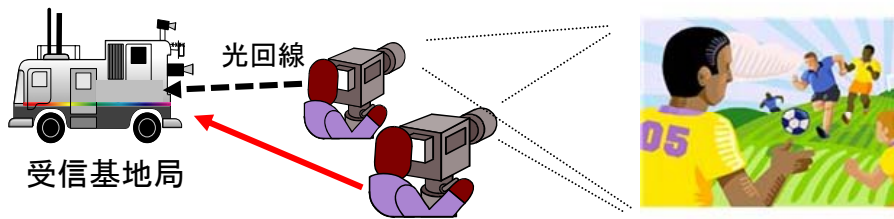　図4は道路を横切る場合や河川を横断する場合などで 120GHz 帯 FPU を仮設して使用する場合である。この利用イメージの場合の伝送距離は 4km 程度である。
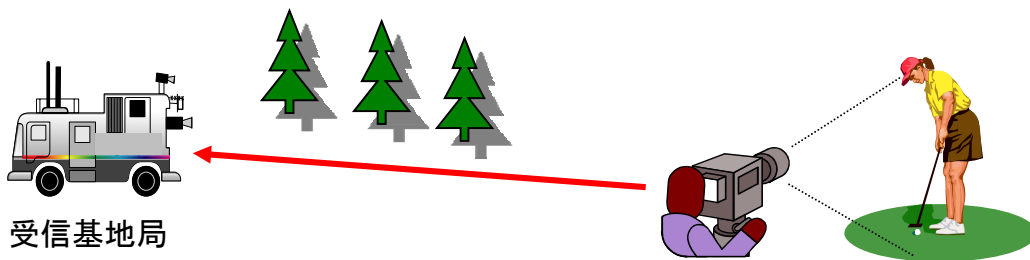
図2　競技場での利用例



図3　ゴルフ場での利用例



図4　道路横断での利用例

## 1.3　スーパーハイビジョンの伝送

　　120GHz 帯 FPU では、スーパーハイビジョンの伝送を想定している。そこで、ITU-R 勧告 BT.2020（参考資料１参照）などを参考に、表１に示す４つの条件を選定して、まず、映像情報量について検討した。ここで条件１と条件２は、ハイビジョンで 60i 及び 60p として良く知られている条件に相当し、条件３と条件４は、スーパーハイビジョン（8K）の開発にあたりフルスペック方式及び Dual Green 方式として進められている条件に相当している。

　　各条件における映像情報量を表２に示す。映像情報量は、４Ｋでは条件２の場合に 9.95 Gbps、８Ｋでは条件４の場合に 19.9 Gbps であり、これらを今回の検討対象とする。

　　なお、将来的には、４Ｋでは条件３（35.8Gbps）、８Ｋでは条件２（39.8Gbps）や条件３（143.3Gbps）などの映像情報量を有する場合も想定されるが、その場合にも、数分の１程度の低い圧縮率の圧縮技術等を用いることにより、今回の検討対象とした条件での帯域で伝送が可能である。

### 表1　検討条件

|  | 条件1<br>（4:2:2、60i） | 条件2<br>（4:2:2、60p） | 条件3<br>(フルスペック) | 条件4<br>（Dual Green） |
|---|---|---|---|---|
| サンプリング構造 | 4:2:2 | 4:2:2 | 4:4:4 | G1,G2,B,R |
| フレーム周波数 | 60i | 60p | 120p | 60p |
| 階調 | 10bit | 10bit | 12bit | 10bit |

### 表2　映像情報量の比較

注：現実の使用が想定されていないケースは、（ ）で示した。

| 画素数 | 条件1 | 条件2 | 条件3 | 条件4 |
|---|---|---|---|---|
| 1920×1080 | 1.24Gbps | 2.49Gbps | （8.96Gbps） | （1.24Gbps） |
| 3840×2160<br>（4K） | （4.98Gbps） | 9.95Gbps | 35.8Gbps<br>圧縮技術等により、条件2<br>の際の帯域で伝送が可能 | （4.98Gbps） |
| 7680×4320<br>（8K） | （19.9Gbps） | 39.8Gbps | 143.3Gbps<br>圧縮技術等により、条件4の際の帯域で伝送が可能 | 19.9Gbps |

　　FPU での伝送時には、映像情報の他に、音声データや制御信号が付加されるので、実際の伝送レートはこれらの値よりは大きくなる。現在のところ、スーパーハイビジョンのカメラとしては、条件 4 の Dual Green 方式（参考資料２）が主流であり、この方式では、映像信号は 16 本の HD-SDI（High-Definition Serial Digital Interface）

信号に変換されて出力される。HD-SDI 信号（参考資料３参照）の伝送ビットレートは 1.485Gbps であり、８Ｋスーパーハイビジョンは 16 本の HD-SDI 信号で構成されていることから、24Gbps の伝送容量が必要となる。

図５に条件４で８Ｋを FPU で伝送する際のシステム構成を示す。この場合、HD-SDI 信号を８本ずつ多重して送信機に入力し、２系統の無線伝送路を確保することで 24Gbps の８Ｋスーパーハイビジョン信号を伝送する構成となっている。この結果、１つの送信機では、少なくとも 12Gbps の情報を伝送することが必要となる。

なお、スーパーハイビジョンの素材伝送では、有線（光ファイバー）伝送が多く用いられていることから、有線系との親和性の確保も重要となっている。このため、図５における MUX と TX の間、RX と DEMUX の間、あるいは MUX 出力と DEMUX 入力の間を光ファイバーで接続する場合が考えられる。その場合には、10 ギガビット・イーサネットなどの規格品に対応するために、１系統の入力信号を 10Gbps 程度に制限する場合もある。
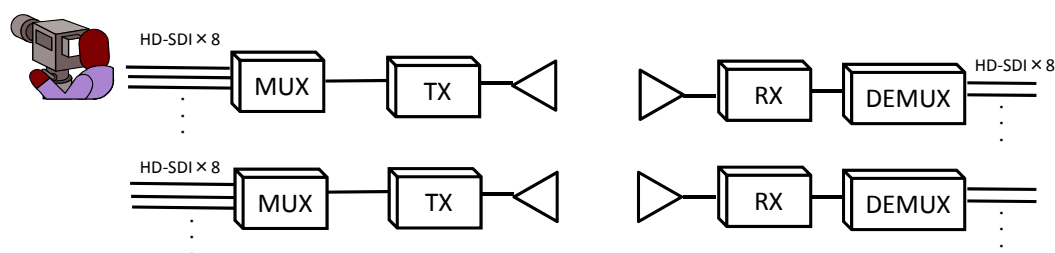


図５　8K 伝送時の無線システムの構成例

４Ｋスーパーハイビジョン信号を伝送する場合、表２条件２（サンプリング構造 4:2:2、フレーム周波数　60p、階調　10bit）の場合には表２のとおり 9.95Gbps が必要であるが、８Ｋスーパーハイビジョンの場合と同様に、８本の HD-SDI 信号で伝送することが想定される。また、通常のハイビジョン伝送において、複数の HD-SDI 信号を当該装置で伝送することも想定される。

1.4　要求条件

以上の検討結果より、120GHz 帯 FPU の要求条件を以下のように定める。


1　競技場やホール等からの固定中継を想定し、短距離仮設型として運用する。
2　伝搬距離は、
　①　競技場などで使用される場合については、雨の中での競技もあり、競技が中断される概ね１時間雨量 60mm の降雨強度において、250m 程度とすることを目標

②ゴルフ中継などで仮設して使用される場合については、１ｋｍ程度とすることを目標

③河川横断等で仮設して使用される場合には、４ｋｍ程度とすることを目標

とする。

3　伝送にあたっては、最大 HD-SDI 信号１６本分を伝送可能とする。

第 2 章　技術的条件

2.1　通信方式

　　取材等で得た映像情報を一方向に伝送するもので、既存の FPU と同様の使用方法が想定されることから、通信方式は、既存の FPU と同様に「単向通信方式」とすることが適当である。

2.2　変調方式

　　本システムでは、想定される伝送容量が大きく、また、使用する周波数が 120GHz と高いため、変調方式は比較的簡易な方式から選択することが現実的と考えられる。特にキャリア信号の強度を直接変調し、受信側では包絡線検波を行う ASK 変調は、最も簡易な回路構成で高速のデータ伝送が行えることから、ミリ波無線で広く用いられている方式である。実際に、120GHz 帯において ASK 変調、包絡線検波を使用した実験試験局で伝送距離 5.8km における 10Gbps 伝送が報告されている。

　　直接変調方式は、多値数を大きくすることが難しいため、将来的にみても４値（QPSK 変調）までが実現可能なものと考えられる。QPSK 変調方式を使用した 120GHz 帯無線システムは実験レベルで試作されており、実験試験局を使用した実証試験で伝送距離 200m における 10Gbps 屋外伝送が報告されている。

　　上記より、本システムの変調方式は、ASK 変調、BPSK 変調及び QPSK 変調とする。

2.3　電波の型式

　　120GHz 帯 FPU は、映像素材伝送に使用される映像信号の他、音声信号や制御監視信号等２つ以上のデジタル信号を送ることが想定されることから、各変調方式による電波の型式は以下のとおりとする。

表 3　各変調方式における電波の型式

| 変調方式 | 電波の型式 |
|---|---|
| ASK変調 | A7W |
| BPSK変調又はQPSK変調 | G7W |

2.4　スーパーハイビジョン伝送に必要となるビットレート

　　現在の８Kスーパーハイビジョンのカメラとしては、Dual Green 方式が主流であるがこの映像信号は 16 本の HD-SDI 信号に変換されて出力される。HD-SDI 信号の伝送ビットレートは 1.485Gbps であり、８Kスーパーハイビジョンが 16 本の HD-SDI 信号で構成

されていることから、８Kスーパーハイビジョンの伝送に必要となるビットレートは 24Gbps となる。

　４Kスーパーハイビジョン信号を伝送する場合には、8 本の HD-SDI 信号に変換されることから、伝送に必要となるビットレートは 12Gbps となる。


2.5　占有周波数帯幅の許容値

　2.4 に記載したように、８Kスーパーハイビジョンを伝送するには 24Gbps の伝送容量が必要になる。

　ASK 変調方式の周波数帯域幅 BW(ASK)については、ベースバンド信号の周波数帯域幅をＢとすると、以下となる。

$$BW(ASK) = 2B \qquad\qquad\qquad (1)$$

　また、PSK 変調方式の周波数帯域幅 BW（PSK）については、以下となる。

$$BW(PSK) = 2B / \log_2 N \quad （N は多値数） \qquad\qquad (2)$$

　しかしながら、デジタル信号伝送では、通常、ロールオフフィルタ等を用いて、使用する周波数帯域幅を制限するが、10Gbps 級の高速デジタルベースバンド信号のロールオフフィルタを製作することは困難なため、高周波フィルタを用いて、伝送性能に影響しない周波数帯域幅を検討した。

　フィルタによる帯域制限を行った場合には、ASK 方式、BPSK 方式、QPSK 方式のうち、所要 C/N を他の方式より多く必要な ASK 方式が最も影響を受けることから、帯域制限による所要 C/N の劣化を、ASK 方式について実験的に確認した。その結果を図６に示す。また、120GHz 帯で使用可能な周波数帯域 18GHz を伝送可能とすることを考えたところ、帯域幅／伝送容量の値が 1.46 倍となる。このときの固定劣化量 2dB を、最大の劣化量として考慮することとし、他の変調方式についても同様とした。

　このことから、120GHz 帯 FPU における占有周波数帯幅の許容値は、ASK 方式、BPSK 方式及び QPSK 方式ともに、17.5GHz とすることが適当である。
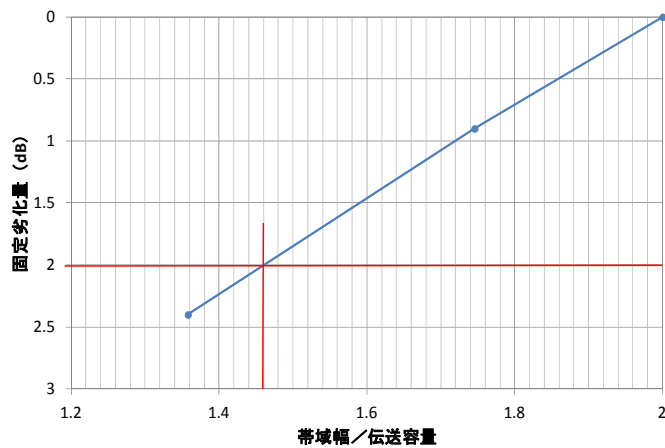
図６　帯域幅を制限したときの固定劣化量

表４　変調方式と占有周波数帯幅の関係

| 変調方式 | 最大伝送容量 | 占有周波数帯幅 |
|---|---|---|
| ASK 方式 | 12Gbps | 17.5GHz |
| BPSK 方式 | 12Gbps | 17.5GHz |
| QPSK 方式 | 24Gbps | 17.5GHz |

　表４のとおり QPSK 方式の最大伝送容量は 24Gbps であることから、2.4 で検討した８Ｋスーパーハイビジョンの伝送が可能である。しかし、ASK 方式及び BPSK 方式では、最大伝送容量は 12Gbps であることから、８Ｋスーパーハイビジョンの伝送は行えないが、２系統の無線通信路を使用することにより、必要となるビットレート 24Gbps が伝送可能となる。

## 2.6　周波数の許容偏差
　120GHz 帯 FPU と同様に高い周波数帯を使用する 60GHz 帯の陸上移動業務の無線局については 200ppm と規定している。120GHz 帯 FPU はイベント時等に仮設して用いられるため、装置を小型軽量化し、可搬性に優れた装置であることが望ましいことから、これと同様、200ppm で規定するのが適当である。

## 2.7　割当周波数
　120GHz 帯 FPU は、2.5 で検討したように、占有周波数帯幅は、17.5GHz 程度であり、2.6 で検討したように、周波数偏差は 200ppm(25MHz 程度)である。したがって、本システムに必要となる周波数の幅は 17.6GHz 程度となる。
　表５に 114.25～136GHz の周波数割当を示す。同表に記載するように 116～134 GHz

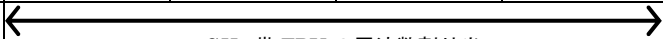（18GHz）の周波数を割り当てれば、占有周波数帯幅を 17.5 GHz 以上確保することが可能である。さらに、中心周波数を 125 GHz とすれば、隣接周波数帯との間にガードバンド 200MHz 程度を確保することが可能であり、隣接周波数帯との周波数共用にも貢献することができる。これらの検討結果から、割り当て周波数は 116〜134GHz、中心周波数は 125GHz とすることが適当である。

表5　114.25 GHz〜136 GHz の国際周波数割当

| 周波数（GHz） | 114.25〜116 | 116〜122.25 | 122.25〜123 | 123〜130 | 130〜134 | 134〜136 |
|---|---|---|---|---|---|---|
| | | ←　120GHz 帯 FPU の周波数割り当て（中心周波数　125 GHz）　→ | | | | |
| 業務 | 地球探査衛星（受動）電波天文宇宙研究（受動） | 地球探査衛星（受動）衛星間宇宙研究（受動） | 固定移動衛星間アマチュア | 固定衛星移動衛星無線航行無線航行衛星電波天文 | 地球探査衛星（能動）固定衛星間移動電波天文 | アマチュアアマチュア衛星電波天文 |

## 2.8　回線の品質

### 2.8.1　所要 C/N

　　本システムは、光ケーブルが敷設困難な場合の代替え手段として用いられることも想定しており、HD-SDI 信号を光ケーブルで伝送した場合と同様のビット誤り率が求められる。現在、HD-SDI 信号のケーブル伝送では、BER$<10^{-10}$ を要求されている。

　　BER$<10^{-10}$ を満足する ASK 変調、BPSK 変調及び QPSK 変調の所要 C/N（理論値）は表6に示すとおりである。したがって、所要 C/N は、これらの変調方式の C/N（理論値）に、送受信機の固定劣化分 5.5dB を加えた値とすることが適当である。

　　なお、固定劣化 5.5dB には、フィルタの帯域制限による 2dB の劣化を含んでいる。
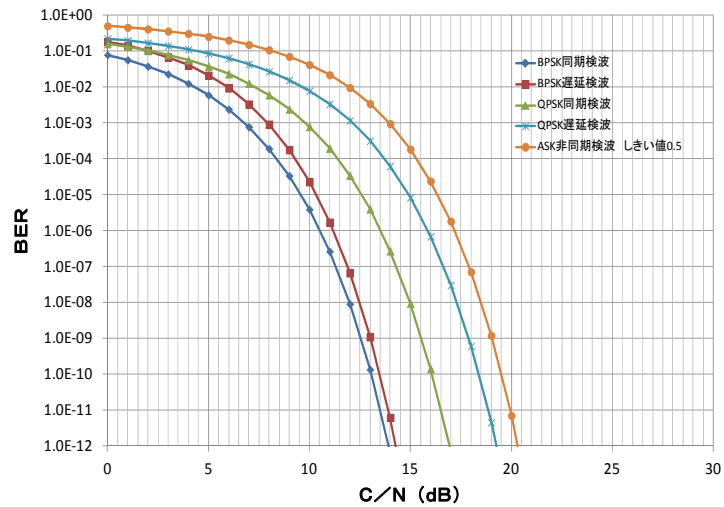
図7　各変調方式の CN-BER 特性（理論値）

表6　各変調方式の所要 C/N

| 変調方式 | 所要 C/N<br>（理論値）（dB） | 所要 C/N<br>（固定劣化考慮後）（dB） |
|---|---|---|
| ASK 方式 | 19.5 | 25.0 |
| BPSK 方式 | 13.5 | 19.0 |
| QPSK 方式 | 18.4 | 23.9 |

2.8.2　C/N 配分（参考資料４）

　　C/N 配分の検討を行うにあたり、120GHz 帯 FPU は、高い周波数帯であるため自由空間伝搬損失が大きいこと、同一周波数帯及び隣接周波数帯を使用する干渉対象局が少ないことから、干渉雑音の影響は小さいものと考えられる。そこで、120GHz 帯 FPU では、C/N 配分を熱雑音に多く割り振り、熱雑音に 70%、干渉雑音に 30%とすることが適当と考えられる。

2.8.3　大気吸収損（参考資料５）

　　回線品質の検討に使用する大気吸収損については、ITU-R 勧告 P.676-9（参考資料６）や伝搬試験の結果に基づき、高温多湿の時（水蒸気密度が 30g/m³：30℃で相対湿度が 100%のとき）の大気吸収損である 3 dB/km とすることが適当である。

2.8.4　降雨減衰量（参考資料７）

　　スポーツ中継の場合、降雨があってもスポーツ競技自体が継続されている限りは回

線の確保が必要になる。このため、降雨強度は、スポーツ競技が中断される、概ね時間雨量 60mm とすることとし、降雨減衰量は 23dB/km とすることが適当である。

### 2.8.5 雑音指数（NF）

120 GHz 帯の受信機に使用された２種類の実験機の低雑音増幅器(LNA)の NF の測定値を図8 に示す。測定における各 LNA の NF は各々 8.9 dB 及び 5.5 dB であった。装置の性能ばらつきや製造コストなど機器の開発状況を考慮し、42GHz 帯 FPU と同様に若干の余裕を持たせ、10dB とすることが適当である。
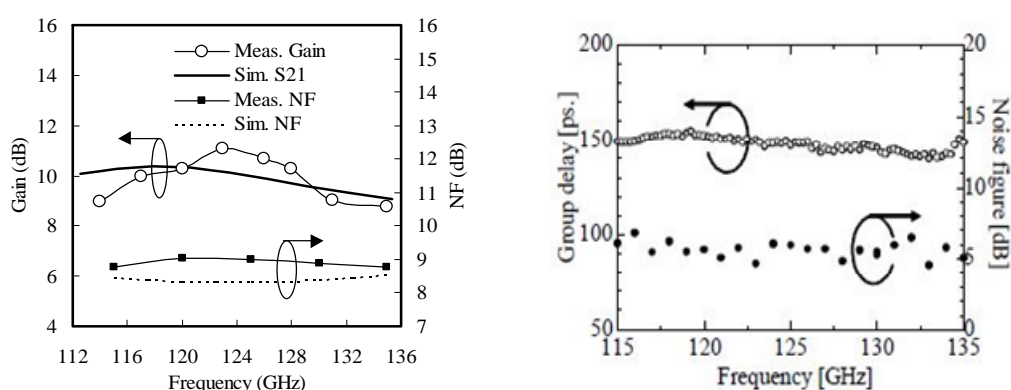


図８　120GHz 帯 LNA の NF の測定値

### 2.8.6 伝送マージン

120GHz 帯 FPU の伝送マージンは、アンテナのポインティング損等を考慮し、6dB とすることが適当である。

### 2.9 空中線の特性

120 GHz 帯における送信空中線としては、ホーンアンテナ（利得 20〜30 dBi 程度）、レンズアンテナ（直径 7.5〜45 cm、利得 25〜50 dBi 程度）、パラボラ（カセグレイン）アンテナ（直径 10 〜60 cm、利得 37〜52 dBi 程度）などがある。

120GHz 帯 FPU においても、42 GHz 帯や 55 GHz 帯の FPU と同様に、利用シーン、伝送距離、伝搬環境に応じて使用する空中線の指向特性や利得は異なるものと考えられる。例えば、伝送距離が短い場合には、利得が低くなるが、ビーム幅が広く、方向調整が容易なアンテナを使用することが考えられる。したがって、空中線の指向特性は、120GHz 帯 FPU の各種の利用シーンに合わせて適切な空中線を利用することが望ましい。最大利得については、直径 60cm のパラボラアンテナで実現可能な値とする。

また、偏波についても、120GHz 帯 FPU の各種の利用シーンに合わせて最適な偏波を利用できることが望ましく、垂直偏波、水平偏波及び円偏波を使用できることが適当と考

える。

## 2.10 最大空中線電力及び空中線電力の許容値

　2.1～2.9 で記載した条件に基づき、回線設計を行った。各変調方式において、2.8.6 で規定した伝送マージンを確保するために必要な空中線電力を逆算したところ表 7 に示すとおりであり、最大空中線電力は 1W とすることが適当である。なお、各変調方式及び伝送距離における回線設計例を参考資料 9 に示す。

　また、送信電力の許容偏差については、無線設備規則 14 条第一項の表中第六（470MHz 以上の無線局の一般則）　を適用し、「上限 50%、下限 50%の範囲内」とすることが適当と考えられる。

表 7　各変調方式で必要な空中線電力

| 変調方式 | 必要な空中線電力（mW） | | | |
|---|---|---|---|---|
| | 降雨時 | | 晴天時 | |
| | 伝送距離（250m） | 伝送距離（1km） | 伝送距離（450m） | 伝送距離（4.4km） |
| ＡＳＫ方式 | 17.5 | 1000 | 17.5 | 1000 |
| ＢＰＳＫ方式 | 4.4 | 250 | 4.4 | 250 |
| ＱＰＳＫ方式 | 13.6 | 770 | 13.6 | 770 |

## 2.11　2系統の並行回線による伝送の検討

　図９に示す同一偏波を使用した並行回線の場合、直径 60cm パラボラアンテナ（利得：51dBi）を 1°離せば、アンテナ利得が最大利得より 12.5dB 以上小さくなり、送受で 25dB 確保できることから、所要 C/N を満足し、並行回線における伝送が可能となる。2 つの無線回線間の角度 α が 1.0 °以上になる無線回線間の距離を、この例における離隔距離として計算したところ、伝送距離 が 500 m の場合では約 8.7 m、伝送距離が 1 km の場合では約 17.5 m となる。なお、2 台の送信機の偏波を変える等により、必要となる無線局間距離をさらに小さくできることが見込まれる。
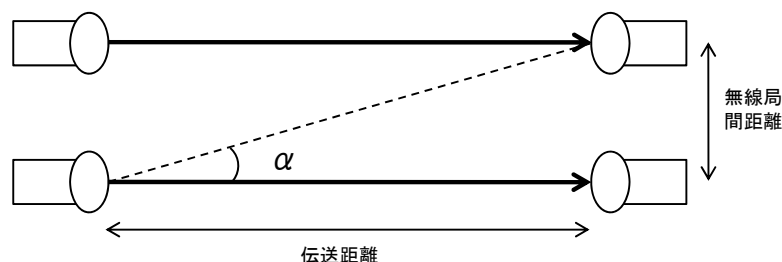


図９　並行回線の模式図

## 2.12 不要発射の強度の許容値

　無線設備規則別表第 3 号におけるスプリアス発射及び不要放射は、960 MHz を超える周波数領域かつ出力 10 W 以下の設備に対しては、「帯域外領域におけるスプリアス発射の強度」は 100μW 以下、「スプリアス領域における不要発射の強度」は 50μW 以下、（参照帯域幅：1 MHz）と定められている。これらの規定については、周波数有効利用の観点から他の無線局との共用が可能となるように定められているが、本周波数帯がきわめて高い周波数帯であり、感度が十分に高い（測定雑音が十分に小さい）測定機器の入手や構成が困難であること等から、80GHz 帯高速無線伝送システムの規定と同様に、「帯域外領域における不要発射の強度」は 100μW 以下、「スプリアス領域における不要発射の強度」は 50μW 以下、（参照帯域幅：1 MHz）とすることが適当である。

## 2.13 受信設備の副次的に発する電波等の限度

　機器のコストや他の無線設備への影響を考慮して、60GHz 帯の陸上移動業務の無線局の基準と同様、50μW 以下とすることが適当と考える。

## 2.14 電波防護指針への適合性

　120GHz 帯 FPU は移動局であることから、電波防護指針への適合性については、電波法施行規則第 21 条の 3 第 1 項第 2 号において適用が除外されているが、固定的に利用するシーンが多いことから、次のとおり適合性を検討した。

　電波法施行規則第 21 条の 3 では、電波の強度と生体への作用との関係が定量的に定められており、運用形態に応じて、これに基づく電波防護の指針に適合するようシステム諸元の設定に配慮する必要がある。

　表 8 に 100kHz から 300GHz の周波数帯での防護基準を示す。この場合において、120GHz 帯における防護指針による電力束密度は、1mW/c㎡ （6 分間平均）となっている。

表 8　電磁界強度(平均時間 6 分間)の基準値（電波法施行規則別表第 2 号の 3 の 2）

| 周　波　数 | 電界強度の実効値 [V/m] | 磁界強度の実効値 [A/m] | 電力束密度 [mW/cm$^2$] |
|---|---|---|---|
| 10kHz － 30kHz | 275 | 72.8 | |
| 30kHz － 3MHz | 275 | 2.18/f | |
| 3MHz － 30MHz | 824/f | 2.18/f | |
| 30MHz － 300MHz | 27.5 | 0.0728 | 0.2 |
| 300MHz － 1.5GHz | 1.585$\sqrt{f}$ | $\sqrt{f}$/237.8 | f/1500 |
| 1.5GHz － 300GHz | 61.4 | 0.163 | 1 |

　f は、ＭＨｚを単位とする周波数

そこで、平成 11 年郵政省告示第 300 号記載の電力束密度の基本算出式から、所要距離を求めた。

　なお、無線設備からの発射される電力束密度の算出方法及び測定方法は次のとおりである。（告示平成 11 年 4 月 27 日第 300 号より）

　S = Pin・G・K / (40πR²)

　S：電力束密度　単位：[mW/cm²]

　Pin：送信空中線入力電力　単位：[W]

　G：送信空中線絶対利得　単位：無し（倍）

　R：送信空中線からの離隔距離　単位：[m]

　K：反射係数　単位：無し（倍）

　（反射を考慮しない：1 、大地面反射のみを考慮：2.56、 水面などの反射を考慮：4）


　2.10 の最大空中線電力の検討等に基づき、120GHz 帯 FPU の諸元を次のように仮定する。

・ 送信電力 1W
・ 空中線利得 51dBi　（送信給電損 1dB を別途想定。人体に近い位置に設置される可能性のある最も大きなものとして想定。）

この場合の所要離隔距離は表9のとおりである。


表９　　電波防護に関する離隔距離算出結果

| 条件 | 所要離隔距離 |
| --- | --- |
| 反射を考慮しない | 28.2 m |
| 大地面反射のみ考慮 | 45.1 m |
| 水面などの反射を考慮 | 56.4 m |


　したがって 120GHz 帯 FPU が送信中の時は、空中線の正面の数十 m 範囲内に立ち入った場合には、電力束密度が基準値を超える可能性がある。

　しかしながら、つぎの運用実態を考慮すると、

　①本システムは、放送素材伝送用途に使用されるため、伝送路が遮蔽されないように、送信装置は設置されるため、人の立ち入る可能性が極めて少ないこと

　②空中線の指向性が極めて鋭い（半値角約 0.4 度）ため、主ビーム幅は数十 m 離れた距離でも 1m 以下であり、人の立ち入りがあった場合でも、一定の場所で停止していない限りは、6 分間の連続した照射とはなりにくいこと

　③伝送路が遮蔽された場合には、伝送に支障が生じ、FPU の運用者が認識できること

等の観点から、人体への影響は生じないものと考えられる。

　また、空中線の指向性が鋭いために、正面以外については十分な減衰が見込まれることから、周囲の安全を確保することは十分に可能である。なお、設置環境によっては、防護柵などを設置することも考慮することも必要である。


## 2.15　他の無線システムとの共用

### 2.15.1　120GHz 帯周波数の割当計画及び利用状況

　　表 10 に 114.25～136 GHz の周波数割当計画を示す。詳細な割当計画は参考資料 10 に示す。

　　表 11 に国内、外国における現在の周波数利用状況の概要を示す。

①同一周波数帯については、国内において利用する無線局の開設はない。また、国内において受信設備の指定はされていない。一方、外国の衛星システムとしては、AURA 衛星システムがある。

②隣接周波数帯については、105-116GHz の周波数帯において、指定を受けている受信設備が長野、鹿児島に一局ずつ存在する。また、134-136GHz では、約 150 局のアマチュア無線局が免許されている。

　　したがって、AURA 衛星システム、電波天文業務の受信設備及びアマチュア無線局について共用検討を行った。


表 10　114.25 GHz～136 GHz の周波数割当

| 周波数（GHz） | 114.25～116 | 116～122.25 | 122.25～123 | 123～130 | 130～134 | 134～136 |
|---|---|---|---|---|---|---|
| 業務 | 地球探査衛星（受動）電波天文宇宙研究（受動） | 地球探査衛星（受動)衛星間宇宙研究（受動) | 固定移動衛星間アマチュア | 固定衛星移動衛星無線航行無線航行衛星電波天文 | 地球探査衛星（能動）固定衛星間移動電波天文 | アマチュアｱﾏﾁｭｱ衛星電波天文 |

表 11　国内、外国における 120GHz 帯周波数の割当計画及び利用状況

| 周波数関係 | 無線システム | 使用周波数帯（GHz） | FPU から見て検討する干渉関係 | 無線局等の開設状況 | | 干渉検討の要否 |
|---|---|---|---|---|---|---|
| | | | | 国内の状況 | 外国の状況（衛星） | |
| 同一 | 地球探査衛星（受動）宇宙研究（受動） | 116-122.25 | 与干渉 | 無線局の開設無し | AURA（非静止、米国） | 要検討 |
| | 衛星間 | 116-122.25 | 与干渉/被干渉 | | 衛星網無し | |
| | 固定移動衛星間アマチュア無線 | 122.25-123 | 与干渉/被干渉 | | | |
| | 固定衛星（宇宙から地球）移動衛星（宇宙から地球）無線航行無線航行衛星 | 123-130 | 与干渉/被干渉 | | | |
| | 地球探査衛星（能動）固定衛星間移動 | 130-134 | 与干渉/被干渉 | | | |
| | 電波天文 | 123-130 130-134 | 与干渉 | 受信設備の指定無し | － | 要検討 |
| 隣接 | 電波天文 | 105-116 | 与干渉 | 指定受信設備：2（長野、鹿児島）114.25-116GHz：全ての電波の発射を禁止 | － | 要検討 |
| | アマチュア無線 | 134-136 | 与干渉/被干渉 | 約 150 局 | － | 要検討 |

2.15.2 干渉検討に使用する 120GHz 帯 FPU の諸元、運用条件

　干渉検討に使用する 120GHz 帯 FPU の諸元及び運用条件を参考資料 11 に示す。また、干渉検討に使用する 120GHz 帯 FPU のアンテナ指向特性の詳細を参考資料 12 に示す。

2.15.3　地上系システムとの干渉検討

2.15.3.1　アマチュア無線との干渉検討（参考資料 13）

　アマチュア無線局が、134～136GHz において 151 局開設されており、現状では、アマチュア無線については隣接周波数帯への干渉検討である。

　アマチュア無線との干渉検討の結果を表 12 に示す。この結果、120GHz 帯 FPU とアマチュア無線の離隔距離を 50m 以上とれば、与干渉／被干渉とも生じない。また、離隔距離 50m は、無線局の存在を視覚的に確認できる距離であることから、送信機

や受信機の設置時に現場で運用調整が可能であり、無線局間の干渉は回避できると考えられる。

表 12 アマチュア無線との干渉検討結果

| 周波数関係 | 無線システム | 使用周波数帯 | FPU から見て検討する干渉関係 | 混信保護値 | 離隔距離 |
|---|---|---|---|---|---|
| 隣接 | アマチュア無線 | 134-136GHz | 与干渉 | -117.8dBm[1],[2] | 20m |
| | | | 被干渉 | -61.4dBm[1] | 50m |

※1 混信保護値は、受信機の熱雑音量と同程度とした。

※2 アマチュア無線の受信帯域幅を 40kHz とした。

2.15.3.2 電波天文業務との干渉検討（参考資料 15）

電波法第 56 条第 1 項に基づき告示されている、日本における受動業務として、100 GHz 超の周波数領域の観測が可能な電波天文台は、「国立天文台（長野県）」と、「国立天文台（鹿児島県）」であり、保護される周波数は、105.0 GHz から 116.0 GHz である。参考資料 14 に日本国内の電波天文の諸元を示す。

（1） 同一周波数帯における電波天文業務への与干渉

同一周波数帯（123-130GHz 及び 130-134GHz）において、指定されている電波天文業務の用に供する受信設備は、現状は無い。

今後に指定される場合も想定し、離隔距離の検討を行ったところ、見通し内の場合は離隔距離が 60 km 以上、見通し外（中間に遮断物が有る場合）の場合は離隔距離が 20 km 以上であれば、120GHz 帯 FPU から電波天文台に届く電力密度は干渉保護基準以下となる。

（2） 隣接周波数帯における電波天文業務への与干渉

隣接周波数帯（105-116GHz）において、指定されている電波天文業務の用に供する受信設備は、長野及び鹿児島の 2 カ所ある。116GHz 以下の周波数帯における電力密度の値は、測定器の測定限界である-55dBm/MHz を仮定した。その結果、見通し内に電波天文がある場合には、離隔距離が 10 km 以上、見通し外（中間に遮断物が有る場合も含む）の場合には、離隔距離が 500m 以上であれば、120GHz 帯 FPU から電波天文台に届く電力密度は干渉保護基準以下となる。

電波天文台との干渉検討結果のまとめを表 13 に示す。

表 13 電波天文台との干渉検討結果

| 周波数関係 | 使用周波数帯（GHz） | 電波天文帯域に与える FPU の電力密度 | 混信保護値 | 離隔距離 |
|---|---|---|---|---|
| 同一 | 123-130<br>130-134 | 0.0dBm/MHz | -198dBm/MHz | 見通し内：60km 以上<br>見通し外：20km 以上 |
| 隣接 | 105-116 | -55dBm/MHz | -198dBm/MHz | 見通し内：10km 以上<br>見通し外：500m 以上 |

　　120GHz 帯 FPU の運用が、電波天文業務の受信設備と表 13 に示す離隔距離以上で行うことで共用は可能である。

　　なお、離隔距離の範囲内で 120GHz 帯 FPU を運用する場合には、事前に電波天文業務の受信設備の運用者との間で運用調整を図ることが必要である。

2.15.4　衛星系システムとの干渉検討（参考資料 17）

　　干渉検討の対象となるのは、現時点では、非静止衛星系システム AURA のみである。非静止衛星系システム AURA との干渉検討に使用した諸元、運用条件を参考資料 17 に示す。干渉検討では、確率論的共用検討の手法を用いた。地球探査衛星では、対地観測モードと大気観測モードで保護基準が異なるため、両モードについて干渉検討を実施した。以下に、各モードでの干渉検討の手法を記載する。

（１）対地観測モード

　　運用されている非静止衛星を用いた地球探査衛星(受動)システムは、16 日間で地球全面を回るため、16 日間を 10 秒毎に衛星の軌道位置を変えて計算を行った。さらに、衛星の各軌道位置で±50 度の衛星搭載アンテナのスキャンを行っていると仮定し、8 時間ごとに 120GHz 帯 FPU のシステムパラメータを想定した運用確率に従って、変えて計算を行った。

（２）大気観測モード

　　非静止衛星を用いた地球探査衛星(受動)の大気観測モードでは、衛星搭載アンテナの挙動が不明なため、以下の 3 つの計算を行った。

（a）大気観測モードの衛星搭載アンテナが、常に衛星の進行方向の一つの地上局システムを指向する場合。

（b）大気観測モードの衛星搭載アンテナが、常に衛星の進行方向を指向する場合。

（c）大気観測モードの衛星搭載アンテナが、常に衛星の進行方向とは逆方向を指向す

る場合。

この場合、(a)のケースが、干渉確率計算の中では最悪シナリオとなる。

表 14 に非静止衛星システムとの干渉検討の結果（参考資料 17）、両観測モードにおいて、干渉電力密度は保護基準よりも十分に小さな値となっており、AURA 衛星システムとの共用は可能と考えられる。

表 14    AURA 衛星システムの干渉検討結果

| 周波数関係 | 無線システム | 使用周波数帯（GHｚ） | FPU から見て検討する干渉関係 | 干渉確率 | | |
|---|---|---|---|---|---|---|
| 同一 | 地球探査衛星（受動） | 116-122.25 | 与干渉 | 対地観測モード許容干渉確率：0.01%以下[※1] | 1W ： 0.000124%<br>0.5W ： 0.000074%<br>0.1W ： 0.000023%<br>0.04W ： 0.000013% | |
| | | | | 大気観測モード許容干渉確率：1%以下[※2] | 1W ： 0.1362%<br>0.5W ： 0.0913%<br>0.1W ： 0.0276%<br>0.04W ： 0.0129% | |

※１    対地観測モードの許容干渉確率に用いた干渉保護値は、ITU-R 勧告 RS.2017 に基づく干渉保護値-166dBW/200MHz を超えるものとして算出

※２    大気観測モードの許容干渉確率に用いた干渉保護値は、ITU-R 勧告 RS.2017 に基づく干渉保護値-189dBW/10MHz を超えるものとして算出

## 2.16  無線設備の測定方法
無線設備の測定方法については、以下のとおりとする。

### 2.16.1  周波数の偏差
送信周波数の測定はアンテナ端子で行い、無変調状態において測定した値を送信周波数とする。測定にはスペクトルアナライザを使用し、スペクトルアナライザの分解能帯域幅は 1 MHz とする。

### 2.16.2  占有周波数帯幅
占有周波数帯幅の測定はアンテナ端子で行い、占有周波数帯幅が最大となる信号により変調された状態で行う。測定にはスペクトルアナライザを使用し、測定時の掃引

周波数幅は無線設備規則に規定する許容値の2倍以上とする。

　変調方式等によりキャリア成分が存在するスペクトルに関しては、変調方式等に応じて、キャリア成分を除去して、占有周波数帯幅の計算を行う。

　送信スペクトル分布から測定系の雑音レベルまで余裕がなく電力積算に影響を与える場合は、分解能帯域幅を 1MHz とした状態で、キャリアリーク等を除く電力最大点から 23 dB 減衰する（スペクトルの強度が、最大点の 0.5 ％相当となる）点の上限周波数と下限周波数の差を用いることができる。

　なお、23 dB 低下した点が複数ある場合は、最も高い周波数と最も低い周波数の幅とする。

## 2.16.3　空中線電力

　空中線電力の測定はアンテナ端子で行う。測定には、高周波電力計を使用する。

　無線設備を通常の変調状態で動作させたときに給電線に供給される電力を測定した値を空中線電力の強度とする。ただし、変調をかけた状態での測定が不可能なものについては、無変調状態において測定した値を送信電力の強度とする。

　平均電力で規定される変調方式（BPSK 変調及び QPSK 変調）の場合は、高周波電力計の測定値を測定結果とすることができる。ただし、尖頭電力で規定される変調方式（ASK 変調）の場合は、平均電力を測定し妥当な換算係数を用い、尖頭電力とすることができる。

## 2.16.4　スプリアス領域における不要発射の強度

　スプリアス領域（無線設備規則別表第 3 号における不要発射の強度の許容値を規定する周波数範囲のうち 30 MHz から 110 GHz 又は中心周波数の 2 倍の周波数のうちいずれか高い周波数までの周波数範囲をいう。以下同じ。）で測定する。スプリアス領域における不要発射の強度の測定はアンテナ端子で行う。

　無線設備を通常の変調状態で動作させたときに給電線に供給される周波数毎の不要発射の平均電力を測定した値又はその値と基本周波数の搬送波電力又は平均電力との差の値を不要発射の強度とする。測定はスペクトルアナライザを使用し、スペクトルアナライザの参照帯域幅は 1 MHz とする。

　給電線として導波管を用いる場合はカットオフ周波数の 0.7 倍とする。なお、導波管が長く十分なカットオフ減衰量が得られる場合は、下限周波数をカットオフ周波数とする。

　上限周波数は基本波周波数の 2 倍とするが、フィルタ等の周波数特性により十分な減衰量が得られる周波数帯は、そのデータをもって当該周波数範囲の測定に代えることが出来る。

また、必要に応じて搬送波抑圧フィルタを使用することとし、その場合は、帯域外領域における不要発射の強度を補正することとする。


2.16.5　帯域外領域における不要発射の強度
　帯域外領域における不要発射の強度の測定はアンテナ端子で行い、無線設備を変調状態で動作させたときのあらゆる不要発射が予想される周波数において不要発射を測定した値又はその値と基本周波数における平均電力との差の値を不要発射の強度とする。測定にはスペクトルアナライザを使用し、スペクトルアナライザの参照帯域幅は 1 MHz とする。
　また、必要に応じて搬送波抑圧フィルタを使用することとし、その場合は、不要発射の強度を補正することとする。


2.16.6　受信設備の副次的に発する電波等の限度
　2.16.5 の測定方法に合わせて測定する。

# 情報通信審議会 情報通信技術分科会 放送システム委員会 構成員

（敬称略、専門委員は五十音順）

| 氏　名 | | 主　要　現　職 |
|---|---|---|
| 主　査 | 伊東　晋 | 東京理科大学　理工学部　教授 |
| 主査代理 | 都竹　愛一郎 | 名城大学　理工学部　教授 |
| 委　員 | 相澤　彰子 | 国立情報学研究所　コンテンツ科学研究系　教授 |
| 専門委員 | 浅見　洋 | 一般社団法人日本CATV技術協会　理事待遇・審議役 |
| 〃 | 井家上　哲史 | 明治大学　理工学部　教授 |
| 〃 | 伊丹　誠 | 東京理科大学　基礎工学部　教授 |
| 〃 | 甲藤　二郎 | 早稲田大学　理工学部　教授 |
| 〃 | 門脇　直人 | 独立行政法人情報通信研究機構　新世代ワイヤレス研究センター長 |
| 〃 | 佐藤　明雄 | 東京工科大学　コンピュータサイエンス学部　教授 |
| 〃 | 関根　かをり | 明治大学　理工学部　教授 |
| 〃 | 高田　潤一 | 東京工業大学大学院　理工学研究科　教授 |
| 〃 | 丹　康雄 | 北陸先端科学技術大学院大学　情報科学研究科　教授 |
| 〃 | 野田　勉 | 一般社団法人日本ケーブルラボ　実用化開発グループ長 |
| 〃 | 松井　房樹 | 一般社団法人電波産業会　常務理事　研究開発本部長 |
| 〃 | 村山　優子 | 岩手県立大学　ソフトウェア情報学部　教授 |
| 〃 | 山田　孝子 | 関西学院大学　総合政策学部　教授 |

情報通信技術分科会　放送システム委員会
120GHz 帯放送事業用無線局検討作業班　構成員

（敬称略、構成員は五十音順）

| 氏　　　名 | | 主　要　現　職 |
|---|---|---|
| 主任 | 高田　潤一 | 東京工業大学 大学院理工学研究科 国際開発工学専攻 教授 |
| 主任代理 | 泉本　貴広 | 日本放送協会 技術局　計画部 チーフエンジニア |
| 構成員 | 亀谷　收 | 国立天文台水沢 VLBI 観測所　電波天文周波数小委員会　副委員長 |
| 〃 | 佐藤　誠 | 日本テレビ放送網株式会社 技術統括局技術開発部 専門部長 |
| 〃 | 島貫　靖 | NTT アドバンステクノロジ株式会社　ネットワークシステム事業本部<br>システム開発ビジネスユニット電波設計チーム 担当課長代理 |
| 〃 | 杉之下　文康 | 日本放送協会 放送技術研究所 放送ネットワーク研究部 主任研究員 |
| 〃 | 立澤　加一 | 国立天文台電波天文周波数小委員会　事務局長 |
| 〃 | 中川　永伸 | 一般財団法人テレコムエンジニアリングセンター　技術グループ　部長 |
| 〃 | 能見　正 | 独立行政法人宇宙航空研究開発機構　周波数管理室長 |
| 〃 | 野路　幸男 | 池上通信機株式会社 開発本部 マーケティング部 技監 |
| 〃 | 枚田　明彦 | 日本電信電話株式会社　マイクロシステムインテグレーション研究所<br>スマートデバイス研究部　主幹研究員 |
| 〃 | 福田　正人 | 株式会社テレビ朝日 技術局　技術統括部 |
| 〃 | 保科　徹 | 日本電気株式会社 放送映像事業部 第一技術部 プロジェクトディレクター |
| 〃 | 宮下　敦 | 株式会社日立国際電気 映像・通信事業部 製品設計統括本部<br>通信装置設計本部 放送設備設計部 部長 |
| 〃 | 宮本　大太郎 | 株式会社テレビ東京 技術局　回線技術部 |
| 〃 | 森本　聡 | 株式会社フジテレビジョン 技術開発局技術開発室開発推進部 副部長 |
| 〃 | 山本　善尚 | 株式会社 TBS テレビ 技術局放送設備計画部 |

参考資料

RECOMMENDATION ITU-R BT.2020

**Parameter values for ultra-high definition television systems for production and international programme exchange**

(2012)

**Scope**

Ultra-high definition television (UHDTV) will provide viewers with an enhanced visual experience primarily by having a wide field of view both horizontally and vertically with appropriate screen sizes relevant to usage at home and in public places. UHDTV applications require system parameters that go beyond the levels of HDTV. This Recommendation specifies UHDTV image system parameters for production and international programme exchange.

The ITU Radiocommunication Assembly,

*considering*

a)      that digital terrestrial television broadcasting (DTTB) service has been introduced by some administrations since 1997 and can provide high quality television programmes through HDTV systems;

b)      that viewers expect future TV systems beyond HDTV to provide improved characteristics compared with the current HDTV systems in terms of a more realistic sensation, greater transparency to the real world, and more accurate visual information;

c)      that ultra-high definition television (UHDTV) is expected to become available in the near future with, *inter alia*, larger screens, higher spatial/temporal resolution, wider colour gamut, wider dynamic range, etc. taking into account developments of display technology;

d)      that ITU-R has been studying extremely high-resolution imagery (EHRI) and an expanded hierarchy of large screen digital imagery (LSDI) image formats and has established ITU-R Recommendations: Recommendation ITU-R BT.1201-1 providing the guidelines of image characteristics for extremely high-resolution imagery, and Recommendation ITU-R BT.1769 offering the parameter values for an expanded hierarchy of LSDI image formats;

e)      that LSDI is a system providing a display on a very large screen, typically for public viewing. This can be used in a wide variety of applications including programme presentations such as dramas, plays, sporting events, concerts, etc.;

f)      that EHRI is a system offering higher resolution than HDTV and can be used for both broadcasting and non-broadcasting applications (e.g. computer graphics, printing and medical applications);

g)      that UHDTV provides viewers with an enhanced visual experience primarily by a wider field of view that covers a considerable part of the human natural visual field with appropriate screen sizes relevant to usage at home and in public places;

h)      that signal formats contributing to increasing the compression efficiency are desirable for UHDTV systems since they have a larger number of pixels than HDTV systems,

*recommends*

**1**      that for UHDTV programme production and international exchange, the specifications described in this Recommendation should be used[1],

*and further recommends*

**2**      that if it is shown that an alternative electro-optical transfer function (EOTF) will provide significant benefits without also imposing significant disadvantages, then this Recommendation should be extended to enable use with an improved EOTF.

NOTE – Future consideration should be given to extend this Recommendation in a complementary manner to include extended image parameters.

TABLE 1

**Picture spatial characteristics**

| Parameter | Values | |
|---|---|---|
| Picture aspect ratio | 16:9 | |
| Pixel count<br>Horizontal × vertical | 7 680 × 4 320 | 3 840 × 2 160 |
| Sampling lattice | Orthogonal | |
| Pixel aspect ratio | 1:1 (square pixels) | |
| Pixel addressing | Pixel ordering in each row is from left to right, and rows are ordered from top to bottom. | |

TABLE 2

**Picture temporal characteristics**

| Parameter | Values |
|---|---|
| Frame frequency (Hz) | 120, 60, 60/1.001, 50, 30, 30/1.001, 25, 24, 24/1.001 |
| Scan mode | Progressive |

---

[1]  Both 3 840 × 2 160 and 7 680 × 4 320 systems of UHDTV will find their main applications for the delivery of television programming to the home where they will provide viewers with an increased sense of "being there" and increased sense of realness by using displays with a screen diagonal of the order of 1.5 metres or more and for large screen (LSDI) presentations in theatres, halls and other venues such as sports venues or theme parks.

Presentation on tablet displays with extremely high resolution will also be attractive for viewers.

The 7 680 × 4 320 system will provide a more enhanced visual experience than the 3 840 × 2 160 system for a wider range of viewing environments.

An increase in the efficiency of video source coding and/or in the capacity of transmission channels, compared to those currently in use, will likely be needed to deliver such programs by terrestrial or satellite broadcasting to the home. Research is under way to achieve this goal. The delivery of such programming will initially be possible by cable or fibre.

TABLE 3

**System colorimetry**

| Parameter | Values | | |
|---|---|---|---|
| Opto-electronic transfer characteristics before non-linear pre-correction | Assumed linear [1] | | |
| Primary colours and reference white [2] | Chromaticity coordinates (CIE, 1931) | x | y |
| | Red primary (R) | 0.708 | 0.292 |
| | Green primary (G) | 0.170 | 0.797 |
| | Blue primary (B) | 0.131 | 0.046 |
| | Reference white (D65) | 0.3127 | 0.3290 |

[1] Picture information can be linearly indicated by the tristimulus values of RGB in the range of 0-1.

[2] The colorimetric values of the picture information can be determined based on the reference RGB primaries and the reference white.

TABLE 4

**Signal format**

| Parameter | Values | |
|---|---|---|
| Signal format | $R'G'B'$ [2] | |
| | Constant luminance $Y'_C C'_{BC} C'_{RC}$ [3] | Non-constant luminance $Y'C'_B C'_R$ [4] |
| Non-linear transfer function | $$E' = \begin{cases} 4.5E, & 0 \le E < \beta \\ \alpha E^{0.45} - (\alpha - 1), & \beta \le E \le 1 \end{cases}$$ where $E$ is voltage normalized by the reference white level and proportional to the implicit light intensity that would be detected with a reference camera colour channel $R$, $G$, $B$; $E'$ is the resulting non-linear signal. $\alpha = 1.099$ and $\beta = 0.018$ for 10-bit system $\alpha = 1.0993$ and $\beta = 0.0181$ for 12-bit system | |

---

[2] $R'G'B'$ may be used for programme exchange when the best quality programme production is of primary importance.

[3] Constant luminance $Y'_C C'_{BC} C'_{RC}$ may be used when the most accurate retention of luminance information is of primary importance or where there is an expectation of improved coding efficiency for delivery (see Report ITU-R BT.2246).

[4] Conventional non-constant luminance $Y'C'_B C'_R$ may be used when use of the same operational practices as those in SDTV and HDTV environments is of primary importance through a broadcasting chain (see Report ITU-R BT.2246).

TABLE 4 *(end)*

| Parameter | Values | |
|---|---|---|
| Derivation of $Y'_C$ and $Y'$ | $Y'_C = \left(0.2627R + 0.6780G + 0.0593B\right)'$ | $Y' = 0.2627R' + 0.6780G' + 0.0593B'$ |
| Derivation of colour difference signals | $C'_{BC} = \begin{cases} \dfrac{B'-Y'_C}{1.9404}, & -0.9702 \leq B'-Y'_C \leq 0 \\[2ex] \dfrac{B'-Y'_C}{1.5816}, & 0 < B'-Y'_C \leq 0.7908 \end{cases}$ $C'_{RC} = \begin{cases} \dfrac{R'-Y'_C}{1.7184}, & -0.8592 \leq R'-Y'_C \leq 0 \\[2ex] \dfrac{R'-Y'_C}{0.9936}, & 0 < R'-Y'_C \leq 0.4968 \end{cases}$ | $C'_B = \dfrac{B'-Y'}{1.8814}$ $C'_R = \dfrac{R'-Y'}{1.4746}$ |

TABLE 5

**Digital representation**

| Parameters | Values | | |
|---|---|---|---|
| Coded signal | $R'$, $G'$, $B'$ or $Y'$, $C'_B$, $C'_R$ or $Y'_C$, $C'_{BC}$, $C'_{RC}$ | | |
| Sampling lattice – $R'$, $G'$, $B'$, $Y'$, $Y'_C$ | Orthogonal, line and picture repetitive co-sited | | |
| Sampling lattice – $C'_B$, $C'_R$ or $C'_{BC}$, $C'_{RC}$ | Orthogonal, line and picture repetitive co-sited with each other. The first (top-left) sample is co-sited with the first $Y'$ samples. | | |
| | 4:4:4 system | 4:2:2 system | 4:2:0 system |
| | Each has the same number of horizontal samples as the $Y'$ $(Y'_C)$ component. | Horizontally subsampled by a factor of two with respect to the $Y'$ $(Y'_C)$ component. | Horizontally and vertically subsampled by a factor of two with respect to the $Y'$ $(Y'_C)$ component. |
| Coding format | 10 or 12 bits per component | | |
| Quantization of $R'$, $G'$, $B'$, $Y'$, $Y'_C$, $C'_B$, $C'_R$, $C'_{BC}$, $C'_{RC}$ | $DR' = INT\left[\left(219 \times R' + 16\right) \times 2^{n-8}\right]$ $DG' = INT\left[\left(219 \times G' + 16\right) \times 2^{n-8}\right]$ $DB' = INT\left[\left(219 \times B' + 16\right) \times 2^{n-8}\right]$ $DY'(DY'_C) = INT\left[\left(219 \times Y'(Y'_C) + 16\right) \times 2^{n-8}\right]$ $DC'_B(DC'_{BC}) = INT\left[\left(224 \times C'_B(C'_{BC}) + 128\right) \times 2^{n-8}\right]$ $DC'_R(DC'_{RC}) = INT\left[\left(224 \times C'_R(C'_{RC}) + 128\right) \times 2^{n-8}\right]$ | | |

TABLE 5 *(end)*

| Parameters | Values | |
|---|---|---|
| Quantization levels | 10-bit coding | 12-bit coding |
| − Black level<br>   *DR′, DG′, DB′, DY′, DY′$_C$*<br>− Achromatic<br>   *DC′$_B$, DC′$_R$, DC′$_{BC}$,*<br>   *DC′$_{RC}$*<br>− Nominal Peak<br>   *DR′, DG′, DB′, DY′, DY′$_C$*<br>   *DC′$_B$, DC′$_R$, DC′$_{BC}$, DC′$_{RC}$* | 64<br><br>512<br><br><br>940<br>64 and 960 | 256<br><br>2 048<br><br><br>3 760<br>256 and 3 840 |
| Quantization level assignment<br>− Video data<br>− Timing reference | 10-bit coding<br>4 through 1 019<br>0-3 and 1 020-1 023 | 12-bit coding<br>16 through 4 079<br>0-15 and 4 080-4 095 |

————————————

## Dual Green 方式

　800 万画素の撮像・表示素子を G 信号に 2 枚、R・B 信号にそれぞれ 1 枚ずつ用いるスーパーハイビジョンの方式。フレーム周波数は 60p、階調は 10 ビットで、SHV の番組制作には、現状、カメラをはじめ、記録装置、編集装置、表示装置などにおいて、この方式の機器が用いられている。

　　各素子の画素位置をずらし、視覚の解像度に大きく寄与する G 信号のサンプル点を 2 倍にすることで等価的に解像度を確保している（ベイヤー配列）。



各画素はR、G、Bを割り当てる。
G₁とG₂画素は斜めにずれている。
（G信号が解像度に最も寄与するため、実質的に縦横方向に2倍の解像度を得られる）
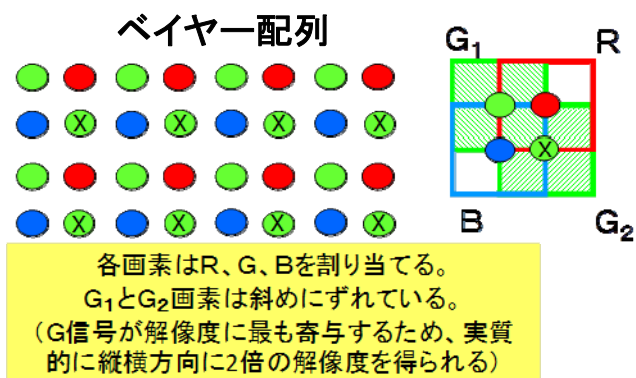
# HD-SDI 信号について

　ハイビジョンカメラなどから出力されるシリアルデジタル信号である HD-SDI 信号は、映像データの他、同期信号である SAV(Start of Active Video)や EAV(End of Active Video)、および LN(Line Number)や CRC(Cyclic Redundancy Check)、音声データなどを格納する補助データ領域のデータで構成されている。図 1 に HD-SDI 信号の構成を示す。図 1 は1125 ラインある映像の 1 ライン分のデータを示している。HD-SDI 信号は、下図のとおり1 ライン 22kbit で構成され、一画面当たり 1125 ライン、輝度信号（Y）と色差信号（$C_B$/$C_R$）を 60i で伝送するので、伝送ビットレートは、1.485Gbps となる。
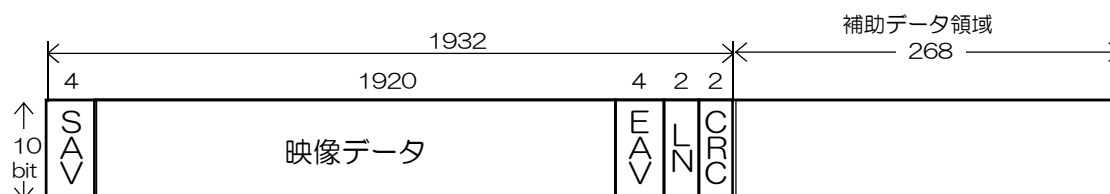


図 1　HD-SDI 信号の構成（映像 1 ライン分のデータ）

<div align="center">

Ｃ／Ｎ配分

</div>

〇ASK 方式

　　25.0dB ────┬── 熱雑音　（70%）　　　　26.5dB
　　　　　　　　└── 干渉雑音（30%）　　　　30.2dB

〇BPSK 方式

　　19.0dB ────┬── 熱雑音　（70%）　　　　20.5dB
　　　　　　　　└── 干渉雑音（30%）　　　　24.2dB

〇QPSK 方式

　　23.9dB ────┬── 熱雑音　（70%）　　　　25.4dB
　　　　　　　　└── 干渉雑音（30%）　　　　29.1dB

# 大気吸収損

　大気吸収損については、ITU-R 勧告 P.676-9（参考資料６）に、Dry（乾燥空気：水蒸気密度が 0g/m³）と Standard（水蒸気密度が 7.5g/m³）における値が、周波数ごとに掲載されている。図 1 に ITU-R 勧告 P.676-9 に記載された各周波数における大気吸収損を示す。120 GHz 帯においては、水蒸気密度が 7.5g/m³ における値は約 1 dB/km となっている。

　図 2 に 120GHz 帯 FPU を使用した 3 km 区間の伝搬試験における水蒸気密度と受信電力の関係を示すが、水蒸気密度が 1g/m³ 増加すると受信電力は 0.31dB m 低下しており、この傾向は ITU-R 勧告 P.676-9 とよく一致している。国内で一般的な最悪ケース（気温 30℃、相対湿度 100%、水蒸気密度 約 30g/m³）では、図 2 に示すとおり、減衰量は伝送距離 3km で約 9dB となる。従って、1km 当りの減衰量は 3 dB/km となる。

　回線設計を行う上で、季節的変動を考慮して、回線品質の検討に使用する大気吸収損の値は、高温多湿のとき（水蒸気密度が 30g/m³：30℃で相対湿度が 100%のとき）の大気吸収損である 3 dB/km とすることが適当である。



図 1　大気吸収定数の周波数依存性

傾きは、水蒸気密度が1g／m³増加すると0.31dBm低下。ITU-R 勧告P.676と良く一致。

気温30℃、相対湿度100%では、水蒸気密度は約30 g／m³。3kmの伝送距離では9dB程度の減衰量（3dB／km）。

図 2　受信電力と水蒸気密度の関係

RECOMMENDATION ITU-R P.676-9

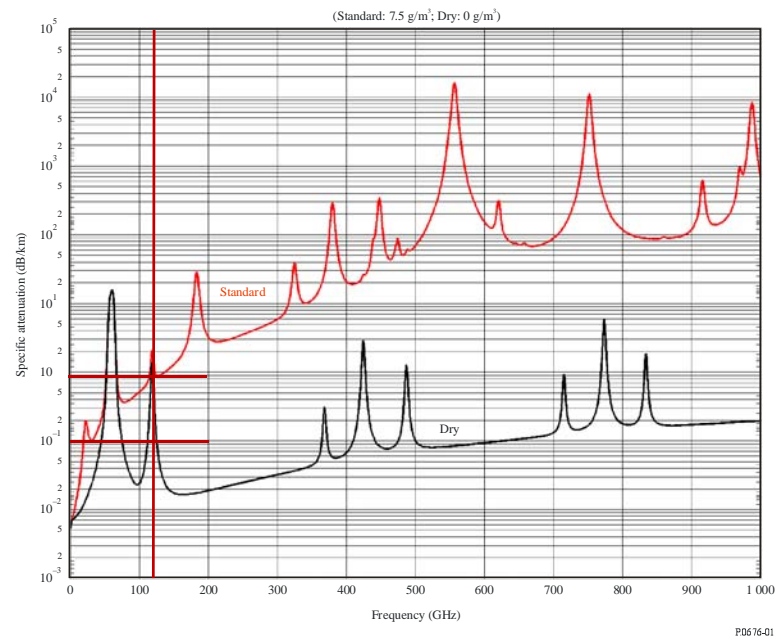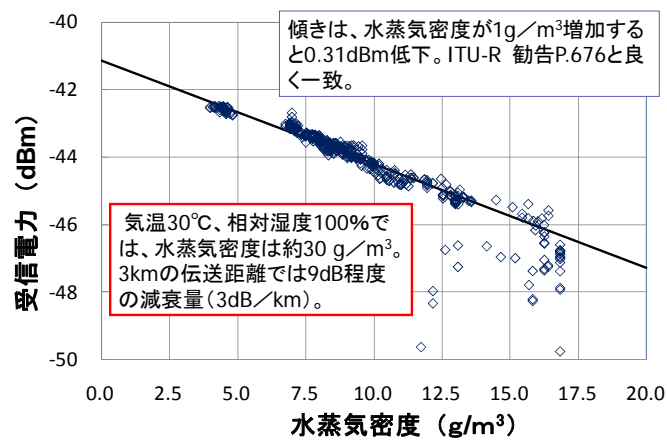# Attenuation by atmospheric gases

(Question ITU-R 201/3)

(1990-1992-1995-1997-1999-2001-2005-2007-2009-2012)

**Scope**

Recommendation ITU-R P.676 provides methods to estimate the attenuation of atmospheric gases on terrestrial and slant paths using:

a)      an estimate of gaseous attenuation computed by summation of individual absorption lines that is valid for the frequency range 1-1 000 GHz, and

b)      a simplified approximate method to estimate gaseous attenuation that is applicable in the frequency range 1-350 GHz.

The ITU Radiocommunication Assembly,

*considering*

a)      the necessity of estimating the attenuation by atmospheric gases on terrestrial and slant paths,

*recommends*

**1**      that, for general application, the procedures in Annex 1 be used to calculate gaseous attenuation at frequencies up to 1 000 GHz;

**2**      that, for approximate estimates of gaseous attenuation in the frequency range 1 to 350 GHz, the computationally less intensive procedure given in Annex 2 be used.

# Annex 1

# Line-by-line calculation of gaseous attenuation

## 1      Specific attenuation

The specific attenuation at frequencies up to 1 000 GHz due to dry air and water vapour, can be evaluated most accurately at any value of pressure, temperature and humidity by means of a summation of the individual resonance lines from oxygen and water vapour, together with small additional factors for the non-resonant Debye spectrum of oxygen below 10 GHz, pressure-induced nitrogen attenuation above 100 GHz and a wet continuum to account for the excess water vapour-absorption found experimentally. Figure 1 shows the specific attenuation using the model, calculated from 0 to 1 000 GHz at 1 GHz intervals, for a pressure of 1 013 hPa, temperature of 15° C for the cases of a water-vapour density of 7.5 g/m³ (Curve A) and a dry atmosphere (Curve B).

Near 60 GHz, many oxygen absorption lines merge together, at sea-level pressures, to form a single, broad absorption band, which is shown in more detail in Fig. 2. This figure also shows the oxygen attenuation at higher altitudes, with the individual lines becoming resolved at lower pressures. Some additional molecular species (e.g. oxygen isotopic species, oxygen vibrationally excited species, ozone, ozone isotopic species, and ozone vibrationally excited species, and other minor species) are not included in the line-by-line prediction method. These additional lines are insignificant for typical atmospheres, but may be important for a dry atmosphere.

For quick and approximate estimates of specific attenuation at frequencies up to 350 GHz, in cases where high accuracy is not required, simplified algorithms are given in Annex 2 for restricted ranges of meteorological conditions.

The specific gaseous attenuation is given by:

$$\gamma = \gamma_o + \gamma_w = 0.1820 f\, N''(f) \qquad \text{dB/km} \qquad (1)$$

where $\gamma_o$ and $\gamma_w$ are the specific attenuations (dB/km) due to dry air (oxygen, pressure-induced nitrogen and non-resonant Debye attenuation) and water vapour, respectively, and where $f$ is the frequency (GHz) and $N''(f)$ is the imaginary part of the frequency-dependent complex refractivity:

$$N''(f) = \sum_i S_i\, F_i + N''_D(f) \qquad (2)$$

$S_i$ is the strength of the $i$-th line, $F_i$ is the line shape factor and the sum extends over all the lines (for frequencies, $f$, above 118.750343 GHz oxygen line, only the oxygen lines above 60 GHz complex should be included in the summation; the summation should begin at $i = 38$ rather than at $i = 1$); $N''_D(f)$ is the dry continuum due to pressure-induced nitrogen absorption and the Debye spectrum.

The line strength is given by:

$$
\begin{aligned}
S_i \;&=\; a_1 \times 10^{-7}\, p\, \theta^3\, \exp\left[a_2\,(1-\theta)\right] & \text{for oxygen} \\[2mm]
&=\; b_1 \times 10^{-1}\, e\, \theta^{3.5}\, \exp\left[b_2\,(1-\theta)\right] & \text{for water vapour}
\end{aligned}
\qquad (3)
$$

where:

$\quad\quad p:$    dry air pressure (hPa)

$\quad\quad e:$    water vapour partial pressure in hPa (total barometric pressure $p_{tot} = p + e$)

$\quad\quad \theta =$    $300/T$

$\quad\quad T:$    temperature (K).

FIGURE 1

**Specific attenuation due to atmospheric gases, calculated at 1 GHz intervals, including line centres**
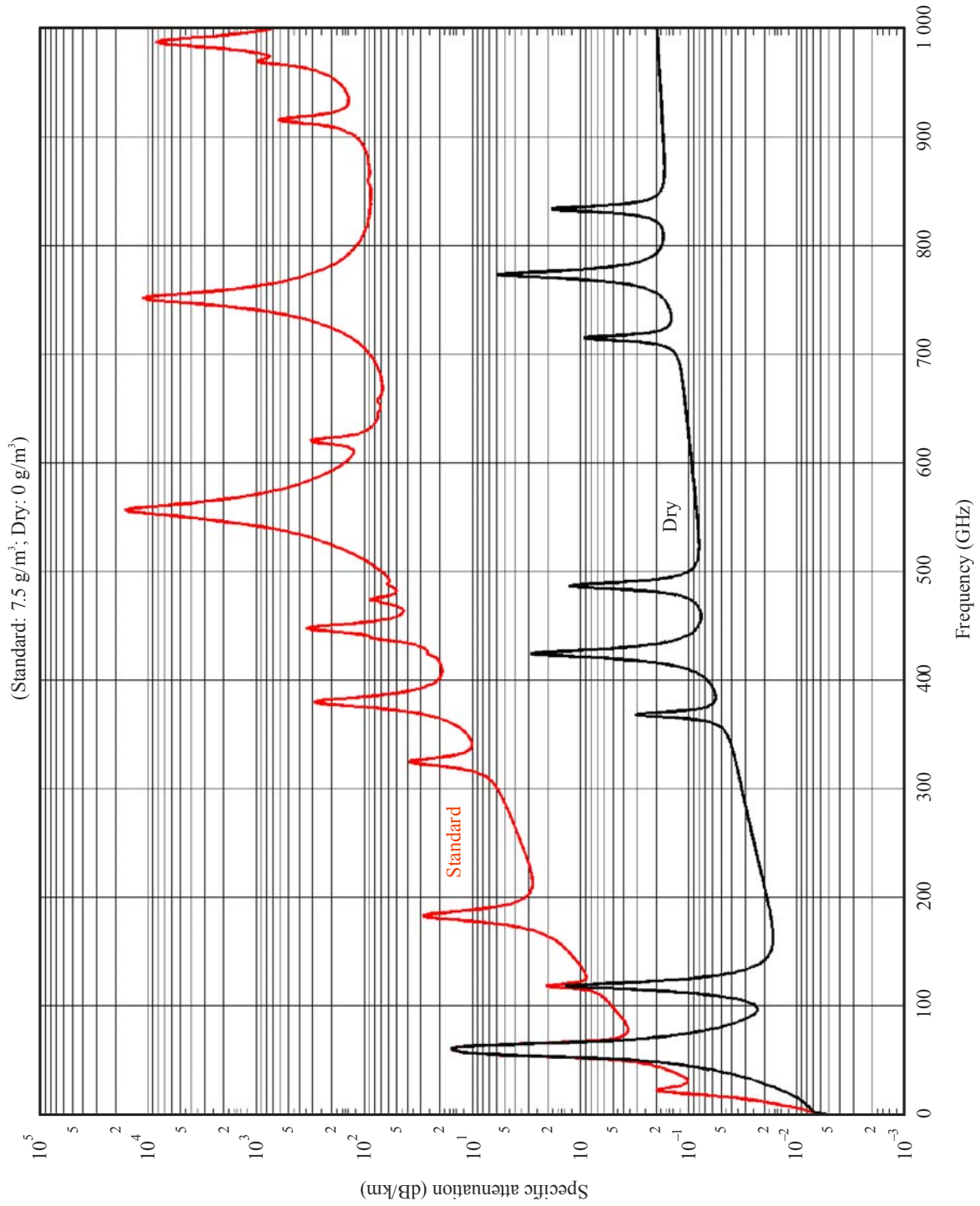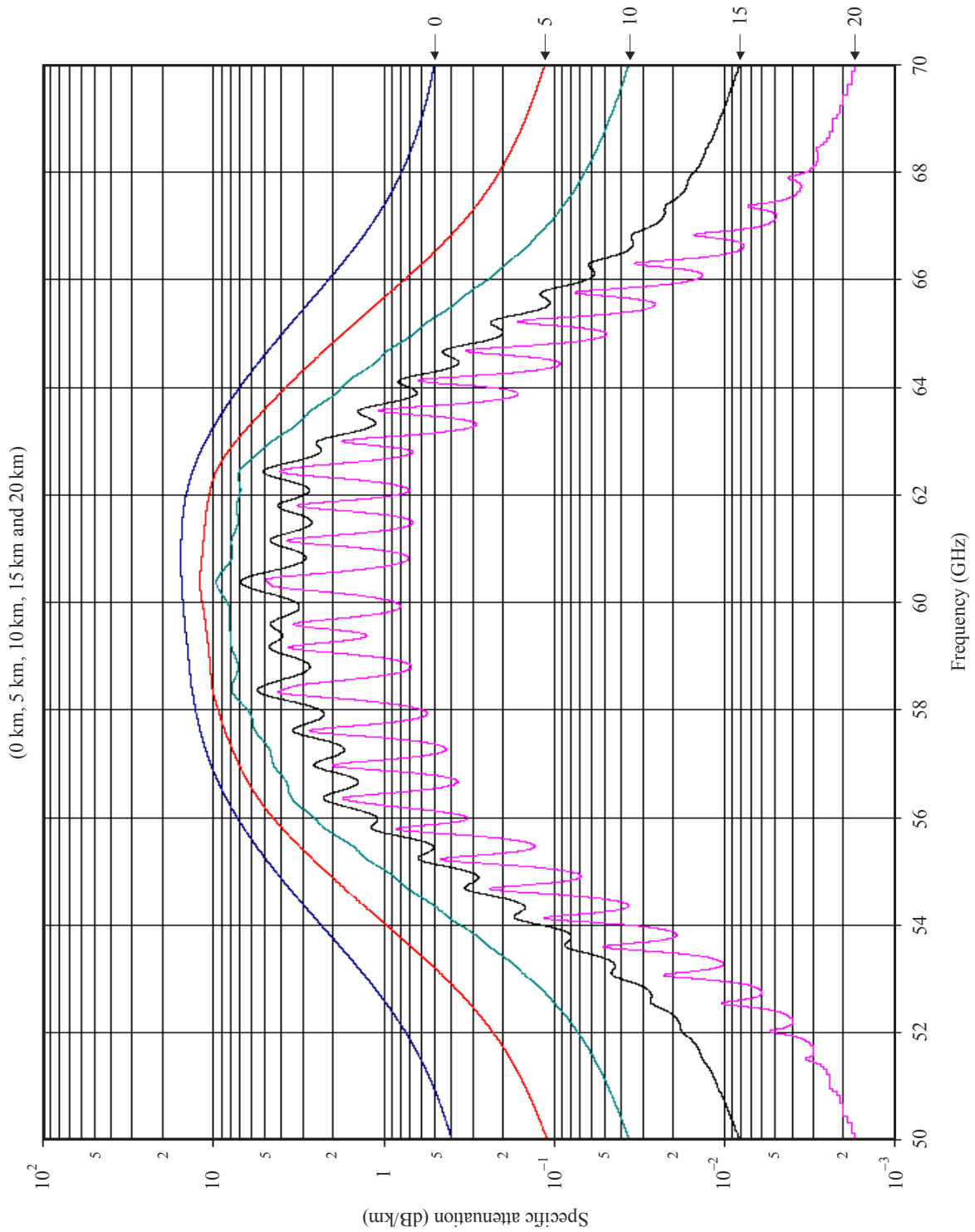
FIGURE 2

**Specific attenuation in the range 50-70 GHz at the altitudes indicated**

Local values of $p$, $e$ and $T$ measured profiles (e.g. using radiosondes) should be used; however, in the absence of local information, the reference standard atmospheres described in Recommendation ITU-R P.835 should be used. (Note that where total atmospheric attenuation is being calculated, the same-water vapour partial pressure is used for both dry-air and water-vapour attenuations.)

The water-vapour partial pressure, $e$, may be obtained from the water-vapour density $\rho$ using the expression:

$$e = \frac{\rho\,T}{216.7} \tag{4}$$

The coefficients $a_1$, $a_2$ are given in Table 1 for oxygen, those for water vapour, $b_1$ and $b_2$, are given in Table 2.

The line-shape factor is given by:

$$F_i = \frac{f}{f_i}\left[\frac{\Delta f - \delta\,(f_i - f)}{(f_i - f)^2 + \Delta f^2} + \frac{\Delta f - \delta\,(f_i + f)}{(f_i + f)^2 + \Delta f^2}\right] \tag{5}$$

where $f_i$ is the line frequency and $\Delta f$ is the width of the line:

$$\Delta f = a_3 \times 10^{-4}\,(p\,\theta^{(0.8 - a_4)} + 1.1\,e\,\theta) \qquad \text{for oxygen}$$
$$= b_3 \times 10^{-4}\,(p\,\theta^{b_4} + b_5\,e\,\theta^{b_6}) \qquad \text{for water vapour} \tag{6a}$$

The line width $\Delta f$ is modified to account for Doppler broadening:

$$\Delta f = \sqrt{\Delta f^2 + 2.25 \times 10^{-6}} \qquad \text{for oxygen}$$
$$= 0.535\Delta f + \sqrt{0.217\Delta f^2 + \frac{2.1316 \times 10^{-12}\,f_i^2}{\theta}} \qquad \text{for water vapour} \tag{6b}$$

$\delta$ is a correction factor which arises due to interference effects in oxygen lines:

$$\delta = (a_5 + a_6\theta) \times 10^{-4}\,(p + e)\,\theta^{0.8} \qquad \text{for oxygen}$$
$$= 0 \qquad \text{for water vapour} \tag{7}$$

The spectroscopic coefficients are given in Tables 1 and 2.

TABLE 1

**Spectroscopic data for oxygen attenuation**

| $f_0$ | $a_1$ | $a_2$ | $a_3$ | $a_4$ | $a_5$ | $a_6$ |
|---|---|---|---|---|---|---|
| 50.474238 | .94 | 9.694 | 8.90 | .0 | 2.400 | 7.900 |
| 50.987749 | 2.46 | 8.694 | 9.10 | .0 | 2.200 | 7.800 |
| 51.503350 | 6.08 | 7.744 | 9.40 | .0 | 1.970 | 7.740 |
| 52.021410 | 14.14 | 6.844 | 9.70 | .0 | 1.660 | 7.640 |
| 52.542394 | 31.02 | 6.004 | 9.90 | .0 | 1.360 | 7.510 |
| 53.066907 | 64.10 | 5.224 | 10.20 | .0 | 1.310 | 7.140 |
| 53.595749 | 124.70 | 4.484 | 10.50 | .0 | 2.300 | 5.840 |
| 54.130000 | 228.00 | 3.814 | 10.70 | .0 | 3.350 | 4.310 |
| 54.671159 | 391.80 | 3.194 | 11.00 | .0 | 3.740 | 3.050 |
| 55.221367 | 631.60 | 2.624 | 11.30 | .0 | 2.580 | 3.390 |
| 55.783802 | 953.50 | 2.119 | 11.70 | .0 | −1.660 | 7.050 |
| 56.264775 | 548.90 | .015 | 17.30 | .0 | 3.900 | −1.130 |
| 56.363389 | 1 344.00 | 1.660 | 12.00 | .0 | −2.970 | 7.530 |
| 56.968206 | 1 763.00 | 1.260 | 12.40 | .0 | −4.160 | 7.420 |
| 57.612484 | 2 141.00 | .915 | 12.80 | .0 | −6.130 | 6.970 |
| 58.323877 | 2 386.00 | .626 | 13.30 | .0 | −2.050 | .510 |
| 58.446590 | 1 457.00 | .084 | 15.20 | .0 | 7.480 | −1.460 |
| 59.164207 | 2 404.00 | .391 | 13.90 | .0 | −7.220 | 2.660 |
| 59.590983 | 2 112.00 | .212 | 14.30 | .0 | 7.650 | −.900 |
| 60.306061 | 2 124.00 | .212 | 14.50 | .0 | −7.050 | .810 |
| 60.434776 | 2 461.00 | .391 | 13.60 | .0 | 6.970 | −3.240 |
| 61.150560 | 2 504.00 | .626 | 13.10 | .0 | 1.040 | −.670 |
| 61.800154 | 2 298.00 | .915 | 12.70 | .0 | 5.700 | −7.610 |
| 62.411215 | 1 933.00 | 1.260 | 12.30 | .0 | 3.600 | −7.770 |
| 62.486260 | 1 517.00 | .083 | 15.40 | .0 | −4.980 | .970 |
| 62.997977 | 1 503.00 | 1.665 | 12.00 | .0 | 2.390 | −7.680 |
| 63.568518 | 1 087.00 | 2.115 | 11.70 | .0 | 1.080 | −7.060 |
| 64.127767 | 733.50 | 2.620 | 11.30 | .0 | −3.110 | −3.320 |
| 64.678903 | 463.50 | 3.195 | 11.00 | .0 | −4.210 | −2.980 |
| 65.224071 | 274.80 | 3.815 | 10.70 | .0 | −3.750 | −4.230 |
| 65.764772 | 153.00 | 4.485 | 10.50 | .0 | −2.670 | −5.750 |
| 66.302091 | 80.09 | 5.225 | 10.20 | .0 | −1.680 | −7.000 |
| 66.836830 | 39.46 | 6.005 | 9.90 | .0 | −1.690 | −7.350 |
| 67.369598 | 18.32 | 6.845 | 9.70 | .0 | −2.000 | −7.440 |
| 67.900867 | 8.01 | 7.745 | 9.40 | .0 | −2.280 | −7.530 |
| 68.431005 | 3.30 | 8.695 | 9.20 | .0 | −2.400 | −7.600 |
| 68.960311 | 1.28 | 9.695 | 9.00 | .0 | −2.500 | −7.650 |
| 118.750343 | 945.00 | .009 | 16.30 | .0 | −.360 | .090 |
| 368.498350 | 67.90 | .049 | 19.20 | .6 | .000 | .000 |
| 424.763124 | 638.00 | .044 | 19.30 | .6 | .000 | .000 |
| 487.249370 | 235.00 | .049 | 19.20 | .6 | .000 | .000 |
| 715.393150 | 99.60 | .145 | 18.10 | .6 | .000 | .000 |
| 773.839675 | 671.00 | .130 | 18.20 | .6 | .000 | .000 |
| 834.145330 | 180.00 | .147 | 18.10 | .6 | .000 | .000 |

TABLE 2

**Spectroscopic data for water-vapour attenuation**

| $f_0$ | $b_1$ | $b_2$ | $b_3$ | $b_4$ | $b_5$ | $b_6$ |
|---|---|---|---|---|---|---|
| 22.235080 | 0.1130 | 2.143 | 28.11 | .69 | 4.800 | 1.00 |
| 67.803960 | 0.0012 | 8.735 | 28.58 | .69 | 4.930 | .82 |
| 119.995940 | 0.0008 | 8.356 | 29.48 | .70 | 4.780 | .79 |
| 183.310091 | 2.4200 | .668 | 30.50 | .64 | 5.300 | .85 |
| 321.225644 | 0.0483 | 6.181 | 23.03 | .67 | 4.690 | .54 |
| 325.152919 | 1.4990 | 1.540 | 27.83 | .68 | 4.850 | .74 |
| 336.222601 | 0.0011 | 9.829 | 26.93 | .69 | 4.740 | .61 |
| 380.197372 | 11.5200 | 1.048 | 28.73 | .54 | 5.380 | .89 |
| 390.134508 | 0.0046 | 7.350 | 21.52 | .63 | 4.810 | .55 |
| 437.346667 | 0.0650 | 5.050 | 18.45 | .60 | 4.230 | .48 |
| 439.150812 | 0.9218 | 3.596 | 21.00 | .63 | 4.290 | .52 |
| 443.018295 | 0.1976 | 5.050 | 18.60 | .60 | 4.230 | .50 |
| 448.001075 | 10.3200 | 1.405 | 26.32 | .66 | 4.840 | .67 |
| 470.888947 | 0.3297 | 3.599 | 21.52 | .66 | 4.570 | .65 |
| 474.689127 | 1.2620 | 2.381 | 23.55 | .65 | 4.650 | .64 |
| 488.491133 | 0.2520 | 2.853 | 26.02 | .69 | 5.040 | .72 |
| 503.568532 | 0.0390 | 6.733 | 16.12 | .61 | 3.980 | .43 |
| 504.482692 | 0.0130 | 6.733 | 16.12 | .61 | 4.010 | .45 |
| 547.676440 | 9.7010 | .114 | 26.00 | .70 | 4.500 | 1.00 |
| 552.020960 | 14.7700 | .114 | 26.00 | .70 | 4.500 | 1.00 |
| 556.936002 | 487.4000 | .159 | 32.10 | .69 | 4.110 | 1.00 |
| 620.700807 | 5.0120 | 2.200 | 24.38 | .71 | 4.680 | .68 |
| 645.866155 | 0.0713 | 8.580 | 18.00 | .60 | 4.000 | .50 |
| 658.005280 | 0.3022 | 7.820 | 32.10 | .69 | 4.140 | 1.00 |
| 752.033227 | 239.6000 | .396 | 30.60 | .68 | 4.090 | .84 |
| 841.053973 | 0.0140 | 8.180 | 15.90 | .33 | 5.760 | .45 |
| 859.962313 | 0.1472 | 7.989 | 30.60 | .68 | 4.090 | .84 |
| 899.306675 | 0.0605 | 7.917 | 29.85 | .68 | 4.530 | .90 |
| 902.616173 | 0.0426 | 8.432 | 28.65 | .70 | 5.100 | .95 |
| 906.207325 | 0.1876 | 5.111 | 24.08 | .70 | 4.700 | .53 |
| 916.171582 | 8.3400 | 1.442 | 26.70 | .70 | 4.780 | .78 |
| 923.118427 | 0.0869 | 10.220 | 29.00 | .70 | 5.000 | .80 |
| 970.315022 | 8.9720 | 1.920 | 25.50 | .64 | 4.940 | .67 |
| 987.926764 | 132.1000 | .258 | 29.85 | .68 | 4.550 | .90 |
| 1 780.000000 | 22 300.0000 | .952 | 176.20 | .50 | 30.500 | 5.00 |

The dry air continuum arises from the non-resonant Debye spectrum of oxygen below 10 GHz and a pressure-induced nitrogen attenuation above 100 GHz.

$$N_D''(f) = f\, p\, \theta^2 \left[ \frac{6.14 \times 10^{-5}}{d\left[1 + \left(\dfrac{f}{d}\right)^2\right]} + \frac{1.4 \times 10^{-12}\, p\, \theta^{1.5}}{1 + 1.9 \times 10^{-5}\, f^{1.5}} \right] \tag{8}$$

where $d$ is the width parameter for the Debye spectrum:

$$d = 5.6 \times 10^{-4}\,(p+e)\theta^{0.8} \tag{9}$$

## 2 Path attenuation

### 2.1 Terrestrial paths

For a terrestrial path, or for slightly inclined paths close to the ground, the path attenuation, $A$, may be written as:

$$A = \gamma\, r_0 = (\gamma_o + \gamma_w)\, r_0 \qquad \text{dB} \tag{10}$$

where $r_0$ is path length (km).

### 2.2 Slant paths

This section gives a method to integrate the specific attenuation calculated using the line-by-line model given above, at different pressures, temperatures and humidities through the atmosphere. By this means, the path attenuation for communications systems with any geometrical configuration within and external to the Earth's atmosphere may be accurately determined simply by dividing the atmosphere into horizontal layers, specifying the profile of the meteorological parameters pressure, temperature and humidity along the path. In the absence of local profiles, from radiosonde data, for example, the reference standard atmospheres in Recommendation ITU-R P.835 may be used, either for global application or for low (annual), mid (summer and winter) and high latitude (summer and winter) sites.

Figure 3 shows the zenith attenuation calculated at 1 GHz intervals with this model for the global reference standard atmosphere in Recommendation ITU-R P.835, with horizontal layers 1 km thick and summing the attenuations for each layer, for the cases of a moist atmosphere (Curve A) and a dry atmosphere (Curve B).

The total slant path attenuation, $A(h, \varphi)$, from a station with altitude, $h$, and elevation angle, $\varphi$, can be calculated as follows when $\varphi \geq 0$:

$$A(h, \varphi) = \int_h^\infty \frac{\gamma(H)}{\sin \Phi}\, \mathrm{d}H \tag{11}$$

where the value of Φ can be determined as follows based on Snell's law in polar coordinates:

$$\Phi = \arccos\left(\frac{c}{(r+H) \times n(H)}\right) \qquad (12)$$

where:

$$c = (r+h) \times n(h) \times \cos\varphi \qquad (13)$$

where $n(h)$ is the atmospheric radio refractive index, calculated from pressure, temperature and water-vapour pressure along the path (see Recommendation ITU-R P.835) using Recommendation ITU-R P.453.

On the other hand, when $\varphi < 0$, there is a minimum height, $h_{min}$, at which the radio beam becomes parallel with the Earth's surface. The value of $h_{min}$ can be determined by solving the following transcendental equation:

$$(r+h_{min}) \times n(h_{min}) = c \qquad (14)$$

This can be easily solved by repeating the following calculation, using $h_{min} = h$ as an initial value:

$$h'_{min} = \frac{c}{n(h_{min})} - r \qquad (15)$$

Therefore, $A(h, \varphi)$ can be calculated as follows:

$$A(h, \varphi) = \int_{h_{min}}^{\infty} \frac{\gamma(H)}{\sin\Phi}\,dH + \int_{h_{min}}^{h} \frac{\gamma(H)}{\sin\Phi}\,dH \qquad (16)$$

In carrying out the integration of equations (11) and (16), care should be exercised in that the integrand becomes infinite at $\Phi = 0$. However, this singularity can be eliminated by an appropriate variable conversion, for example, by using $u^4 = H - h$ in equation (11) and $u^4 = H - h_{min}$ in equation (16).

A numerical solution for the attenuation due to atmospheric gases can be implemented with the following algorithm.

To calculate the total attenuation for a satellite link, it is necessary to know not only the specific attenuation at each point of the link but also the length of path that has that specific attenuation. To derive the path length it is also necessary to consider the ray bending that occurs in a spherical Earth.

Using Fig. 4 as a reference, $a_n$ is the path length through layer $n$ with thickness $\delta_n$ that has refractive index $n_n$. $\alpha_n$ and $\beta_n$ are the entry and exiting incidence angles. $r_n$ are the radii from the centre of the Earth to the beginning of layer $n$. $a_n$ can then be expressed as:

$$a_n = -r_n \cos\beta_n + \frac{1}{2}\sqrt{4\,r_n^2\cos^2\beta_n + 8\,r_n\,\delta_n + 4\,\delta_n^2} \qquad (17)$$

The angle $\alpha_n$ can be calculated from:

$$\alpha_n = \pi - \arccos\left(\frac{-a_n^2 - 2\,r_n\,\delta_n - \delta_n^2}{2\,a_n\,r_n + 2\,a_n\,\delta_n}\right) \qquad (18)$$

$\beta_1$ is the incidence angle at the ground station (the complement of the elevation angle φ). $\beta_{n+1}$ can be calculated from $\alpha_n$ using Snell's law that in this case becomes:

$$\beta_{n+1} = \arcsin\left(\frac{n_n}{n_{n+1}}\sin \alpha_n\right)$$                                        (19)

where $n_n$ and $n_{n+1}$ are the refractive indexes of layers $n$ and $n + 1$.

Equation (19) may become invalid at very low elevation angles (φ < 1°) when radiosonde data from certain regions of the world susceptible to ducting conditions are used as input. In such cases, air layers with radio refractivity gradients smaller in magnitude than −157 N/km are present and the ray-tracing algorithm (equations (17) to (19)), based on geometrical optics, is no longer applicable. The arcsine function in equation (19) becomes complex under these anomalous conditions since its argument is then slightly larger than 1. It should be noted that equation (19) is valid for all elevation angles when the reference standard atmospheres described in Recommendation ITU-R P.835 are used as input, since these idealized atmospheres – clearly without strong negative refractivity gradients – do not support such anomalous propagation conditions.

FIGURE 3

**Zenith attenuation due to atmospheric gases, calculated at 1 GHz intervals, including line centres**



P0676-03

(Standard: 7.5 g/m³ at sea level; Dry: 0 g/m³)
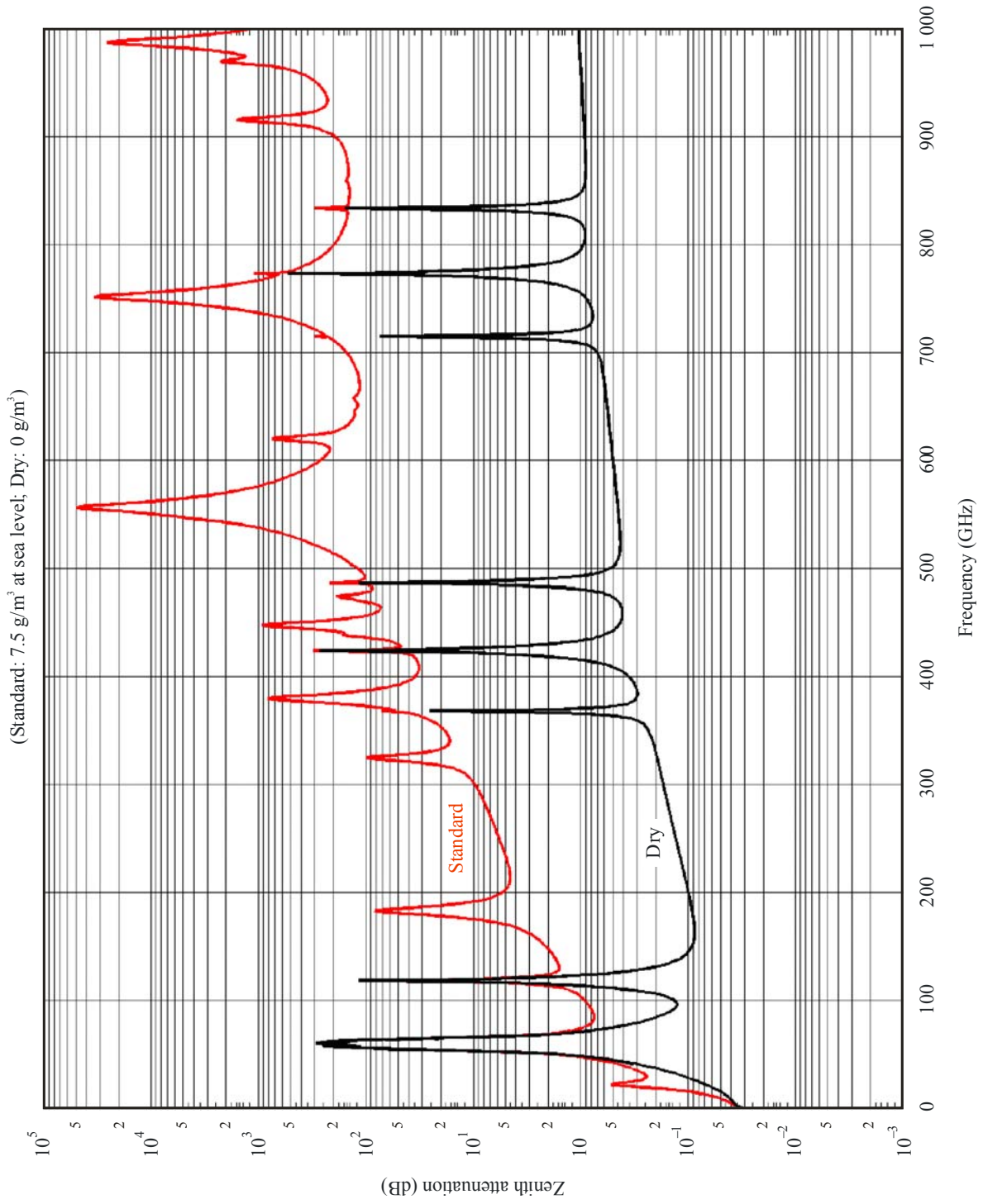
The remaining frequency dependent (dispersive) term has a marginal influence on the result (around 1%) but can be calculated from the method shown in the ITU-R Handbook on Radiometeorology.

The total attenuation can be derived using:

$$A_{gas} = \sum_{n=1}^{k} a_n \, \gamma_n \qquad \text{dB} \qquad (20)$$

where $\gamma_n$ is the specific attenuation derived from equation (1).

To ensure an accurate estimate of the path attenuation, the thickness of the layers should increase exponentially, from 10 cm at the lowest layer (ground level) to 1 km at an altitude of 100 km, according to the following equation:

$$\delta_i = 0.0001 \, \exp\left\{\frac{i-1}{100}\right\} \qquad \text{km} \qquad (21)$$

from $i = 1$ to 922, noting that $\delta_{922} \cong 1.0$ km and $\sum_{i=1}^{922} \delta_i \cong 100$ km.

For Earth-to-space applications, the integration should be performed at least up to 30 km, and up to 100 km at the oxygen line-centre frequencies.

FIGURE 4



P.0676-04

49
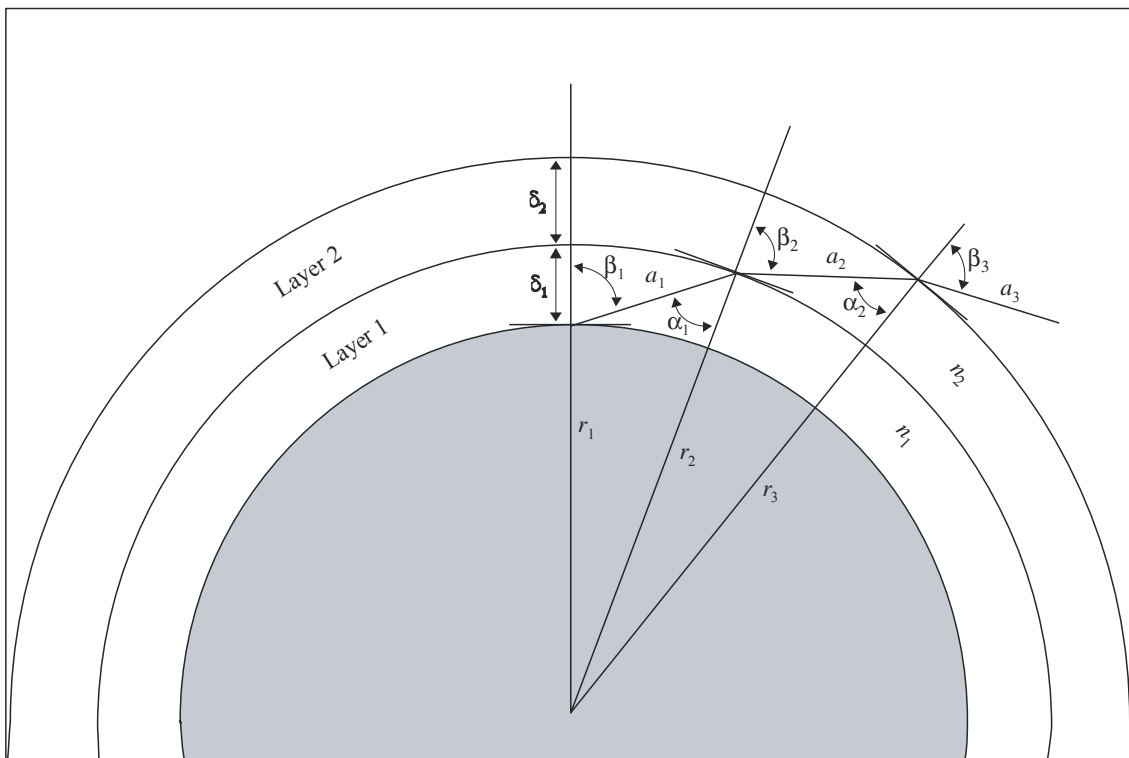
**3** **Dispersive effects**

The effects of dispersion are discussed in the ITU-R Handbook on Radiometeorology, which contains a model for calculating dispersion based on the line-by-line calculation. For practical purposes, dispersive effects should not impose serious limitations on millimetric terrestrial communication systems operating with bandwidths of up to a few hundred MHz over short ranges (for example, less than about 20 km), especially in the window regions of the spectrum, at frequencies removed from the centres of major absorption lines. For satellite communication systems, the longer path lengths through the atmosphere will constrain operating frequencies further to the window regions, where both atmospheric attenuation and the corresponding dispersion are low.

# Annex 2

## Approximate estimation of gaseous attenuation in the frequency range 1-350 GHz

This Annex contains simplified algorithms for quick, approximate estimation of gaseous attenuation for a limited range of meteorological conditions and a limited variety of geometrical configurations.

**1** **Specific attenuation**

The specific attenuation due to dry air and water vapour, from sea level to an altitude of 10 km, can be estimated using the following simplified algorithms, which are based on curve-fitting to the line-by-line calculation, and agree with the more accurate calculations to within an average of about ±10% at frequencies removed from the centres of major absorption lines. The absolute difference between the results from these algorithms and the line-by-line calculation is generally less than 0.1 dB/km and reaches a maximum of 0.7 dB/km near 60 GHz. For altitudes higher than 10 km, and in cases where higher accuracy is required, the line-by-line calculation should be used.

For dry air, the attenuation $\gamma_o$ (dB/km) is given by the following equations:

For $f \leq 54$ GHz:

$$\gamma_o = \left[ \frac{7.2 \, r_t^{2.8}}{f^2 + 0.34 \, r_p^2 \, r_t^{1.6}} + \frac{0.62\xi_3}{(54 - f)^{1.16\xi_1} + 0.83 \, \xi_2} \right] f^2 r_p^2 \times 10^{-3} \qquad (22a)$$

For 54 GHz $< f \leq$ 60 GHz:

$$\gamma_o = \exp\left[ \frac{\ln \gamma_{54}}{24}(f - 58)(f - 60) - \frac{\ln \gamma_{58}}{8}(f - 54)(f - 60) + \frac{\ln \gamma_{60}}{12}(f - 54)(f - 58) \right] \qquad (22b)$$

For 60 GHz $< f \leq$ 62 GHz:

$$\gamma_o = \gamma_{60} + (\gamma_{62} - \gamma_{60})\frac{f - 60}{2} \qquad (22c)$$

For 62 GHz $< f \le$ 66 GHz:

$$\gamma_o = \exp\left[\frac{\ln\gamma_{62}}{8}(f-64)(f-66) - \frac{\ln\gamma_{64}}{4}(f-62)(f-66) + \frac{\ln\gamma_{66}}{8}(f-62)(f-64)\right] \quad (22d)$$

For 66 GHz $< f \le$ 120 GHz:

$$\gamma_o = \left\{3.02\times10^{-4}r_t^{3.5} + \frac{0.283\,r_t^{3.8}}{(f-118.75)^2 + 2.91r_p^2 r_t^{1.6}} + \frac{0.502\xi_6[1-0.0163\xi_7(f-66)]}{(f-66)^{1.4346\xi_4}+1.15\xi_5}\right\}f^2 r_p^2 \times 10^{-3} \quad (22e)$$

For 120 GHz $< f \le$ 350 GHz:

$$\gamma_o = \left[\frac{3.02\times10^{-4}}{1+1.9\times10^{-5}f^{1.5}} + \frac{0.283r_t^{0.3}}{(f-118.75)^2 + 2.91r_p^2 r_t^{1.6}}\right]f^2 r_p^2 r_t^{3.5}\times10^{-3}+\delta \quad (22f)$$

with:

$$\xi_1 = \varphi(r_p, r_t, 0.0717, -1.8132, 0.0156, -1.6515) \quad (22g)$$

$$\xi_2 = \varphi(r_p, r_t, 0.5146, -4.6368, -0.1921, -5.7416) \quad (22h)$$

$$\xi_3 = \varphi(r_p, r_t, 0.3414, -6.5851, 0.2130, -8.5854) \quad (22i)$$

$$\xi_4 = \varphi(r_p, r_t, -0.0112, 0.0092, -0.1033, -0.0009) \quad (22j)$$

$$\xi_5 = \varphi(r_p, r_t, 0.2705, -2.7192, -0.3016, -4.1033) \quad (22k)$$

$$\xi_6 = \varphi(r_p, r_t, 0.2445, -5.9191, 0.0422, -8.0719) \quad (22l)$$

$$\xi_7 = \varphi(r_p, r_t, -0.1833, 6.5589, -0.2402, 6.131) \quad (22m)$$

$$\gamma_{54} = 2.192\varphi(r_p, r_t, 1.8286, -1.9487, 0.4051, -2.8509) \quad (22n)$$

$$\gamma_{58} = 12.59\varphi(r_p, r_t, 1.0045, 3.5610, 0.1588, 1.2834) \quad (22o)$$

$$\gamma_{60} = 15.0\varphi(r_p, r_t, 0.9003, 4.1335, 0.0427, 1.6088) \quad (22p)$$

$$\gamma_{62} = 14.28\varphi(r_p, r_t, 0.9886, 3.4176, 0.1827, 1.3429) \quad (22q)$$

$$\gamma_{64} = 6.819\varphi(r_p, r_t, 1.4320, 0.6258, 0.3177, -0.5914) \quad (22r)$$

$$\gamma_{66} = 1.908\varphi(r_p, r_t, 2.0717, -4.1404, 0.4910, -4.8718) \quad (22s)$$

$$\delta = -0.00306\varphi(r_p, r_t, 3.211, -14.94, 1.583, -16.37) \quad (22t)$$

$$\varphi(r_p, r_t, a, b, c, d) = r_p^a r_t^b \exp[c(1-r_p)+d(1-r_t)] \quad (22u)$$

where:

$f$:     frequency (GHz)

$r_p =$    $p_{tot}/1013$, where $p_{tot}$ represents total air pressure

$r_t =$    $288/(273 + t)$

$p$:     pressure (hPa)

$t$:     temperature (°C), where mean temperature values can be obtained from maps given in Recommendation ITU-R P.1510, when no adequate temperature data are available.

For water vapour, the attenuation $\gamma_w$ (dB/km) is given by:

$$
\begin{aligned}
\gamma_w = \Bigg\{ & \frac{3.98\eta_1 \exp[2.23(1-r_t)]}{(f-22.235)^2 + 9.42\eta_1^2} g(f,22) + \frac{11.96\eta_1 \exp[0.7(1-r_t)]}{(f-183.31)^2 + 11.14\eta_1^2} \\
& + \frac{0.081\eta_1 \exp[6.44(1-r_t)]}{(f-321.226)^2 + 6.29\eta_1^2} + \frac{3.66\eta_1 \exp[1.6(1-r_t)]}{(f-325.153)^2 + 9.22\eta_1^2} \\
& + \frac{25.37\eta_1 \exp[1.09(1-r_t)]}{(f-380)^2} + \frac{17.4\eta_1 \exp[1.46(1-r_t)]}{(f-448)^2} \\
& + \frac{844.6\eta_1 \exp[0.17(1-r_t)]}{(f-557)^2} g(f,557) + \frac{290\eta_1 \exp[0.41(1-r_t)]}{(f-752)^2} g(f,752) \\
& + \frac{8.3328\times10^4\eta_2 \exp[0.99(1-r_t)]}{(f-1\,780)^2} g(f,1\,780) \Bigg\} f^2 r_t^{2.5} \rho \times 10^{-4}
\end{aligned}
\tag{23a}
$$

with:

$$
\eta_1 = 0.955 r_p r_t^{0.68} + 0.006\rho
\tag{23b}
$$

$$
\eta_2 = 0.735\, r_p r_t^{0.5} + 0.0353\, r_t^4 \rho
\tag{23c}
$$

$$
g(f, f_i) = 1 + \left( \frac{f - f_i}{f + f_i} \right)^2
\tag{23d}
$$

where $\rho$ is the water-vapour density (g/m³).

Figure 5 shows the specific attenuation from 1 to 350 GHz at sea-level for dry air and water vapour with a density of 7.5 g/m³.

## 2     Path attenuation

## 2.1     Terrestrial paths

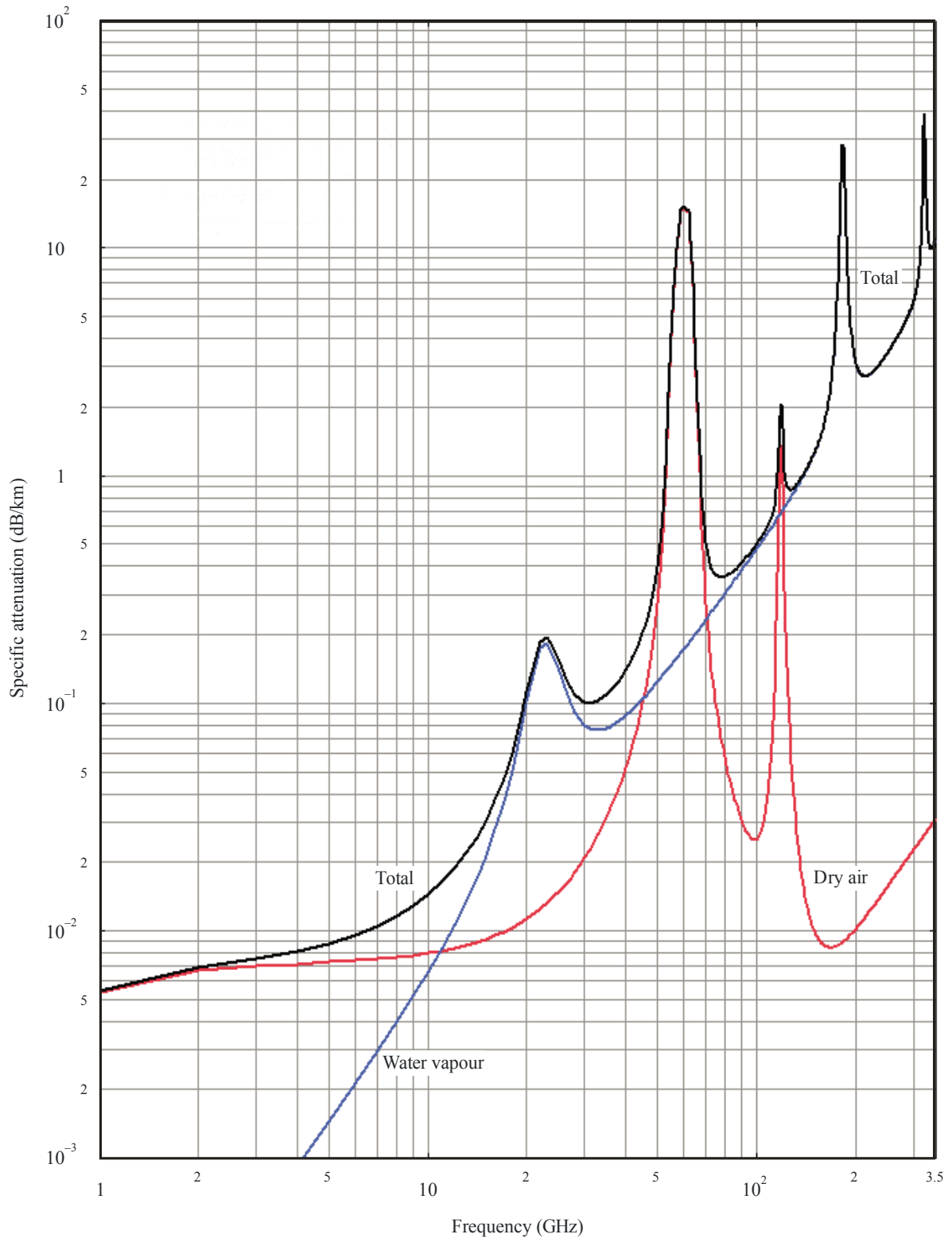For a horizontal path, or for slightly inclined paths close to the ground, the path attenuation, $A$, may be written as:

$$
A = \gamma r_0 = (\gamma_o + \gamma_w) r_0 \quad \text{dB}
\tag{24}
$$

where $r_0$ is the path length (km).

FIGURE 5

**Specific attenuation due to atmospheric gases**



Frequency (GHz)

Pressure: 1 013 hPa
Temperature: 15° C
Water vapour density: 7.5 g/m$^3$

P.0676-05

## 2.2 Slant paths

This section contains simple algorithms for estimating the gaseous attenuation along slant paths through the Earth's atmosphere, by defining an equivalent height by which the specific attenuation calculated in § 1 may be multiplied to obtain the zenith attenuation. The equivalent heights are dependent on pressure, and can hence be employed for determining the zenith attenuation from sea level up to an altitude of about 10 km. The resulting zenith attenuations are accurate to within ±10% for dry air and ±5% for water vapour from sea level up to altitudes of about 10 km, using the pressure, temperature and water-vapour density appropriate to the altitude of interest. For altitudes higher than 10 km, and particularly for frequencies within 0.5 GHz of the centres of resonance lines at any altitude, the procedure in Annex 1 should be used. Note that the Gaussian function in equation (25b) describing the oxygen equivalent height in the 60 GHz band can yield errors higher than 10% at certain frequencies, since this procedure cannot reproduce the structure shown in Fig. 7. The expressions below were derived from zenith attenuations calculated with the procedure in Annex 1, integrating the attenuations numerically over a bandwidth of 500 MHz; the resultant attenuations hence effectively represent approximate minimum values in the 50-70 GHz band. The path attenuation at elevation angles other than the zenith may then be determined using the procedures described later in this section.

For dry air, the equivalent height is given by:

$$h_o = \frac{6.1}{1+0.17\,r_p^{-1.1}}(1+t_1+t_2+t_3) \tag{25a}$$

where:

$$t_1 = \frac{4.64}{1+0.066\,r_p^{-2.3}}\exp\left[-\left(\frac{f-59.7}{2.87+12.4\exp\,(-7.9\,r_p)}\right)^2\right] \tag{25b}$$

$$t_2 = \frac{0.14\exp\,(2.12\,r_p)}{(f-118.75)^2+0.031\exp(2.2\,r_p)} \tag{25c}$$

$$t_3 = \frac{0.0114}{1+0.14\,r_p^{-2.6}}f\,\frac{-0.0247+0.0001f+1.61\times10^{-6}f^2}{1-0.0169f+4.1\times10^{-5}f^2+3.2\times10^{-7}f^3} \tag{25d}$$

with the constraint that:

$$h_o \leq 10.7\,r_p^{0.3}\quad\text{when }f<70\,\text{GHz} \tag{25e}$$

and for water vapour, the equivalent height is:

$$h_w = 1.66\left(1+\frac{1.39\sigma_w}{(f-22.235)^2+2.56\sigma_w}+\frac{3.37\sigma_w}{(f-183.31)^2+4.69\sigma_w}+\frac{1.58\sigma_w}{(f-325.1)^2+2.89\sigma_w}\right) \tag{26a}$$

for $f \leq 350$ GHz

$$\sigma_w = \frac{1.013}{1+\exp[-8.6\,(r_p-0.57)]} \tag{26b}$$

The zenith attenuation between 50 to 70 GHz is a complicated function of frequency, as shown in Fig. 7, and the above algorithms for equivalent height can provide only an approximate estimate, in general, of the minimum levels of attenuation likely to be encountered in this frequency range. For greater accuracy, the procedure in Annex 1 should be used.

The concept of equivalent height is based on the assumption of an exponential atmosphere specified by a scale height to describe the decay in density with altitude. Note that scale heights for both dry air and water vapour may vary with latitude, season and/or climate, and that water vapour distributions in the real atmosphere may deviate considerably from the exponential, with corresponding changes in equivalent heights. The values given above are applicable up to altitudes of about 10 km.

The total zenith attenuation is then:

$$A = \gamma_o \, h_o + \gamma_w \, h_w \quad \text{dB} \tag{27}$$

Figure 6 shows the total zenith attenuation at sea level, as well as the attenuation due to dry air and water vapour, using the mean annual global reference atmosphere given in Recommendation ITU-R P.835. Between 50 and 70 GHz greater accuracy can be obtained from the 0 km curve in Fig. 7 which was derived using the line-by-line calculation as described in Annex 1.

### 2.2.1    Elevation angles between 5° and 90°

### 2.2.1.1    Earth-space paths

For an elevation angle, $\varphi$, between 5° and 90°, the path attenuation is obtained using the cosecant law, as follows:

For path attenuation based on surface meteorological data:

$$A = \frac{A_o + A_w}{\sin \varphi} \quad \text{dB} \tag{28}$$

where   $A_o = h_o \, \gamma_o$   and   $A_w = h_w \, \gamma_w$

and for path attenuation based on integrated water vapour content:

$$A(P) = \frac{A_o + A_w(P)}{\sin \varphi} \quad \text{dB} \tag{29}$$

where $A_w(P)$ is given in § 2.3.

### 2.2.1.2    Inclined paths

To determine the attenuation values on an inclined path between a station situated at altitude $h_1$ and another at a higher altitude $h_2$, where both altitudes are less than 10 km above mean sea level, the values $h_o$ and $h_w$ in equation (28) must be replaced by the following $h_o'$ and $h_w'$ values:

$$h_o' = h_o \left[ e^{-h_1/h_o} - e^{-h_2/h_o} \right] \quad \text{km} \tag{30}$$

$$h_w' = h_w \left[ e^{-h_1/h_w} - e^{-h_2/h_w} \right] \quad \text{km} \tag{31}$$

it being understood that the value $\rho$ of the water-vapour density used in equation (23) is the hypothetical value at sea level calculated as follows:

$$\rho = \rho_1 \times \exp\left( h_1/2 \right) \tag{32}$$

where $\rho_1$ is the value corresponding to altitude $h_1$ of the station in question, and the equivalent height of water vapour density is assumed as 2 km (see Recommendation ITU-R P.835).

Equations (30), (31) and (32) use different normalizations for the dry air and water-vapour equivalent heights. While the mean air pressure referred to sea level can be considered constant around the world (equal to 1 013 hPa), the water-vapour density not only has a wide range of

climatic variability but is measured at the surface (i.e. at the height of the ground station). For values of surface water-vapour density, see Recommendation ITU-R P.836.

## 2.2.2 Elevation angles between 0º and 5º

### 2.2.2.1 Earth-space paths

In this case, Annex 1 of this Recommendation should be used. The same Annex should also be used for elevations less than zero.

### 2.2.2.2 Inclined paths

The attenuation on an inclined path between a station situated at altitude $h_1$ and a higher altitude $h_2$ (where both altitudes are less than 10 km above mean sea level), can be determined from the following:

$$A = \gamma_o \sqrt{h_o} \left[ \frac{\sqrt{R_e + h_1} \cdot F(x_1) \, e^{-h_1 / h_o}}{\cos \varphi_1} - \frac{\sqrt{R_e + h_2} \cdot F(x_2) \, e^{-h_2 / h_o}}{\cos \varphi_2} \right]$$

$$+ \gamma_w \sqrt{h_w} \left[ \frac{\sqrt{R_e + h_1} \cdot F(x_1') \, e^{-h_1 / h_w}}{\cos \varphi_1} - \frac{\sqrt{R_e + h_2} \cdot F(x_2') \, e^{-h_2 / h_w}}{\cos \varphi_2} \right] \qquad \text{dB} \qquad (33)$$

where:

   $R_e$:  effective Earth radius including refraction, given in Recommendation ITU-R P.834, expressed in km (a value of 8 500 km is generally acceptable for the immediate vicinity of the Earth's surface)

   $\varphi_1$:  elevation angle at altitude $h_1$

   F:  function defined by:

$$F(x) = \frac{1}{0.661 \, x + 0.339 \sqrt{x^2 + 5.51}} \qquad (34)$$

$$\varphi_2 = \arccos \left( \frac{R_e + h_1}{R_e + h_2} \cos \varphi_1 \right) \qquad (35a)$$

$$x_i = \tan \varphi_i \sqrt{\frac{R_e + h_i}{h_o}} \qquad \text{for } i = 1, 2 \qquad (35b)$$

$$x_i' = \tan \varphi_i \sqrt{\frac{R_e + h_i}{h_w}} \qquad \text{for } i = 1, 2 \qquad (35c)$$

it being understood that the value $\rho$ of the water vapour density used in equation (23) is the hypothetical value at sea level calculated as follows:

$$\rho = \rho_1 \cdot \exp \left( h_1 / 2 \right) \qquad (36)$$

where $\rho_1$ is the value corresponding to altitude $h_1$ of the station in question, and the equivalent height of water vapour density is assumed as 2 km (see Recommendation ITU-R P.835).

Values for $\rho_1$ at the surface can be found in Recommendation ITU-R P.836. The different formulation for dry air and water vapour is explained at the end of § 2.2.

FIGURE 6

**Total, dry air and water-vapour zenith attenuation from sea level**
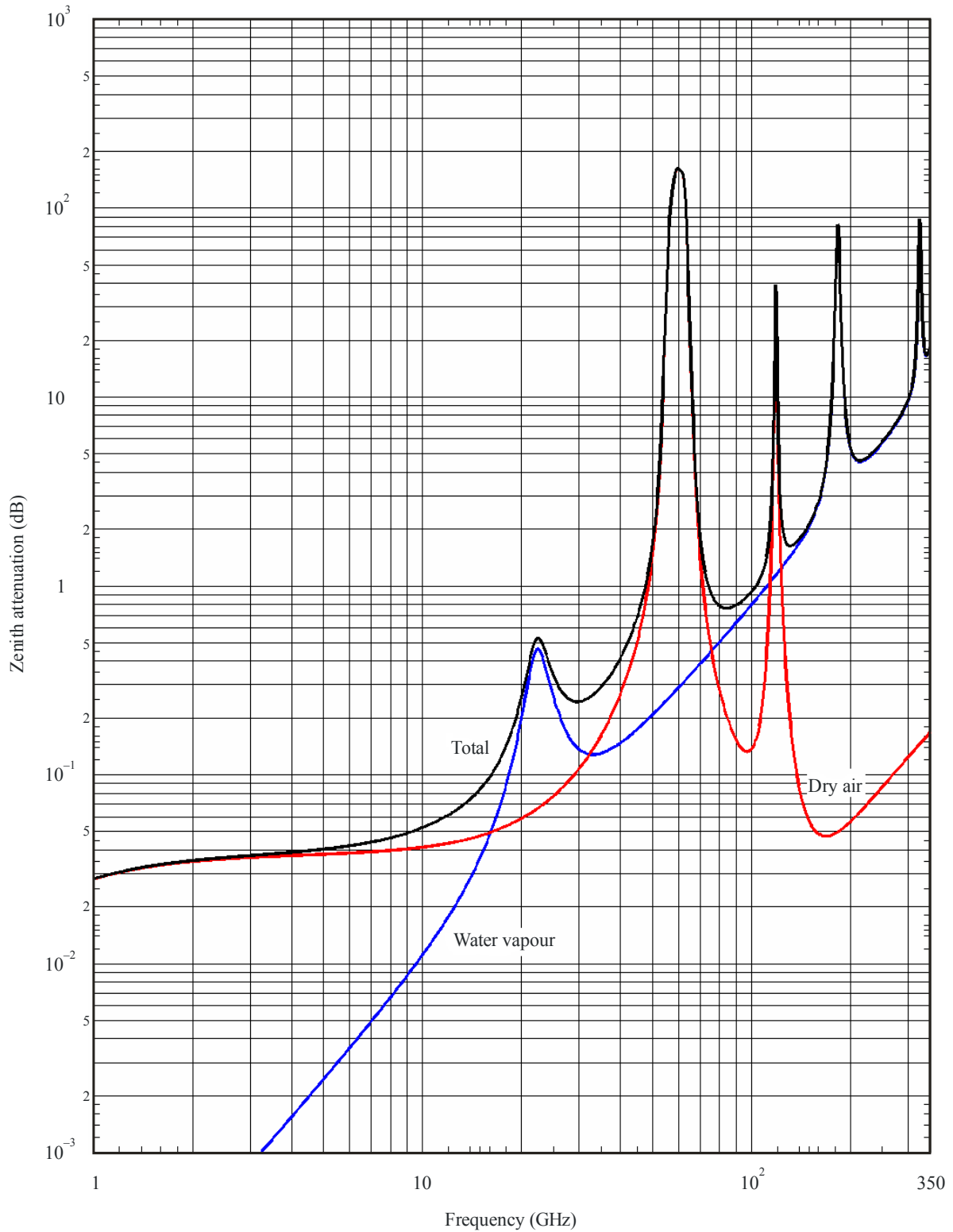


Surface pressure: 1 013 hPa
Surface temperature: 15° C
Surface water-vapour density: 7.5 g/m$^3$

P.0676-06

FIGURE 7

**Zenith oxygen attenuation from the altitudes indicated, calculated at intervals of 50 MHz, including line centres (0 km, 5 km, 10 km, 15 km and 20 km)**
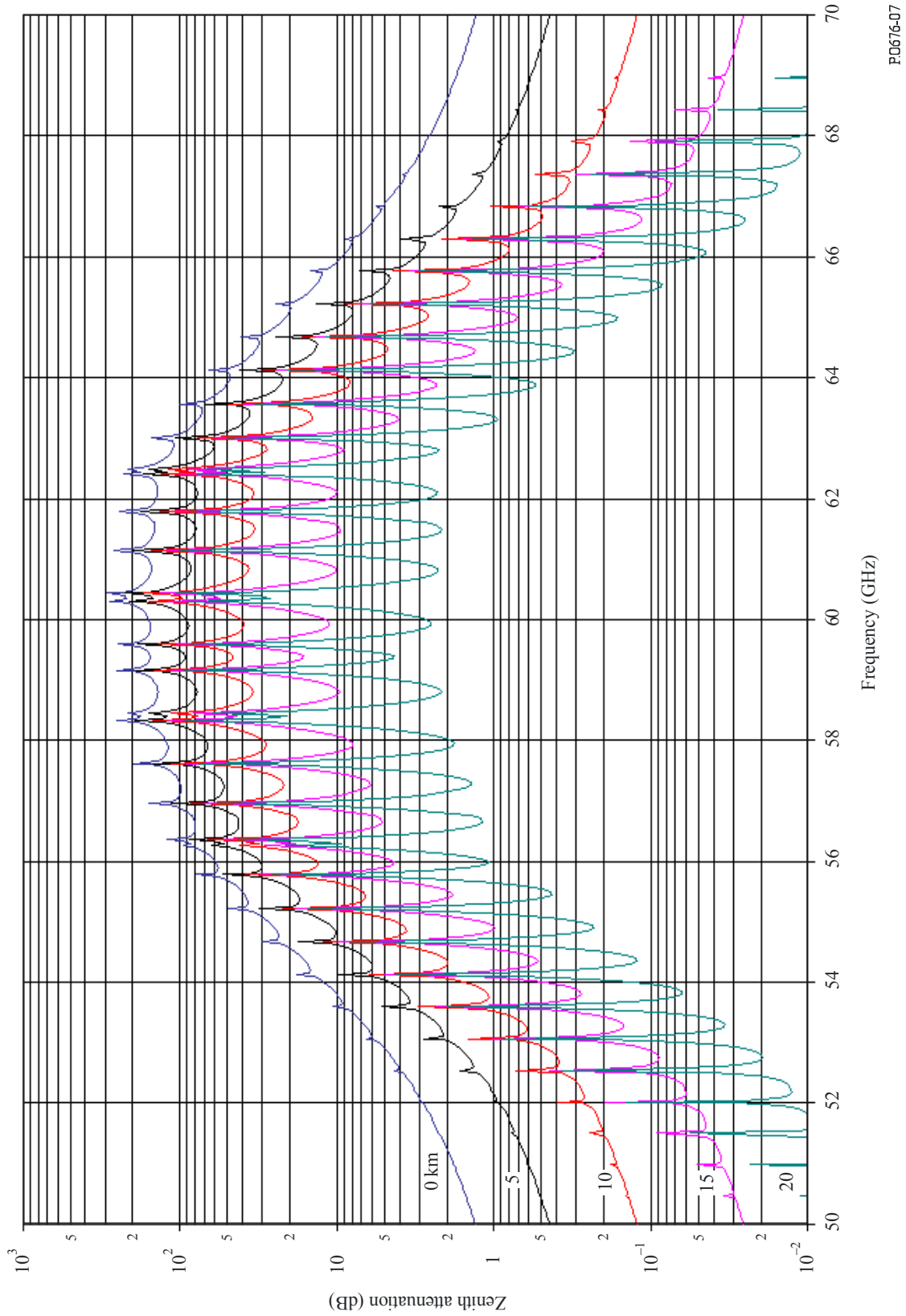
## 2.3    Zenith path water-vapour attenuation

The above method for calculating slant path attenuation by water vapour relies on the knowledge of the profile of water-vapour pressure (or density) along the path. In cases where the integrated water vapour content along the path, $V_t$, is known, an alternative method may be used. The total water-vapour attenuation can be estimated as:

$$A_w(P) = \frac{0.0173\,V_t(P)\,\gamma_w(f, p_{ref}, \rho_{v,ref}, t_{ref})}{\gamma_w(f_{ref}, p_{ref}, \rho_{v,ref}, t_{ref})} \qquad \text{dB} \qquad (37)$$

where:

$f$ :     frequency (GHz)

$f_{ref}$ :     20.6 (GHz)

$p_{ref} =$     780 (hPa)

$\rho_{v,ref} = \quad \dfrac{V_t(P)}{4}$ (g/m$^3$)

$t_{ref} = \quad 14 \ln\left(\dfrac{0.22\,V_t(P)}{4}\right) + 3$ (°C)

$V_t(P)$:     integrated water vapour content at the required percentage of time (kg/m$^2$ or mm), which can be obtained either from radiosonde profiles, radiometric measurements, or Recommendation ITU-R P.836 (kg/m$^2$ or mm)

$\gamma_w(f, p, \rho, t)$:     specific attenuation as a function of frequency, pressure, water-vapour density, and temperature calculated from equation (23a) (dB/km).

———————

## 降雨減衰量

　降雨減衰量については、ITU-R 勧告 P.838-3（参考資料８）に各周波数における降雨強度と降雨減衰量の関係が示されている。図 1 に P.838-3 に示された 120GHz 帯における降雨強度と降雨減衰量の関係を示す。また、120GHz 帯 FPU を使用して実施した屋外伝搬実験の結果も示している。理論値と実験結果はよく一致している。

　スポーツ中継の場合、降雨があってもスポーツ競技自体が継続されている限りは回線の確保が必要になる。スポーツ競技が中断される降雨強度は、概ね 60mm/h である。降雨強度 60mm/h の場合の降雨減衰量は、ITU-R 勧告 P.838-3 では 23dB/km となる。したがって回線設計では、降雨減衰係数の値として 23dB/km を使用することが適当である。
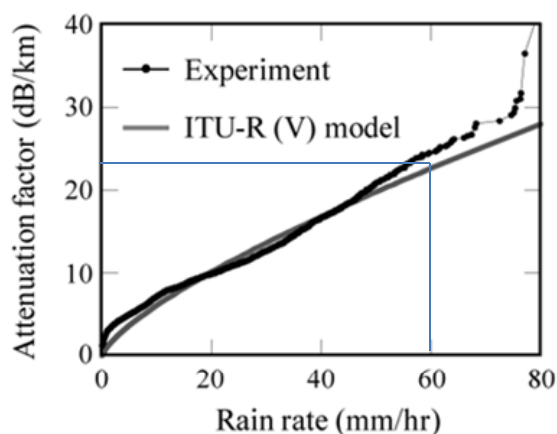


図 1　120GHz 帯における降雨減衰量と降雨強度の関係

RECOMMENDATION  ITU-R  P.838-3

# Specific attenuation model for rain for use in prediction methods

(Question ITU-R 201/3)

(1992-1999-2003-2005)

The ITU Radiocommunication Assembly,

*considering*

a)      that there is a need to calculate the attenuation due to rain from a knowledge of rain rates,

*recommends*

**1**      that the following procedure be used.

The specific attenuation $\gamma_R$ (dB/km) is obtained from the rain rate $R$ (mm/h) using the power-law relationship:

$$\gamma_R = kR^{\alpha} \tag{1}$$

Values for the coefficients $k$ and $\alpha$ are determined as functions of frequency, $f$ (GHz), in the range from 1 to 1 000 GHz, from the following equations, which have been developed from curve-fitting to power-law coefficients derived from scattering calculations:

$$\log_{10} k = \sum_{j=1}^{4} a_j \exp\left[-\left(\frac{\log_{10} f - b_j}{c_j}\right)^2\right] + m_k \log_{10} f + c_k \tag{2}$$

$$\alpha = \sum_{j=1}^{5} a_j \exp\left[-\left(\frac{\log_{10} f - b_j}{c_j}\right)^2\right] + m_\alpha \log_{10} f + c_\alpha \tag{3}$$

where:

$f$:    frequency (GHz)

$k$:    either $k_H$ or $k_V$

$\alpha$:    either $\alpha_H$ or $\alpha_V$.

Values for the constants for the coefficient $k_H$ for horizontal polarization are given in Table 1 and for the coefficient $k_V$ for vertical polarization in Table 2. Table 3 gives the values for the constants for the coefficient $\alpha_H$ for horizontal polarization, and Table 4 gives the values for the constants for the coefficient $\alpha_V$ for vertical polarization.

TABLE 1

**Coefficients for $k_H$**

| $j$ | $a_j$ | $b_j$ | $c_j$ | $m_k$ | $c_k$ |
|---|---|---|---|---|---|
| 1 | −5.33980 | −0.10008 | 1.13098 | | |
| 2 | −0.35351 | 1.26970 | 0.45400 | | |
| 3 | −0.23789 | 0.86036 | 0.15354 | −0.18961 | 0.71147 |
| 4 | −0.94158 | 0.64552 | 0.16817 | | |

TABLE 2

**Coefficients for $k_V$**

| $j$ | $a_j$ | $b_j$ | $c_j$ | $m_k$ | $c_k$ |
|---|---|---|---|---|---|
| 1 | −3.80595 | 0.56934 | 0.81061 | | |
| 2 | −3.44965 | −0.22911 | 0.51059 | | |
| 3 | −0.39902 | 0.73042 | 0.11899 | −0.16398 | 0.63297 |
| 4 | 0.50167 | 1.07319 | 0.27195 | | |

TABLE 3

**Coefficients for $\alpha_H$**

| $j$ | $a_j$ | $b_j$ | $c_j$ | $m_\alpha$ | $c_\alpha$ |
|---|---|---|---|---|---|
| 1 | −0.14318 | 1.82442 | −0.55187 | | |
| 2 | 0.29591 | 0.77564 | 0.19822 | | |
| 3 | 0.32177 | 0.63773 | 0.13164 | 0.67849 | −1.95537 |
| 4 | −5.37610 | −0.96230 | 1.47828 | | |
| 5 | 16.1721 | −3.29980 | 3.43990 | | |

TABLE 4

**Coefficients for $\alpha_V$**

| $j$ | $a_j$ | $b_j$ | $c_j$ | $m_\alpha$ | $c_\alpha$ |
|---|---|---|---|---|---|
| 1 | −0.07771 | 2.33840 | −0.76284 | | |
| 2 | 0.56727 | 0.95545 | 0.54039 | | |
| 3 | −0.20238 | 1.14520 | 0.26809 | −0.053739 | 0.83433 |
| 4 | −48.2991 | 0.791669 | 0.116226 | | |
| 5 | 48.5833 | 0.791459 | 0.116479 | | |

For linear and circular polarization, and for all path geometries, the coefficients in equation (1) can be calculated from the values given by equations (2) and (3) using the following equations:

$$k = [k_H + k_V + (k_H - k_V)\cos^2\theta \cos 2\tau]/2 \qquad (4)$$

$$\alpha = [k_H\alpha_H + k_V\alpha_V + (k_H\alpha_H - k_V\alpha_V)\cos^2\theta \cos 2\tau]/2k \qquad (5)$$

where $\theta$ is the path elevation angle and $\tau$ is the polarization tilt angle relative to the horizontal ($\tau = 45°$ for circular polarization).

For quick reference, the coefficients $k$ and $\alpha$ are shown graphically in Figs. 1 to 4, and Table 5 lists numerical values for the coefficients at given frequencies.

FIGURE 1

**$k$ coefficient for horizontal polarization**



Frequency (GHz)
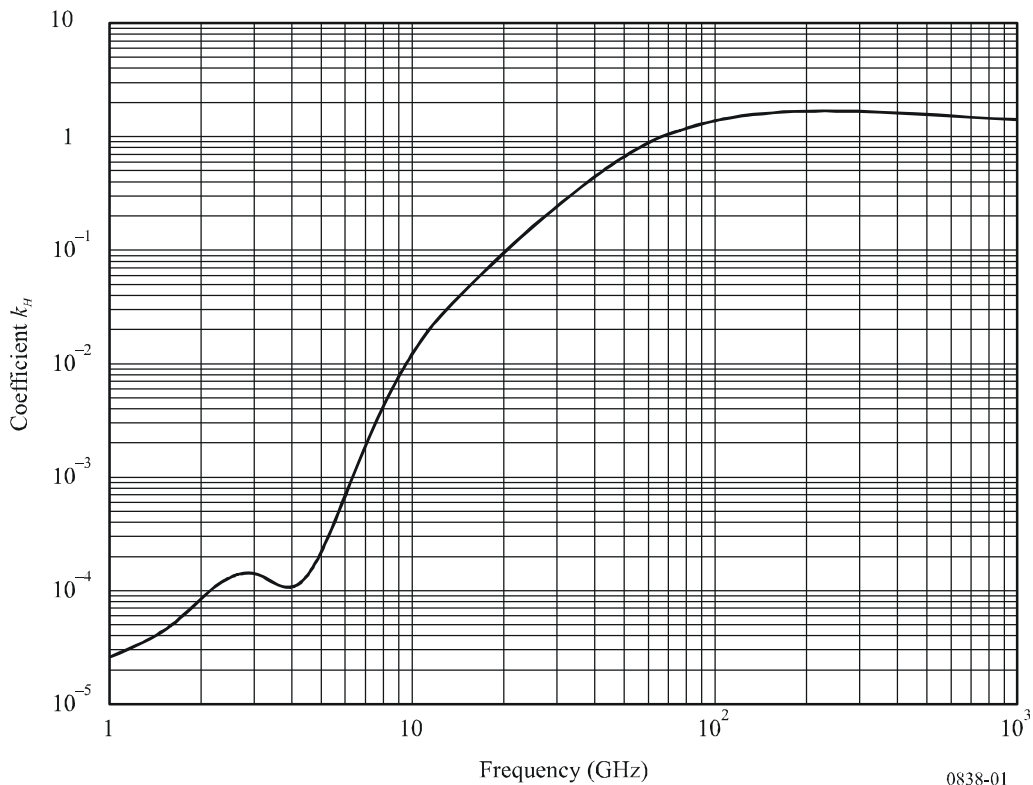
0838-01

FIGURE 2

**α coefficient for horizontal polarization**



0838-02
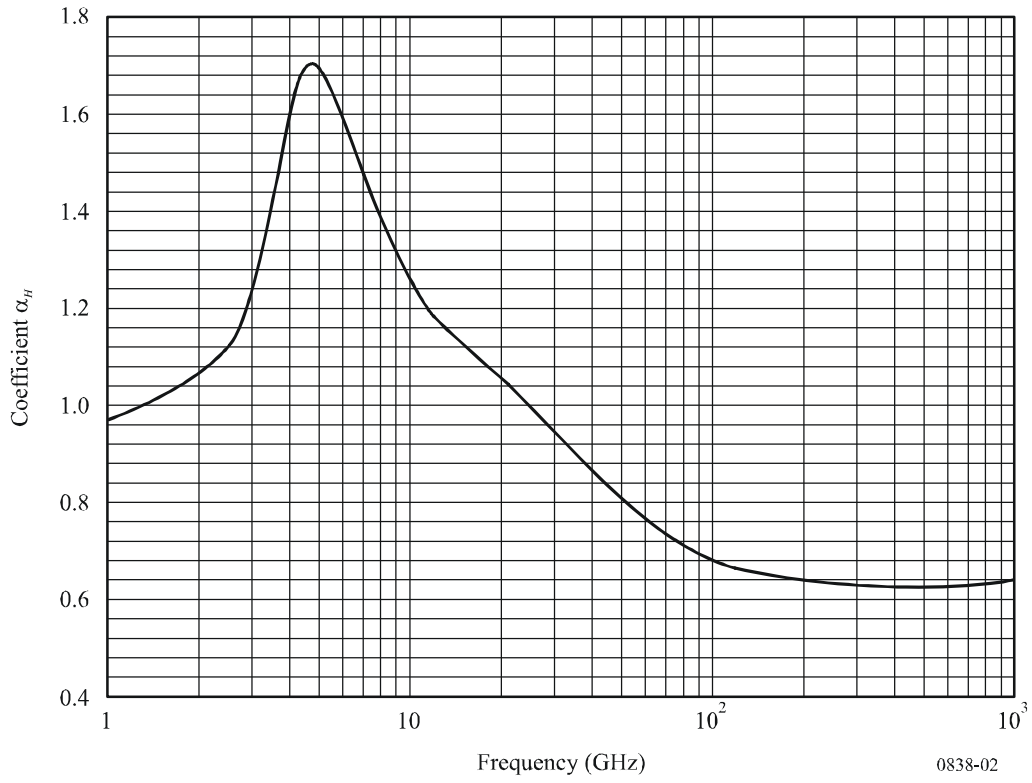
FIGURE 3

***k* coefficient for vertical polarization**



0838-03

FIGURE 4

**α coefficient for vertical polarization**



0838-04
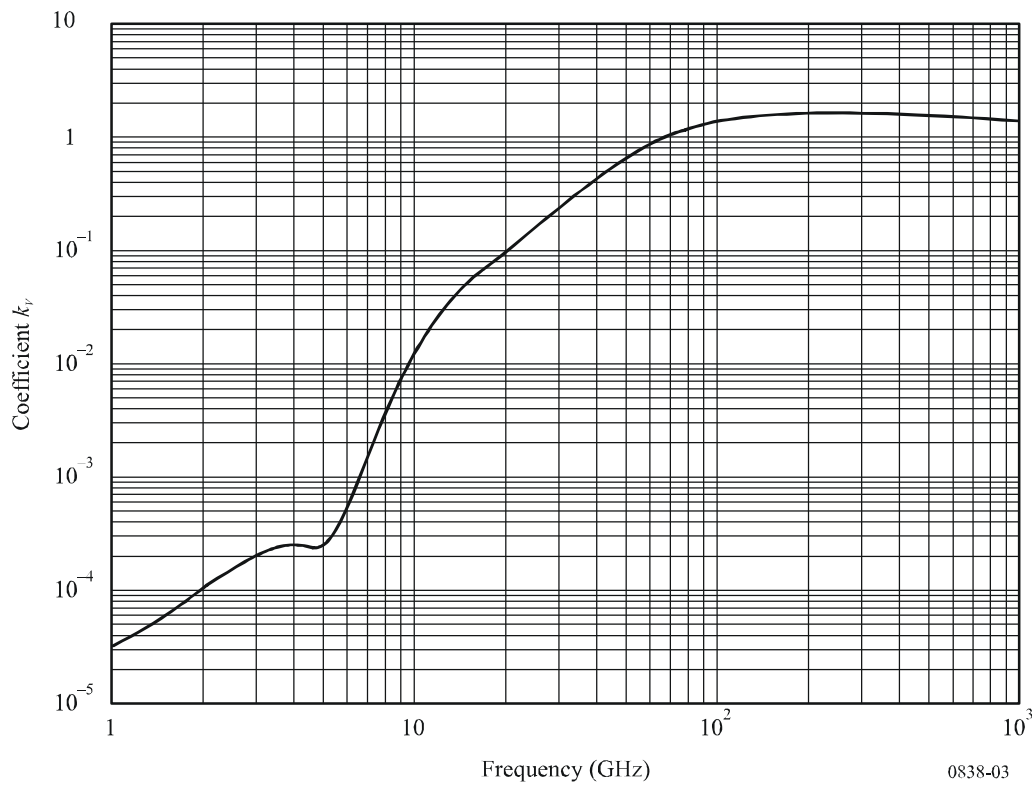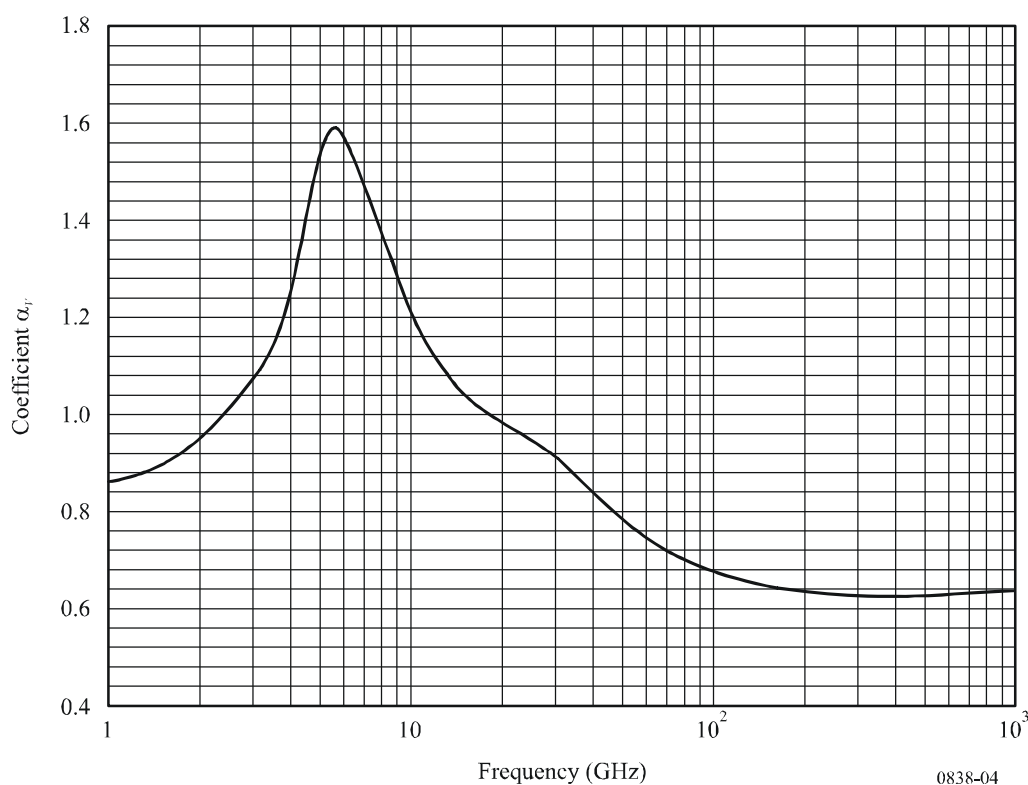
TABLE 5

**Frequency-dependent coefficients for estimating specific rain attenuation using equations (4), (5) and (1)**

| Frequency (GHz) | $k_H$ | $\alpha_H$ | $k_V$ | $\alpha_V$ |
|---|---|---|---|---|
| 1 | 0.0000259 | 0.9691 | 0.0000308 | 0.8592 |
| 1.5 | 0.0000443 | 1.0185 | 0.0000574 | 0.8957 |
| 2 | 0.0000847 | 1.0664 | 0.0000998 | 0.9490 |
| 2.5 | 0.0001321 | 1.1209 | 0.0001464 | 1.0085 |
| 3 | 0.0001390 | 1.2322 | 0.0001942 | 1.0688 |
| 3.5 | 0.0001155 | 1.4189 | 0.0002346 | 1.1387 |
| 4 | 0.0001071 | 1.6009 | 0.0002461 | 1.2476 |
| 4.5 | 0.0001340 | 1.6948 | 0.0002347 | 1.3987 |
| 5 | 0.0002162 | 1.6969 | 0.0002428 | 1.5317 |
| 5.5 | 0.0003909 | 1.6499 | 0.0003115 | 1.5882 |
| 6 | 0.0007056 | 1.5900 | 0.0004878 | 1.5728 |
| 7 | 0.001915 | 1.4810 | 0.001425 | 1.4745 |
| 8 | 0.004115 | 1.3905 | 0.003450 | 1.3797 |
| 9 | 0.007535 | 1.3155 | 0.006691 | 1.2895 |
| 10 | 0.01217 | 1.2571 | 0.01129 | 1.2156 |

TABLE 5 (*continued*)

| Frequency (GHz) | $k_H$ | $\alpha_H$ | $k_V$ | $\alpha_V$ |
|---|---|---|---|---|
| 11 | 0.01772 | 1.2140 | 0.01731 | 1.1617 |
| 12 | 0.02386 | 1.1825 | 0.02455 | 1.1216 |
| 13 | 0.03041 | 1.1586 | 0.03266 | 1.0901 |
| 14 | 0.03738 | 1.1396 | 0.04126 | 1.0646 |
| 15 | 0.04481 | 1.1233 | 0.05008 | 1.0440 |
| 16 | 0.05282 | 1.1086 | 0.05899 | 1.0273 |
| 17 | 0.06146 | 1.0949 | 0.06797 | 1.0137 |
| 18 | 0.07078 | 1.0818 | 0.07708 | 1.0025 |
| 19 | 0.08084 | 1.0691 | 0.08642 | 0.9930 |
| 20 | 0.09164 | 1.0568 | 0.09611 | 0.9847 |
| 21 | 0.1032 | 1.0447 | 0.1063 | 0.9771 |
| 22 | 0.1155 | 1.0329 | 0.1170 | 0.9700 |
| 23 | 0.1286 | 1.0214 | 0.1284 | 0.9630 |
| 24 | 0.1425 | 1.0101 | 0.1404 | 0.9561 |
| 25 | 0.1571 | 0.9991 | 0.1533 | 0.9491 |
| 26 | 0.1724 | 0.9884 | 0.1669 | 0.9421 |
| 27 | 0.1884 | 0.9780 | 0.1813 | 0.9349 |
| 28 | 0.2051 | 0.9679 | 0.1964 | 0.9277 |
| 29 | 0.2224 | 0.9580 | 0.2124 | 0.9203 |
| 30 | 0.2403 | 0.9485 | 0.2291 | 0.9129 |
| 31 | 0.2588 | 0.9392 | 0.2465 | 0.9055 |
| 32 | 0.2778 | 0.9302 | 0.2646 | 0.8981 |
| 33 | 0.2972 | 0.9214 | 0.2833 | 0.8907 |
| 34 | 0.3171 | 0.9129 | 0.3026 | 0.8834 |
| 35 | 0.3374 | 0.9047 | 0.3224 | 0.8761 |
| 36 | 0.3580 | 0.8967 | 0.3427 | 0.8690 |
| 37 | 0.3789 | 0.8890 | 0.3633 | 0.8621 |
| 38 | 0.4001 | 0.8816 | 0.3844 | 0.8552 |
| 39 | 0.4215 | 0.8743 | 0.4058 | 0.8486 |
| 40 | 0.4431 | 0.8673 | 0.4274 | 0.8421 |
| 41 | 0.4647 | 0.8605 | 0.4492 | 0.8357 |
| 42 | 0.4865 | 0.8539 | 0.4712 | 0.8296 |
| 43 | 0.5084 | 0.8476 | 0.4932 | 0.8236 |
| 44 | 0.5302 | 0.8414 | 0.5153 | 0.8179 |
| 45 | 0.5521 | 0.8355 | 0.5375 | 0.8123 |
| 46 | 0.5738 | 0.8297 | 0.5596 | 0.8069 |
| 47 | 0.5956 | 0.8241 | 0.5817 | 0.8017 |
| 48 | 0.6172 | 0.8187 | 0.6037 | 0.7967 |

TABLE 5 (*continued*)

| Frequency (GHz) | $k_H$ | $\alpha_H$ | $k_V$ | $\alpha_V$ |
|---|---|---|---|---|
| 49 | 0.6386 | 0.8134 | 0.6255 | 0.7918 |
| 50 | 0.6600 | 0.8084 | 0.6472 | 0.7871 |
| 51 | 0.6811 | 0.8034 | 0.6687 | 0.7826 |
| 52 | 0.7020 | 0.7987 | 0.6901 | 0.7783 |
| 53 | 0.7228 | 0.7941 | 0.7112 | 0.7741 |
| 54 | 0.7433 | 0.7896 | 0.7321 | 0.7700 |
| 55 | 0.7635 | 0.7853 | 0.7527 | 0.7661 |
| 56 | 0.7835 | 0.7811 | 0.7730 | 0.7623 |
| 57 | 0.8032 | 0.7771 | 0.7931 | 0.7587 |
| 58 | 0.8226 | 0.7731 | 0.8129 | 0.7552 |
| 59 | 0.8418 | 0.7693 | 0.8324 | 0.7518 |
| 60 | 0.8606 | 0.7656 | 0.8515 | 0.7486 |
| 61 | 0.8791 | 0.7621 | 0.8704 | 0.7454 |
| 62 | 0.8974 | 0.7586 | 0.8889 | 0.7424 |
| 63 | 0.9153 | 0.7552 | 0.9071 | 0.7395 |
| 64 | 0.9328 | 0.7520 | 0.9250 | 0.7366 |
| 65 | 0.9501 | 0.7488 | 0.9425 | 0.7339 |
| 66 | 0.9670 | 0.7458 | 0.9598 | 0.7313 |
| 67 | 0.9836 | 0.7428 | 0.9767 | 0.7287 |
| 68 | 0.9999 | 0.7400 | 0.9932 | 0.7262 |
| 69 | 1.0159 | 0.7372 | 1.0094 | 0.7238 |
| 70 | 1.0315 | 0.7345 | 1.0253 | 0.7215 |
| 71 | 1.0468 | 0.7318 | 1.0409 | 0.7193 |
| 72 | 1.0618 | 0.7293 | 1.0561 | 0.7171 |
| 73 | 1.0764 | 0.7268 | 1.0711 | 0.7150 |
| 74 | 1.0908 | 0.7244 | 1.0857 | 0.7130 |
| 75 | 1.1048 | 0.7221 | 1.1000 | 0.7110 |
| 76 | 1.1185 | 0.7199 | 1.1139 | 0.7091 |
| 77 | 1.1320 | 0.7177 | 1.1276 | 0.7073 |
| 78 | 1.1451 | 0.7156 | 1.1410 | 0.7055 |
| 79 | 1.1579 | 0.7135 | 1.1541 | 0.7038 |
| 80 | 1.1704 | 0.7115 | 1.1668 | 0.7021 |
| 81 | 1.1827 | 0.7096 | 1.1793 | 0.7004 |
| 82 | 1.1946 | 0.7077 | 1.1915 | 0.6988 |
| 83 | 1.2063 | 0.7058 | 1.2034 | 0.6973 |
| 84 | 1.2177 | 0.7040 | 1.2151 | 0.6958 |
| 85 | 1.2289 | 0.7023 | 1.2265 | 0.6943 |
| 86 | 1.2398 | 0.7006 | 1.2376 | 0.6929 |

TABLE 5 (*end*)

| Frequency (GHz) | $k_H$ | $\alpha_H$ | $k_V$ | $\alpha_V$ |
|---|---|---|---|---|
| 87 | 1.2504 | 0.6990 | 1.2484 | 0.6915 |
| 88 | 1.2607 | 0.6974 | 1.2590 | 0.6902 |
| 89 | 1.2708 | 0.6959 | 1.2694 | 0.6889 |
| 90 | 1.2807 | 0.6944 | 1.2795 | 0.6876 |
| 91 | 1.2903 | 0.6929 | 1.2893 | 0.6864 |
| 92 | 1.2997 | 0.6915 | 1.2989 | 0.6852 |
| 93 | 1.3089 | 0.6901 | 1.3083 | 0.6840 |
| 94 | 1.3179 | 0.6888 | 1.3175 | 0.6828 |
| 95 | 1.3266 | 0.6875 | 1.3265 | 0.6817 |
| 96 | 1.3351 | 0.6862 | 1.3352 | 0.6806 |
| 97 | 1.3434 | 0.6850 | 1.3437 | 0.6796 |
| 98 | 1.3515 | 0.6838 | 1.3520 | 0.6785 |
| 99 | 1.3594 | 0.6826 | 1.3601 | 0.6775 |
| 100 | 1.3671 | 0.6815 | 1.3680 | 0.6765 |
| 120 | 1.4866 | 0.6640 | 1.4911 | 0.6609 |
| 150 | 1.5823 | 0.6494 | 1.5896 | 0.6466 |
| 200 | 1.6378 | 0.6382 | 1.6443 | 0.6343 |
| 300 | 1.6286 | 0.6296 | 1.6286 | 0.6262 |
| 400 | 1.5860 | 0.6262 | 1.5820 | 0.6256 |
| 500 | 1.5418 | 0.6253 | 1.5366 | 0.6272 |
| 600 | 1.5013 | 0.6262 | 1.4967 | 0.6293 |
| 700 | 1.4654 | 0.6284 | 1.4622 | 0.6315 |
| 800 | 1.4335 | 0.6315 | 1.4321 | 0.6334 |
| 900 | 1.4050 | 0.6353 | 1.4056 | 0.6351 |
| 1 000 | 1.3795 | 0.6396 | 1.3822 | 0.6365 |

# 120GHz 帯 FPU の回線設計例

## 表 1 ASK 方式における回線設計例（晴天時）

1 競技場などで使用される場合（晴天時）

| 項目 | 記号 | 単位 | 数値 | 備考 |
|---|---|---|---|---|
| 送信周波数 | f | GHz | 125 | |
| 波長 | λ | mm | 2.40 | |
| 帯域幅 | B | GHz | 17.5 | |
| 送信電力 | w | mW | 17.5 | |
| 送信電力 | W | dBm | 12.4 | |
| 送信給電損 | Lt | dB | 1.0 | |
| 送信アンテナ利得 | Gt | dBi | 44.0 | |
| 送信EIPR | WGt/Lt | dBm | 55.4 | W−Lt+Gt |
| 伝送距離 | d | km | 0.45 | |
| 大気吸収損 | Lo | dB | 1.4 | 3dB/km |
| 降雨損 | Lra | dB | 0.0 | 1分間降雨強度=0mm/h |
| 自由空間伝搬損 | Ld | dB | 127.4 | |
| 受信アンテナ利得 | Gr | dBi | 44.0 | |
| 受信給電損 | Lr | dB | 1.0 | |
| 受信電力 | Ci | dBm | −30.4 | (WGt/Lt)−(Lo+Lra+Ld)+Gr−Lr |
| 雑音指数 | F | dB | 10.0 | |
| ボルツマン定数 | k | dBm/(Hz・K) | −198.6 | k=1.38E−23 |
| 標準温度 | $T_0$ | dBK | 24.8 | $T_0$=300 |
| 帯域幅 | B | dBHz | 102.4 | |
| 雑音電力 | Ni | dBm | −61.4 | Ni=$kT_0BF$ |
| 受信C／N | C/N | dB | 31.0 | |
| 所要C／N | | dB | 25.0 | |
| 伝送マージン | | dB | 6.0 | |

2 河川横断などで使用される場合（晴天時）

| 項目 | 記号 | 単位 | 数値 | 備考 |
|---|---|---|---|---|
| 送信周波数 | f | GHz | 125 | |
| 波長 | λ | mm | 2.40 | |
| 帯域幅 | B | GHz | 17.5 | |
| 送信電力 | w | mW | 1000.0 | |
| 送信電力 | W | dBm | 30.0 | |
| 送信給電損 | Lt | dB | 1.0 | |
| 送信アンテナ利得 | Gt | dBi | 51.0 | |
| 送信EIPR | WGt/Lt | dBm | 80.0 | W−Lt+Gt |
| 伝送距離 | d | km | 4.4 | |
| 大気吸収損 | Lo | dB | 13.1 | 3dB/km |
| 降雨損 | Lra | dB | 0.0 | 1分間降雨強度=0mm/h |
| 自由空間伝搬損 | Ld | dB | 147.2 | |
| 受信アンテナ利得 | Gr | dBi | 51.0 | |
| 受信給電損 | Lr | dB | 1.0 | |
| 受信電力 | Ci | dBm | −30.3 | (WGt/Lt)−(Lo+Lra+Ld)+Gr−Lr |
| 雑音指数 | F | dB | 10.0 | |
| ボルツマン定数 | k | dBm/(Hz・K) | −198.6 | k=1.38E−23 |
| 標準温度 | $T_0$ | dBK | 24.8 | $T_0$=300 |
| 帯域幅 | B | dBHz | 102.4 | |
| 雑音電力 | Ni | dBm | −61.4 | Ni=$kT_0BF$ |
| 受信C／N | C/N | dB | 31.1 | |
| 所要C／N | | dB | 25.0 | |
| 伝送マージン | | dB | 6.1 | |

| 晴天時 | 短距離用 | 長距離用 |
|---|---|---|
| 空中線電力 | 17.5mW | 1W |
| 伝搬距離 | 450m | 4.4km |

## 表 2　BPSK 方式における回線設計例（晴天時）

### 1　競技場などで使用される場合（晴天時）

| 項目 | 記号 | 単位 | 数値 | 備考 |
|---|---|---|---|---|
| 送信周波数 | f | GHz | 125 | |
| 波長 | λ | mm | 2.40 | |
| 帯域幅 | B | GHz | 17.5 | |
| 送信電力 | w | mW | 4.4 | |
| 送信電力 | W | dBm | 6.4 | |
| 送信給電損 | Lt | dB | 1.0 | |
| 送信アンテナ利得 | Gt | dBi | 44.0 | |
| 送信EIRP | WGt/Lt | dBm | 49.4 | W-Lt+Gt |
| 伝送距離 | d | km | 0.45 | |
| 大気吸収損 | Lo | dB | 1.4 | 3dB/km |
| 降雨損 | Lra | dB | 0.0 | 1分間降雨強度=0mm/h |
| 自由空間伝搬損 | Ld | dB | 127.4 | |
| 受信アンテナ利得 | Gr | dBi | 44.0 | |
| 受信給電損 | Lr | dB | 1.0 | |
| 受信電力 | Ci | dBm | -36.4 | (WGt/Lt)-(Lo+Lra+Ld)+Gr-Lr |
| 雑音指数 | F | dB | 10.0 | |
| ボルツマン定数 | k | dBm/(Hz・K) | -198.6 | k=1.38E-23 |
| 標準温度 | $T_0$ | dBK | 24.8 | $T_0$=300 |
| 帯域幅 | B | dBHz | 102.4 | |
| 雑音電力 | Ni | dBm | -61.4 | Ni=k$T_0$BF |
| 受信C／N | C/N | dB | 25.0 | |
| 所要C／N | | dB | 19.0 | |
| 伝送マージン | | dB | 6.0 | |

### 2　河川横断などで使用される場合（晴天時）

| 項目 | 記号 | 単位 | 数値 | 備考 |
|---|---|---|---|---|
| 送信周波数 | f | GHz | 125 | |
| 波長 | λ | mm | 2.40 | |
| 帯域幅 | B | GHz | 17.5 | |
| 送信電力 | w | mW | 250.0 | |
| 送信電力 | W | dBm | 24.0 | |
| 送信給電損 | Lt | dB | 1.0 | |
| 送信アンテナ利得 | Gt | dBi | 51.0 | |
| 送信EIRP | WGt/Lt | dBm | 74.0 | W-Lt+Gt |
| 伝送距離 | d | km | 4.4 | |
| 大気吸収損 | Lo | dB | 13.1 | 3dB/km |
| 降雨損 | Lra | dB | 0.0 | 1分間降雨強度=0mm/h |
| 自由空間伝搬損 | Ld | dB | 147.2 | |
| 受信アンテナ利得 | Gr | dBi | 51.0 | |
| 受信給電損 | Lr | dB | 1.0 | |
| 受信電力 | Ci | dBm | -36.4 | (WGt/Lt)-(Lo+Lra+Ld)+Gr-Lr |
| 雑音指数 | F | dB | 10.0 | |
| ボルツマン定数 | k | dBm/(Hz・K) | -198.6 | k=1.38E-23 |
| 標準温度 | $T_0$ | dBK | 24.8 | $T_0$=300 |
| 帯域幅 | B | dBHz | 102.4 | |
| 雑音電力 | Ni | dBm | -61.4 | Ni=k$T_0$BF |
| 受信C／N | C/N | dB | 25.0 | |
| 所要C／N | | dB | 19.0 | |
| 伝送マージン | | dB | 6.0 | |

| 晴天時 | 短距離用 | 長距離用 |
|---|---|---|
| 空中線電力 | 4.4mW | 250mW |
| 伝搬距離 | 450m | 4.4km |

## 表3　QPSK方式における回線設計例（晴天時）

### 1 競技場などで使用される場合（晴天時）

| 項目 | 記号 | 単位 | 数値 | 備考 |
|---|---|---|---|---|
| 送信周波数 | f | GHz | 125 | |
| 波長 | λ | mm | 2.40 | |
| 帯域幅 | B | GHz | 17.5 | |
| 送信電力 | w | mW | 13.6 | |
| 送信電力 | W | dBm | 11.3 | |
| 送信給電損 | Lt | dB | 1.0 | |
| 送信アンテナ利得 | Gt | dBi | 44.0 | |
| 送信EIPR | WGt/Lt | dBm | 54.3 | W−Lt+Gt |
| 伝送距離 | d | km | 0.45 | |
| 大気吸収損 | Lo | dB | 1.4 | 3dB/km |
| 降雨損 | Lra | dB | 0.0 | 1分間降雨強度=0mm/h |
| 自由空間伝搬損 | Ld | dB | 127.4 | |
| 受信アンテナ利得 | Gr | dBi | 44.0 | |
| 受信給電損 | Lr | dB | 1.0 | |
| 受信電力 | Ci | dBm | −31.5 | (WGt/Lt)−(Lo+Lra+Ld)+Gr−Lr |
| 雑音指数 | F | dB | 10.0 | |
| ボルツマン定数 | k | dBm/(Hz・K) | −198.6 | k=1.38E−23 |
| 標準温度 | $T_0$ | dBK | 24.8 | $T_0$=300 |
| 帯域幅 | B | dBHz | 102.4 | |
| 雑音電力 | Ni | dBm | −61.4 | Ni=k$T_0$BF |
| 受信C／N | C/N | dB | 29.9 | |
| 所要C／N | | dB | 23.9 | |
| 伝送マージン | | dB | 6.0 | |

### 2 河川横断などで使用される場合（晴天時）

| 項目 | 記号 | 単位 | 数値 | 備考 |
|---|---|---|---|---|
| 送信周波数 | f | GHz | 125 | |
| 波長 | λ | mm | 2.40 | |
| 帯域幅 | B | GHz | 17.5 | |
| 送信電力 | w | mW | 770.0 | |
| 送信電力 | W | dBm | 28.9 | |
| 送信給電損 | Lt | dB | 1.0 | |
| 送信アンテナ利得 | Gt | dBi | 51.0 | |
| 送信EIPR | WGt/Lt | dBm | 78.9 | W−Lt+Gt |
| 伝送距離 | d | km | 4.4 | |
| 大気吸収損 | Lo | dB | 13.1 | 3dB/km |
| 降雨損 | Lra | dB | 0.0 | 1分間降雨強度=0mm/h |
| 自由空間伝搬損 | Ld | dB | 147.2 | |
| 受信アンテナ利得 | Gr | dBi | 51.0 | |
| 受信給電損 | Lr | dB | 1.0 | |
| 受信電力 | Ci | dBm | −31.5 | (WGt/Lt)−(Lo+Lra+Ld)+Gr−Lr |
| 雑音指数 | F | dB | 10.0 | |
| ボルツマン定数 | k | dBm/(Hz・K) | −198.6 | k=1.38E−23 |
| 標準温度 | $T_0$ | dBK | 24.8 | $T_0$=300 |
| 帯域幅 | B | dBHz | 102.4 | |
| 雑音電力 | Ni | dBm | −61.4 | Ni=k$T_0$BF |
| 受信C／N | C/N | dB | 29.9 | |
| 所要C／N | | dB | 23.9 | |
| 伝送マージン | | dB | 6.0 | |

| 晴天時 | 短距離用 | 長距離用 |
|---|---|---|
| 空中線電力 | 13.6mW | 770mW |
| 伝搬距離 | 450m | 4.4km |

## 表 4　ASK 方式における回線設計例（雨天時）

**1　競技場などで使用される場合（雨天時）**

| 項目 | 記号 | 単位 | 数値 | 備考 |
|---|---|---|---|---|
| 送信周波数 | f | GHz | 125 | |
| 波長 | λ | mm | 2.40 | |
| 帯域幅 | B | GHz | 17.5 | |
| 送信電力 | w | mW | 17.5 | |
| 送信電力 | W | dBm | 12.4 | |
| 送信給電損 | Lt | dB | 1.0 | |
| 送信アンテナ利得 | Gt | dBi | 44.0 | |
| 送信EIPR | WGt/Lt | dBm | 55.4 | W−Lt+Gt |
| 伝送距離 | d | km | 0.25 | |
| 大気吸収損 | Lo | dB | 0.8 | 3dB/km |
| 降雨損 | Lra | dB | 5.8 | 1分間降雨強度=60mm/h |
| 自由空間伝搬損 | Ld | dB | 122.3 | |
| 受信アンテナ利得 | Gr | dBi | 44.0 | |
| 受信給電損 | Lr | dB | 1.0 | |
| 受信電力 | Ci | dBm | −30.4 | (WGt/Lt)−(Lo+Lra+Ld)+Gr−Lr |
| 雑音指数 | F | dB | 10.0 | |
| ボルツマン定数 | k | dBm/(Hz・K) | −198.6 | k=1.38E−23 |
| 標準温度 | $T_0$ | dBK | 24.8 | $T_0$=300 |
| 帯域幅 | B | dBHz | 102.4 | |
| 雑音電力 | Ni | dBm | −61.4 | Ni=k$T_0$BF |
| 受信C／N | C/N | dB | 31.0 | |
| 所要C／N | | dB | 25.0 | |
| 伝送マージン | | dB | 6.0 | |

**2　河川横断などで使用される場合（雨天時）**

| 項目 | 記号 | 単位 | 数値 | 備考 |
|---|---|---|---|---|
| 送信周波数 | f | GHz | 125 | |
| 波長 | λ | mm | 2.40 | |
| 帯域幅 | B | GHz | 17.5 | |
| 送信電力 | w | mW | 1000.0 | |
| 送信電力 | W | dBm | 30.0 | |
| 送信給電損 | Lt | dB | 1.0 | |
| 送信アンテナ利得 | Gt | dBi | 51.0 | |
| 送信EIPR | WGt/Lt | dBm | 80.0 | W−Lt+Gt |
| 伝送距離 | d | km | 1.0 | |
| 大気吸収損 | Lo | dB | 3.0 | 3dB/km |
| 降雨損 | Lra | dB | 23.0 | 1分間降雨強度=60mm/h |
| 自由空間伝搬損 | Ld | dB | 134.4 | |
| 受信アンテナ利得 | Gr | dBi | 51.0 | |
| 受信給電損 | Lr | dB | 1.0 | |
| 受信電力 | Ci | dBm | −30.4 | (WGt/Lt)−(Lo+Lra+Ld)+Gr−Lr |
| 雑音指数 | F | dB | 10.0 | |
| ボルツマン定数 | k | dBm/(Hz・K) | −198.6 | k=1.38E−23 |
| 標準温度 | $T_0$ | dBK | 24.8 | $T_0$=300 |
| 帯域幅 | B | dBHz | 102.4 | |
| 雑音電力 | Ni | dBm | −61.4 | Ni=k$T_0$BF |
| 受信C／N | C/N | dB | 31.0 | |
| 所要C／N | | dB | 25.0 | |
| 伝送マージン | | dB | 6.0 | |

| 晴天時 | 短距離用 | 長距離用 |
|---|---|---|
| 空中線電力 | 17.5mW | 1W |
| 伝搬距離 | 250m | 1km |

## 表 5　BPSK 方式における回線設計例（雨天時）

### 1　競技場などで使用される場合（雨天時）

| 項目 | 記号 | 単位 | 数値 | 備考 |
|---|---|---|---|---|
| 送信周波数 | f | GHz | 125 | |
| 波長 | λ | mm | 2.40 | |
| 帯域幅 | B | GHz | 17.5 | |
| 送信電力 | w | mW | 4.4 | |
| 送信電力 | W | dBm | 6.4 | |
| 送信給電損 | Lt | dB | 1.0 | |
| 送信アンテナ利得 | Gt | dBi | 44.0 | |
| 送信EIPR | WGt/Lt | dBm | 49.4 | W−Lt+Gt |
| 伝送距離 | d | km | 0.25 | |
| 大気吸収損 | Lo | dB | 0.8 | 3dB/km |
| 降雨損 | Lra | dB | 5.8 | 1分間降雨強度=60mm/h |
| 自由空間伝搬損 | Ld | dB | 122.3 | |
| 受信アンテナ利得 | Gr | dBi | 44.0 | |
| 受信給電損 | Lr | dB | 1.0 | |
| 受信電力 | Ci | dBm | −36.4 | (WGt/Lt)−(Lo+Lra+Ld)+Gr−Lr |
| 雑音指数 | F | dB | 10.0 | |
| ボルツマン定数 | k | dBm/(Hz・K) | −198.6 | k=1.38E−23 |
| 標準温度 | $T_0$ | dBK | 24.8 | $T_0$=300 |
| 帯域幅 | B | dBHz | 102.4 | |
| 雑音電力 | Ni | dBm | −61.4 | Ni=kT$_0$BF |
| 受信C／N | C/N | dB | 25.0 | |
| 所要C／N | | dB | 19.0 | |
| 伝送マージン | | dB | 6.0 | |

### 2　河川横断などで使用される場合（雨天時）

| 項目 | 記号 | 単位 | 数値 | 備考 |
|---|---|---|---|---|
| 送信周波数 | f | GHz | 125 | |
| 波長 | λ | mm | 2.40 | |
| 帯域幅 | B | GHz | 17.5 | |
| 送信電力 | w | mW | 250.0 | |
| 送信電力 | W | dBm | 24.0 | |
| 送信給電損 | Lt | dB | 1.0 | |
| 送信アンテナ利得 | Gt | dBi | 51.0 | |
| 送信EIPR | WGt/Lt | dBm | 74.0 | W−Lt+Gt |
| 伝送距離 | d | km | 1.0 | |
| 大気吸収損 | Lo | dB | 3.0 | 3dB/km |
| 降雨損 | Lra | dB | 23.0 | 1分間降雨強度=60mm/h |
| 自由空間伝搬損 | Ld | dB | 134.4 | |
| 受信アンテナ利得 | Gr | dBi | 51.0 | |
| 受信給電損 | Lr | dB | 1.0 | |
| 受信電力 | Ci | dBm | −36.4 | (WGt/Lt)−(Lo+Lra+Ld)+Gr−Lr |
| 雑音指数 | F | dB | 10.0 | |
| ボルツマン定数 | k | dBm/(Hz・K) | −198.6 | k=1.38E−23 |
| 標準温度 | $T_0$ | dBK | 24.8 | $T_0$=300 |
| 帯域幅 | B | dBHz | 102.4 | |
| 雑音電力 | Ni | dBm | −61.4 | Ni=kT$_0$BF |
| 受信C／N | C/N | dB | 25.0 | |
| 所要C／N | | dB | 19.0 | |
| 伝送マージン | | dB | 6.0 | |

| 晴天時 | 短距離用 | 長距離用 |
|---|---|---|
| 空中線電力 | 4.4mW | 250mW |
| 伝搬距離 | 250m | 1km |

## 表 6　QPSK 方式における回線設計例（雨天時）

1　競技場などで使用される場合（雨天時）

| 項目 | 記号 | 単位 | 数値 | 備考 |
|---|---|---|---|---|
| 送信周波数 | f | GHz | 125 | |
| 波長 | λ | mm | 2.40 | |
| 帯域幅 | B | GHz | 17.5 | |
| 送信電力 | w | mW | 13.6 | |
| 送信電力 | W | dBm | 11.3 | |
| 送信給電損 | Lt | dB | 1.0 | |
| 送信アンテナ利得 | Gt | dBi | 44.0 | |
| 送信EIPR | WGt/Lt | dBm | 54.3 | W−Lt+Gt |
| 伝送距離 | d | km | 0.25 | |
| 大気吸収損 | Lo | dB | 0.8 | 3dB/km |
| 降雨損 | Lra | dB | 5.8 | 1分間降雨強度=60mm/h |
| 自由空間伝搬損 | Ld | dB | 122.3 | |
| 受信アンテナ利得 | Gr | dBi | 44.0 | |
| 受信給電損 | Lr | dB | 1.0 | |
| 受信電力 | Ci | dBm | −31.5 | (WGt/Lt)−(Lo+Lra+Ld)+Gr−Lr |
| 雑音指数 | F | dB | 10.0 | |
| ボルツマン定数 | k | dBm/(Hz・K) | −198.6 | k=1.38E−23 |
| 標準温度 | $T_0$ | dBK | 24.8 | $T_0$=300 |
| 帯域幅 | B | dBHz | 102.4 | |
| 雑音電力 | Ni | dBm | −61.4 | Ni=k$T_0$BF |
| 受信C／N | C/N | dB | 29.9 | |
| 所要C／N | | dB | 23.9 | |
| 伝送マージン | | dB | 6.0 | |

2　河川横断などで使用される場合（雨天時）

| 項目 | 記号 | 単位 | 数値 | 備考 |
|---|---|---|---|---|
| 送信周波数 | f | GHz | 125 | |
| 波長 | λ | mm | 2.40 | |
| 帯域幅 | B | GHz | 17.5 | |
| 送信電力 | w | mW | 770.0 | |
| 送信電力 | W | dBm | 28.9 | |
| 送信給電損 | Lt | dB | 1.0 | |
| 送信アンテナ利得 | Gt | dBi | 51.0 | |
| 送信EIPR | WGt/Lt | dBm | 78.9 | W−Lt+Gt |
| 伝送距離 | d | km | 1.0 | |
| 大気吸収損 | Lo | dB | 3.0 | 3dB/km |
| 降雨損 | Lra | dB | 23.0 | 1分間降雨強度=60mm/h |
| 自由空間伝搬損 | Ld | dB | 134.4 | |
| 受信アンテナ利得 | Gr | dBi | 51.0 | |
| 受信給電損 | Lr | dB | 1.0 | |
| 受信電力 | Ci | dBm | −31.5 | (WGt/Lt)−(Lo+Lra+Ld)+Gr−Lr |
| 雑音指数 | F | dB | 10.0 | |
| ボルツマン定数 | k | dBm/(Hz・K) | −198.6 | k=1.38E−23 |
| 標準温度 | $T_0$ | dBK | 24.8 | $T_0$=300 |
| 帯域幅 | B | dBHz | 102.4 | |
| 雑音電力 | Ni | dBm | −61.4 | Ni=k$T_0$BF |
| 受信C／N | C/N | dB | 29.9 | |
| 所要C／N | | dB | 23.9 | |
| 伝送マージン | | dB | 6.0 | |

| 晴天時 | 短距離用 | 長距離用 |
|---|---|---|
| 空中線電力 | 13.6mW | 770mW |
| 伝搬距離 | 250m | 1km |

# 周波数割当計画
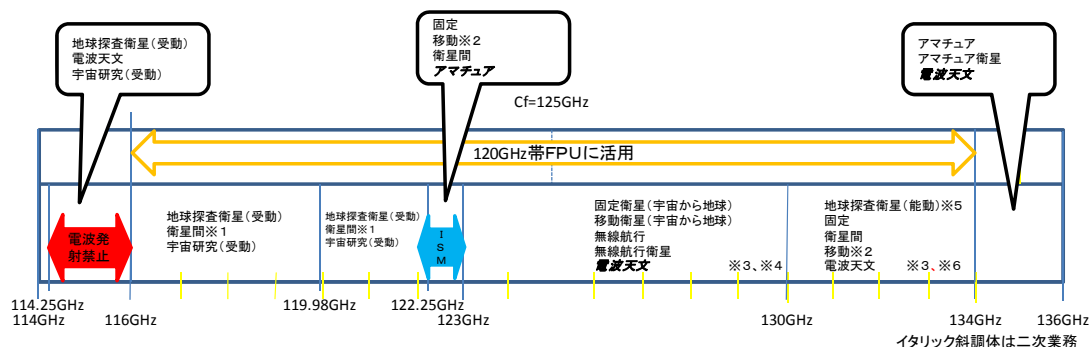


※１　衛星間業務によるこの周波数帯の使用は、静止衛星軌道の衛星に限定される。すべての条件及びすべての変調方式に対して、地表面から１０００ｋｍまでの高度及び受動検知器が存在する全ての静止軌道位置の近傍で、衛星間業務の局により生じる単一入射電力束密度は、全ての仰角において－１４８ｄＢ（Ｗ／（㎡・ＭＨｚ））を超えてはならない。（J287）

※２　航空移動業務によるこの周波数帯の使用は、衛星間業務に有害な混信を生じさせないことを条件とする（無線通信規則第５．４３号参照）。（J277）

※３　（略）、１２８．３３－１２８．５９ＧＨｚ、１２９．２３－１２９．４９ＧＨｚ、１３０－１３４ＧＨｚ、（略）の周波数帯の使用は、電波天文業務を有害な混信から保護するための実行可能な全ての措置を執らなければならない。宇宙局又は航空機上の局からの電波の発射は、電波天文業務に対する著しく重大な混信源となり得る(無線通信規則第 4.5 号、第 4.6 号及び第 29 条参照）。（J36）

※４　この周波数帯は、移動衛星業務又は無線航行衛星業務に関連して、特定の固定地点の陸上局を接続する衛星回線の使用にも使用することができる。（J268）

※５　地球探査衛星業務（能動）による使用は、１３３．５－１３４ＧＨｚの周波数帯に限る。（J288）

※６　宇宙局の送信設備及び関連する電波天文業務の用に供する受信設備の運営体は、１３０－１３４ＧＨｚの周波数帯における地球探査衛星業務（能動）の宇宙局から電波天文受信機の空中線の主ビームに向けられた送信により発生する干渉を極力避けるため、相互に運用を計画するものとする。（J285）

## 干渉検討に使用する 120GHz 帯 FPU の諸元、及び運用条件

1　120GHz 帯 FPU の諸元

①　中心周波数、及び、帯域

・中心周波数　125GHz

・帯域：116〜134 GHz

②　空中線電力

・空中線電力は、1 波当たり、1W, 500mW, 100mW, 40mW

・帯域外領域におけるスプリアス発射の強度の許容値：100 μW／1 MHz 以下

・スプリアス領域における不要発射の強度の許容値　　：50 μW／1 MHz 以下

③　空中線利得

　アンテナ種類は、パラボラアンテナ、ホーンアンテナを想定した。

　パラボラアンテナは、（60 cmφ 51 dBi）、（45 cmφ 49 dBi）、（20 cmφ 40 dBi）の三種類とした。ホーンアンテナは、20 cmφ で、24 dBi の一種類とした。干渉検討に使用したアンテナの指向特性は参考資料 12 に記載している。

2　大気減衰

　衛星と 120GHz 帯 FPU の位置関係及び使用周波数での適切な大気減衰を用いる。勧告 ITU-R P.676-9Annex 2 を用いて計算した大気減衰量を図 1 に示す。
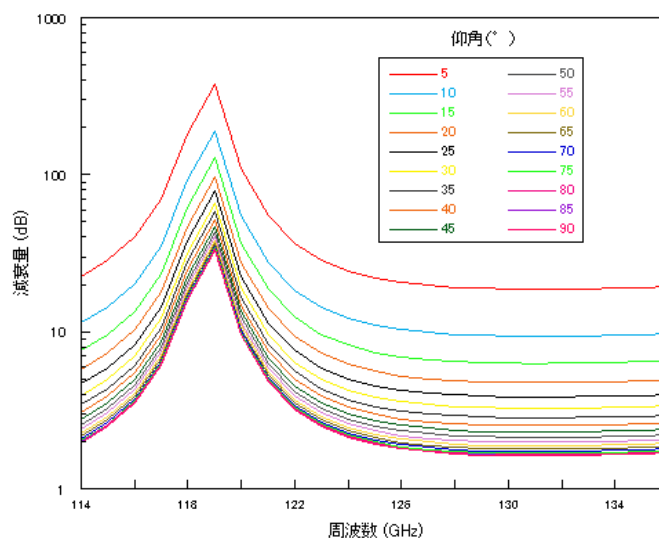


図 1　120GHz 帯域の仰角別大気減衰量

## 3 120GHz 帯 FPU の運用方法

### 3.1 日本に存在する 120GHz 帯 FPU の送信機数、同時運用確率、運用時間率について

共用検討を実施するに当り、将来に渡り、日本に存在すると想定される移動局として利用される 120GHz 帯 FPU の送信機数、高周波帯での無線局であることを考慮した同時運用確率、さらに、高周波帯の無線局が、番組等の素材伝送で使用されることを想定した運用時間率について、以下の値を仮定して計算に使用した。

①合計　300 局

②同時運用確率を 1%（常時 3 局が、日本国内で送信）

③運用時間率を 0.1%（8.76 時間固定されて連続送信）

④運用されているアンテナの 90 %がパラボラアンテナであり、10 %がホーンアンテナの利用を仮定した。また、運用されているパラボラアンテナのうち 20 %が 60 cmφ、60 %が 45 cmφ、残りの 20 %が 20 cmφ を利用すると仮定した。

### 3.2 最大運用仰角、または、運用仰角確率について

FPU としての運用なので、仰角、方位角は規定しない。ただし、実際の運用では水平方向から±5 度がほとんどであり、それ以上の仰角、伏角については、運用の可能性が低いため、干渉検討でのみ適用する運用仰角確率を以下の通りとした。なお、アンテナを直上に振る可能性はないため、仰角が 80 度以上になる運用確率は 0 である。

|仰角｜＜＝20 度　　　　　90%

45 度＞＝｜仰角｜＞20 度　　9%

80 度＞＝｜仰角｜＞45 度　　1%

｜仰角｜＞80 度　　　　　　0%

# 干渉検討に使用する 120GHz 帯 FPU のアンテナ指向特性

① パラボラアンテナ参照指向特性

　パラボラアンテナの放射パタンの測定値を基に、パラボラアンテナの参照指向特性を下記の式 1 及び式 2 で定義した。パラボラアンテナの指向特性は、測定した結果、その利得、サイドローブとも口径による顕著な差がみられないことから、全ての口径で同一の式を用いることとした。さらに、式 1 及び式 2 は 45 cmφ パラボラで連続しており、使用する利得によっては、不連続が発生しても、そのまま計算で用いた。なお、衛星業務との確率論的な共用検討では、運用の度に設置位置が変わる地上局からの干渉波が、全てサイドローブピークから発射されるわけではなく、サイドローブのヌルから発射される場合もあるため、サイドローブの平均レベルとして、ピークサイドローブレベルから 3 dB 下げた、パラボラアベレージサイドローブの参照指向特性を使用した。

パラボラピークサイドローブ：

$G(\varphi) = G_{max}$ 　　　　for 　0° ＜ φ ＜ 　1°

$G(\varphi) = 47 - 25\log\varphi$ 　for 　1° ≦ φ ＜ 　76°

$G(\varphi) = 0$ 　　　　for 　76° ≦ φ ≦ 180° 　　（式 1）

パラボラアベレージサイドローブ（干渉確率計算で使用）：

$G(\varphi) = G_{max}$ 　　　　for 　0° ＜ φ ＜ 　1°

$G(\varphi) = 44 - 25\log\varphi$ 　for 　1° ≦ φ ＜ 　76°

$G(\varphi) = -3$ 　　　　for 　76° ≦ φ ≦ 180° 　　（式 2）

② ホーンアンテナ参照指向特性

　パラボラアンテナと同様、ホーンアンテナの放射パタンの測定値を基に、ホーンアンテナの参照指向特性を下記の式 3 及び式 4 で定義した。ホーンアンテナでは、E 面と H 面で放射パタンが異なるが、最悪値を共用検討に使用するため、E 面での測定値を使用して参照指向特性を求めた。なお、衛星業務との確率論的な共用検討では、パラボラアンテナと同様、運用の度に設置位置が変わる地上局からの干渉波が、全てサイドローブピークから発射されるわけではなく、サイドローブのヌルから発射される場合もあるため、サイドローブの平均レベルとして、ピークサイドローブレベルから 3 dB 下げたホーンアンテナアベレージサイドローブの参照指向特性を使用した。

ホーンアンテナピークサイドローブ：

$G(\varphi) = G_{max}$          for    0°   <   φ   <    1°

$G(\varphi) = G_{max} - 0.07 \times \varphi^2$    for    1°   ≦   φ   <   10°

$G(\varphi) = 46 - 29\log\varphi$      for   10°   ≦   φ   <   48°

$G(\varphi) = -3$            for   48°   ≦   φ   ≦   180°      （式 3）


ホーンアンテナアベレージサイドローブ（干渉確率計算で使用）：

$G(\varphi) = G_{max}$          for    0°   <   φ   <    1°

$G(\varphi) = G_{max} - 0.07 \times \varphi^2$    for    1°   ≦   φ   <   10°

$G(\varphi) = 43 - 29\log\varphi$      for   10°   ≦   φ   <   90°

$G(\varphi) = -14$          for   90°   ≦   φ   ≦   180°      （式 4）

① 対地観測モード（地球表面を垂直方向に近い角度で観測するモード）

ITU-R 勧告 RS.2017 に基づく干渉保護値-166dBW/200MHz を超える干渉確率を表 4 に示す。ITU-R 勧告 RS. 2017 に基づく対地観測モードの地球探査衛星(受動)業務の保護基準値－166 dBW／200 MHz を超える干渉確率が 0.01 ％未満となっており、非静止衛星の対地観測モードは、1 W の出力において共用が可能となっている。

表 4　対地観測モードでの地球探査衛星(受動)センサーへの干渉確率

| Mobile Station Transmit Power (Watts) | % of time －166 dBW／200 MHz Exceeded |
|---|---|
| 1 | 0.000124 |
| 0.5 | 0.000074 |
| 0.1 | 0.000023 |
| 0.04 | 0.000013 |

② 大気観測モード

ITU-R 勧告 RS. 2017 に基づく大気観測モードの地球探査衛星(受動)業務の保護基準値－189 dBW／10 MHz を超える干渉確率を表 5 に示す。ITU-R 勧告 RS. 2017 に基づく大気観測モードの地球探査衛星(受動)業務の保護基準値－189 dBW／10 MHz を超える干渉確率が 1 ％未満となっており、大気観測モードの非静止衛星(受動)の全ての例で、1 W の出力で共用が可能であることを示している。

表 5　大気観測モードでの地球探査衛星(受動)センサーへの干渉確率

| Mobile Station Transmit Power (Watts) | % of time －189 dBW／10 MHz Exceeded |
|---|---|
| 1 | 0.1362 |
| 0.5 | 0.0913 |
| 0.1 | 0.0276 |
| 0.04 | 0.0129 |

# アマチュア無線との干渉検討

　干渉検討に使用するアマチュア無線及び 120GHz 帯 FPU の諸元を以下のように定義する。

アマチュア無線業務の諸元
　・空中線電力：200mW （23dBm）
　・アマチュア無線の帯域外に落ち込む電力を空中線電力の 0.5%と仮定：1mW
　・アンテナ利得：20dBi（±10 度）
　・受信信号帯域幅：40kHz
　・受信信号帯域幅における熱雑音量：-117.8dBm（40kHz）

120GHz 帯 FPU の諸元
　・妨害波電力密度　-45.0dBm/MHz（測定機の測定限界の値で仮定）
　・空中線利得　20.0dBi（±10 度）
　・熱雑音量：-61.4dBm

以下の計算は、134GHz で行った。
① 　アマチュア無線から FPU への被干渉検討結果
　50m の見通し範囲にアマチュア無線がある場合、FPU への干渉電力密度は以下の式で求められる。
　受信電力= 妨害波送信電力＋送信空中線利得＋受信空中線利得－（自由空間伝搬損失
　　　　　＋大気減衰）（大気減衰定数：0.93 dB／km(勧告 ITU-R P.676-9）を適用）
　P ＝ 0.0(dBm)＋20.0(dBi)＋20.0(dBi)－(109.0(dB)＋0.05dB))
　　＝－69.0(dBm)
　以上により、離隔距離を 50 m 以上とれば、アマチュア無線から FPU への被干渉電力は、FPU の熱雑音以下になり、共用は可能である。

② 　FPU からアマチュア無線への与干渉検討結果
　20m の見通し範囲にアマチュア無線がある場合、FPU からの与干渉電力は以下の式で求められる。
　受信電力= 妨害波送信電力密度＋送信空中線利得＋受信空中線利得－（自由空間伝搬
　　　　　損失＋大気減衰）－帯域換算値（1MHz→40kHz）

（大気減衰定数：0.93 dB／km(勧告 ITU-R P.676-9）を適用）

P ＝ -45.0(dBm/MHz)＋20.0(dBi)＋20.0(dBi)－(101.0(dB)＋0.02(dB))-14.0(dB)

＝－120.0 (dBm)

　この計算結果より、離隔距離を 20 m 以上とれば、FPU からアマチュア無線への与干渉電力はアマチュア無線の受信信号帯域幅の熱雑音以下になり、共用は可能である。

# 日本国内の電波天文台の諸元

表 1　日本国内の電波天文台の諸元

|  | 国立天文台<br>（長野県） | 国立天文台<br>（鹿児島県） | 名古屋大学<br>（愛知県） |
|---|---|---|---|
| 地点（北緯） | 35°56′40″ | 31°27′51″ | 35° 09′ 07″ |
| 地点（東経） | 138°28′21″ | 130°30′26″ | 136° 58′ 14″ |
| 地点標高（m） | 1343 | 57.5 | 75 |
| アンテナ高（m） | 22 | 12 | 6 |

## 電波天文業務の受信設備との干渉検討

### ①　同一周波数帯（123-130GHz, 130-134GHz）を使用する場合

検討で使用した諸元を以下に示す。

電波天文業務の受信設備の諸元

・アンテナ利得：0 dBi（仰角 0 度）

・混信保護値：-189 dBW／8 GHz（ITU-R 勧告 RA. 769-2（参考資料 16）の 89GHz
　　帯“continuum observations”の基準値を採用）　→　-198 dBm／MHz

120GHz 帯 FPU の諸元

・空中線電力密度　0.0dBm/MHz（30dBm/1GHz の場合）

・空中線利得　20.0dBi（±10 度）

電波天文業務のアンテナの指向性については、電波天文業務のアンテナは主に天空を指向しており、 120GHz 帯 FPU は地上回線であるため、共用検討で用いる電波天文業務のアンテナ利得は、仰角 0 度で水平面無指向性とみなし 0 dBi を使用した。また、大気減衰定数は、勧告 ITU-R P.676-9（参考資料６）Annex 2 の手法を用いて、水平方向の伝搬路で算出した。周波数は 125GHz において計算した。

（１）　電波天文が見通し範囲にある場合

　　　伝送距離が 60 km とした場合の受信電力密度は以下のようになる。

受信電力密度 ＝ 妨害波送信電力密度＋送信空中線利得＋受信空中線利得
　　　　　　　　　－（自由空間伝搬損失＋大気減衰）
　　　　　　　（大気減衰定数：0.87 dB／km(勧告 ITU-R P.676-9) を適用）
P　＝0.0（dBm／MHz）＋20.0(dBi)＋ 0.0(dBi) －(169.9(dB)＋52.2(dB))
　　＝－202.1（dBm／MHz）

　　　即ち、見通し範囲では、伝送距離が 60 km 以上で、電波天文台での 120GHz 帯
FPU からの受信電力密度は、当該周波数帯における最大許容受信電力密度
　　－189dBW／8GHz＝－198dBm／MHz
を下回る。

（２） 同一周波数帯で電波天文台が見通し範囲外にある場合

電波天文台が見通し外にある場合、つまり、遮断物が有る場合については、ナイフエッジ回折損失があるとした。図１に示す回線の場合、伝送距離を 20 km とし、その中間点に高さ 100 m の遮断物が有る場合のナイフエッジ回折損失は以下のようになる。
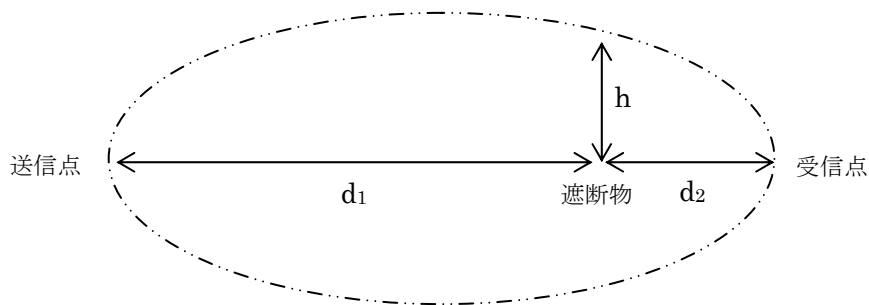


図１　ナイフエッジ回折損失の計算に使用する配置

λ ：0.0024 m　（周波数　125 GHz）

$d_1$ ：10000 m

$d_2$ ：10000 m

h ：100 m

ナイフエッジ回折損失 J(v)は次式で近似される。

$$J(v) = 6.9 + 20 \log \left\{ \sqrt{(v-0.1)^2 + 1} + v - 0.1 \right\}$$

$$v = h \sqrt{\frac{2}{\lambda} \left( \frac{1}{d1} + \frac{1}{d2} \right)}$$

したがって、回折損失 Ld＝45.1（dB）となる。

以上からナイフエッジ 100 m の遮断物が中間にある伝送距離 20 km における電波天文台における 120GHz 帯 FPU からの受信電力密度は以下のとおりとなる。

受信電力密度 ＝ 妨害波送信電力密度＋送信空中線利得＋受信空中線利得

－（自由空間伝搬損失＋大気減衰）－山岳回折損

（大気減衰定数：0.87 dB／km(勧告 ITU-R P.676-9）を適用）

P ＝0.0(dBm／MHz)＋20.0(dBi)＋ 0.0(dBi) －(160.4(dB)＋17.4(dB))－45.1 (dB)

＝－202.9 (dBm／MHz)

よって、電波天文台における受信電力密度は当該周波数帯における最大許容受信電力密度

－189 dBW／8 GHz＝－198 dBm／MHz

を下回る。

② 隣接周波数帯（105-116GHz）を使用する場合
　検討で使用した諸元を以下に示す。

　電波天文業務の受信設備の諸元
　・アンテナ利得：0 dBi（仰角 0 度）
　・混信保護値：-189 dBW／8 GHz（ITU-R 勧告 RA. 769-2 の 89GHz 帯“continuum
　　observations”の基準値を採用）　→　 -198 dBm／MHz

　120GHz 帯 FPU の諸元
　・空中線電力密度　-55dBm/MHz　（注）
　・空中線利得　20.0dBi（±10 度）
　注 ： 116GHz 以下の周波数帯における電力は、測定機の測定限界である
　　　-55dBm/MHz とした（実験機による値：図２参照）。また、干渉計算は、120GHz
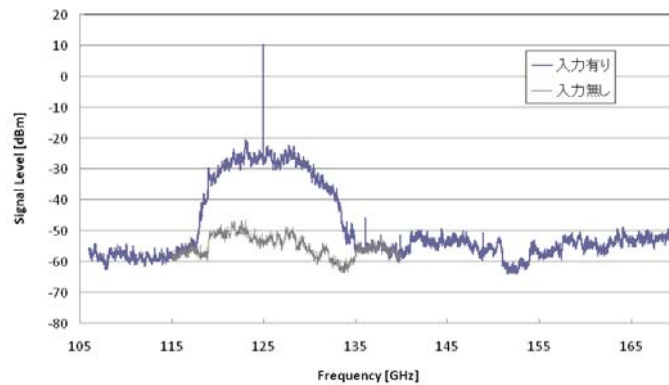　　　帯 FPU で使用する周波数に最も近い 116GHz で行った。



図２　120GHz 帯 FPU の送信スペクトル例

（１）電波天文台が見通し範囲にある場合
　　伝送距離が 10 km とした場合の受信電力密度は以下のようになる。
　　受信電力密度 ＝ 妨害波送信電力密度＋送信空中線利得＋受信空中線利得
　　　　　　　　　－（自由空間伝搬損失＋大気減衰）
　　　　　　　　　（大気減衰定数：1.02 dB／km(勧告 ITU-R P.676-9) を適用）
　　P ＝－55 (dBm／MHz)＋20.0(dBi)＋0.0 (dBi)　－(153.7(dB)＋10.2 (dB))
　　　 ＝－198.9 (dBm／MHz)
　　即ち、見通し範囲では、伝送距離が 10 km 以上で、電波天文台での 120GHz 帯

FPUからの受信電力密度は、当該周波数帯における最大許容受信電力密度

　　－189dBW／8GHz＝－198dBm／MHz

を下回る。


（２）電波天文台が見通し範囲外にある場合

　　電波天文台が見通し外にある場合、つまり、遮断物が有る場合については、ナイフエッジ回折損失があるとした。図１に示す回線の場合、伝送距離を 500m とし、その中間点に高さ 10 m の遮断物が有る場合のナイフエッジ回折損失は、①（２）と同様に計算した結果、Ld＝40.8（dB）となる。

　　$\lambda$　：0.00259 m　　（周波数　116 GHz）

　　$d_1$　：250 m

　　$d_2$　：250 m

　　h　：10 m


　　ナイフエッジ 10 m の遮断物が中間にある伝送距離 500 m における電波天文台における 120GHz 帯 FPU からの受信電力密度は以下のとおりとなる。

　　受信電力密度 ＝ 妨害波送信電力密度＋送信空中線利得＋受信空中線利得

　　　　　　　　　　－（自由空間伝搬損失＋大気減衰）－山岳回折損

　　P ＝-55.0(dBm／MHz)＋20.0(dBi)＋0.0(dBi)－(127.7(dB)＋0.5dB)－40.8dB

　　　＝－204.0（dBm／MHz）

　　よって、電波天文台における受信電力密度は、当該周波数帯における最大許容受信電力密度

　　－189 dBW／8 GHz＝－198 dBm／MHz

を下回る。

# Rec. ITU-R RA.769-2

# RECOMMENDATION ITU-R RA.769-2

## Protection criteria used for radio astronomical measurements

(Question ITU-R 145/7)

(1992-1995-2003)

The ITU Radiocommunication Assembly,

*considering*

a)    that many of the most fundamental astronomical advances made in the past five decades, (e.g. the discovery of radio galaxies, quasars, and pulsars, the direct measurement of neutral hydrogen, the direct measurement of distances of certain external galaxies, and establishment of a positional reference frame accurate to ~20 arc µs) have been made through radio astronomy, and that radio astronomical observations are expected to continue making fundamental contributions to our understanding of the Universe, and that they provide the only way to investigate some cosmic phenomena;

b)    that the development of radio astronomy has also led to major technological advances, particularly in receiving and imaging techniques, and to improved knowledge of fundamental radio-noise limitations of great importance to radiocommunication, and promises further important results;

c)    that radio astronomers have made useful astronomical observations from the Earth's surface in all available atmospheric windows ranging from 2 MHz to 1 000 GHz and above;

d)    that the technique of space radio astronomy, which involves the use of radio telescopes on space platforms, provides access to the entire radio spectrum above about 10 kHz, including parts of the spectrum not accessible from the Earth due to absorption in atmosphere;

e)    that protection from interference is essential to the advancement of radio astronomy and associated measurements;

f)    that radio astronomical observations are mostly performed with high-gain antennas or arrays, to provide the highest possible angular resolution, and consequently main beam interference does not need to be considered in most situations, except when there is the possibility of receiver damage;

g)    that most interference that leads to the degradation of astronomical data is received through the far side lobes of the telescope;

h)    that the sensitivity of radio astronomical receiving equipment, which is still steadily improving, particularly at millimetre wavelengths, and that it greatly exceeds the sensitivity of communications and radar equipment;

j)    that typical radio astronomical observations require integration times of the order of a few minutes to hours, but that sensitive observations, particularly of spectral lines, may require longer periods of recording, sometimes up to several days;

k)      that some transmissions from spacecraft can introduce problems of interference to radio astronomy and that these cannot be avoided by choice of site for an observatory or by local protection;

l)      that interference to radio astronomy can be caused by terrestrial transmissions reflected by the Moon, by aircraft, and possibly by artificial satellites;

m)      that some types of high spatial-resolution interferometric observations require simultaneous reception, at the same radio frequency, by widely separated receiving systems that may be located in different countries, on different continents, or on space platforms;

n)      that propagation conditions at frequencies below about 40 MHz are such that a transmitter operating anywhere on the Earth might cause interference detrimental to radio astronomy;

o)      that some degree of protection can be achieved by appropriate frequency assignments on a national rather than an international basis;

p)      that WRCs have made improved allocations for radio astronomy, particularly above 71 GHz, but that protection in many bands, particularly those shared with other radio services, may still need careful planning;

q)      that technical criteria concerning interference detrimental to the radio astronomy service (RAS) have been developed, which are set out in Tables 1, 2, and 3,

*recommends*

**1**      that radio astronomers should be encouraged to choose sites as free as possible from interference;

**2**      that administrations should afford all practicable protection to the frequencies and sites used by radio astronomers in their own and neighbouring countries and when planning global systems, taking due account of the levels of interference given in Annex 1;

**3**      that administrations, in seeking to afford protection to particular radio astronomical observations, should take all practical steps to reduce all unwanted emissions falling within the band of the frequencies to be protected for radio astronomy to the absolute minimum. Particularly those emissions from aircraft, high altitude platform stations, spacecraft and balloons;

**4**      that when proposing frequency allocations, administrations take into account that it is very difficult for the RAS to share frequencies with any other service in which direct line-of-sight paths from the transmitters to the observatories are involved. Above about 40 MHz sharing may be practicable with services in which the transmitters are not in direct line-of-sight of the observatories, but coordination may be necessary, particularly if the transmitters are of high power.

# Annex 1

# Sensitivity of radio astronomy systems

## 1 General considerations and assumptions used in the calculation of interference levels

### 1.1 Detrimental-level interference criterion

The sensitivity of an observation in radio astronomy can be defined in terms of the smallest power level change $\Delta P$ in the power level $P$ at the radiometer input that can be detected and measured. The sensitivity equation is:

$$\frac{\Delta P}{P} = \frac{1}{\sqrt{\Delta f_0 t}} \tag{1}$$

where:

     $P$ and $\Delta P$:    power spectral density of the noise

         $\Delta f_0$:    bandwidth

         $t$:    integration time. $P$ and $\Delta P$ in equation (1) can be expressed in temperature units through the Boltzmann's constant, $k$:

$$\Delta P = k\,\Delta T; \quad \text{also} \quad P = k\,T \tag{2}$$

Thus we may express the sensitivity equation as:

$$\Delta T = \frac{T}{\sqrt{\Delta f_0 t}} \tag{3}$$

where:

$$T = T_A + T_R$$

This result applies for one polarization of the radio telescope. $T$ is the sum of $T_A$ (the antenna noise temperature contribution from the cosmic background, the Earth's atmosphere and radiation from the Earth) and $T_R$, the receiver noise temperature. Equations (1) or (3) can be used to estimate the sensitivities and interference levels for radio astronomical observations. The results are listed in Tables 1 and 2. An observing (or integration) time, $t$, of 2 000 s is assumed, and interference threshold levels, $\Delta P_H$, given in Tables 1 and 2 are expressed as the interference power within the bandwidth $\Delta f$ that introduces an error of 10% in the measurement of $\Delta P$ (or $\Delta T$), i.e.:

$$\Delta P_H = 0.1\,\Delta P\,\Delta f \tag{4}$$

In summary, the appropriate columns in Tables 1 and 2 may be calculated using the following methods:

–      $\Delta T$, using equation (3),

–      $\Delta P$, using equation (2),

–      $\Delta P_H$, using equation (4).

The interference can also be expressed in terms of the pfd incident at the antenna, either in the total bandwidth or as a spectral pfd, $S_H$, per 1 Hz of bandwidth. The values given are for an antenna having a gain, in the direction of arrival of the interference, equal to that of an isotropic antenna (which has an effective area of $c^2/4\pi f^2$, where $c$ is the speed of the light and $f$ the frequency). The gain of an isotropic radiator, 0 dBi, is used as a general representative value for the side-lobe level, as discussed under § 1.3.

Values of $S_H \Delta f$ (dB(W/m$^2$)), are derived from $\Delta P_H$ by adding:

$$20 \log f - 158.5 \qquad \text{dB} \qquad\qquad (5)$$

where $f$ (Hz). $S_H$ is then derived by subtracting $10 \log \Delta f$ (Hz) to allow for the bandwidth.

## 1.2     Integration time

The calculated sensitivities and interference levels presented in Tables 1 and 2 are based on assumed integration times of 2 000 s. Integration times actually used in astronomical observations cover a wide range of values. Continuum observations made with single-antenna telescopes (as distinct from interferometric arrays) are well represented by the integration time of 2 000 s, typical of good quality observations. On the other hand 2 000 s is less representative of spectral line observations. Improvements in receiver stability and the increased use of correlation spectrometers have allowed more frequent use of longer integration times required to observe weak spectral lines, and spectral line observations lasting several hours are quite common. A more representative integration time for these observations would be 10 h. For a 10 h integration, the threshold interference level is 6 dB more stringent than the values given in Table 2. There are also certain observations of time varying phenomena, e.g. observations of pulsars, stellar or solar bursts, and interplanetary scintillations for which much shorter time periods may be adequate.

## 1.3     Antenna response pattern

Interference to radio astronomy is almost always received through the antenna side lobes, so the main beam response to interference need not be considered.

The side-lobe model for large paraboloid antennas in the frequency range 2 to 30 GHz, given in Recommendation ITU-R SA.509 is a good approximation of the response of many radio astronomy antennas and is adopted throughout this Recommendation as the radio astronomy reference antenna. In this model, the side-lobe level decreases with angular distance (degrees) from the main beam axis and is equal to $32 - 25 \log \varphi$ (dBi) for $1° < \varphi < 48°$. The effect of an interfering signal clearly depends upon the angle of incidence relative to the main beam axis of the antenna, since the side-lobe gain, as represented by the model, varies from 32 to $-10$ dBi as a function of this angle. However, it is useful to calculate the threshold levels of interference strength for a particular value of side-lobe gain, that we choose as 0 dBi, and use in Tables 1 to 3. From the model, this side-lobe level occurs at an angle of 19.05° from the main beam axis. Then a signal at the detrimental threshold level defined for 0 dBi side-lobe gain will exceed the criterion for the detrimental level at the receiver input if it is incident at the antenna at an angle of less than 19.05°. The solid angle

within a cone of angular radius 19.05° is 0.344 sr, which is equal to 5.5% of the $2\pi$ sr of the sky above the horizon that a radio telescope is able to observe at any given time. Thus if the probability of the angle of incidence of interference is uniformly distributed over the sky, about 5.5% of interfering signals would be incident within 19.05° of the main beam axis of an antenna pointed towards the sky. Note also that the 5.5% figure is in line with the recommended levels of data loss to radio astronomy observations in percentage of time, specified in Recommendation ITU-R RA.1513.

The particular case of non-GSO satellites presents a dynamic situation, that is, the positions of the satellites relative to the beam of the radio astronomy antenna show large changes within the time scale of the 2 000 s integration time. Analysis of interference in this case requires integrating the response over the varying side-lobe levels, for example, using the concept of epfd defined in No. 22.5C of the Radio Regulations (RR). In addition it is usually necessary to combine the responses to a number of satellites within a particular system. In such calculations it is suggested that the antenna response pattern for antennas of diameter greater than 100 $\lambda$ in Recommendation ITU-R S.1428 be used to represent the radio astronomy antenna, until a model based specifically on radio astronomy antennas is available; see § 2.2 for further discussion.

## 1.4 Bandwidth

Equation (1) shows that observations of the highest sensitivity are obtained when radio astronomers make use of the widest possible bandwidth. Consequently, in Table 1 (continuum observations), $\Delta f$ is assumed to be the width of the allocated radio astronomy bands for frequencies up to 71 GHz. Above 71 GHz a value of 8 GHz is used, which is a representative bandwidth generally used on radio astronomy receivers in this range. In Table 2 (spectral line observations) a channel bandwidth $\Delta f$ equal to the Doppler shift corresponding to 3 km/s in velocity is used for entries below 71 GHz. This value represents a compromise between the desired high spectral resolution and the sensitivity. There are a very large number of astrophysically important lines above 71 GHz, as shown in Recommendation ITU-R RA.314 and only a few representative values for the detrimental levels are given in Table 2 for the range 71-275 GHz. The channel bandwidth used to compute the detrimental levels above 71 GHz is 1 000 kHz (1 MHz) in all cases. This value was chosen for practical reasons. While it is slightly wider than the spectral channel width customary in radio astronomy receivers at these frequencies, it is used as the standard reference bandwidth for space services above 15 GHz.

## 1.5 Receiver noise temperature and antenna temperature

The receiver noise temperatures in Tables 1 and 2 are representative of the systems in use in radio astronomy. For frequencies above 1 GHz these are cryogenically cooled amplifiers or mixers. The quantum effect places a theoretical lower limit of $hf/k$ on the noise temperature of such devices, where $h$ and $k$ are Planck's and Boltzmann's constants, respectively. This limit becomes important at frequencies above 100 GHz, where it equals 4.8 K. Practical mixers and amplifiers for bands at 100 GHz and higher provide noise temperatures greater than $hf/k$ by a factor of about four. Thus, for frequencies above 100 GHz, noise temperatures equal to $4hf/k$ are used in Tables 1 and 2.

The antenna temperatures in the Tables are also representative of practical systems in use in radio astronomy. They include the effects of the ionosphere or the neutral atmosphere, ground pickup in side lobes resulting from spillover or scattering, ohmic losses, and the cosmic microwave background. At frequencies above 100 GHz the atmospheric losses due to water vapour in the neutral atmosphere become very important. For these frequencies the values given are typical of the terrestrial sites used for major millimetric-wave radio astronomy facilities, such as Mauna Kea, Hawaii, or the Llano de Chajnantor at an elevation of 5 000 m in Chile, which is the site chosen for a major international radio astronomy array for frequencies in the range 30 GHz to 1 THz.

## 2 Special cases

The levels given in Tables 1 and 2 are applicable to terrestrial sources of interfering signals. The detrimental pfd and spectral pfd shown in Tables 1 and 2 assume that interference is received through a 0 dBi side lobe, and should be regarded as the general interference criteria for high sensitivity radio astronomy observations, when the interference does not enter the near side lobes.

### 2.1 Interference from GSO satellites

Interference from GSO satellites is a case of particular importance. Because the power levels in Tables 1 and 2 were calculated based on a 0 dBi antenna gain, interference detrimental to radio astronomy will be encountered when a reference antenna, such as described in Recommendation ITU-R SA.509, is pointed within 19.05° of a satellite radiating at levels in accordance with those listed in the Tables. A series of such transmitters located around the GSO would preclude radio astronomy observations with high sensitivity from a band of sky 38.1° wide and centred on the orbit. The loss of such a large area of sky would impose severe restrictions on radio astronomy observations.

In general, it would not be practical to suppress the unwanted emissions from satellites to below the detrimental level when the main beam of a radio telescope is pointed directly towards the satellite. A workable solution is suggested by observing the projection of the GSO in celestial coordinates as viewed from the latitudes of a number of major radio astronomy observations (see Recommendation ITU-R RA.517). If it were possible to point a radio telescope to within 5° of the GSO without encountering detrimental interference, then for that telescope a band of sky 10° wide would be unavailable for high-sensitivity observations. For a given observatory this would be a serious loss. However, for a combination of radio telescopes located at northern and southern latitudes, operating at the same frequencies, the entire sky would be accessible. A value of 5° should therefore be regarded as the requirement for minimum angular spacing between the main beam of a radio astronomy antenna and the GSO.

In the model antenna response of Recommendation ITU-R SA.509, the side-lobe level at an angle of 5° from the main beam is 15 dBi. Thus, to avoid interference detrimental to a radio telescope meeting the antenna side-lobe performance of Recommendation ITU-R SA.509, pointed to within 5° of the transmitter, it is desirable that the satellite emissions be reduced 15 dB below the pfd given in Tables 1 and 2. When satellites are spaced at intervals of only a few degrees along the GSO, the emission levels associated with the individual transmitters must be even lower to meet the requirement that the sum of the powers of all the interfering signals received should be 15 dB below $\Delta P_H$ in Tables 1 and 2.

It is recognized that the emission limitations discussed above cannot, in practice, be achieved so as to enable sharing of the same frequency band between radio astronomy and down-link transmissions from satellites to take place. The limitations are, however, applicable to unwanted emission from the satellite transmitters, which fall within the radio astronomy bands listed in Tables 1 and 2. These emission limitations have implications for the space services responsible for the interference, which require careful evaluation. Furthermore, the design of new radio astronomy antennas should strive to minimize the level of side-lobe gain near the main beam as an important means of reducing interference from transmitters in the GSO.

## 2.2 Interference from non-GSO satellites

In the case of non-GSO satellites, and in particular for low-Earth orbit satellites, the systems usually involve constellations of many individual satellites. Thus determination of interference levels requires analysis of the combined effect of many signals, most of which are received through far side lobes of the radio astronomy antenna. A more detailed side-lobe model than that of Recommendation ITU-R SA.509 is therefore desirable, and it is proposed that the model in Recommendation ITU-R S.1428 be used until such time as a more representative model for radio astronomy antennas is obtained. In using this proposed model the case for antennas with diameter greater than $100 \lambda$ is generally appropriate for radio astronomy applications. It should be noted that Note 1 of Recommendation ITU-R S.1428, which allows cross-polarized components to be ignored, cannot be applied since radio astronomy antennas generally receive signals in two orthogonal polarizations simultaneously. The motion of non-GSO satellites across the sky during a 2 000 s integration period requires that the interference level be averaged over this period, that is, the response to each satellite must be integrated as the satellite moves through the side-lobe pattern. One system of analysis that includes these requirements is the epfd method described in RR No. 22.5C. Values of epfd represent the pfd of a signal entering the antenna through the centre of the main beam that would produce an equivalent level of interference power. Since the threshold levels of detrimental interference in Tables 1 and 2 correspond to pfd received with an antenna gain of 0 dBi, it is necessary to compare them with values of ($epfd + G_{mb}$), where $G_{mb}$ is the main beam gain, to determine whether the interference exceeds the detrimental level. Making use of the epfd method, Recommendation ITU-R S.1586 has recently been developed for interference calculations between radio astronomy telescopes and FSS non-GSO satellite systems. A similar Recommendation, Recommendation ITU-R M.1583 was developed for interference calculations between radio astronomy telescopes and MSS and radionavigation-satellite service non-GSO satellite systems. The applicability of the protection criteria given in Tables 1 and 2 is described in Recommendation ITU-R RA.1513.

## 2.3 The response of interferometers and arrays to radio interference

Two effects reduce the response to interference. These are related to the frequency of the fringe oscillations that are observed when the outputs of two antennas are combined, and to the fact that the components of the interfering signal received by different and widely-spaced antennas will suffer different relative time delays before they are recombined. The treatment of these effects is more complicated than that for single antennas in § 1. Broadly speaking, if the strength of the received interfering signal remains constant, the effect is reduced by a factor roughly equal to the

mean time of one natural fringe oscillation divided by the data averaging time. This typically ranges from some seconds for a compact array with the longest projected spacing $L' \sim 10^3 \lambda$, where $\lambda$ is the wavelength, to less than 1 ms for intercontinental arrays with $L' \sim 10^7 \lambda$. Thus, compared to a single radio telescope, the interferometer has a degree of immunity to interference which, under reasonable assumptions increases with the array size expressed in wavelengths.

The greatest immunity from interference occurs for interferometers and arrays in which the separation of the antennas is sufficiently great that the chance of occurrence of correlated interference is very small (e.g. for very long baseline interferometry (VLBI)). In this case, the above considerations do not apply. The tolerable interference level is determined by the requirement that the power level of the interfering signal should be no more than 1% of the receiver noise power to prevent serious errors in the measurement of the amplitude of the cosmic signals. The interference levels for typical VLBI observations are given in Table 3, based on the values of $T_A$ and $T_R$ given in Table 1.

It must be emphasized that the use of large interferometers and arrays is generally confined to studies of discrete, high-brightness sources, with angular dimensions no more than a few tenths of a second of arc for VLBI. For more general studies of radio sources, the results in Tables 1 and 2 apply and are thus appropriate for the general protection of radio astronomy.

TABLE 1

**TABLE 1**

**Threshold levels of interference detrimental to radio astronomy continuum observations**

| Centre frequency [1] $f_c$ (MHz) | Assumed bandwidth $\Delta f$ (MHz) | Minimum antenna noise temperature $T_A$ (K) | Receiver noise temperature $T_R$ (K) | System sensitivity [2] (noise fluctuations) | | Threshold interference levels [2] [3] | | |
|---|---|---|---|---|---|---|---|---|
| | | | | Temperature $\Delta T$ (mK) | Power spectral density $\Delta P$ (dB(W/Hz)) | Input power $\Delta P_H$ (dBW) | pfd $S_H \Delta f$ (dB(W/m²)) | Spectral pfd $S_H$ (dB(W/(m² · Hz))) |
| (1) | (2) | (3) | (4) | (5) | (6) | (7) | (8) | (9) |
| 13.385 | 0.05 | 50 000 | 60 | 5 000 | −222 | −185 | −201 | −248 |
| 25.610 | 0.12 | 15 000 | 60 | 972 | −229 | −188 | −199 | −249 |
| 73.8 | 1.6 | 750 | 60 | 14.3 | −247 | −195 | −196 | −258 |
| 151.525 | 2.95 | 150 | 60 | 2.73 | −254 | −199 | −194 | −259 |
| 325.3 | 6.6 | 40 | 60 | 0.87 | −259 | −201 | −189 | −258 |
| 408.05 | 3.9 | 25 | 60 | 0.96 | −259 | −203 | −189 | −255 |
| 611 | 6.0 | 20 | 60 | 0.73 | −260 | −202 | −185 | −253 |
| 1 413.5 | 27 | 12 | 10 | 0.095 | −269 | −205 | −180 | −255 |
| 1 665 | 10 | 12 | 10 | 0.16 | −267 | −207 | −181 | −251 |
| 2 695 | 10 | 12 | 10 | 0.16 | −267 | −207 | −177 | −247 |
| 4 995 | 10 | 12 | 10 | 0.16 | −267 | −207 | −171 | −241 |
| 10 650 | 100 | 12 | 10 | 0.049 | −272 | −202 | −160 | −240 |
| 15 375 | 50 | 15 | 15 | 0.095 | −269 | −202 | −156 | −233 |
| 22 355 | 290 | 35 | 30 | 0.085 | −269 | −195 | −146 | −231 |
| 23 800 | 400 | 15 | 30 | 0.050 | −271 | −195 | −147 | −233 |
| 31 550 | 500 | 18 | 65 | 0.083 | −269 | −192 | −141 | −228 |
| 43 000 | 1 000 | 25 | 65 | 0.064 | −271 | −191 | −137 | −227 |
| 89 000 | 8 000 | 12 | 30 | 0.011 | −278 | −189 | −129 | −228 |
| 150 000 | 8 000 | 14 | 30 | 0.011 | −278 | −189 | −124 | −223 |
| 224 000 | 8 000 | 20 | 43 | 0.016 | −277 | −188 | −119 | −218 |
| 270 000 | 8 000 | 25 | 50 | 0.019 | −276 | −187 | −117 | −216 |

[1]  Calculation of interference levels is based on the centre frequency shown in this column although not all regions have the same allocations.

[2]  An integration time of 2 000 s has been assumed; if integration times of 15 min, 1 h, 2 h, 5 h or 10 h are used, the relevant values in the Table should be adjusted by +1.7, −1.3, −2.8, −4.8 or −6.3 dB respectively.

[3]  The interference levels given are those which apply for measurements of the total power received by a single antenna.  Less stringent levels may be appropriate for other types of measurements, as discussed in § 2.2. For transmitters in the GSO, it is desirable that the levels be adjusted by −15 dB, as explained in § 2.1.

## TABLE 2[*]

**Threshold levels of interference detrimental to radio astronomy spectral-line observations**

| Frequency $f$ (MHz) | Assumed spectral line channel bandwidth $\Delta f$ (kHz) | Minimum antenna noise temperature $T_A$ (K) | Receiver noise temperature $T_R$ (K) | System sensitivity[(2)] (noise fluctuations) | | Threshold interference levels[(1) (2)] | | |
|---|---|---|---|---|---|---|---|---|
| | | | | Temperature $\Delta T$ (mK) | Power spectral density $\Delta P_S$ (dB(W/Hz)) | Input power $\Delta P_H$ (dBW) | pfd $S_H \Delta f$ (dB(W/m²)) | Spectral pfd $S_H$ (dB(W/(m² · Hz))) |
| (1) | (2) | (3) | (4) | (5) | (6) | (7) | (8) | (9) |
| 327 | 10 | 40 | 60 | 22.3 | −245 | −215 | −204 | −244 |
| 1 420 | 20 | 12 | 10 | 3.48 | −253 | −220 | −196 | −239 |
| 1 612 | 20 | 12 | 10 | 3.48 | −253 | −220 | −194 | −238 |
| 1 665 | 20 | 12 | 10 | 3.48 | −253 | −220 | −194 | −237 |
| 4 830 | 50 | 12 | 10 | 2.20 | −255 | −218 | −183 | −230 |
| 14 488 | 150 | 15 | 15 | 1.73 | −256 | −214 | −169 | −221 |
| 22 200 | 250 | 35 | 30 | 2.91 | −254 | −210 | −162 | −216 |
| 23 700 | 250 | 35 | 30 | 2.91 | −254 | −210 | −161 | −215 |
| 43 000 | 500 | 25 | 65 | 2.84 | −254 | −207 | −153 | −210 |
| 48 000 | 500 | 30 | 65 | 3.00 | −254 | −207 | −152 | −209 |
| 88 600 | 1 000 | 12 | 30 | 0.94 | −259 | −209 | −148 | −208 |
| 150 000 | 1 000 | 14 | 30 | 0.98 | −259 | −209 | −144 | −204 |
| 220 000 | 1 000 | 20 | 43 | 1.41 | −257 | −207 | −139 | −199 |
| 265 000 | 1 000 | 25 | 50 | 1.68 | −256 | −206 | −137 | −197 |

[*] This Table is not intended to give a complete list of spectral-line bands, but only representative examples throughout the spectrum.

[(1)] An integration time of 2 000 s has been assumed; if integration times of 15 min, 1 h, 2 h, 5 h or 10 h are used, the relevant values in the Table should be adjusted by +1.7, −1.3, −2.8, −4.8 or −6.3 dB respectively.

[(2)] The interference levels given are those which apply for measurements of the total power received by a single antenna. Less stringent levels may be appropriate for other types of measurements, as discussed in § 2.2. For transmitters in the GSO, it is desirable that the levels need to be adjusted by −15 dB, as explained in § 2.1.

COLUMN DESCRIPTIONS FOR TABLES 1 AND 2

**Column**

(1)     Centre frequency of the allocated radio astronomy band (Table 1) or nominal spectral line frequency (Table 2).

(2)     Assumed or allocated bandwidth (Table 1) or assumed typical channel widths used for spectral line observations (Table 2).

(3)     Minimum antenna noise temperature includes contributions from the ionosphere, the Earth's atmosphere and radiation from the Earth.

(4)     Receiver noise temperature representative of a good radiometer system intended for use in high sensitivity radio astronomy observations.

(5)     Total system sensitivity (mK) as calculated from equation (1) using the combined antenna and receiver noise temperatures, the listed bandwidth and an integration time of 2 000 s.

(6)     Same as (5) above, but expressed in noise power spectral density using the equation $\Delta P = k\,\Delta T$, where $k = 1.38 \times 10^{-23}$ (J/K) (Boltzmann's constant). The actual numbers in the Table are the logarithmic expression of $\Delta P$.

(7)     Power level at the input of the receiver considered harmful to high sensitivity observations, $\Delta P_H$. This is expressed as the interference level which introduces an error of not more than 10% in the measurement of $\Delta P$; $\Delta P_H = 0.1\,\Delta P\,\Delta f$: the numbers in the Table are the logarithmic expression of $\Delta P_H$.

(8)     pfd in a spectral line channel needed to produce a power level of $\Delta P_H$ in the receiving system with an isotropic receiving antenna. The numbers in the Table are the logarithmic expression of $S_H\,\Delta f$.

(9)     Spectral pfd needed to produce a power level $\Delta P_H$ in the receiving system with an isotropic receiving antenna. The numbers in the Table are the logarithmic expression of $S_H$. To obtain the corresponding power levels in a reference bandwidth of 4 kHz or 1 MHz add 36 dB or 60 dB, respectively.

TABLE  3

**Threshold interference levels for VLBI observations**

| Centre frequency (MHz) | Threshold level (dB(W/m² · Hz))) |
|---|---|
| 325.3 | −217 |
| 611 | −212 |
| 1 413.5 | −211 |
| 2 695 | −205 |
| 4 995 | −200 |
| 10 650 | −193 |
| 15 375 | −189 |
| 23 800 | −183 |
| 43 000 | −175 |
| 86 000 | −172 |

## 非静止衛星系システムとの干渉検討

　非静止衛星である米国の AURA の衛星諸元を表１に示す。（ITU-R 勧告 RS.1861（参考資料 18））

<p align="center">表１　非静止衛星 AURA システムの諸元</p>

| AURA システムの諸元 | | 備　　　考 |
|---|---|---|
| 打ち上げ | 2004 年 7 月 15 日 | |
| ミッション | 地球のオゾン、大気の品質及び気候の観測 | |
| センサー | リム　サウンダー | |
| 高度 | 705km | 非静止軌道 |
| 傾斜角 | 98.2 度 | |
| 周期 | 16 日 | |
| 最大空中線利得 | 60dBi | |
| アンテナの観測スキャン角度 | ±50° | 183GHz 帯衛星（AMSU-B）のデータを流用 |

　地球探査衛星(受動)業務の干渉保護基準は、ITU-R 勧告 RS.2017（参考資料 19）に記載されている。116〜122.25GHz の地球探査衛星（受動）の保護基準を表２に示す。

　ここで、表２の Scan mode に記載されている「N」は、Nadir scan mode の頭文字で、地球表面を垂直方向に近い角度で観測するモードで、本報告書の中では、以下、「対地観測モード」と呼称する。また、同様に「L」は、Limb scan mode の頭文字で、地表面から宇宙空間の間の大気を観測するモードで、以下、「大気観測モード」と呼称する。

　対地観測モードの地球探査衛星(受動)業務の保護基準値−166 dBW／200 MHz を超える干渉確率が 0.01%未満である。

　非静止衛星を用いた地球探査衛星（受動）業務の衛星搭載アンテナ指向特性は、勧告 ITU-R RS.1813-1（参考資料 20）で記載されているアンテナのピーク参照指向特性の式、及び平均参照指向特性の計算式を 120GHz 帯に拡張して用いた。その他、本システムのアンテナが対地観測モードを行う際のアンテナの挙動についての情報がないため、ITU-R 勧告 RS.1416（参考資料 21）に記載のある 183 GHz の非静止衛星を用いた地球探査衛星(受動)システムの対地観測モードのパラメータを適用した。表３に、そのパラメータを示す。本検討では、下記の表中にある、アンテナの観測スキャン角度（衛星の鉛直方向から±50

度）の情報を用いた。

表2　地球探査衛星(受動)の保護基準　（ITU-R Rec.RS.2017 より）

| Frequency band(s) (GHz) | Reference bandwidth (MHz) | Maximum interference level (dBW) | Percentage of area or time permissible interference level may be exceeded[1] (%) | Scan mode (N, C, L)[2] |
|---|---|---|---|---|
| 115.25-122.25 | 200/10[3] | −166/−189[3] | 0.01/1[3] | N, L |

[1] For a 0.01% level, the measurement area is a square on the Earth of 2 000 000 km², unless otherwise justified; for a 0.1% level, the measurement area is a square on the Earth of 10 000 000 km² unless otherwise justified; for a 1% level, the measurement time is 24 h, unless otherwise justified.

[2] N: Nadir, Nadir scan modes concentrate on sounding or viewing the Earth's surface at angles of nearly perpendicular incidence. The scan terminates at the surface or at various levels in the atmosphere according to the weighting functions. L: Limb, Limb scan modes view the atmosphere "on edge" and terminate in space rather than at the surface, and accordingly are weighted zero at the surface and maximum at the tangent point height. C: Conical, Conical scan modes view the Earth's surface by rotating the antenna at an offset angle from the nadir direction.

[3] First number for nadir or conical scanning modes and second number for microwave limb sounding applications.

表3　183 GHz で運用される非静止衛星（受動）システムの対地観測モードのパラメータ

| Parameter | AMSU-B |
|---|---|
| Antenna main-beam gain (dBi) | 45 |
| Antenna back-lobe gain (dBi) | −14 |
| Antenna beamwidth at half power points (degrees) | 1.15 |
| Sensor altitude range (km) | 500 to 1 000  850 (nominal) |
| Interference criteria per bandwidth (dB(W／200 MHz)) | −160 |
| Antenna measurement scan angles (from nadir) (degrees) | ±50 |
| Cold calibration angle (from orbital plane) (degrees) | 90 ± 4 |
| Cold calibration angle range (from nadir) (degrees) | 65 to 85  83 (nominal) |

以下に干渉検討結果を示す。

RECOMMENDATION ITU-R RS.1861*

# Typical technical and operational characteristics of Earth exploration-satellite service (passive) systems using allocations between 1.4 and 275 GHz

(Question ITU-R 243/7)

(2010)

**Scope**

This Recommendation provides typical technical and operational characteristics of Earth exploration-satellite service (passive) systems using allocations between 1.4 and 275 GHz for utilization in sharing studies.

The ITU Radiocommunication Assembly,

*considering*

a)      that Earth exploration-satellite service (EESS) (passive) observations may receive emissions from active services;

b)      that there are exclusive EESS (passive) allocations in which all emissions are prohibited by RR No. 5.340;

c)      that EESS (passive) is allocated on a co-primary basis with active services in certain bands;

d)      that studies considering protection for EESS (passive) systems are taking place within ITU-R;

e)      that in order to perform compatibility and sharing studies with EESS (passive) systems, the technical and operational characteristics of those systems must be known,

*recommends*

**1**      that the technical and operational parameters presented in Annex 1 of this Recommendation should be taken into account in studies considering EESS (passive) systems using allocations between 1.4 and 275 GHz.

# Annex 1

## 1      Introduction

Passive sensors are used in the remote sensing of the Earth and its atmosphere by Earth exploration and meteorological satellites in certain frequency bands allocated to the Earth exploration-satellite service (EESS) (passive). The products of these passive sensor operations are used extensively in meteorology, climatology, and other disciplines for operational and scientific purposes. However, these sensors are sensitive to any emissions within their allocated band. Therefore, any RF emissions above a certain level may constitute interference to the passive sensors using those bands.

---

*      This Recommendation should be brought to the attention of Radiocommunication Study Group 1.

This is mainly due to the fact that passive sensors may not be able to differentiate the wanted signal from the interference and that interference may not be identifiable in the passive sensor products.

## 2        Current missions and predicted deployments

Several administrations and at least one recognized international organization operated more than 24 satellites in the EESS (passive) at the end of the year 2007. An additional two to three are anticipated to be deployed per year for the foreseeable future. Individual satellites typically carry one to three passive sensing payloads operating below 275 GHz. Each payload may conduct measurements simultaneously at 3 to 15 frequencies as well as on two polarizations at a single frequency.

## 3        Typical orbits

EESS (passive) systems operate in non-geostationary satellite orbit (non-GSO). Orbits are typically circular with an altitude between 350 and 1 400 km. Many EESS (passive) systems operate in a sun-synchronous orbit. Some sensors make measurements at the same place on the Earth every day, while others will repeat observations only after a longer (often more than two weeks) repeat period.

In certain circumstances, multiple satellites operate in formation. Formation flying EESS satellites allow the capability to measure a portion of the atmosphere or surface of the Earth using both multiple instruments and multiple orientations. Measurements from multiple spacecraft will be separated within an amount of time shorter than the time constant of the phenomena being measured. Nominally this separation is on the order of 5 to 15 min, but can be as little as 15 s.

Two formations are used between multiple systems operating in non-GSO. In one formation, two or more satellites directly follow each other performing measurements of the same parcel of atmosphere or the Earth's surface as demonstrated by satellites A and B in Fig. 1. In the other formation, a nadir pointing passive sensor conducts a measurement while another spacecraft conducts a near-simultaneous measurement at the Earth's limb as demonstrated by satellites A and C in Fig. 1.

## 4        Types of measurements

All EESS passive sensing systems perform a form of radiometry. Radiometry senses how much energy a body radiates given its temperature. The amount of energy radiated from a perfect "blackbody" varies with frequency and is given by Planck's equation. However, no substance is truly a perfect blackbody radiator. Frequencies of particular interest for EESS (passive) applications are provided in Recommendation ITU-R RS.515.

The amount of energy radiated is also dependent on the radiating substance. Within a passive sensor's field of view, there may be multiple radiators in *inter alia* atmosphere, water vapour, suspended ice particles, and cloud liquid water, emitting in the sensor's bandwidth. Measurements not conducted on the Earth's limb will also receive background emissions from water, soil, surface ice, or some combination of all three.

A single passive sensor cannot by itself identify how much energy is radiated by each substance in its field of view. For this reason, data products of most value are derived by comparing measurements from multiple sensors operating at multiple frequencies. By performing radiometric measurements at multiple frequencies, the types of each natural emitter (e.g. water vapour, suspended ice, $O_3$, etc.) and their concentrations may be derived. As the data from any one sensor

may be compared with that of multiple other sensors, any interference received by one sensor may corrupt multiple other measurements.

FIGURE 1

**Formation flying orientations**



1861-01
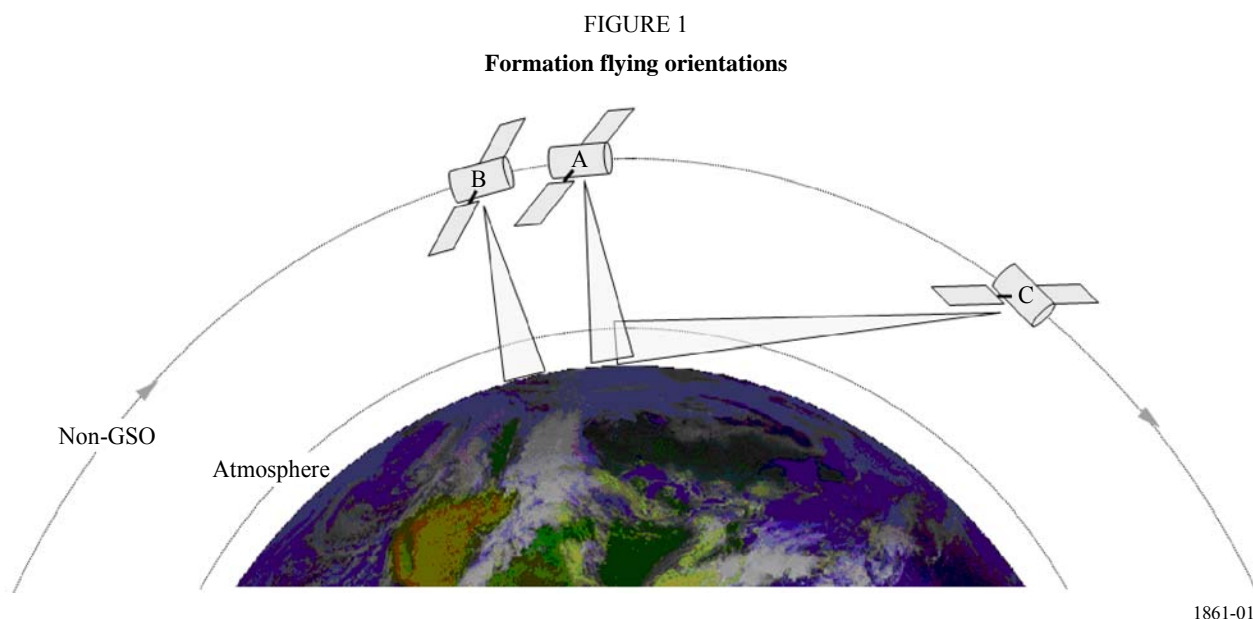
## 4.1 Fixed-pointing, multiple frequency and polarization radiometric sensing

Sensing concurrently at multiple frequencies and polarizations offers the possibilities of identifying the presence of multiple natural emitters present in the field of view of the sensor as well as to create profiles of their concentrations. Profiling (a.k.a. sounding) sensors may be nadir-pointing or pointed at the limb of the Earth. Applications of profiling sensors includes the determination of atmospheric chemistry profiles of $H_2O$, $O_3$, $ClO$, $BrO$, $HCl$, $OH$, $HO_2$, $HNO_3$, $HCN$, and $N_2O$ through limb measurements.

Fixed pointing radiometers are also used to determine path delay of the radar signals used for altimeters caused by atmospheric water vapour.

Radiometers designed for the whole Earth viewing perform continuous, hemispheric microwave soundings of temperature and humidity profiles as well as rain mapping.

## 4.2 Conical scanning radiometers

Many passive microwave sensors designed for imaging the Earth's surface features use a conical scan configuration turning around the nadir direction because it is important, for the interpretation of surface measurements, to maintain a constant ground incidence angle along the entire scan-lines since the footprints will remain constant in size, and also because the polarization characteristics of the signal have an angular dependence. Conical scanning antennas gather information over wide areas as shown in Fig. 2. Scans are typically performed by rotating the antenna at an offset angle from the nadir direction. Conical scanning radiometers are used to monitor various water processes including precipitation, oceanic water vapour, cloud water, near-surface wind speed, sea surface temperature, soil moisture, snow cover, and sea ice parameters. They can also be used to provide information on the integrated column precipitation content, its area distribution, and its intensity.

FIGURE 2

**Geometry of conical scan passive microwave radiometers**
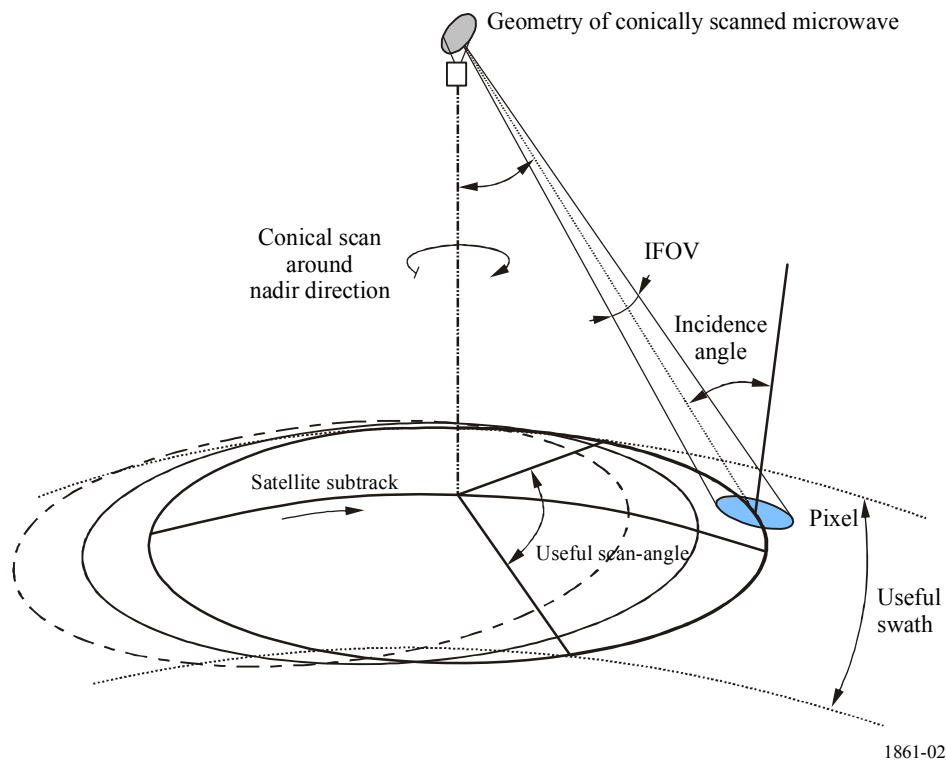


1861-02

## 4.3 Cross-track scanning radiometers

Scanning radiometric measurements gather information over wide areas creating virtual maps of the parameter being measured. This data product determines the horizontal spatial variability of a parameter rather than measuring the parameters at specific points. Scanning measurements are also typically performed at multiple frequencies and polarizations.

Typical applications of cross-track scanning radiometers include the measurement of temperature profiles in the upper atmosphere (especially the stratosphere) and to provide a cloud-filtering capability for tropospheric temperature observations. They also are used to provide daily global observations of temperature and moisture profiles at high temporal resolution, and to measure cloud liquid water content and provide qualitative estimates of precipitation rate.

Scans are typically performed in a cross-track pattern across the surface of the Earth as shown in Fig. 3. Cross-track scanning is performed by physically rotating a reflector 360°. As the reflector is directed away from the surface of the Earth, sensor channels are still used as calibrations are performed by measuring the cosmic background (i.e. cold sky) in addition to a known "warm" source on the spacecraft, as shown in Fig. 4.

FIGURE 3

**Typical cross-track Earth scanning pattern**



1861-03
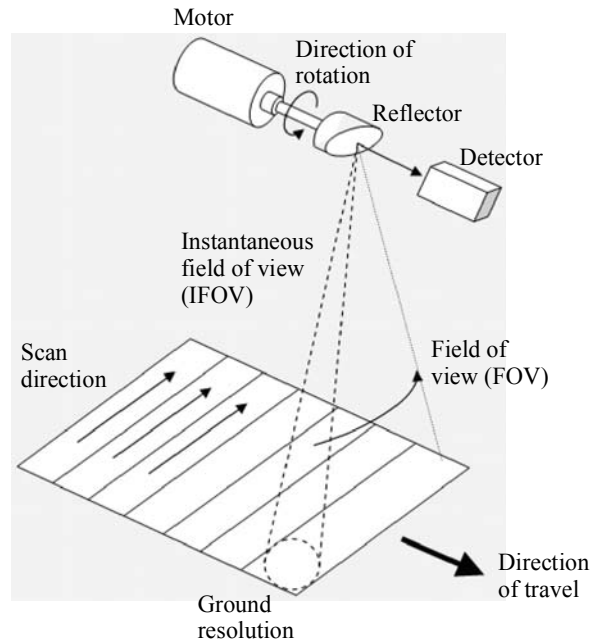
FIGURE 4

**Typical sensing scanning pattern over 360°**



*Note 1* – All angles with respect to nadir.
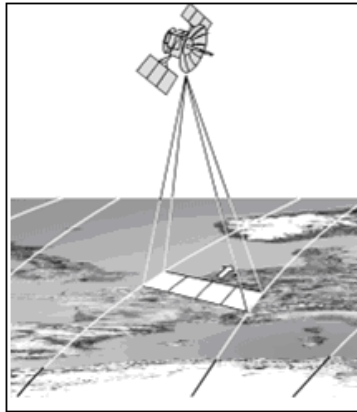
1861-04
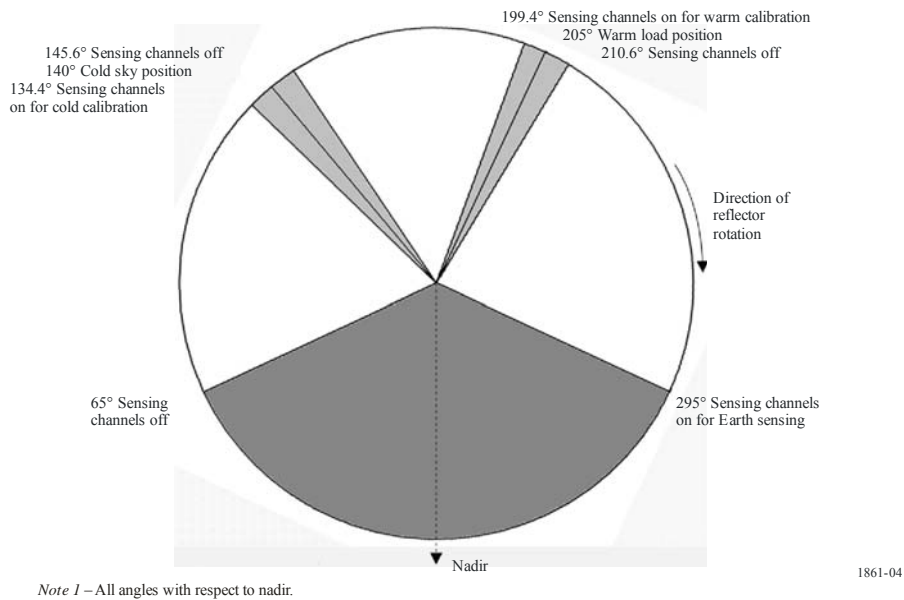
## 4.4 Push-broom radiometers

A "push-broom" (along track) sensor consists of a line of sensors arranged perpendicular to the flight direction of the spacecraft, as illustrated in Fig. 5. Different areas of the surface are detected as the spacecraft flies forward. The push-broom is a purely static instrument with no moving parts.

The major feature of the push-broom is that all resolution elements in a scan line are acquired simultaneously, and not sequentially as with mechanically scanned sensors, enabling this type of sensor to significantly increase the achievable radiometric resolution. Push-broom sensors can be used for a variety of applications, including temperature profiles measurements of the atmosphere, and soil moisture and ocean salinity measurements.

FIGURE 5

**Typical push-broom radiometer configuration**



1861-05

## 5     Definition of parameters

TABLE 1

**List of technical and operational EESS parameters for passive sensors**

| |
|---|
| Sensor type |
| **Orbit parameters** |
| Altitude |
| Inclination |
| Eccentricity |
| Repeat period |
| **Sensor antenna parameters** |
| Number of beams |
| Reflector diameter |
| Maximum antenna gain |
| Polarization |
| –3 dB beamwidth |
| Instantaneous field of view |
| Off-nadir pointing angle |
| Incidence angle at Earth |

TABLE 1 (*end*)

| –3 dB beam dimensions |
| Swath width |
| Main beam efficiency |
| Beam dynamics |
| Sensor antenna pattern |
| Cold calibration antenna gain |
| Cold calibration horizontal angle (degrees relative to satellite track) |
| Cold calibration vertical angle (degrees relative to nadir direction) |
| **Sensor receiver parameters** |
| Sensor integration time |
| Channel bandwidth |
| Horizontal resolution |
| Vertical resolution |

TABLE 2

**Definitions of parameters**

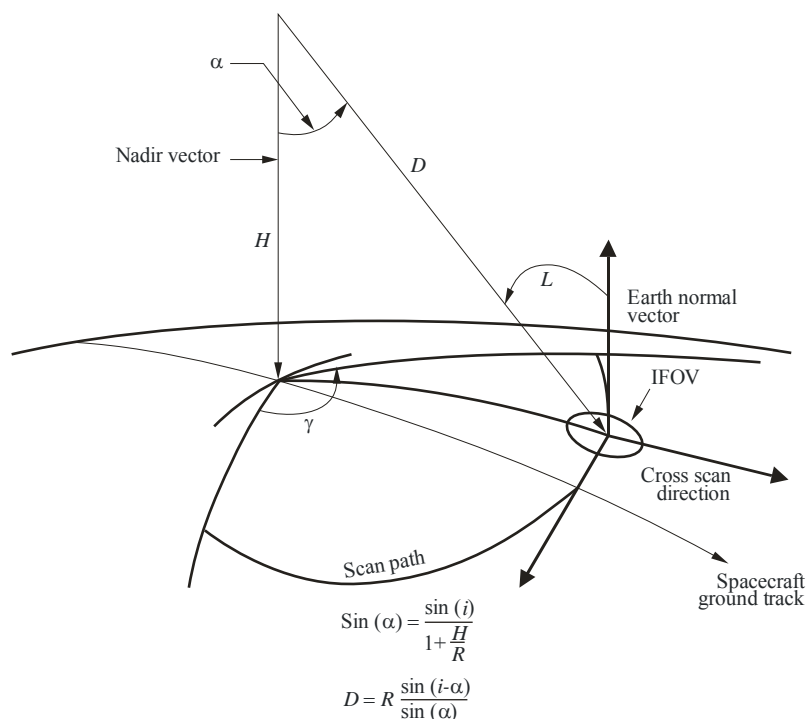| Parameter | Definition |
|---|---|
| Sensor type | Various types of radiometers are possible depending on the technology of the radiometer: interferometric radiometer, conical scan, nadir, push-broom, limb radiometer |
| **Orbit parameters** | |
| Altitude | The height above the mean sea level |
| Inclination | Angle between the equator and the plane of the orbit |
| Eccentricity | The ratio of the distance between the foci of the (elliptical) orbit to the length of the major axis |
| Repeat period | The time for the footprint of the antenna beam to return to (approximately) the same geographic location |
| **Sensor antenna parameters** Antenna characteristics vary among sensors. Measured antenna patterns are provided in § 6, where available. A reference radiation pattern is currently being developed for use in other cases | |
| Number of beams | The number of beams is the number of locations on Earth from which data are acquired at one time |
| Reflector diameter | Diameter of the antenna reflector |
| Maximum antenna gain | The maximum antenna gain can be the real one, or, if it is not known, it can be computed using the antenna efficiency η and $D$ diameter of the reflector (when applicable), with the formula: $$\text{Maximum\_antenna\_gain} = \eta\left(\pi\frac{D}{\lambda}\right)^2$$ |
| Polarization | Specification of linear or circular polarization |
| −3 dB beamwidth | The −3 dB beamwidth, $\theta_{3dB}$, is defined as the angle between the two directions in which the radiation intensity is one-half the maximum value |

TABLE 2 (*end*)

| Parameter | Definition |
|---|---|
| Instantaneous field of view | The instantaneous field of view (IFOV) is the area over which the detector is sensitive to radiation. By knowing the altitude of the satellite, the dimension of the IFOV can be calculated on the Earth's surface at the nadir point: the IFOV is generally expressed in km × km. The IFOV is a measure of the size of the resolution element.<br><br>In a scanning system the IFOV refers to the solid angle subtended by the detector when the scanning motion is stopped. For conical scan radiometers, two values are usually computed:<br>– along-track: in the direction of the platform motion (along the in-track direction);<br>– cross-track: in the direction orthogonal to the motion of the sensor platform.<br>For nadir scan radiometers, such as that shown in Fig. 3, the nadir IFOV = $H\theta_{3dB}$, where $H$ is the height of the satellite and $\theta_{3dB}$ is the half-power beamwidth.<br>See also Fig. 6 |
| Off-nadir pointing angle | The angle between the nadir and the pointing direction. It is the angle α in Fig. 6 |
| Incidence angle at Earth | The angle between the pointing direction and the normal to the Earth's surface. It is the angle $i$ as in Fig. 6 |
| –3 dB beam dimensions | The linear dimensions of the beam on the Earth (at the –3 dB level) |
| Swath width | The swath width is defined as the linear ground distance covered in the cross-track direction. For a scanning radiometer, it depends on the angular field of view (AFOV) or scanning angle. For a nadir radiometer, it depends on the off nadir angle. The field of view (FOV) is the total range of viewing of a sensor into the direction of the target. The cross-track component of the FOV is equivalent to the swath width |
| Main beam efficiency | The main beam area is defined as the angular size of a cone with an opening angle equal to 2.5 times the measured –3 dB beamwidth. The main beam efficiency is defined as the ratio of the energy received in the main beam to the energy received in the complete antenna pattern |
| Beam dynamics | The beam dynamics is defined as follows:<br>– For conical scans, it is the rotating speed of the beam;<br>– For mechanical nadir scans, it is the number of scans per second |
| Sensor antenna pattern | Antenna gain as a function of off-axis angle |
| Cold calibration antenna gain | Antenna gain in the direction of (cold) space. This could be the maximum gain of the primary antenna or the secondary antenna |
| Cold calibration horizontal angle | Horizontal angle (degrees relative to satellite track) of the cold calibration measurement. This angle is measured in the tangent plane relative to the along-track direction |
| Cold calibration vertical angle | Vertical angle (degrees relative to nadir direction) of the cold calibration measurement. This angle is measured out from the tangent plane |
| **Sensor receiver parameters** | |
| Sensor integration time | The *sensor integration time* corresponds to the short period of time allocated for the radiative measurement of the instantaneous area of observation by the detector of a sensor |
| Channel bandwidth | The *channel bandwidth* is the range of frequencies around a centre frequency used by the passive sensor |
| **Measurement spatial resolution** | |
| Horizontal resolution | The *spatial resolution* is often defined as the ability to distinguish between two closely spaced objects on an image. It is generally expressed in both horizontal (usually cross-track IFOV size) and vertical (along-track) resolutions. (Note that "vertical", in this sense, does not refer to altitude.) |
| Vertical resolution | |

FIGURE 6

**Scanning configuration**



$$\text{Sin}\,(\alpha) = \frac{\sin\,(i)}{1 + \dfrac{H}{R}}$$

$$D = R\,\frac{\sin\,(i\text{-}\alpha)}{\sin\,(\alpha)}$$

*i*: incidence angle at footprint centre
α: angle off nadir
γ: total scan angle
*H*: height above mean sea level
*D*: distance to field of view centre
*R*: radius of Earth (not shown in diagram)

1861-06

Note that the field of view's projection on the Earth's surface becomes elliptical due to the increased incidence angle from nadir to the edge of the swath width (half swath).

# 6 Parameters of typical systems

This section provides typical parameters of passive sensors for EESS (passive) bands between 1 GHz and 275 GHz. Table 3 lists the EESS (passive) bands and the section in this text that contains the passive sensor parameters for each band. A consistent set of parameters is used for each band to support worst-case static analyses and dynamic analyses to determine interference levels into passive sensors.

TABLE 3

**List of EESS (passive) bands**

| EESS (passive) band | Section (§) containing passive sensor parameters |
|---|---|
| 1 400-1 427 MHz | 6.1 |
| 6 425-7 250 MHz | 6.2 |
| 10.6-10.7 GHz | 6.3 |
| 18.6-18.8 GHz | 6.4 |
| 21.2-21.4 GHz | 6.5 |
| 23.6-24 GHz | 6.6 |
| 31.3-31.8 GHz | 6.7 |
| 36-37 GHz | 6.8 |
| 50.2-50.4 GHz | 6.9 |
| 52.6-54.25 GHz | 6.10 |
| 54.25-59.3 GHz | 6.11 |
| 86-92 GHz | 6.12 |
| 114.25-122.25 GHz | 6.13 |
| 148.5-151.5 GHz | 6.14 |
| 155.5-158.5 GHz | 6.15 |
| 164-167 GHz | 6.16 |
| 174.8-191.8 GHz | 6.17 |

## 6.1      Typical parameters of passive sensors operating in the 1 400-1 427 MHz band

Frequencies near 1 400 MHz are ideal for measuring soil moisture, and also for measuring sea surface salinity and vegetation biomass. Soil moisture is a key variable in the hydrologic cycle with significant influence on evaporation, infiltration and runoff. In the vadose zone[1], soil moisture governs the rate of water uptake by vegetation. Sea surface salinity has an influence on deep thermohaline circulation and the meridional heat transport. Variations in salinity influence the near surface dynamics of tropical oceans. To date, there is no capability to measure soil moisture and sea surface salinity directly on a global basis, so the protection of this passive band is essential.

Some remote sensing missions will collect soil moisture data in the entire passive microwave band under consideration from 1 400 to 1 427 MHz. Others will use the same band to collect measurements of ocean salinity with the goal of observing and modelling the processes that relate sea surface salinity variations to climatic changes in the hydrologic cycle, and to understand how these variations influence the general ocean circulation. Still other missions will use a different technological approach and will measure both soil moisture and ocean salinity.

Table 4 provides the characteristics and parameters of sensors on these missions.

---

[1]   The "vadose zone" is the portion of Earth between the land surface and the zone of saturation which extends from the top of the ground surface to the water table.

TABLE 4

**EESS (passive) sensor characteristics in the 1 400-1 427 MHz band**

|  | **Sensor A1** | **Sensor A2** | **Sensor A3** |
|---|---|---|---|
| Sensor type | Interferometric radiometer | Conical scan | Push broom |
| **Orbit parameters** | | | |
| Altitude | 757 km | 670 km | 657 km |
| Inclination | 98° | | |
| Eccentricity | 0 | | |
| Repeat period | 3 days | 3 days | 7 days |
| **Sensor antenna parameters** | | | |
| Number of beams | 1 | 1 | 3 |
| Reflector diameter | N/A | 6.2 m | 2.5 m |
| Maximum beam gain | 9 dBi | 37 dBi | 29.1, 28.8, 28.5 dBi |
| Polarization | V, H | | |
| –3 dB beamwidth | 71.6° | 2.6° | 6.1°, 6.3°, 6.6° |
| Off-nadir pointing angle | 25° | 35.5° | 25.8°, 33.8°, 40.3° |
| Beam dynamics | Fixed | 14.6 rpm | Fixed |
| Incidence angle at Earth | 2°/48° | 39.9° | 28.7°, 37.8°, 45.6° |
| –3 dB beam dimensions | 50 km (35 km centre of FOV) | 50.1 × 38.5 km | 94 × 76 km, 120 × 84 km 156 × 97 km |
| Instantaneous field of view | 756 km | Same as –3 dB dimensions, above | |
| Main beam efficiency | N/A | 91% | 94%, 92.4%, 90.4% |
| Swath width | 1 000 km | 1 000 km | 407 km |
| Sensor antenna pattern | Fig. 7a | Fig. 7b | Fig. 7c |
| Cold calibration ant. gain | N/A | | |
| Cold calibration angle (degrees re. satellite track) | N/A | | |
| Cold calibration angle (degrees re. nadir direction) | N/A | | |
| **Sensor receiver parameters** | | | |
| Sensor integration time | 1.2 s | 84 ms | 6 s |
| Channel bandwidth | 27 MHz | | 26 MHz |
| **Measurement spatial resolution** | | | |
| Horizontal resolution | 40 km | 39 km | 64, 75, 90 km |
| Vertical resolution | N/A | | |

FIGURE 7a

**Sensor A1 antenna pattern for the 1 400-1 427 MHz band**
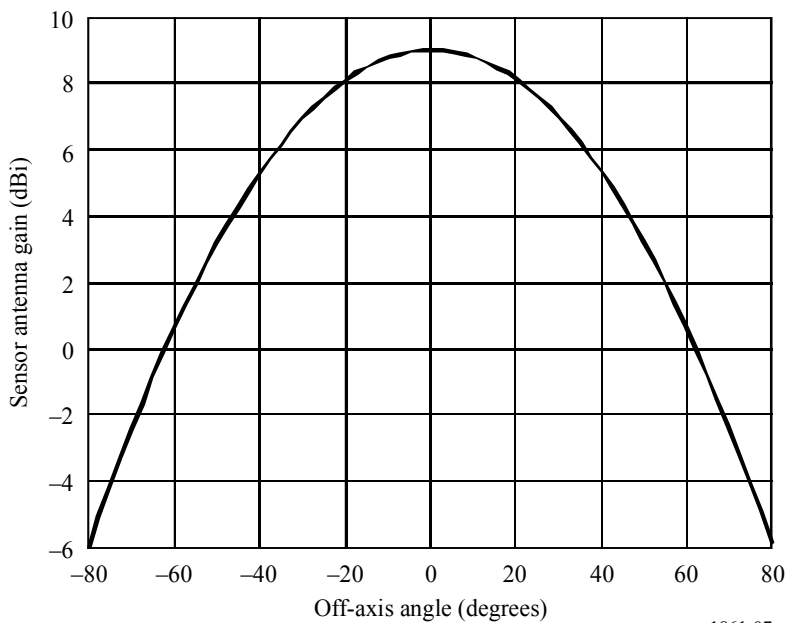


1861-07a

FIGURE 7b

**Sensor A2 antenna patterns for the 1 400-1 427 MHz band**



Φ = 0° cut
Φ = 90° cut
XPol

1861-07b

FIGURE 7c

**Sensor A3 antenna patterns for the 1 400-1 427 MHz band**
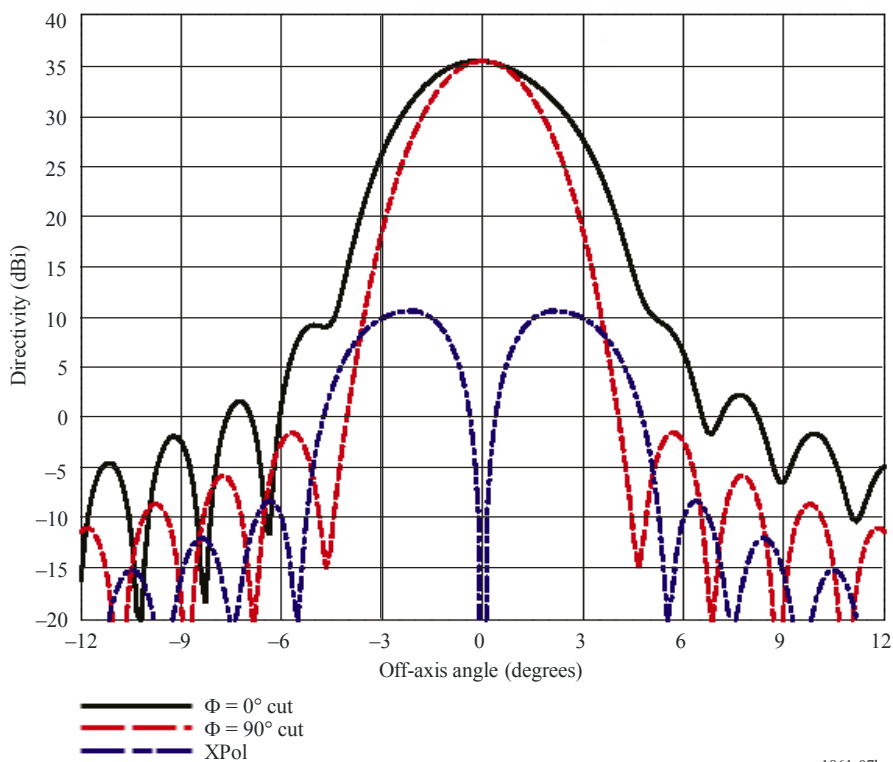


1861-07c
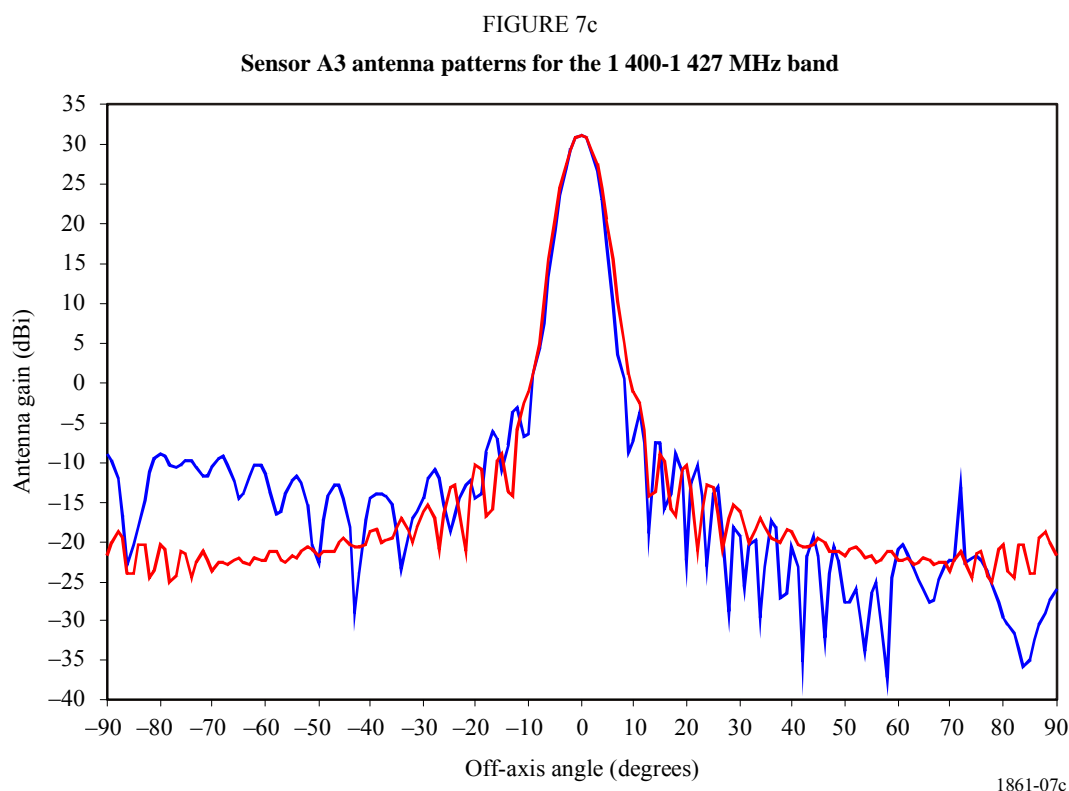
## 6.2 Typical parameters of passive sensors operating in the 6.425-7.25 GHz band

The 6-7 GHz band channel is essential for observing global soil moisture, global sea surface temperature, temperature of sea ice and sea surface wind through cloud, in combination with other channels.

In measurement of soil moisture, measurement in higher frequencies is strongly influenced by vegetation and the atmosphere, and the 6-7 GHz band is the most suitable for relatively higher spatial resolution measurements. In the case of measurement of sea surface temperature, measurement in higher frequencies is strongly influenced by the atmosphere and lower temperature is more difficult to measure in higher frequencies, making the 6-7 GHz band the most suitable.

Table 5 summarizes the parameters of passive sensors that are or will be operating in the 6.425-7.25 GHz band.

## 6.3 Typical parameters of passive sensors operating in the 10.6-10.7 GHz band

The band 10.6-10.7 GHz is of primary interest to measure rain, snow, sea state, and ocean wind. Table 6 summarizes the parameters of passive sensors that are or will be operating in the 10.6-10.68 GHz band.

TABLE 5

**EESS (passive) sensor characteristics in the 6.425-7.25 GHz band**

| | Sensor B1 | Sensor B2 | Sensor B3 | Sensor B4 |
|---|---|---|---|---|
| Sensor type | Conical scan | | | |
| **Orbit parameters** | | | | |
| Altitude | 705 km | 828 km | 835 km | 699.6 km |
| Inclination | 98.2° | 98.7° | 98.85° | 98.186° |
| Eccentricity | 0.0015 | 0 | 0 | 0.002 |
| Repeat period | 16 days | 17 days | N/A | 16 days |
| **Sensor antenna parameters** | | | | |
| Number of beams | 1 | | | |
| Reflector diameter | 1.6 m | 2.2 m | 0.6 m | 2.0 m |
| Maximum beam gain | 38.8 dBi | | | 40.6 dBi |
| Polarization | V, H | | | |
| –3 dB beamwidth | 2.2° | 1.65° | | 1.8° |
| Off-nadir pointing angle | 47.5° | 46.8° | 55.4° | 47.5° |
| Beam dynamics | 40 rpm | 31.6 rpm | 2.88 s scan period | 40 rpm |
| Incidence angle at Earth | 55° | 55.7° | 65° | 55° |
| –3 dB beam dimensions | 40 km (cross-track) | 24 km | | 35 km (cross-track) |
| Instantaneous field of view | 43 km × 75 km | 68 km × 40 km | 112 km × 260 km | 35 km × 61 km |
| Main beam efficiency | 95.1% | 95% | | 92% |
| Swath width | 1 450 km | 1 700 km | 2 000 km | 1 450 km |
| Sensor antenna pattern | See Rec. ITU-R RS.1813 | | | |
| Cold calibration ant. gain | 25.1 dBi | N/A | | 25.6 dBi |
| Cold calibration angle (degrees re. satellite track) | 115.5º | N/A | | 115.5º |
| Cold calibration angle (degrees re. nadir direction) | 97.0º | N/A | | 97.0º |
| **Sensor receiver parameters** | | | | |
| Sensor integration time | 2.5 ms | 5 ms | N/A | 2.5 ms |
| Channel bandwidth | 350 MHz centred at 6.925 GHz | 350 MHz centred at 6.625 GHz | 350 MHz centred at 6.9 GHz | 350 MHz centred at 6.925 GHz and at 7.3 GHz |
| **Measurement spatial resolution** | | | | |
| Horizontal resolution | 43 km | 15-50 km | 38 km | 35 km |
| Vertical resolution | 74 km | 24 km | 38 km | 61 km |

TABLE 6

**EESS (passive) sensor characteristics in the 10.6-10.7 GHz band**

|  | **Sensor C1** | **Sensor C2** | **Sensor C3** | **Sensor C4** | **Sensor C5** |
|---|---|---|---|---|---|
| Sensor type | Conical scan | | | | |
| **Orbit parameters** | | | | | |
| Altitude | 817 km | 705 km | 833 km | 835 km | 699.6 km |
| Inclination | 98° | 98.2° | 98.7° | 98.85° | 98.186° |
| Eccentricity | 0 | 0.0015 | 0 | 0 | 0.002 |
| Repeat period | N/A | 16 days | 17 days | N/A | 16 days |
| **Sensor antenna parameters** | | | | | |
| Number of beams | 1 | | 2 | 1 | |
| Reflector diameter | 0.9 m | 1.6 m | 2.2 m | 0.6 m | 2.0 m |
| Maximum beam gain | 36 dBi | 42.3 dBi | 45 dBi | 36 dBi | 44.1 dBi |
| Polarization | H, V | | H, V, R, L | H, V | |
| –3 dB beamwidth | 2.66° | 1.4° | 1.02° | 3.28° | 1.2° |
| Instantaneous field of view | 56 km × 30 km | 51 km × 29 km | 48 km × 28 km | 76 km × 177 km | 41 km × 21 km |
| Main beam efficiency | | 94.8% | 95% | | 93% |
| Off-nadir pointing angle | 44.3° | 47.5° | 47° | 55.4° | 47.5° |
| Beam dynamics | 20 rpm | 40 rpm | 31.6 rpm | 2.88 s scan period | 40 rpm |
| Incidence angle at Earth | 52° | 55° | 58.16° | 65° | 55° |
| –3 dB beam dimensions | 56.7 km (cross-track) | 27.5 km (cross-track) | 42.9 km (cross-track) | N/A | 23 km (cross-track) |
| Swath width | 1 594 km | 1 450 km | 1 600 km | 2 000 km | 1 450 km |
| Sensor antenna pattern | See Rec. ITU-R RS.1813 | Fig. 8a | Fig. 8b | See Rec. ITU-R RS.1813 | |
| Cold calibration ant. gain | N/A | 29.1 dBi | N/A | | 29.6 dBi |
| Cold calibration angle (degrees re. satellite track) | N/A | 115.5º | N/A | | 115.5º |
| Cold calibration angle (degrees re. nadir direction) | N/A | 97.0º | N/A | | 97.0º |
| **Sensor receiver parameters** | | | | | |
| Sensor integration time | 1 ms | 2.5 ms | 2.47 ms | N/A | 2.5 ms |
| Channel bandwidth | 100 MHz | 100 MHz centred at 10.65 GHz | | | |
| **Measurement spatial resolution** | | | | | |
| Horizontal resolution | 38 km | 27 km | 15 km | 38 km | 23 km |
| Vertical resolution | 38 km | 47 km | 15 km | 38 km | 41 km |

FIGURE 8a

**Sensor C1 antenna pattern envelope for the 10.6-10.7 GHz band**
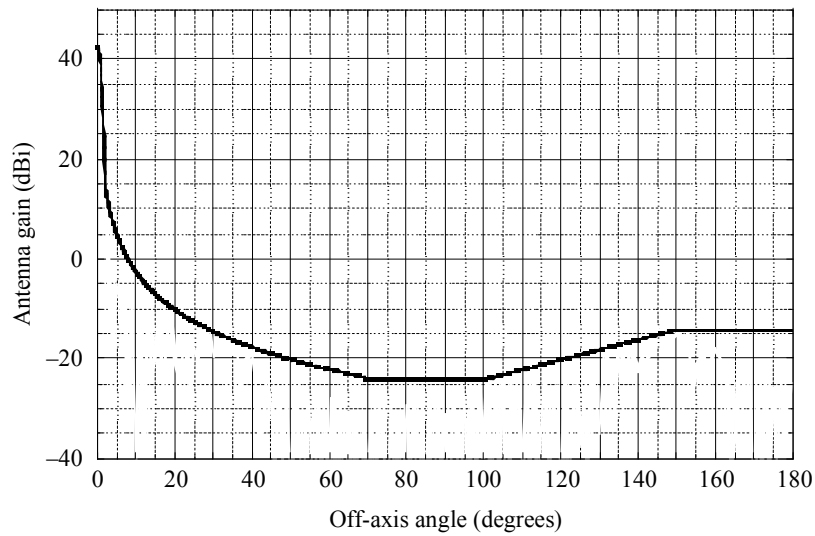


1861-08a

FIGURE 8b

**Sensor C2 antenna pattern envelope for the 10.6-10.7 GHz band**
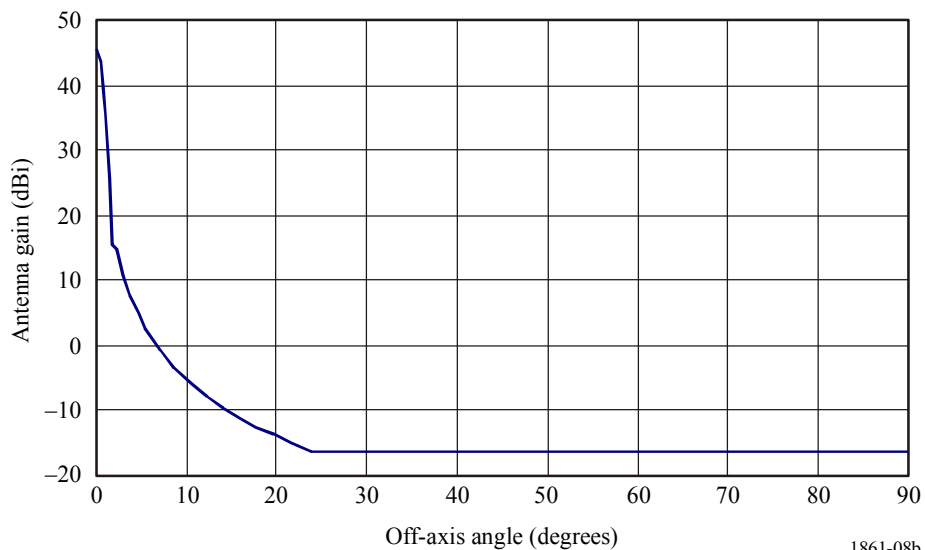


1861-08b

## 6.4     Typical parameters of passive sensors operating in the 18.6-18.8 GHz band

The 18.6-18.8 GHz band is essential for observing global rain rates, sea state, sea ice, water vapour, ocean wind speed, soil emissivity, and humidity. Table 7 summarizes the parameters of passive sensors that are or will be operating in the 18.6-18.8 GHz band.

TABLE 7

**EESS (passive) sensor characteristics in the 18.6-18.8 GHz band**

| | Sensor D1 | Sensor D2 | Sensor D3 | Sensor D4 | Sensor D5 |
|---|---|---|---|---|---|
| Sensor type | Conical scan | | | | |
| **Orbit parameters** | | | | | |
| Altitude | 828 km | 705 km | 865.6 km | 835 km | 699.6 km |
| Inclination | 98.7° | 98.2° | 20° | 98.85° | 98.186° |
| Eccentricity | 0 | 0.0015 | 0 | 0 | 0.002 |
| Repeat period | 17 days | 16 days | 7 days | | 16 days |
| **Sensor antenna parameters** | | | | | |
| Number of beams | 3 | 1 | | 1 | |
| Reflector diameter | 2.2 m | 1.6 m | 0.65 m | 0.6 m | 2.0 m |
| Maximum beam gain | | 47.6 dBi | | | 49.4 dBi |
| Polarization | V, H, LHC, RHC, +45°, −45° | V, H | | | |
| −3 dB beamwidth | 0.64° | 0.8° | 0.67° | 1.9° | 0.65° |
| Instantaneous field of view | 24 km × 15.5 km | 27 km × 16 km | 10 km | 45 km × 104 km | 22 km × 13 km |
| Main beam efficiency | 95% | 95.8% | 96% | | 94% |
| Off-nadir pointing angle | 46.6° | 47.5° | 44.5° | 55.4° | 47.5° |
| Beam dynamics | 31.6 rpm | 40 rpm | 20 rpm | 2.88 s scan period | 40 rpm |
| Incidence angle at Earth | 53.6° | 55.0° | 52.3° | 65° | 55.0° |
| −3 dB beam dimensions | 9 km | 13 km (cross-track) | 10 km | 28 km | 16 km (cross-track) |
| Swath width | 1 700 km | 1 450 km | | 2 000 km | 1 450 km |
| Sensor antenna pattern | See Rec. ITU-R RS.1813 | | | | |
| Cold calibration ant. gain | N/A | 32.8 dBi | N/A | | 33.9 dBi |
| Cold calibration angle (degrees re. satellite track) | N/A | 115.5º | N/A | | 115.5º |
| Cold calibration angle (degrees re. nadir direction) | N/A | 97.0º | N/A | | 97.0º |
| **Sensor receiver parameters** | | | | | |
| Sensor integration time | 1.2 ms | 2.5 ms | N/A | | 2.5 ms |
| Channel bandwidth | 200 MHz centred at 18.7 GHz | | N/A | 200 MHz centred at 18.7 GHz | |
| **Measurement spatial resolution** | | | | | |
| Horizontal resolution | 9 km | 16 km | 40 km | 38 km | 13 km |
| Vertical resolution | 9 km | 27 km | 40 km | 38 km | 22 km |

### 6.5        Typical parameters of passive sensors operating in the 21.2-21.4 GHz band

The 21.2-21.4 GHz band in addition to the 23.6-24 GHz band are used for measurements of water vapour and liquid water both on the Earth's surface and in the atmosphere. They are on either side of the 22.235 GHz water-vapour spectral line. Atmospheric measurements are used with oxygen, $O_2$, temperature measurements to remove the effect of water vapour on temperature profiles. Table 8 summarizes the parameters of passive sensors that are or will be operating in the 21.2-21.4 GHz band.

TABLE 8

**EESS (passive) sensor characterstics in the 21.2-21.4 GHz band**

|  | **Sensor E1** | **Sensor E2** |
|---|---|---|
| Sensor type | Mechanical nadir scan | Push-broom[1] |
| **Orbit parameters** | | |
| Altitude | 833 km | 850 km |
| Inclination | 98.6° | 98° |
| Eccentricity | 0 | |
| Repeat period | 9 days | |
| **Sensor antenna parameters** | | |
| Number of beams | 1 beam; 30 earth fields per 8 s scan period | 90 |
| Maximum beam gain | 34.4 dBi | 45 dBi |
| Reflector diameter | 0.3 m | 0.9 m |
| Polarization | V | H, V |
| −3 dB beamwidth | 3.3° | 1.1° |
| Instantaneous field of view | Nadir FOV: 48.5 km<br>Outer FOV: 149.1 × 79.4 km | 16 km × 2 282 km |
| Main beam efficiency | 95% | |
| Off-nadir pointing angle | ±48.33° cross-track | |
| Beam dynamics | 8 s scan period | N/A (beams are unchanging) |
| Incidence angle at Earth | | |
| −3 dB beam dimensions | 45 km | 16 km |
| Total FOV cross/along-track | Outer FOV: 149.1 × 79.4 km<br>Nadir FOV: 48.5 km | 100/1.1° |
| Swath width | 2 343 km | 2 282 km |
| Sensor antenna pattern | −10 dBi back lobe gain | −12 dBi back lobe gain |

[1]   Push-broom is a concept that has not yet been implemented at this frequency.

TABLE 8 (*end*)

|  | **Sensor E1** | **Sensor E2** |
|---|---|---|
| **Sensor antenna parameters (*cont.*)** | | |
| Cold calibration ant. gain | 34.4 dBi | 35 dBi |
| Cold calibration angle (degrees re. satellite track) | 90° | |
| Cold calibration angle (degrees re. nadir direction) | 83° | |
| **Sensor receiver parameters** | | |
| Sensor integration time | 158 m | N/A |
| Channel bandwidth | 270 MHz centred at 23.8 GHz | N/A |
| **Measurement spatial resolution** | | |
| Horizontal resolution | 45 km | 16 km |
| Vertical resolution | N/A | 16 km |

## 6.6 Typical parameters of passive sensors operating in the 23.6-24 GHz band

In case of a sounder, passive measurements around frequencies 23.8 GHz (total water vapour content), 31.5 GHz (window channel) and 90 GHz (liquid water) provide auxiliary data which play a predominant role in the retrieval process of temperature measurements performed in the $O_2$ absorption spectrum. These auxiliary measurements must have radiometric and geometric performances and availability criteria consistent with those of the temperature measurements. In case of a conical scanning radiometer, it is possible to measure horizontal water vapour distribution with other channels. The main characteristics of the sensors are given in Table 9.

TABLE 9

**EESS (passive) sensor characteristics in the 23.6-24 GHz band**

| | Sensor F1 | Sensor F2 | Sensor F3 | Sensor F4 | Sensor F5 | Sensor F6 | Sensor F7 | Sensor F8 |
|---|---|---|---|---|---|---|---|---|
| Sensor type | Conical scan | | | Mechanical nadir scan | | Conical scan | Push-broom | Conical scan |
| **Orbit parameters** | | | | | | | | |
| Altitude | 817 km | 705 km | 828 km | 833 km 822 km* | 824 km | 835 km | 850 km | 699.6 km |
| Inclination | 20° | 98.2° | 98.7° | 98.6° 98.7°* | 98.7° | 98.85° | 98° | 98.186° |
| Eccentricity | 0 | 0.0015 | 0 | 0 0.001 | 0 | | | 0.002 |
| Repeat period | 7 days | 16 days | 17 days | 9 days 29 days* | 9 days | | | 16 days |
| **Sensor antenna parameters** | | | | | | | | |
| Number of beams | 1 | | | 30 earth fields per 8 s scan period | 2 | 1 | 90 | 1 |
| Reflector diameter | 0.6 m | 1.6 m | 2.2 m | 0.3 m 0.274 m* | 0.203 m | 0.6 m | 0.9 m | 48.5 dBi |
| Maximum beam gain | 40 dBi | 46.7 dBi | 52 dBi | 34.4 dBi | 30.4 dBi | 43 dBi | 45 dBi | 2.0 m |
| Polarization | H, V | | | V QV* | QV | H, V | | H, V |
| −3 dB beamwidth | 1. 81° | 0.9° | 0.64° | 3.3° | 5.2° | 1.5° | 1.1° | 0.75° |
| Instantaneous field of view | 63 km × 38 km | 32 km × 18 km | 18 km × 12 km | Nadir FOV: 48.5 km Outer FOV: 149.1 × 79.4 km 147 × 79 km* | Nadir FOV: 74.8 km Outer FOV: 323.1 × 141.8 km | 36 km × 86 km | 16 km × 2 282 km | 26 km × 15 km |
| Main beam efficiency | 96% | 94.8% | 95% | | | | | 94% |
| Off-nadir pointing angle | 44.5° | 47.5° | 46.6° | ±48.33° cross-track | ±52.725° cross-track | 55.4° | | 47.5° |

TABLE 9 (*end*)

| | Sensor F1 | Sensor F2 | Sensor F3 | Sensor F4 | Sensor F5 | Sensor F6 | Sensor F7 | Sensor F8 |
|---|---|---|---|---|---|---|---|---|
| **Sensor antenna parameters (*cont.*)** | | | | | | | | |
| Beam dynamics | 31.9 rpm | 40 rpm | 31.6 rpm | 8 s scan period | 8/3 s scan period cross-track; 96 earth fields per scan period | 2.88 s scan period | 90 resolution elements/ line | 40 rpm |
| Incidence angle at Earth | 52.3° | 55° | 53.63° | 0° (nadir) 57.5°* | | 65° | | 55° |
| −3 dB beam dimensions | 38.7 km (cross-track) | 18 km (cross-track) | 14.1 km (cross-track) | 45 km 48 km* | 76 km | 22 km | 16 km | 15 km (cross-track) |
| Swath width | 1 607 km | 1 450 km | 1 688 km | 2 343 km 2 186 km* | 2 503 km | 2 000 km | 2 282 km | 1 450 km |
| Sensor antenna pattern | See Rec. ITU-R RS.1813 | Fig. 9b | See Rec. ITU-R RS.1813 | Fig. 9c | See Rec. ITU-R RS.1813 | | −12 dBi back lobe gain | See Rec. ITU-R RS.1813 |
| Cold calibration ant. gain | N/A | 32.1 dBi | N/A | 34.4 dBi | 30.4 dBi | N/A | 35 dBi | 32.4 dBi |
| Cold calibration angle (degrees re. satellite track) | N/A | 115.5° | N/A | 90° −90° ± 3.9°* | 0 | N/A | 90° | 115.5° |
| Cold calibration angle (degrees re. nadir direction) | N/A | 97.0° | N/A | 83° | 82.175° | N/A | 83° | N/A |
| **Sensor receiver parameters** | | | | | | | | |
| Sensor integration time | 1 ms | 2.5 ms | 1.2 ms | 158 ms | 18 ms | N/A | | 2.5 ms |
| Channel bandwidth | 400 MHz | 400 MHz centred at 23.8 GHz | | 270 MHz centred at 23.8 GHz | | 400 MHz centred at 23.8 GHz | N/A | 400 MHz centred at 23.8 GHz |
| **Measurement spatial resolution** | | | | | | | | |
| Horizontal resolution | 40 km | 18 km | 17.6 km | 45 km 48 km* | 75 km | 38 km | 16 km | 15 km |
| Vertical resolution | N/A | 30 km | N/A | 45 km 48 km* | 75 km | 38 km | 16 km | 25 km |

NOTE 1 – * Indicates that a particular sensor is flown on different missions, with different orbit and sensor parameters.

FIGURE 9a

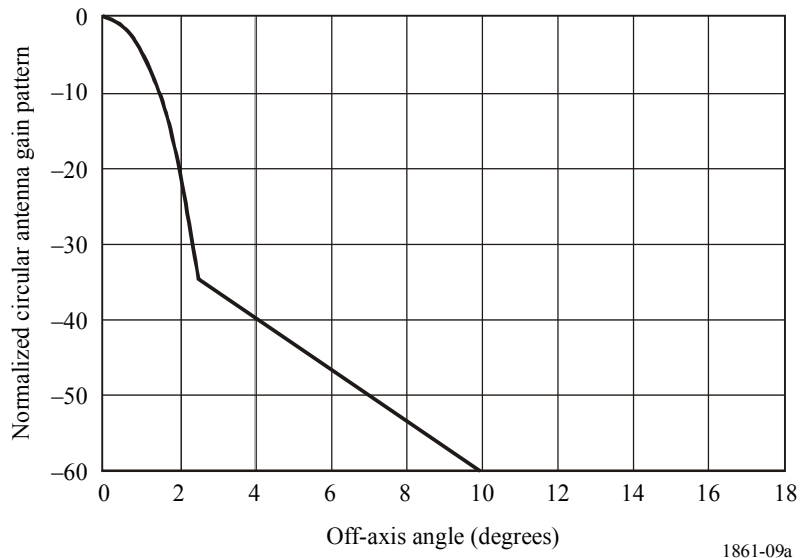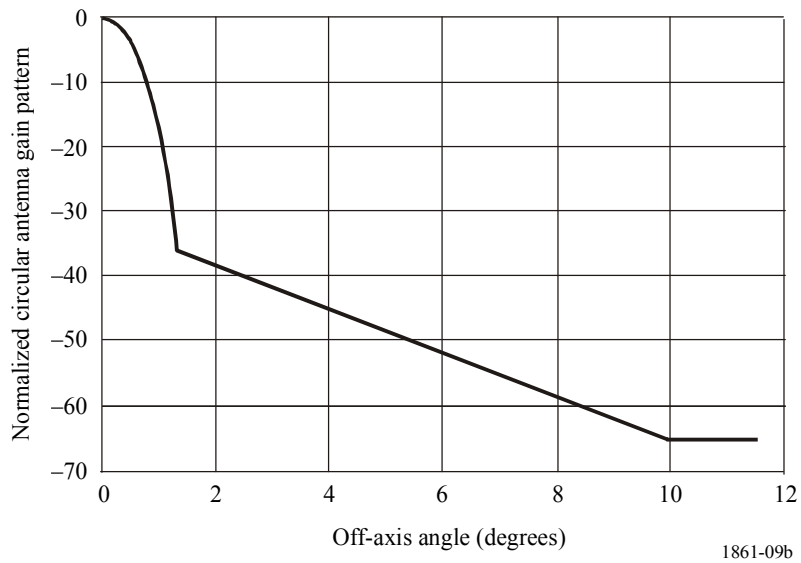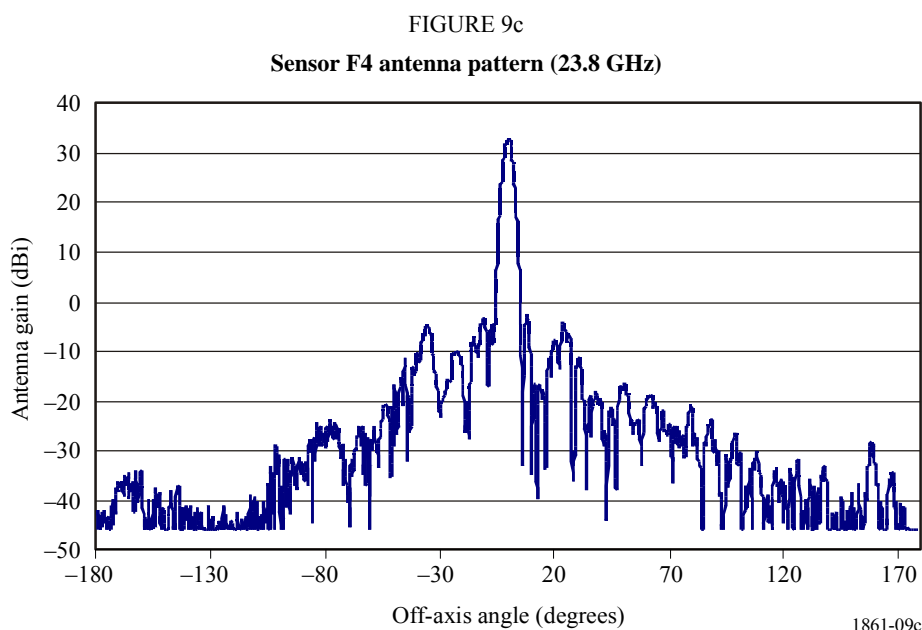**Sensor F1 antenna pattern envelope for the 23.6-24 GHz band**



1861-09a

FIGURE 9b

**Sensor F2 antenna pattern envelope for the 23.6-24 GHz band**



1861-09b

FIGURE 9c

**Sensor F4 antenna pattern (23.8 GHz)**



1861-09c

## 6.7    Typical parameters of passive sensors operating in the 31.3-31.8 GHz band

Passive measurements around frequencies 23.8 GHz (total water vapour content), 31.5 GHz (window channel) and 90 GHz (liquid water) provide auxiliary data which play a predominant role in the retrieval process of temperature measurements performed in the $O_2$ absorption spectrum. These auxiliary measurements must have radiometric and geometric performances and availability criteria consistent with those of the temperature measurements.

This band is one of the bands used for close-to-nadir atmospheric sounding in conjunction with the bands such as 23.8 GHz and 50.3 GHz for the characterization each layer of the Earth's atmosphere. The 31.3-31.5 GHz band will also be used in conjunction with the band 31.5-31.8 GHz as a "split window". This will allow a comparison of the measurements conducted in the two sub-bands to check the quality of the data. This will then allow using the full band when the quality is expected good to increase the sensitivity of the sensor.

Table 10 summarizes the parameters of passive sensors that are or will be operating in the 31.3-31.8 GHz band.

TABLE 10

**EESS (passive) sensor characteristics in the 31.3-31.8 GHz band**

|  | **Sensor G1** | **Sensor G2** | **Sensor G3** |
|---|---|---|---|
| Sensor type | Nadir scan | | Conical scan |
| **Orbit parameters** | | | |
| Altitude | 833 km<br>822 km* | 824 km | 835 km |
| Inclination | 98.6° | 98.7° | 98.85° |
| Eccentricity | 0.001 | 0 | 0 |
| Repeat period | 9 days<br>29 days* | 9 days | |

TABLE 10 (*end*)

| | Sensor G1 | Sensor G2 | Sensor G3 |
|---|---|---|---|
| **Sensor antenna parameters** | | | |
| Number of beams | 30 earth fields per 8 s scan period | 2 | 1 |
| Maximum beam gain | 34.4 dBi | 30.4 dBi | 45 dBi |
| Reflector diameter | 0.30 m<br>0.274 m* | 0.203 m | 0.6 m |
| Polarization | V<br>QV* | QV | H, V |
| –3 dB beamwidth | 3.3° | 5.2° | 1.1° |
| Off-nadir pointing angle | ±48.33° cross-track | ±52.725° cross-track | 55.4° |
| Beam dynamics | 8 s scan period | 8/3 s scan period cross-track; 96 earth fields per scan period | 2.88 s scan period |
| Incidence angle at Earth | 0<br>57.5°* | 0 | 65° |
| –3 dB beam dimensions | 49.1 km | 75 km | 16 km |
| Instantaneous field of view | Nadir FOV: 48.5 km<br>Outer FOV: 149.1 × 79.4 km<br>147 × 79 km* | Nadir FOV: 74.8 km<br>Outer FOV: 323.1.1 × 141.8 km | 30 km × 69 km |
| Main beam efficiency | 95% | | |
| Swath width | 2 343 km<br>2 186 km* | 2 500 km | 2 000 km |
| Sensor antenna pattern | See Rec. ITU-R RS.1813 | | |
| Cold calibration ant. gain | 34.4 dBi | 30.4 dBi | N/A |
| Cold calibration angle (degrees re. satellite track) | 90°<br>−90° ± 3.9°* | 0 | N/A |
| Cold calibration angle (degrees re. nadir direction) | 83.33° | 82.175° | N/A |
| **Sensor receiver parameters** | | | |
| Sensor integration time | 158 ms | 18 ms | N/A |
| Channel bandwidth | 180 MHz centred at 31.4 GHz | | 0.5 GHz |
| **Measurement spatial resolution** | | | |
| Horizontal resolution | 44 km<br>48 km* | 75 km | 38 km |
| Vertical resolution | 44 km<br>48 km* | 75 km | 38 km |

NOTE 1 – * Indicates that a particular sensor is flown on different missions, with different orbit and sensor parameters.

## 6.8 Typical parameters of passive sensors operating in the 36-37 GHz band

The band 36-37 GHz is vital for the study of global water circulation, rain rates, snow, sea ice, and clouds. Table 11 summarizes the parameters of passive sensors that are or will be operating in the 36-37 GHz band.

TABLE 11

**EESS (passive) sensor characteristics in the 36-37 GHz band**

|  | Sensor H1 | Sensor H2 | Sensor H3 | Sensor H4 | Sensor H5 |
|---|---|---|---|---|---|
| Sensor type | Conical scan | | | | |
| **Orbit parameters** | | | | | |
| Altitude | 865.6 km | 705 km | 828 km | 835 km | 699.6 km |
| Inclination | 20° | 98.2° | 98.7° | 98.85° | 98.186° |
| Eccentricity | 0 | 0.0015 | 0 | 0 | 0.002 |
| Repeat period | 7 days | 16 days | 17 days |  | 16 days |
| **Sensor antenna parameters** | | | | | |
| Number of beams | | | 2 | 1 | |
| Reflector diameter | 0.65 m | 1.6 m | 2.2 m | 0.6 m | 2.0 m |
| Maximum beam gain | 45 dBi | 53.1 dBi | 55 dBi | 46 dBi | 54.8 dBi |
| Polarization | H | H, V | | | |
| −3 dB beamwidth | 1.8° | 0.42° | 0.44° | 1° | 0.35° |
| Instantaneous field of view | 62 km × 38 km | 14 km × 8 km | 16 km × 12 km | 26 km × 60 km | 12 km × 7 km |
| Main beam efficiency | 96% | 93.9% | 95% |  | 93% |
| Off-nadir pointing angle | 44.5° | 47.5° | 46.8° | 55.4° | 47.5° |
| Beam dynamics | 31.9 rpm | 40 rpm | 31.6 rpm | 2.88 s scan period | 40 rpm |
| Incidence angle at Earth | 52.3° | 55° | 55.7° | 65° | 55° |
| −3 dB beam dimensions | 38 km (cross-track) | 8.2 km (cross-track) | 12 km (cross-track) | 15 km | 6.8 km (cross-track) |
| Swath width | 1 607 km | 1 450 km | 1 700 km | 2 000 km | 40 rpm |
| Sensor antenna pattern | See Rec. ITU-R RS.1813 | See Fig. 10 | See Rec. ITU-R RS.1813 | | |
| Cold calibration ant. gain | N/A | 36.5 dBi | N/A | | 39.3 dBi |
| Cold calibration angle (degrees re. satellite track) | N/A | 115.5º | N/A | | 115.5º |
| Cold calibration angle (degrees re. nadir direction) | N/A | 97.0 | N/A | | 97.0 |

TABLE 11 (*end*)

|                                | Sensor H1 | Sensor H2 | Sensor H3 | Sensor H4 | Sensor H5 |
|--------------------------------|-----------|-----------|-----------|-----------|-----------|
| **Sensor receiver parameters** |           |           |           |           |           |
| Sensor integration time        | 1 ms      | 2.5 ms    | 1.2 ms    | N/A       | 2.5 ms    |
| Channel bandwidth              | 1 GHz     | 1 GHz centred at 36.5 GHz |           |           |           |
| **Measurement spatial resolution** |       |           |           |           |           |
| Horizontal resolution          | 40 km     | 8.2 km    | 12 km     | 38 km     | 6.8 km    |
| Vertical resolution            | N/A       | 14 km     | 6 km      | 38 km     | 12 km     |

FIGURE 10

**Sensor H2 antenna pattern envelope for the 36-37 GHz band**
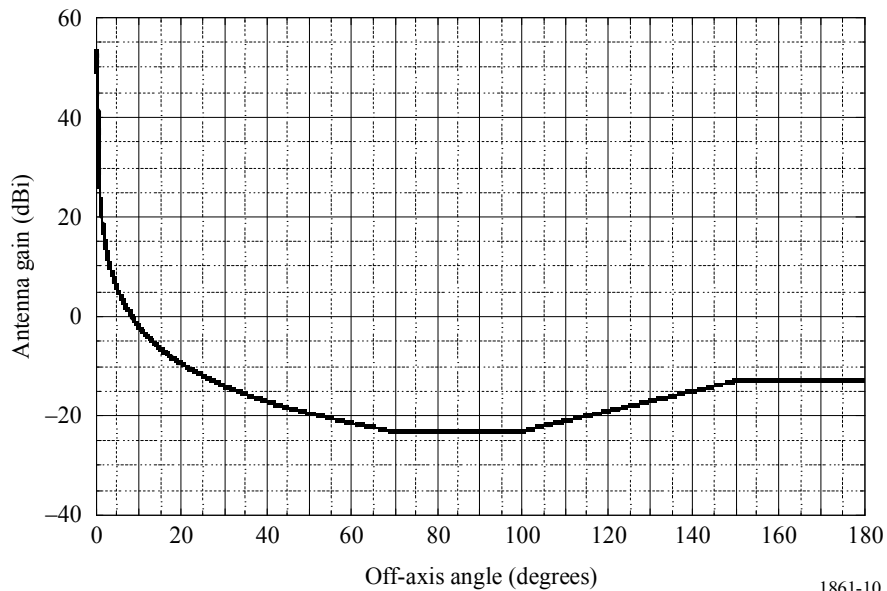


1861-10

## 6.9      Typical parameters of passive sensors operating in the 50.2-50.4 GHz band

This frequency band is one of several bands between 50 GHz and 60 GHz that are used collectively to provide three-dimensional temperature profiles of the atmosphere. Table 12 summarizes the parameters of passive sensors that are or will be operating in the 50.2-50.4 GHz band.

TABLE 12

**EESS (passive) sensor characteristics in the 50.2-50.4 GHz band**

|  | **Sensor I1** | **Sensor I2** | **Sensor I3** | **Sensor I4** |
|---|---|---|---|---|
| Sensor type | Conical scan | Mechanical nadir scan | Push-broom | Mechanical nadir scan |
| **Orbit parameters** | | | | |
| Altitude | 828 km | 833 km 822 km* | 850 km | 824 km |
| Inclination | 98.7° | 98.6° 98.7°* | 98° | 98.7° |
| Eccentricity | 0 | 0 0.001* | 0 | 0 |
| Repeat period | 17 days | 9 days 29 days* |  | 9 days |
| **Sensor antenna parameters** | | | | |
| Number of beams | 1 | 30 earth fields per 8 s scan period | 90 | 2 |
| Reflector diameter | 2.2 m | 0.15 m | 0.5 m | 0.203 m |
| Maximum beam gain |  | 34.4 dBi | 45 dBi | 37.9 dBi |
| Polarization | V | V QV* | H, V | QH |
| −3 dB beamwidth | 0.39° | 3.3° | 1.1° | 2.2° |
| Instantaneous field of view | 16 km × 12 km | Nadir FOV: 48.5 km Outer FOV: 149.1 × 79.4 km 147 × 79 km* | 16 km × 2 282 km | Nadir FOV: 31.6 km Outer FOV: 136.7 × 60 km |
| Main beam efficiency | 95% | | | 95% |
| Off-nadir pointing angle | 46.8° | ±48.33° cross-track |  | ±52.725° cross-track |
| Beam dynamics | 31.6 rpm | 8 s scan period | 90 resolution elements per swath | 8/3 s scan period cross-track; 96 earth fields per scan period |
| Incidence angle at Earth | 55.7° | 57.5° |  |  |
| −3 dB beam dimensions | 6 km | 48 km (at nadir) | 16 km (at nadir) | 2.2°32 km |
| Swath width | 1 700 km | 2 343 km 2 186 km | 2 282 km | 2 500 km |
| Sensor antenna pattern | See Rec. ITU-R RS.1813 | | | |
| Cold calibration ant. gain | N/A | 34.4 dBi | 35 dBi | 37.9 dBi |

TABLE 12 (*end*)

|  | **Sensor I1** | **Sensor I2** | **Sensor I3** | **Sensor I4** |
|---|---|---|---|---|
| **Sensor antenna parameters (*cont.*)** | | | | |
| Cold calibration angle (degrees re. satellite track) | N/A | 90° −90° ± 3.9°* | 90° | 0 |
| Cold calibration angle (degrees re. nadir direction) | N/A | 83.33° | 83° | 82.175° |
| **Sensor receiver parameters** | | | | |
| Sensor integration time | 1.2 ms | 165 ms | N/A | 18 ms |
| Channel bandwidth | 134 MHz centred at 50.3 GHz | 180 MHz centred at 50.3 GHz | N/A | 180 MHz centred at 50.3 GHz |
| **Measurement spatial resolution** | | | | |
| Horizontal resolution | 6 km | 48 km | 16 km | 32 km |
| Vertical resolution | 6 km | 48 km | 16 km | 32 km |

NOTE 1 – * Indicates that a particular sensor is flown on different missions, with different orbit and sensor parameters.

## 6.10 Typical parameters of passive sensors operating in the 52.6-54.25 GHz band

This band is one of the bands used for close-to-nadir atmospheric sounding in conjunction with the bands at 23.8 GHz, 31.5 GHz and 50.3 GHz to characterize each layer of the atmosphere.

Table 13 summarizes the parameters of passive sensors that are or will be operating in the 52.6-54.25 GHz band.

TABLE 13

**EESS (passive) sensor characteristics in the 52.6-54.25 GHz band**

|  | **Sensor J1** | **Sensor J2** | **Sensor J3** | **Sensor J4** |
|---|---|---|---|---|
| Sensor type | Mechanical nadir scan | Conical scan | Mechanical nadir scan | Conical scan |
| **Orbit parameters** | | | | |
| Altitude | 833 km 822 km* | 828 km | 824 km | 835 km |
| Inclination | 98.6° 98.7°* | 98.7° | | 98.85° |
| Eccentricity | 0 0.001* | 0 | | |
| Repeat period | 9 days 29 days* | 17 days | 9 days | N/A |
| **Sensor antenna parameters** | | | | |
| Number of beams | 30 earth fields per 8 s scan period | 1 | 2 | 1 |
| Reflector diameter | 0.15 m | 2.2 m | 0.203 m | 0.6 m |

TABLE 13 (*end*)

| | Sensor J1 | Sensor J2 | Sensor J3 | Sensor J4 |
|---|---|---|---|---|
| **Sensor antenna parameters (*cont.*)** | | | | |
| Maximum beam gain | 34.4 dBi | 54 dBi | 37.9 dBi | 39 dBi |
| Polarization | V, H QV, QH* | V | QH | V |
| –3 dB beamwidth | 3.3° | 0.39° | 2.2° | 2.2° |
| Instantaneous field of view | Nadir FOV: 48.5 km Outer FOV: 149.1 × 79.4 km 147 × 79 km* | 16 km × 12 km | Nadir FOV: 31.6 km Outer FOV: 136.7 × 60 km | Outer FOV 18 × 43 km |
| Main beam efficiency | 95% | 95% | 95% | |
| Off-nadir pointing angle | ±48.33° cross-track | 46.8° | ±52.725° cross-track | 55.4° |
| Beam dynamics | 8 s scan period | 31.6 rpm | 8/3 s scan period cross-track; 96 earth fields per scan period | 2.88 s scan period |
| Incidence angle at Earth | 0 57.5°* | 55.7° | | 65° |
| –3 dB beam dimensions | 48 km | 6 km | 32 km | 32 km |
| Swath width | 2 343 km 2 186 km* | 1 700 km | 2 500 km | 2 000 km |
| Sensor antenna pattern | See Rec. ITU-R RS.1813 | | | |
| Cold calibration ant. gain | 34.4 dBi | N/A | 37.9 dBi | N/A |
| Cold calibration angle (degrees re. satellite track) | 90° −90° ± 3.9°* | N/A | 0 | N/A |
| Cold calibration angle (degrees re. nadir direction) | 83.33° | N/A | 82.175° | N/A |
| **Sensor receiver parameters** | | | | |
| Sensor integration time | 165 ms | 1.2 ms | 18 ms | N/A |
| Channel bandwidth | 400 MHz centred at 52.8 GHz 170 MHz centred at 53.596 GHz | 960 MHz centred at 53.57 GHz | 400 MHz centred at 52.8 GHz 170 MHz centred at 53.596 GHz | 400 MHz centred at 52.8 GHz, 53.3 GHz, 53.8 GHz |
| **Measurement spatial resolution** | | | | |
| Horizontal resolution | 47 km 48 km* | 6 km | 32 km | 32 km |
| Vertical resolution | 47 km 48 km* | 6 km | 32 km | 32 km |

NOTE 1 – * Indicates that a particular sensor is flown on different missions, with different orbit and sensor parameters.

## 6.11 Typical parameters of passive sensors operating in the bands between 54.25 and 59.3 GHz

The band 54.25-59.3 GHz is of primary interest for atmospheric temperature profiling ($O_2$ absorption lines). Table 14 summarizes the parameters of passive sensors that are or will be operating between 54.25 and 59.3 GHz. The frequency range from 54.25 to 60.3 GHz is covered by many smaller bands with varying bandwidths and polarizations (see Tables 15 and 16).

TABLE 14

**EESS (passive) sensor characteristics operating between 54.25 and 59.3 GHz**

|  | Sensor K1 | Sensor K2 | Sensor K3 | Sensor K4 |
|---|---|---|---|---|
| Sensor type | Conical scan | Mechanical nadir scan | Mechanical nadir scan | Conical scan |
| **Orbit parameters** | | | | |
| Altitude | 828 km | 824 km | 833 km 822 km* | 835 km |
| Inclination | 98.7° | | 98.6° 98.7°* | 98.85° |
| Eccentricity | 0 | | 0 0.001* | 0 |
| Repeat period | 17 days | 9 days | 9 days 29 days* | |
| **Sensor antenna parameters** | | | | |
| Number of beams | 2 | | 30 earth fields per 8 s scan period | 1 |
| Reflector diameter | 2.2 m | 0.203 m | 0.15 m | 0.6 m |
| Maximum beam gain | 60 dBi | 37.9 dBi | 34.4 dBi | 51 dBi |
| Polarization | See Table 15 | See Table 16 | See Table 17 | See Table 18 |
| –3 dB beamwidth | 0.39° | 2.2° | 3.3° | 0.6° |
| Instantaneous field of view | 16 km × 12 km | Nadir FOV: 31.6 km Outer FOV: 136.7 × 60 km | Nadir FOV: 48.5 km (3.3°) Outer FOV: 149.1 × 79.4 km 147 × 79 km* | Outer FOV 18 × 43 km |
| Main beam efficiency | 95% | | | |
| Off-nadir pointing angle | 46.8° | ±52.73° cross-track | ±48.33° cross-track | 55.4° |
| Beam dynamics | 31.6 rpm | 8/3 s scan period cross-track; 96 earth fields per scan period | 8 s scan period | 2.88 s scan period |
| Incidence angle at Earth | 55.7° | | 0 57.5°* | 65° |

TABLE 14 (*end*)

| | Sensor K1 | Sensor K2 | Sensor K3 | Sensor K4 |
|---|---|---|---|---|
| **Sensor antenna parameters (*cont.*)** | | | | |
| −3 dB beam dimensions | 3 km | 31.6 km | 48.5 km<br>48 km* | 18 km × 43 km |
| Swath width | 1 700 km | 2 500 km | 2 343 km | 2 000 km |
| Sensor antenna pattern | See Rec. ITU-R RS.1813 | | | |
| Cold calibration ant. gain | N/A | 37.9 dBi | 34.4 dBi | N/A |
| Cold calibration angle (degrees re. satellite track) | N/A | 0 | 90°<br>−90° ± 3.9°* | N/A |
| Cold calibration angle (degrees re. nadir direction) | N/A | 82.175° | 83.33° | N/A |
| **Sensor receiver parameters** | | | | |
| Sensor integration time | 1.2 ms | 18 ms | 165 ms | N/A |
| Channel bandwidth | See Table 15 | See Table 16 | See Table 17 | See Table 18 |
| **Measurement spatial resolution** | | | | |
| Horizontal resolution | 3 km | 32 km | 48 km | 18 km |
| Vertical resolution | 3 km | 32 km | 48 km | 18 km |

NOTE 1 – * Indicates that a particular sensor is flown on different missions, with different orbit and sensor parameters.

TABLE 15

**Sensor K1 passive sensor characteristics for channels between 54.25 and 60.5 GHz**

| Centre frequency (GHz) | Channel bandwidth (MHz) | Polarization |
|---|---|---|
| 54.380 | 440 | V |
| 54.905 | 350 | V |
| 55.490 | 340 | V |
| 56.660 | 300 | V |
| 59.380 | 280 | V |
| 59.940 | 440 | V |
| 60.3712 | 57.6 | L |
| 60.4080 | 16 | L |
| 60.4202 | 8.4 | L |
| 60.5088 | 44.8 | L |
| 60.434776 | 25 | L |

TABLE 16

**Sensor K2 passive sensor characteristics for channels
between 54.25 and 59.3 GHz**

| Centre frequency (GHz) | Channel bandwidth (MHz) | Polarization |
|---|---|---|
| 54.4 | 400 | QH |
| 54.94 | 400 | QH |
| 55.5 | 330 | QH |
| 57.290344 | 330 | QH |
| 57.073344, 57.507344 | 78 | QH |
| 57.660544, 57.564544, 57.016144, 56.920144 | 36 | QH |
| 57.634544, 57.590544, 56.990144, 56.946144 | 16 | QH |
| 57.622544, 57.602544, 56.978144, 56.958144 | 8 | QH |
| 57.617044, 57.608044, 56.972644, 56.963644 | 3 | QH |

TABLE 17

**Sensor K3 passive sensor characteristics for channels
between 54.25 and 59.3 GHz**

| Centre frequency (GHz) | Channel bandwidth (MHz) | Polarization |
|---|---|---|
| 54.4 | 400 | H, QH* |
| 54.94 | 400 | V, QV* |
| 55.5 | 330 | H, QH* |
| 57.290344 | 330 | H, QH* |
| 57.073344, 57.507344 | 78 | H, QH* |
| 57.660544, 57.564544, 57.016144, 56.920144 | 36 | H, QH* |
| 57.634544, 57.590544, 56.990144, 56.946144 | 16 | H, QH* |
| 57.622544, 57.602544, 56.978144, 56.958144 | 8 | H, QH* |
| 57.617044, 57.608044, 56.972644, 56.963644 | 3 | H, QH* |

NOTE 1 – * Indicates that a particular sensor is flown on different missions, with different parameters.

TABLE 18

**Sensor K4 passive sensor characteristics for channels
between 54.25 and 60.5 GHz**

| Centre frequency (GHz) | Channel bandwidth (MHz) | Polarization | Altitude of peak sensitivity (km) |
|---|---|---|---|
| 54.64 | 400 MHz | V | 10 |
| 55.63 | 400 MHz | V | 14 |
| $57.290344 \pm 0.322 \pm 0.1$ | 50 MHz | V | 20 |
| $57.290344 \pm 0.322 \pm 0.05$ | 20 MHz | V | 25 |
| $57.290344 \pm 0.322 \pm 0.025$ | 10 MHz | V | 29 |
| $57.290344 \pm 0.322 \pm 0.001$ | 5 MHz | V | 35 |
| $57.290344 \pm 0.322 \pm 0.005$ | 3 MHz | V | 42 |

**6.12 Typical parameters of passive sensors operating in the bands between 86 and 92 GHz**

The 86-92 GHz passive sensor band is essential for the measurement of clouds, oil spills, ice, snow, and rain. It is also used as a reference window for temperature soundings near 118 GHz. Table 19 summarizes the parameters of passive sensors that are or will be operating between 86 and 92 GHz.

TABLE 19

**EESS (passive) sensor characteristics operating between 86 and 92 GHz**

| | Sensor L1 | Sensor L2 | Sensor L3 | Sensor L4 | Sensor L5 | Sensor L6 | Sensor L7 | Sensor L8 |
|---|---|---|---|---|---|---|---|---|
| Sensor type | Conical scan | | | Mechanical nadir scan | | | Conical scan | |
| **Orbit parameters** | | | | | | | | |
| Altitude | 867 km | 705 km | 833 km | 833 km<br>822 km* | | 824 km | 835 km | 700 km |
| Inclination | 20° | 98.2° | 98.7° | 98.6°<br>98.7°* | | 98.7° | 98.85° | 98.2° |
| Eccentricity | 0 | 0.0015 | 0 | 0<br>0.001* | | 0 | | 0.002 |
| Repeat period | 7 days | 16 days | 17 days | 9 days<br>29 days* | | 9 days | N/A | 16 days |
| **Sensor antenna parameters** | | | | | | | | |
| Number of beams | 1 | 2 | 1 | 30 earth fields per 8 s scan period | 30 earth fields per 8 s scan period<br><br>1 beam (steerable in 90 earth fields per scan period)* | 2 | | |
| Reflector diameter | 0.65 m | 1.6 m | 2.2 m | 0.15 m | 0.3 m<br>0.22 m* | 0.203 m | 0.6 m | 2 m |
| Maximum beam gain | 50 dBi | 60.5 dBi | 56 dBi | 34.4 dBi | 47 dBi<br>44.8 dBi* | 37.9 dBi | 54 dBi | 62.4 dBi |
| Polarization | H, V | | | H<br>QV* | | QV | H, V | |
| −3 dB beamwidth | 0.43° | 0.18° | 0.39° | 3.3° | 1.1° | 2.2° | 0.4° | 0.15° |
| Instantaneous field of view | 10 km × 17 km | A: 6.2 km × 3.6 km<br>B: 5.9 km × 3.5 km | 16 km × 12 km | Nadir FOV: 48.5 km<br>Outer FOV: 149.1 × 79.4 km<br>147 × 79 km* | Nadir FOV: 16 km (1.1°)<br>Outer FOV: 53 × 27 km* | Nadir FOV: 31.6 km × 31.6 km<br>Outer FOV: 136.7 × 60 km | 12 km × 28 km | A: 5.1 km × 2.9 km<br>B: 5.0 km × 2.9 km |
| Main beam efficiency | 96.2% | 96% | 95% | | | | N/A | 91% |

TABLE 19 (*end*)

| | Sensor L1 | Sensor L2 | Sensor L3 | Sensor L4 | Sensor L5 | Sensor L6 | Sensor L7 | Sensor L8 |
|---|---|---|---|---|---|---|---|---|
| **Sensor antenna parameters (*cont.*)** | | | | | | | | |
| Off-nadir pointing angle | 44.5° | 47.5° | 46.98° | ±48.33° cross-track | ±48.95° 49.4°* | ±52.725° cross-track | N/A | 47.5° |
| Beam dynamics | 20 rpm | 40 rpm | 31.6 rpm | 8 s scan period | 8/3 s scan period | 8/3 s scan period cross-track; 96 earth fields per scan period | 2.88 s scan period | 40 rpm |
| Incidence angle at Earth | 53.5° | A :55.0° B :54.5° | 55.77° | 30 positions 57.5°* | Various angles from 0° 59°* | | 35° | 55° |
| Swath width | 1 700 km | 1 450 km | 1 700 km | 2 343 km 2 186 km* | 2 343 km 2 193 km* | 2 500 km | 2 000 km | 1 450 km |
| Cold calibration ant. Gain | N/A | 40.4 dBi | N/A | 34.4 dBi | 34.4 dBi 44.8 dBi* | 37.9 dBi | N/A | 43.4 dBi |
| Cold calibration angle (degrees re. satellite track) | N/A | 115.5º | N/A | 90° −90° ± 3.9°* | End of scan (at 48.95°) −90° ± 3.9°* | 0 | N/A | 115.5º |
| Cold calibration angle (degrees re. nadir direction) | N/A | 97.0º | N/A | 83.33° | 83.33° 73.6 (66° to 81°)* | 82.175° | N/A | 97.0º |
| **Sensor receiver parameters** | | | | | | | | |
| Sensor integration time | 2 ms | 1.2 ms | | 180 ms 165 ms* | 185 ms 18 ms* | 18 ms | N/A | 1.2 ms |
| Channel bandwidth | 2 700 MHz centred at 89 GHz | 3 000 MHz centred at 89 GHz | 6 000 MHz centred at 89 GHz | | Centred at 89 GHz ± 500 MHz, each with a bandwidth of 1 000 MHz 2 800 MHz centred at 89 GHz* | 2 000 MHz centred at 87-91.9 GHz | 2 GHz | 3 000 MHz centred at 89 GHz |
| **Measurement spatial resolution** | | | | | | | | |
| Horizontal resolution | 10 km | 3.5 km | 6 km | 40.5 km 48 km* | 40.5 km 16 km* | 32 km | 19 km | 2.9 km |
| Vertical resolution | N/A | 6.1 km | 6 km | 48 km | 16 km | 32 km | 6 km | 5.1 km |

NOTE 1 – * Indicates that a particular sensor is flown on different missions, with different orbit and sensor parameters.

**6.13    Typical parameters of passive sensors operating in the bands between 114.25 and 122.25 GHz**

The band 114.25-122.25 GHz is of primary interest for atmospheric temperature profiling ($O_2$ absorption lines). Table 20 summarizes the parameters of passive sensors that are or will be operating between 114.25 and 122.25 GHz.

TABLE 20

**EESS (passive) sensor characteristics operating
between 114.25 and 122.25 GHz**

|  | **Sensor M1** |
|---|---|
| Sensor type | Limb sounder |
| **Orbit parameters** | |
| Altitude | 705 km |
| Inclination | 98.2° |
| Eccentricity | 0.0015 |
| Repeat period | 16 days |
| **Sensor antenna parameters** | |
| Number of beams | 2 |
| Reflector diameter | 1.6 m × 0.8 m |
| Maximum beam gain | 60 dBi |
| Polarization | 2 orthogonal |
| −3 dB beamwidth | 0.19° × 0.245° |
| Instantaneous field of view | 6.5 km × 13 km |
| Main beam efficiency | N/A |
| Off-nadir pointing angle | Limb |
| Beam dynamics | N/A |
| Incidence angle at Earth | N/A |
| −3 dB beam dimensions | 3 km |
| Swath width | N/A |
| Sensor antenna pattern | N/A |
| Cold calibration ant. gain | N/A |
| Cold calibration angle (degrees re. satellite track) | N/A |
| Cold calibration angle (degrees re. nadir direction) | N/A |
| **Sensor receiver parameters** | |
| Sensor integration time | 0.166 s |
| Channel bandwidth | N/A |
| **Measurement spatial resolution** | |
| Horizontal resolution | 13 km |
| Vertical resolution | 6.5 km |

### 6.14 Typical parameters of passive sensors operating in the bands between 148.5 and 151.5 GHz

The 148.5-151.5 GHz passive sensor band is essential for the measurement of $N_2O$, Earth's surface temperature, and cloud parameters. It is also used as a reference window for temperature soundings. Table 21 summarizes the parameters of passive sensors that are or will be operating between 148.5 and 151.5 GHz.

TABLE 21

**EESS (passive) sensor characteristics operating
between 148.5 and 151.5 GHz**

|  | **Sensor N1** |
|---|---|
| Sensor type | Cross-track nadir scan |
| **Orbit parameters** | |
| Altitude | 705 km |
| Inclination | 98.2° |
| Eccentricity | 0.0015 |
| Repeat period | 16 days |
| **Sensor antenna parameters** | |
| Number of beams | 1 |
| Reflector diameter | 0.219 m |
| Maximum beam gain | 45 dB |
| Polarization | Linear |
| –3 dB beamwidth | 1.1° |
| Main beam efficiency | > 95% |
| Off-nadir pointing angle | ±48.95° |
| Beam dynamics | Scan period of 8/3 s |
| Incidence angle at Earth | 56.9° |
| –3 dB beam dimensions | 13.5 km |
| Swath width | 1 650 km |
| Sensor antenna pattern | See Fig. 11 |
| Cold calibration ant. gain | 45 dB |
| Cold calibration angle (degrees re. satellite track) | 90° |
| Cold calibration angle (degrees re. nadir direction) | 65-81° |
| **Sensor receiver parameters** | |
| Sensor integration time | 18 ms |
| Channel bandwidth | 4 000 MHz @ 150 GHz |
| **Measurement spatial resolution** | |
| Horizontal resolution | 13.5 km |
| Vertical resolution | 13.5 km |

FIGURE 11

**Sensor N1 antenna pattern for the 148.5 and 151.5 GHz band**
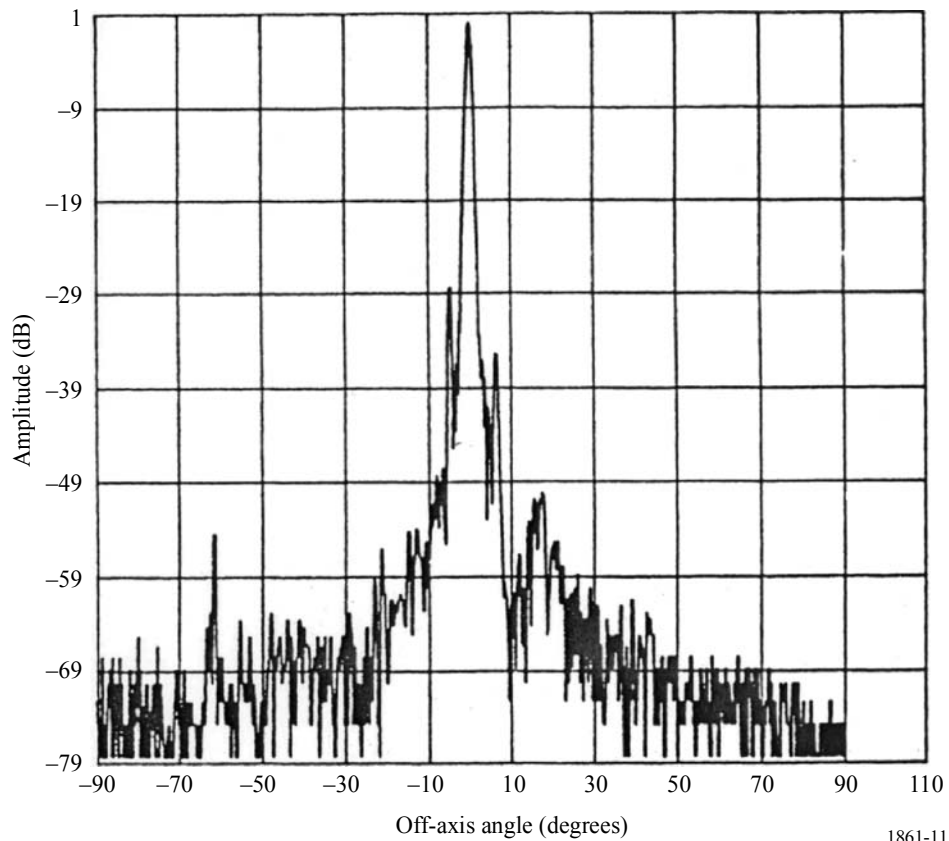


1861-11

## 6.15    Typical parameters of passive sensors operating in the bands between 155.5-158.5 GHz

The band 155.5-158.5 GHz is of primary interest to measure Earth and cloud parameters. Table 22 summarizes the parameters of passive sensors that are or will be operating between 155.5-158.5 GHz.

TABLE 22

**EESS (passive) sensor characteristics operating between 155.5-158.5 GHz**

|  | **Sensor O1** | **Sensor O2** |
|---|---|---|
| Sensor type | Conical scan | Cross-track nadir scan |
| **Orbit parameters** | | |
| Altitude | 865 km | 822 km |
| Inclination | 20° | 98.7° |
| Eccentricity | 0 | 0.001 |
| Repeat period | 7 days | 29 days |
| **Sensor antenna parameters** | | |
| Number of beams | | 1 |
| Reflector diameter | 0.65 m | 0.22 m |
| Maximum beam gain | 60 dBi | 44.8 dBi |
| Polarization | H, V | QV |
| –3 dB beamwidth | | 1.1° |
| Instantaneous field of view | | Nadir FOV: 16 km<br>Outer FOV: 53 × 27 km |
| Main beam efficiency | 96% | 95% |
| Off-nadir pointing angle | 44.5° | 49.45° |
| Beam dynamics | 20 rpm | Scan period of 8/3s |
| Incidence angle at Earth | 52.3° | 59° |
| –3 dB beam dimensions | 3 km | 16 km |
| Swath width | | 2 193 km |
| Sensor antenna pattern | | |
| Cold calibration ant. gain | N/A | 44.8 dBi |
| Cold calibration angle (degrees re. satellite track) | N/A | −90° ± 3.9° |
| Cold calibration angle (degrees re. nadir direction) | N/A | 73.6<br>(66° to 81°) |
| **Sensor receiver parameters** | | |
| Sensor integration time | N/A | 18 ms |
| Channel bandwidth | 2 GHz | < 2.8 GHz |
| **Measurement spatial resolution** | | |
| Horizontal resolution | 6 km | 16 km |
| Vertical resolution | 6 km | 16 km |

## 6.16 Typical parameters of passive sensors operating in the bands between 164 and 167 GHz

The band 164-167 GHz is of primary interest to measure $N_2O$, cloud water and ice, rain, CO, and ClO. Table 23 summarizes the parameters of passive sensors that are or will be operating between 164 and 167 GHz.

TABLE 23

**EESS (passive) sensor characteristics operating between 164 and 167 GHz**

|  | **Sensor P1** | **Sensor P2** |
|---|---|---|
| Sensor type | Conical scan | Mechanical nadir scan |
| **Orbit parameters** | | |
| Altitude | 828 km | 824 km |
| Inclination | 98.7° | |
| Eccentricity | 0 | |
| Repeat period | 17 days | 9 days |
| **Sensor antenna parameters** | | |
| Number of beams | 2 | |
| Reflector diameter | 0.48 × 0.71 m | 0.127 m |
| Maximum beam gain | 54 dBi | 43.9 dBi |
| Polarization | V | QH |
| –3 dB beamwidth | 0.39° | 1.1° |
| Instantaneous field of view | 16 km × 12 km | Nadir FOV: 15.8 km Outer FOV: 68.4 × 30 km |
| Main beam efficiency | 95% | |
| Off-nadir pointing angle | 46.8° | ±52.725° cross-track |
| Beam dynamics | 31.6 rpm | 8/3 s scan period cross-track; 96 earth fields per scan period |
| Incidence angle at Earth | 55.5° | 0° |
| –3 dB beam dimensions | 6 km | 1.1°16 km |
| Swath width | 1 700 km | 2 500 km |
| Sensor antenna pattern | | |
| Cold calibration ant. gain | N/A | 43.9 dBi |
| Cold calibration angle (degrees re. satellite track) | N/A | 0 |
| Cold calibration angle (degrees re. nadir direction) | N/A | 82.175° |
| **Sensor receiver parameters** | | |
| Sensor integration time | 1.2 ms | 18 ms |
| Channel bandwidth | 1 425 MHz centred at 166 ± 0.7875 GHz | 3 000 MHz centred at 164-167 GHz |
| Measurement spatial resolution | | |
| Horizontal resolution | 12 km | 32 km |
| Vertical resolution | 12 km | 32 km |

## 6.17 Typical parameters of passive sensors operating in the bands between 174.8 and 191.8 GHz

The 174.8-191.8 GHz passive sensor band is essential for $N_2O$ and $O_3$ measurements, in addition to water vapour profiling. Table 24 summarizes the parameters of passive sensors that are or will be operating between 174.8 and 191.8 GHz.

TABLE 24

**EESS (passive) sensor characteristics operating between 174.8 and 191.8 GHz**

| | Sensor Q1 | Sensor Q2 | Sensor Q3 | Sensor Q4 | Sensor Q5 | Sensor Q6 | Sensor Q7 |
|---|---|---|---|---|---|---|---|
| Sensor type | Conical scan | Cross-track scan | Limb sounder | Mechanical nadir scan | Conical scan | Nadir scan | |
| **Orbit parameters** | | | | | | | |
| Altitude | 828 km | 705 km | | 824 km | 835 km | 867 km | 822 km |
| Inclination | 98.7° | 98.2° | | 98.7° | 98.85° | 20° | 98.7° |
| Eccentricity | 0 | | | | | | 0.001 |
| Repeat period | 17 days | 16 days | | 9 days | N/A | 7 days | 29 days |
| **Sensor antenna parameters** | | | | | | | |
| Number of beams | 2 | 1 | 2 | 96 earth fields per scan period | 6 | | 1 (steerable in 90 earth fields per scan period) |
| Reflector diameter | 0.48 × 0.71 m | 0.219 m | 1.6 × 0.8 m | 0.127 m | 0.6 m | 0.2 m | 0.22 m |
| Maximum beam gain | 54 dBi | 45 dBi | 60 dBi | 43.9 dBi | 60 dBi | 49 dBi | 44.8 dBi |
| Polarization | V | Linear | V | QH | V | H | QV |
| −3 dB beamwidth | 0.39° | 1.1° | 0.19° × 0.245° | 1.1° | 0.2° | 0.66° | 1.1° |
| Instantaneous field of view | 16 km × 12 km | 14 km | 4.5 km × 9 km | Nadir FOV: 15.8 km Outer FOV: 68.4 × 30 km | Outer FOV: 8 × 19 km | At nadir 10 km × 10 km At swath limit 14 km × 22 km | Nadir FOV: 16 km Outer FOV: 53 × 27 km |
| Main beam efficiency | 95% | | N/A | 95% | N/A | 97% | 95% |
| Off-nadir pointing angle | 46.8° | ±48.95° | N/A | ±52.725° cross-track | 55.4° | 42° | 49.4° |

TABLE 24 (*continued*)

| | Sensor Q1 | Sensor Q2 | Sensor Q3 | Sensor Q4 | Sensor Q5 | Sensor Q6 | Sensor Q7 |
|---|---|---|---|---|---|---|---|
| **Sensor antenna parameters** (*cont.*) | | | | | | | |
| Beam dynamics | 31.6 rpm | 8/3 s scan period | Scans continuously in tangent height from the surface to ~92 km in 24.7 s 240 scans/ orbit | 8/3 s scan period cross-track | 2.88 sscan period | 1 revolution per 1.639 s | 8/3 s scan period cross-track |
| Incidence angle at Earth | 55.5 | 56.9° | N/A | | 65° | 55° | 59° |
| −3 dB beam dimensions | 3 km | 13.5 km | 3 km | 16 km | 8 km × 19 km | 10 km × 10 km | 16 km |
| Swath width | 1 700 km | 1 650 km | N/A | 2 500 km | 2 000 km | 1 700 km | 2 193 km |
| Sensor antenna pattern | | See Fig. 12 | | | | | |
| Cold calibration ant. gain | N/A | 45 dB | N/A | 43.9 dBi | N/A | | 44.8 dBi |
| Cold calibration angle (degrees re. satellite track) | N/A | 90° | N/A | 0 | N/A | | −90° ± 3.9° |
| Cold calibration angle (degrees re. nadir direction) | N/A | 65° to 81° | N/A | 82.175° | N/A | | 73.6 (66° to 81°) |

TABLE 24 (*end*)

| | **Sensor Q1** | **Sensor Q2** | **Sensor Q3** | **Sensor Q4** | **Sensor Q5** | **Sensor Q6** | **Sensor Q7** |
|---|---|---|---|---|---|---|---|
| **Sensor receiver parameters** | | | | | | | |
| Sensor integration time | 1.2 ms | 18 ms | 0.166 s | 18 ms | N/A | 7.34 ms | 18 ms |
| Channel bandwidth | 1 275 MHz centred at 183.31 ± 0.7875 GHz, 3 500 MHz centred at 183.31 ± 3.1 GHz , 4 500 MHz centred at 183.31 ± 7.7 GHz | 1 000 MHz centred at 183.31 ± 1.00 GHz, 2 000 MHz centred at 183.31 ± 3.00 GHz, 4 000 MHz centred at 183.31 ± 7.00 GHz | N/A | See Table 25 | 1.5 GHz centred at 183.31 ± 7 GHz, 1.0 GHz centred at 183.31 ± 3 GHz, 0.5 GHz centred at 183.31 ± 1 GHz | 6 channels from 200 MHz to 2 GHz centred at 183.31 GHz | 0.5 GHz centred at 183.311 ± 1 GHz, 1.0 GHz centred at 183.311 ± 3 GHz, 1.1 GHz centred at 190.311 ± 1 GHz |
| **Measurement spatial resolution** | | | | | | | |
| Horizontal resolution | 6 km | 13.5 km | 9 km | 16 km | 8 km | 10 km cross-track | 16 km |
| Vertical resolution | 6 km | 13.5 km | 4.5 km | 16 km | 8 km | 10 km | 16 km |

FIGURE 12

**Sensor Q2 antenna pattern for the 174.8 and 191.8 GHz band**



1861-12
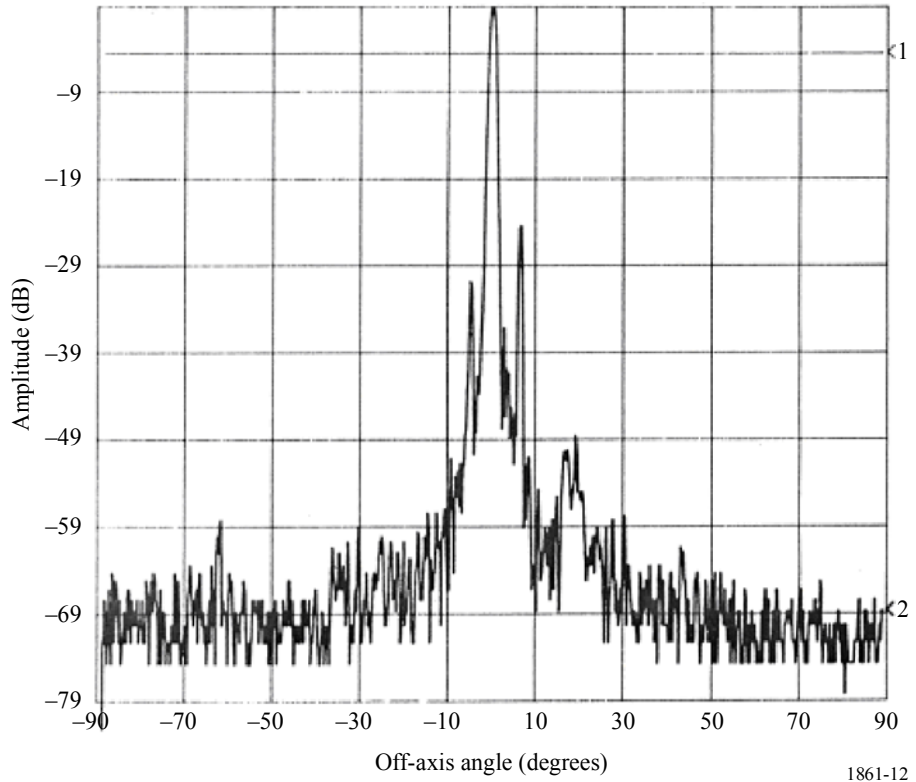
TABLE 25

**Sensor Q4 passive sensor characteristics for channels
between 174.8 and 191.8 GHz**

| Centre frequency (GHz) | Channel bandwidth (MHz) | Polarization |
|---|---|---|
| 183.31 ± 4.5 | 2 000 | QH |
| 183.31 ± 1.8 | 1 000 | QH |
| 190.31 | < 2 200 | V |

# RECOMMENDATION ITU-R RS.2017

# Performance and interference criteria for satellite passive remote sensing

(2012)

**Scope**

This Recommendation provides information on the performance and interference criteria for satellite passive remote sensing of the Earth and its atmosphere for microwave passive sensors.

The ITU Radiocommunication Assembly,

*considering*

a)      that certain frequency bands, including some absorption bands of atmospheric gases (e.g. $O_2$ (oxygen) and $H_2O$ (water vapour)), have been allocated for spaceborne passive microwave remote sensing;

b)      that some of these bands are also allocated to other radiocommunication services;

c)      that performance criteria are a necessary prerequisite to the establishment of interference and sharing criteria;

d)      that surface brightness temperature, the atmospheric temperature at points along a path and absorption coefficients can be determined from measurements of the sensor antenna temperature, $T_A$;

e)      that the surface brightness temperature and the absorption coefficients, in turn, depend upon the physical properties of the surface or atmosphere that are to be sensed;

f)      that studies have established measurement sensitivity requirements;

g)      that interference criteria should be compatible with performance objectives;

h)      that interference criteria are a necessary prerequisite to the establishment of sharing criteria;

j)      that interference criteria can be stated in terms of interference power within a reference bandwidth;

k)      that passive microwave remote sensing is performed in absorption bands to obtain important three-dimensional atmospheric data that are used in particular to initialize numerical weather prediction (NWP) models;

l)      that studies have established that measurements in absorption bands are extremely vulnerable to interference because, in general, there is no possibility to detect and to reject data that are contaminated by interference, and because propagation of undetected contaminated data into NWP models may have a destructive impact on the reliability/quality of weather forecasting;

m)      that three-dimensional measurements of atmospheric temperature or gas concentration are performed in the absorption bands including those in the range 52.6-59.3 GHz, 115.25-122.25 GHz, 174.8-191.8 GHz, as well as the auxiliary window channels at 23.6-24 GHz, 31.3-31.8 GHz, 50.2-50.4 GHz and 86-92 GHz;

n)      that performance requirements for passive sensors can be stated in terms of measurement sensitivity, $\Delta T_e$, and availability, measured at the satellite, assuming that degradation from other elements in the system will be small;

o)      that the sensitivities of radiometric passive sensors are generally expressed as a temperature differential, $\Delta T_e$, given by:

$$\Delta T_e = \alpha \, T_s / \sqrt{Bt} \qquad K$$

where:

$\Delta T_e$ :  radiometric resolution (root-mean-square (r.m.s.) uncertainty in estimation of total system noise, $T_s$);

$\alpha$ :  receiver system constant;

$T_s$ :  system noise temperature (K) (antenna temperature and receiver noise temperature);

$B$ :  spectral resolution (of spectro-radiometer) or "reference bandwidth" of a single radiometric channel (Hz);

$t$ :  sensor integration time (s);

p)       that the radiometer threshold, or minimum discernible power change, is given by:

$$\Delta P = k \, \Delta T_e \, B \qquad W$$

where $k$ is Boltzmann's constant = $1.38 \times 10^{-23}$ J/K,

*recommends*

**1**       that the measurement sensitivities suitable for satellite passive remote sensing of the Earth's land, oceans and atmosphere indicated in Table 1 should be used as performance criteria;

**2**       that in bands used for satellite passive remote sensing, the required minimum availability of passive sensor data for each band should be as specified in column 3 (Data availability) of Table 1;

**3**       that the permissible interference level for spaceborne passive sensors should be set at 20% of $\Delta P$;

**4**       that permissible interference levels and reference bandwidths for the frequency bands preferred for satellite passive sensing of the Earth's land, oceans and atmosphere as specified in Table 2 should be used in any interference assessment or sharing studies;

**5**       that the interference level in Table 2 should not be exceeded for more than a percentage of sensor viewing area or a percentage of measurement time as given in column 4 of Table 2.

TABLE 1

**Performance criteria for satellite passive remote sensing up to 1 000 GHz**

| Frequency band(s) (GHz) | Required $\Delta T_e$ (K) | Data availability[1] (%) | Scan mode (N, C, L)[2] |
|---|---|---|---|
| 1.370-1.427 | 0.05 | 99.9 | N, C |
| 2.64-2.70 | 0.1 | 99.9 | N |
| 4.2-4.4 | 0.05 | 99.9 | N, C |
| 6.425-7.25 | 0.05 | 99.9 | N, C |
| 10.6-10.7 | 0.1 | 99.9 | N, C |
| 15.2-15.4 | 0.1 | 99.9 | N, C |
| 18.6-18.8 | 0.1 | 99.9 | N, C |
| 21.2-21.4 | 0.05 | 99.9 | N |
| 22.21-22.5 | 0.05 | 99.9 | N |
| 23.6-24 | 0.05 | 99.99 | N, C |
| 31.3-31.8 | 0.05 | 99.99 | N, C |
| 36-37 | 0.1 | 99.9 | N, C |
| 50.2-50.4 | 0.05 | 99.99 | N, C |
| 52.6-59.3 | 0.05 | 99.99 | N, C |
| 86-92 | 0.05 | 99.99 | N, C |
| 100-102 | 0.005 | 99 | L |
| 109.5-111.8 | 0.005 | 99 | L |
| 114.25-116 | 0.005 | 99 | L |
| 115.25-122.25 | 0.05/0.005[3] | 99.99/99[3] | N, L |
| 148.5-151.5 | 0.1/0.005[3] | 99.99/99[3] | N, L |
| 155.5-158.5[4] | 0.1 | 99.99 | N, C |
| 164-167 | 0.1/0.005[3] | 99.99/99[3] | N, C, L |
| 174.8-191.8 | 0.1/0.005[3] | 99.99/99[3] | N, C, L |
| 200-209 | 0.005 | 99 | L |
| 226-231.5 | 0.2/0.005[3] | 99.99/99[3] | N, L |
| 235-238 | 0.005 | 99 | L |
| 250-252 | 0.005 | 99 | L |
| 275-285.4 | 0.005 | 99 | L |
| 296-306 | 0.2/0.005[3] | 99.99/99[3] | N, L |
| 313.5-355.6 | 0.3/0.005[3] | 99.99/99[3] | N, C, L |
| 361.2-365 | 0.3/0.005[3] | 99.99/99[3] | N, L |
| 369.2-391.2 | 0.3/0.005[3] | 99.99/99[3] | N, L |
| 397.2-399.2 | 0.3/0.005[3] | 99.99/99[3] | N, L |
| 409-411 | 0.005 | 99 | L |
| 416-433.46 | 0.4/0.005[3] | 99.99/99[3] | N, L |
| 439.1-466.3 | 0.4/0.005[3] | 99.99/99[3] | N, C, L |

TABLE 1 (*end*)

| Frequency band(s) (GHz) | Required $\Delta T_e$ (K) | Data availability[1] (%) | Scan mode (N, C, L)[2] |
|---|---|---|---|
| 477.75-496.75 | 0.005 | 99 | L |
| 497-502 | 0.5/0.005[3] | 99.99/99[3] | N, L |
| 523-527 | 0.5 | 99.99 | N |
| 538-581 | 0.5/0.005[3] | 99.99/99[3] | N, L |
| 611.7-629.7 | 0.005 | 99 | L |
| 634-654 | 0.6/0.005[3] | 99.99/99[3] | N, L |
| 656.9-692 | 0.6/0.005[3] | 99.99/99[3] | N, C, L |
| 713.4-717.4 | 0.005 | 99 | L |
| 729-733 | 0.005 | 99 | L |
| 750-754 | 0.005 | 99 | L |
| 771.8-775.8 | 0.005 | 99 | L |
| 823.15-845.15 | 0.8/0.005[3] | 99.99/99[3] | N, C, L |
| 850-854 | 0.005 | 99 | L |
| 857.9-861.9 | 0.005 | 99 | L |
| 866-882 | 0.8 | 99.99 | N, C |
| 905.17-927.17 | 0.9/0.005[3] | 99.99/99[3] | N, L |
| 951-956 | 0.005 | 99 | L |
| 968.31-972.31 | 0.005 | 99 | L |
| 985.9-989.9 | 0.005 | 99 | L |

[1] Data availability is the percentage of area or time for which accurate data is available for a specified sensor measurement area or sensor measurement time. For a 99.99% data availability, the measurement area is a square on the Earth of 2 000 000 km², unless otherwise justified; for a 99.9% data availability, the measurement area is a square on the Earth of 10 000 000 km² unless otherwise justified; for a 99% data availability the measurement time is 24 h, unless otherwise justified.

[2] N: Nadir, Nadir scan modes concentrate on sounding or viewing the Earth's surface at angles of nearly perpendicular incidence. The scan terminates at the surface or at various levels in the atmosphere according to the weighting functions. L: Limb, Limb scan modes view the atmosphere "on edge" and terminate in space rather than at the surface, and accordingly are weighted zero at the surface and maximum at the tangent point height. C: Conical, Conical scan modes view the Earth's surface by rotating the antenna at an offset angle from the nadir direction.

[3] First number for nadir or conical modes and second number for microwave limb sounding applications.

[4] This band is needed until 2018 to accommodate existing and planned sensors.

TABLE 2

**Interference criteria for satellite passive remote sensing up to 1 000 GHz**

| Frequency band(s) (GHz) | Reference bandwidth (MHz) | Maximum interference level (dBW) | Percentage of area or time permissible interference level may be exceeded[1] (%) | Scan mode (N, C, L)[2] |
|---|---|---|---|---|
| 1.370-1.427 | 27 | −174 | 0.1 | N, C |
| 2.64-2.70 | 10 | −176 | 0.1 | N |
| 4.2-4.4 | 200 | −166 | 0.1 | N, C |
| 6.425-7.25 | 200 | −166 | 0.1 | N, C |
| 10.6-10.7 | 100 | −166 | 0.1 | N, C |
| 15.2-15.4 | 50 | −169 | 0.1 | N, C |
| 18.6-18.8 | 200 | −163 | 0.1 | N, C |
| 21.2-21.4 | 100 | −169 | 0.1 | N |
| 22.21-22.5 | 100 | −169 | 0.1 | N |
| 23.6-24 | 200 | −166 | 0.01 | N, C |
| 31.3-31.8 | 200 | −166 | 0.01 | N, C |
| 36-37 | 100 | −166 | 0.1 | N, C |
| 50.2-50.4 | 200 | −166 | 0.01 | N, C |
| 52.6-59.3 | 100 | −169 | 0.01 | N, C |
| 86-92 | 100 | −169 | 0.01 | N, C |
| 100-102 | 10 | −189 | 1 | L |
| 109.5-111.8 | 10 | −189 | 1 | L |
| 114.25-116 | 10 | −189 | 1 | L |
| 115.25-122.25 | 200/10[3] | −166/−189[3] | 0.01/1[3] | N, L |
| 148.5-151.5 | 500/10[3] | −159/−189[3] | 0.01/1[3] | N, L |
| 155.5-158.5[4] | 200 | −163 | 0.01 | N, C |
| 164-167 | 200/10[3] | −163/−189[3] | 0.01/1[3] | N, C, L |
| 174.8-191.8 | 200/10[3] | −163/−189[3] | 0.01/1[3] | N, C, L |
| 200-209 | 3 | −194 | 1 | L |
| 226-231.5 | 200/3[3] | −160/−194[3] | 0.01/1[3] | N, L |
| 235-238 | 3 | −194 | 1 | L |
| 250-252 | 3 | −194 | 1 | L |
| 275-285.4 | 3 | −194 | 1 | L |
| 296-306 | 200/3[3] | −160/−194[3] | 0.01/1[3] | N, C, L |
| 313.5-355.6 | 200/3[3] | −158/−194[3] | 0.01/1[3] | N, C, L |
| 361.2-365 | 200/3[3] | −158/−194[3] | 0.01/1[3] | N, L |
| 369.2-391.2 | 200/3[3] | −158/−194[3] | 0.01/1[3] | N, L |

TABLE 2 (*end*)

| Frequency band(s) (GHz) | Reference bandwidth (MHz) | Maximum interference level (dBW) | Percentage of area or time permissible interference level may be exceeded[1] (%) | Scan mode (N, C, L)[2] |
|---|---|---|---|---|
| 397.2-399.2 | 200/3[3] | −158/−194[3] | 0.01/1[3] | N, L |
| 409-411 | 3 | −194 | 1 | N |
| 416-433.46 | 200/3[3] | −157/−194[3] | 0.01/1[3] | N, L |
| 439.1-466.3 | 200/3[3] | −157/−194[3] | 0.01/1[3] | N, C, L |
| 477.75-496.75 | 3 | −194 | 1 | L |
| 497-502 | 200/3[3] | −156/−194[3] | 0.01/1[3] | N, L |
| 523-527 | 200 | −156 | 0.01 | N |
| 538-581 | 200/3[3] | −156/−194[3] | 0.01/1[3] | N, L |
| 611.7-629.7 | 3 | −194 | 1 | L |
| 634-654 | 200/3[3] | −155/−194[3] | 0.01/1[3] | N, L |
| 656.9-692 | 200/3[3] | −155/−194[3] | 0.01/1[3] | N, C, L |
| 713.4-717.4 | 3 | −194 | 1 | L |
| 729-733 | 3 | −194 | 1 | L |
| 750-754 | 3 | −194 | 1 | L |
| 771.8-775.8 | 3 | −194 | 1 | L |
| 823.15-845.15 | 200/3[3] | −154/−194[3] | 0.01/1[3] | N, C, L |
| 850-854 | 3 | −194 | 1 | L |
| 857.9-861.9 | 3 | −194 | 1 | L |
| 866-882 | 200 | −154 | 0.01 | C |
| 905.17-927.17 | 200/3[3] | −153/−194[3] | 0.01/1[3] | N, L |
| 951-956 | 3 | −194 | 1 | L |
| 968.31-972.31 | 3 | −194 | 1 | L |
| 985.9-989.9 | 3 | −194 | 1 | L |

[1]  For a 0.01% level, the measurement area is a square on the Earth of 2 000 000 km$^2$, unless otherwise justified; for a 0.1% level, the measurement area is a square on the Earth of 10 000 000 km$^2$ unless otherwise justified; for a 1% level, the measurement time is 24 h, unless otherwise justified.

[2]  N: Nadir, Nadir scan modes concentrate on sounding or viewing the Earth's surface at angles of nearly perpendicular incidence. The scan terminates at the surface or at various levels in the atmosphere according to the weighting functions. L: Limb, Limb scan modes view the atmosphere "on edge" and terminate in space rather than at the surface, and accordingly are weighted zero at the surface and maximum at the tangent point height. C: Conical, Conical scan modes view the Earth's surface by rotating the antenna at an offset angle from the nadir direction.

[3]  First number for nadir or conical scanning modes and second number for microwave limb sounding applications.

[4]  This band is needed until 2018 to accommodate existing and planned sensors.

———————————

RECOMMENDATION ITU-R RS.1813-1

# Reference antenna pattern for passive sensors operating in the Earth exploration-satellite service (passive) to be used in compatibility analyses in the frequency range 1.4-100 GHz

(2009-2011)

**Scope**

This Recommendation provides a reference antenna pattern for Earth exploration-satellite service (EESS) passive sensors to be used in compatibility studies in the frequency range 1.4-100 GHz when no other information is available on actual sensor antennas.

The ITU Radiocommunication Assembly,

*considering*

a) that reference satellite antenna patterns, which reflect to the maximum extent possible the actual antenna gain, are desirable for use in compatibility studies in the case of aggregate interference from multiple sources;

b) that antennas used for spaceborne passive sensors in the Earth exploration-satellite service (EESS) (passive) are usually designed to maximize main beam efficiency and minimize energy received through antenna side lobes;

c) that the impact of a dominating interference source on single pixel measurements or peak interference assessments may require consideration of maxima in the antenna side lobe pattern,

*noting*

a) that characteristics of passive sensors operating between 1.4 GHz and 100 GHz have been taken into account for the derivation of the proposed antenna pattern,

*recommends*

**1** that, in the absence of an actual antenna pattern, the following equations for the average antenna pattern of a spaceborne passive sensor should be used, for antenna diameters greater than 2 times the wavelength:

$$G(\varphi) = G_{max} - 1.8 \times 10^{-3} \left( \frac{D}{\lambda} \varphi \right)^2 \qquad \text{for} \quad 0° \le \varphi \le \varphi_m$$

$$G(\varphi) = \max\left( G_{max} - 1.8 \times 10^{-3} \left( \frac{D}{\lambda} \varphi \right)^2, 33 - 5\log\left(\frac{D}{\lambda}\right) - 25\log(\varphi) \right) \quad \text{for} \quad \varphi_m < \varphi \le 69°$$

$$G(\varphi) = -13 - 5\log\left(\frac{D}{\lambda}\right) \qquad \text{for} \quad 69° < \varphi \le 180°$$

In the case of $G(\varphi) < -23$ dBi, the value $-23$ dBi is to be used, where:

$$G_{max} = 10 \log\left(\eta\pi^2 \frac{D^2}{\lambda^2}\right)$$

$$\varphi_m = \frac{22\lambda}{D}\sqrt{5.5 + 5\log(\frac{D}{\lambda}\eta^2)}$$

$G_{max}$:    maximum antenna gain (dBi)

$G(\varphi)$:    gain (dBi) relative to an isotropic antenna

$\varphi$:    off-axis angle (degrees)

$D$:    antenna diameter (m)

$\lambda$:    wavelength (m)

$\eta$:    antenna efficiency (if $\eta$ is unknown, 60% can be assumed as a representative value);

**2**     that in cases where a few interference sources dominate, or where peak interference values are required in the analysis, the following equations for the antenna pattern for spaceborne passive sensors should be used, for antenna diameters greater than 2 times the wavelength:

$$G(\varphi) = G_{max} - 1.8 \times 10^{-3}\left(\frac{D}{\lambda}\varphi\right)^2 \qquad\qquad \text{for} \quad 0° \le \varphi \le \varphi_m$$

$$G(\varphi) = \max\left(G_{max} - 1.8 \times 10^{-3}\left(\frac{D}{\lambda}\varphi\right)^2, 40 - 5\log\left(\frac{D}{\lambda}\right) - 25\log(\varphi)\right) \quad \text{for} \quad \varphi_m < \varphi \le 69°$$

$$G(\varphi) = -6 - 5\log\left(\frac{D}{\lambda}\right) \qquad\qquad\qquad \text{for} \quad 69° < \varphi \le 180°$$

In the case of $G(\varphi) < -23$ dBi, the value $-23$ dBi is to be used, where:

$$G_{max} = 10 \log\left(\eta\pi^2 \frac{D^2}{\lambda^2}\right)$$

$$\varphi_m = \frac{22\lambda}{D}\sqrt{5.5 + 5\log\left(\frac{D}{\lambda}\eta^2\right)}$$

RECOMMENDATION ITU-R RS.1416*, ** **参考資料**21

# SHARING BETWEEN SPACEBORNE PASSIVE SENSORS AND THE INTER-SATELLITE SERVICE OPERATING NEAR 118 AND 183 GHz

(Question ITU-R 228/7)

(1999)

The ITU Radiocommunication Assembly,

*considering*

a)      that Resolution 723 (WRC-97) resolves to address the allocations of frequency bands above 71 GHz to passive services;

b)      that Recommendation ITU-R RS.515 indicates that the band 115-122 GHz is necessary for spaceborne passive sensing to obtain vertical temperature profiles;

c)      that Recommendation ITU-R RS.515 indicates that the band 175-192 GHz is necessary for spaceborne passive sensing to obtain vertical water vapour profiles;

d)      that weather forecasting is an important tool essential to all human economic activities, and also plays a predominant role in early identification and warnings of potentially dangerous phenomena;

e)      that atmospheric temperature and water vapour profiles are essential data needed for weather forecasting on a global basis;

f)      that the oxygen absorption band around 118 GHz and the water vapour absorption band around 183 GHz represent a unique natural resource for remote temperature and water vapour profile sensing in the atmosphere;

g)      that these passive measurements are extremely vulnerable to interference because the natural variability of the atmosphere makes it impossible to recognize and to filter measurements contaminated by interference;

h)      that contaminated passive sensor measurements can have a dramatic, adverse impact on climate studies and the quality of weather predictions,

*recognizing*

a)      that the bands 116-126 GHz, 174.5-182 GHz, and 185-190 GHz are currently allocated to the inter-satellite service (ISS);

b)      that Recommendation ITU-R RS.1029 provides interference criteria for the passive sensors in the bands 115-122 GHz and 175-192 GHz;

c)      that studies conducted in the bands 116-122 GHz, 174.5-182 GHz and 185-190 GHz have shown that the inter-satellite links (ISLs) in a non-geostationary (non-GSO) satellite system can cause interference to the passive sensors well in excess of these protection criteria (see Annex 1);

d)      that studies conducted in these bands have shown that ISLs in GSO satellite systems can share the band with passive sensors with suitable restrictions on the power flux-density (pfd) produced by GSO satellites at the sensor orbital altitude (see Annex 1);

e)      that No. S9.7 of the Radio Regulations of the specifies that satellite stations using the geostationary-satellite orbit must consider and coordinate with other space radiocommunication systems,

*recommends*

**1**      that, in view of *recognizing* b) and c), passive sensors and ISLs of non-GSO satellite systems should not operate on a co-frequency basis in the bands 116-122 GHz, 174.5-182 GHz and 185-190 GHz;

---

\*      This Recommendation should be brought to the attention of Radiocommunication Study Group 4.

\*\*      Radiocommunication Study Group 7 made editorial amendments to this Recommendation.

**2**          that, in view of *recognizing* d), passive sensors and ISLs of GSO satellite systems can share the 116-122 GHz band provided that the single-entry pfd at all altitudes from 0 to 1 000 km above the Earth's surface and in the vicinity of all geostationary orbital positions occupied by passive sensors, produced by a station in ISS, for all conditions and for all methods of modulation, does not exceed –148 dB(W/(m$^2$ · 200 MHz)) for all angles of arrival;

**3**          that, in view of *recognizing* d) and e), passive sensors and ISLs of GSO satellite systems can share the 174.5-182 GHz and 185-190 GHz bands provided that the single-entry pfd at all altitudes from 0 to 1 000 km above the Earth's surface and in the vicinity of all geostationary orbital positions occupied by passive sensors, produced by a station in the ISS, for all conditions and for all methods of modulation, does not exceed –144 dB(W/(m$^2$ · 200 MHz)) for all angles of arrival.

ANNEX  1

# Feasibility of sharing between the Earth exploration-satellite service (EESS) (spaceborne passive sensors) and the ISS operating near 118 and 183 GHz

## 1          Introduction

The frequency bands near 118 and 183 GHz are allocated to the EESS on a primary basis for passive sensors as shown in Table 1. The allocation near 118 GHz is shared with other services. Near 183 GHz, the passive services have an exclusively allocated band. A need has been identified in this band to expand the frequency range over which passive measurements can be made, and therefore the passive sensors may have to share with active services in adjacent bands. It is important that frequency sharing be examined:

–          to determine if currently allocated sharing at 118 GHz adequately protects the passive sensors; and

–          to determine if the expansion of the range over which passive sensors operate near 183 GHz would create potential sharing problem with other services.

TABLE  1

**EESS allocations at 116-126 GHz and near 183 GHz**

| Frequency band (GHz) | Allocation to services (all worldwide) |
|---|---|
| 116-126 | EESS  (PASSIVE)<br>FIXED<br>INTER-SATELLITE<br>MOBILE<br>SPACE  RESEARCH  (PASSIVE) |
| 174.5-176.5 | EESS  (PASSIVE)<br>FIXED<br>INTER-SATELLITE<br>MOBILE<br>SPACE  RESEARCH  (PASSIVE) |
| 176.5-182 | FIXED<br>INTER-SATELLITE<br>MOBILE |
| 182-185 | EESS  (PASSIVE)<br>RADIO  ASTRONOMY<br>SPACE  RESEARCH  (PASSIVE) |
| 185-190 | FIXED<br>INTER-SATELLITE<br>MOBILE |

## 2       Equipment characteristics

### 2.1       Passive sensors

#### 2.1.1       Low-Earth orbiting (LEO) scanning sensors

The LEO passive sensor used in this analysis is modelled from the advanced microwave sensing unit (AMSU). The AMSU-B is already deployed at 183 GHz and represents the current technology in microwave sensors.

The operation of the sensor is highly dependent upon a mechanically scanned antenna. The reflector moves within a cylindrical shroud. The cylinder has an opened area that allows the antenna to receive radiation across about ±50° of the Earth's surface and into the night sky up to about 85° from nadir. The antenna scans the Earth, moves to the sky for a cold calibration measurement, and then moves inside the shroud for a warm calibration measurement. The angle at which the antenna takes the cold measurement is constrained by the Earth limb and the area of the shroud needed to cover the antenna for a warm measurement. The calibration measurements are used to measure the receiving system gain. The AMSU scanning scheme has the advantage over other schemes that all receiving components remain the same between atmospheric and calibration measurements.

This scanning and calibration method is used on LEO sensors. Because the orbit is sun-synchronous, the sensor can always make a cold measurement at the same location relative to the spacecraft. Most other arrangements would risk having the calibration antenna point toward the sun and not produce a cold measurement.

#### 2.1.2       Geostationary orbiting sensors

Sensors have been proposed to operate in the geostationary orbit. A scanning type of antenna similar to the AMSU would sweep the visible portion of the Earth to about ±8° from the spacecraft's nadir. If this sensor uses cold space for calibration it could either point its scanning antenna away from the Earth similarly to the AMSU or have a separate antenna for calibration pointed at any convenient location. The cold calibration antenna must not only avoid the Earth but also the sun and preferably the moon. The AMSU sensor in sun-synchronous orbit can calibrate at the same location relative to the spacecraft and always avoid pointing toward the sun. If the geostationary satellite points anywhere within its orbital plane, it is likely to point at some time toward the sun or the moon and corrupt the cold measurement. It is therefore assumed that the geostationary satellite would point the cold calibration antenna in some direction that does not cause the antenna to aim near the sun, Earth or moon. Most isolation for the calibration antenna would occur if pointed normal to the equatorial plane. This points the calibration antenna at least 67° from the ecliptic where the directional gain would be relatively low.

#### 2.1.3       Push-broom sensors

At this time no push-broom sensors are in operation and no calibration method has been strictly defined. The push-broom sensor operates true to the analogy by having a series of small antenna beams across the spacecraft's track. Like bristles in the broom, the multiple beams sweep along the track. This system is not mechanical: each antenna beam is fixed. Therefore the Earth pointed beams cannot be used for cold calibration. If a separate antenna is used, it is not as constrained as the AMSU antenna in gain or calibration angle. The single constraint is that it must point toward cold space. If sun-synchronous orbits are used, the best direction is away from the sun, which is where the AMSU points. However the push-broom can use angles above the 85° limit imposed by the AMSU shroud.

#### 2.1.4       Limb sounding sensors

Limb sounding sensors would have characteristics that differ from the AMSU-B, but are not addressed in this analysis.

#### 2.1.5       Sensor characteristics

Sensor characteristics are given in Table 2 for the AMSU and GSO sensors. Two modes of operation for the sensor are considered in this analysis:

–       the scanning mode; and

–       the calibration mode.

The pointing angles for these two modes are given in Table 2.

TABLE 2

**Passive sensor characteristics**

| Parameter | AMSU-B | GSO |
|---|---|---|
| Antenna main-beam gain (dBi) | 45 | 66 |
| Antenna back-lobe gain (dBi) | –14 | –14 |
| Antenna beamwidth at half power points (degrees) | 1.15 | 0.102 |
| Sensor altitude range (km) | 500 to 1 000<br>850 (nominal) | 35 786 |
| Interference criteria per bandwidth (dB(W/200 MHz)) | –160 | –160 |
| Antenna measurement scan angles (from nadir) (degrees) | ± 50 | ± 8 |
| Cold calibration angle (from orbital plane) (degrees) | 90 ± 4 | 90 |
| Cold calibration angle range (from nadir) (degrees) | 65 to 85<br>83 (nominal) | 90 (nominal) |

The practical operational range for sensors in LEOs is between about 500 and 1 000 km. Operational or planned sensor systems in this band orbit at a nominal altitude of 833 km. However, orbits achieved by currently operating systems vary in altitude by as much as 20 km.

## 2.2     Inter-satellite systems

### 2.2.1     Modelled systems

The characteristics of an inter-satellite system modelled in this analysis are listed in Table 3. It is assumed to be a broadband digital system with a data rate of 200 Mbit/s, chosen to match the reference bandwidth of the sensor. This analysis is also applicable to broader band systems that have proportionally higher power.

TABLE 3

**ISL  parameters**

| Parameter | Value |
|---|---|
| Antenna mainbeam gain (dBi) | 45, 50, 55 or 60 |
| Antenna back-lobe gain (dBi) | –10 |
| System noise temperature (K) | 2 000 at 118 GHz and 3 000 at 183 GHz |
| Performance criterion of link, $C/N$ (dB) | 12 |

The link performance is chosen as a $C/N$ of 12 dB. This includes an $E_b/N_0$ of 10 dB for QPSK modulation and a 2 dB implementation loss. The system noise temperature is derived from the system design of ISLs in lower bands and the receivers built for the AMSU-B. A range of antenna gains between 45 and 60 dBi are examined. Generally, the 45 dBi antenna is chosen for low altitude links and the higher 55 or 60 dBi-antenna gain for higher altitudes and longer links. The antenna side-lobe patterns are modelled using the single feed circular beam antenna pattern from Recommendation ITU-R S.672.

The analysis was limited to scanning sensors and inter-satellite systems in circular orbits. ISLs are limited to a network of satellites with the same orbital altitude.

## 2.2.2 Operational systems in other bands

No known inter-satellite systems currently operate in the bands addressed in this analysis. In the ITU records Belarus, Malaysia, and the United States of America have advanced filed their intentions to operate space-to-space systems in the 116 to 126 GHz band. No advanced filings appeared for ISLs near 183 GHz. Of those that operate in other bands, most are either at the GSO or at LEOs nominally 700 to 800 km. A few operate above the sensor at orbits that range from 1 000 to 10 350 km. These systems use multiple satellite constellations to achieve full Earth coverage.

Table 4 lists several operating or proposed non-GSO ISL satellite constellations. The geocentric angles subtended by the links are listed for each constellation.

TABLE 4

**Example non-GSO satellite constellations**

| System | Number of orbits | Number of satellites per orbit | Separation within the orbit (degrees) | Separation between orbits (degrees) | Orbital altitude (km) |
|---|---|---|---|---|---|
| System A | 6 | 11 | 32.7 | 60 | 780 |
| System B | 3 | 4 | 90 | 120 | 10 350 |
| System C | 8 | 6 | 60 | 45 | 1 414 |
| System D | 4 | 8 | 45 | 90 | 775 |
| System E | 21 | 40 | 9 | 17.1 | 700 |
| System F | 6 | 8 | 45 | 60 | 950 |
| System G | 4 | 6 | 60 | 90 | 800 |
| System H | 2 | 5 | 72 | 180 | 500 |
| System I | 6 | 4 | 90 | 60 | 1 000 |

Existing or planned GSO satellite systems operating in other bands do not have, in general, evenly spaced satellites. For example, a look at one system shows five links with varying geocentric angles: 149°, 31°, 85°, 85° and 125°. Table 5 shows the maximum longitudinal spacing for ten GSO constellations along with their antenna gains.

TABLE 5

**Parameters of example GSO inter-satellite systems**

| System | 1 | 2 | 3 | 4 | 5 | 6 | 7 | 8 | 9 | 10 |
|---|---|---|---|---|---|---|---|---|---|---|
| Antenna gain (dBi) | 58.5 | 59 | 58 | 46 | 55.5 | 60.3 | 53 | 50.3 | 49.1 | 55.7 |
| Maximum longitudinal spacing (degrees) | 162.6 | 162.6 | 78.6 | 10.1 | 67.3 | 162.6 | 53.9 | 111.1 | 77.4 | 136.4 |

# 3      Approach

This analysis considers a broad range of parameters for ISL constellations and determines what restrictions on these parameters would permit co-channel sharing. Sharing is considered to be feasible only if the restrictions on the ISL parameters permit the development of systems similar to systems that are planned for other bands.

Unacceptable interference to the Earth-exploration satellite (passive) service is determined by two criteria. First is an interference threshold of –160 dB(W/200 MHz). Interference above this level is considered to be unacceptable. This power level corresponds to 20% of the sensitivity (Recommendation ITU-R RS.1029) of the sensor. Interference received above this level will increase the temperature reading that the satellite is making and corrupt long-term temperature averages. Another –3 dB will be added to the sensitivity to account for sharing with between space and terrestrial services. The second criterion is temporal and is applied when the first criterion, threshold level, is exceeded. The interference should not exceed the threshold for more than 0.01% of the time. This percentage is given in *recommends* 4 of Recommendation ITU-R RS.1029.

## 3.1      Analysis organization

The analysis is presented in two investigations. The first is interference to LEO sensors from ISLs in orbits from close to the Earth to the geostationary orbit. The second investigation is interference into sensors in the geostationary orbit from both GSO and non-GSO ISLs.

Each of these investigations starts with a static analysis that identifies the circumstances under which interference can occur. These circumstances are mainly the orbits of the ISLs and the position of the ISL transmitter relative to the sensor. These interference parameters are applied to a temporal analysis which identifies how many transmitters could operate without exceeding the temporal criterion. Circumstances are then investigated to determine if interference can be avoided by restricting operating parameters of the ISLs or the passive sensors. Finally the restrictions are determined for the number of ISLs, length of inter-satellite paths, and pointing restrictions of sensor antennas. These restrictions are compared to those of operating or planned systems in other bands to determine if the constraints are practicable.

## 3.2      Establishment of geometries causing interference

The analysis examines antenna coupling for all possible orientations of the sensor and ISL transmitter. The analysis of relative positions of the sensor satellite and the interfering satellites is performed to find those positions or orientations that cause interference. This investigation considers altitude differences, geocentric angles between the sensor and the ISL transmitter, and antenna orientations. The ISLs are first analysed with the path centre 200 km above the Earth to keep the path above the atmosphere. The inter-satellite path length in terms of geocentric angle is then reduced while observing the maximum interference orientations to determine the maximum length of the link that precludes unacceptable interference. The results of this analysis identify the specific orientations and configurations that cause interference. It bounds the relationship between geocentric angle and altitude that precludes interference.

An algorithm was set up to calculate the received power of an interfering satellite at the sensor for variations of altitude, inter-satellite path length, geocentric angle between the sensor and interfering satellite, and ISL antenna gain. The received power at the sensor was calculated from the geocentric angle between the sensor and the ISL transmitter. The geocentric angles varied from the horizon to the sensor's nadir as shown in Fig. 1.

The power of the transmitter is calculated to maintain a constant link performance, as specified in Table 3, taking into account the distance of the ISL path and the gains of the two antennas. The height of the inter-satellite path and the geocentric angle are related and define the length of the ISL path. This geometry is illustrated in Fig. 2.

FIGURE 1

**Visibility angles between the sensor and the ISL transmitter**
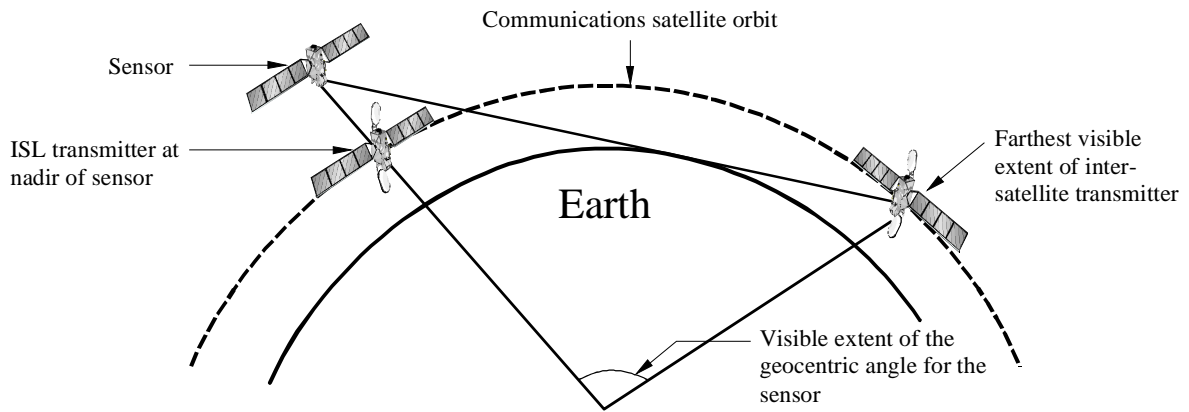


1416-01

FIGURE 2

**ISL geometry**
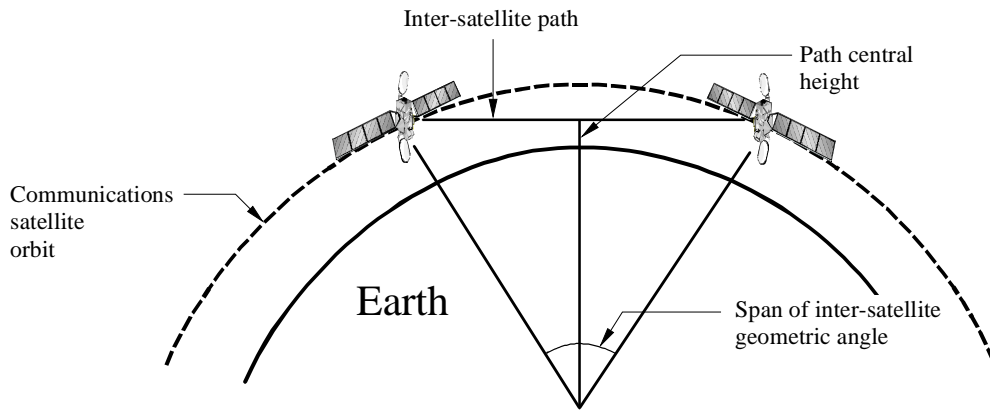


1416-02

The path length of the ISL was evaluated using equation (1):

$$d_{link} \; = \; 2 \sqrt{\left(R_e \; + \; Alt_{non\text{-}GSO}\right)^2 \; - \; \left(R_e \; + \; Alt_{centre}\right)^2} \tag{1}$$

where:

$d_{link}$ : distance (m) from the ISL transmitting satellite to the ISL receiving satellite

$R_e$ : radius of the Earth = 6 378 140 m

$Alt_{non\text{-}GSO}$ : altitude of the non-GSO orbit (m)

$Alt_{centre}$ : altitude of the centre of the non-GSO link path (m) (see Fig. 2).

The power of the ISL transmitter was calculated using equation (2):

$$P_t = -20 \log \left( \frac{0.3}{4\pi f d_{link}} \right) + 10 \log (k\,T\,B)\, 2\,G_{ISL} + 12 \qquad (2)$$

where:

    $P_t$:         ISL power (dBW)

    $f$:         tuned frequency of the sensor in (Hz)

    $k$:         Boltzman's constant $= 1{,}38 \times 10^{-23}$ J/K

    $B$:         reference bandwidth of the sensor (Hz)

    $T$:         noise temperature of the ISL receiver ($K$)

    $G_{ISL}$:         gain of the ISL antennas (dBi) (assumed to be equal for transmitter and receiver)

    12:         performance level of the ISL receiver (rapport $C/N = 12$ dB).

The calculated transmitter power is then used to determine the received interference power considering the path length between the sensor and the transmitter plus the relative gains of the respective antennas toward each other. The received power at the sensor is calculated for all geocentric angular distances from the mutual horizon to the point where the satellites are in line with the centre of the Earth (see Fig. 1). The power to the sensor receiver was calculated using equation (3).

$$P_r = P_t + G_{ISL}(\varphi) + G_{sensor}(\alpha) + L_{fs} \qquad (3)$$

where:

    $P_r$:         received interference power (dBW)

    $G_{ISL}(\varphi)$:         angle dependent gain of the ISL transmitting antenna

    $\varphi$:         off-main-beam angle from the ISL transmitting antenna to the sensor receiver

    $G_{sensor}(\alpha)$:         angle dependent gain of the sensor antenna toward the ISL transmitter

    $\alpha$:         off-boresight angle of the sensor antenna toward he ISL transmitter

    $L_{fs}$:         free-space loss (dB) between the ISL transmitter to the sensor receiver.

The relationship of the received power vs. geocentric angle was plotted as parameters were varied. This identified the worst interference situations and showed what combinations of these parameters would eliminate interference.

## 3.3 Temporal analysis of interference-causing constellations

The output of the previous section identifies sensor and interfering satellite orientations that cause interference, primarily via main beam coupling. The temporal criterion of 0.01% is applied to these orientations.

The analysis considers interference from constellations orbiting above and below the sensor. The ISL constellation is analysed as if it were a random distribution of ISL satellites on a sphere.

Interference is considered to come from any position on the ISL constellation sphere for which the signal received at the sensor from that position exceeds the interference threshold. At each position, excessive interference comes from a small elliptical or circular area on the sphere whose area is determined from the antenna main beam gain and the distance of that sphere from sensor. These small areas are the intersections of the sensor antenna's main beam with the constellation sphere.

Because of the assumption of a random distribution of satellites on the ISL constellation sphere, an area ratio can represent the amount of interference over time. For a single satellite, this is the ratio of the interference area on the sphere to the total surface area of the sphere.

The temporal analysis provides the percentage of time that a single satellite in an ISL constellation exceeds the interference threshold. Comparison of this number to the temporal criterion of 0.01% determines the maximum number of ISL satellites allowed to exceed the interference power threshold.

The static analysis is repeated for the geostationary orbiting sensors but because ISLs in the GSO are fixed, no temporal analysis is needed. A temporal analysis will be presented using the area ratio technique for interference from LEO satellite constellations.

## 3.4 Comparison

In summary, the initial interference analysis provides restrictions in orbital altitude and geocentric angle that avoid interference. For those satellite configurations that do not conform to these restrictions, a temporal analysis determines the number of satellites that can exceed the power threshold while conforming to the 0.01% temporal criterion. Parameters of satellite constellations planned for other bands are compared to these restrictions in order to evaluate whether these restrictions are practical for satellite systems to share these bands with passive sensors.

## 4 Analysis

### 4.1 Interference to LEO sensors

#### 4.1.1 Identification of circumstances causing interference

Initially it is necessary to determine under what circumstances, if any, the power levels of an ISL could exceed the interference threshold of the sensor. To investigate this, a series of calculations were performed with the sensor and ISL transmitter at various orientations to each other. To represent the worst case orientations, the sensor, ISL, and Earth centre are in the same plane. The ISL transmitter is approaching the sensor normal to the sensor's orbital plane. The ISL antenna is aimed in the direction of the sensor. Figure 1 shows the range of angles from the horizon to the nadir of the sensor over which calculations were performed. Figures 3 and 4 are graphs of interference power into the sensor from ISLs over the range of angles illustrated in Fig. 1. Figure 3 represents interference power for the sensor in the scan mode and Figure 4 shows it in the calibration.

FIGURE 3

**Interference power - Scan mode**
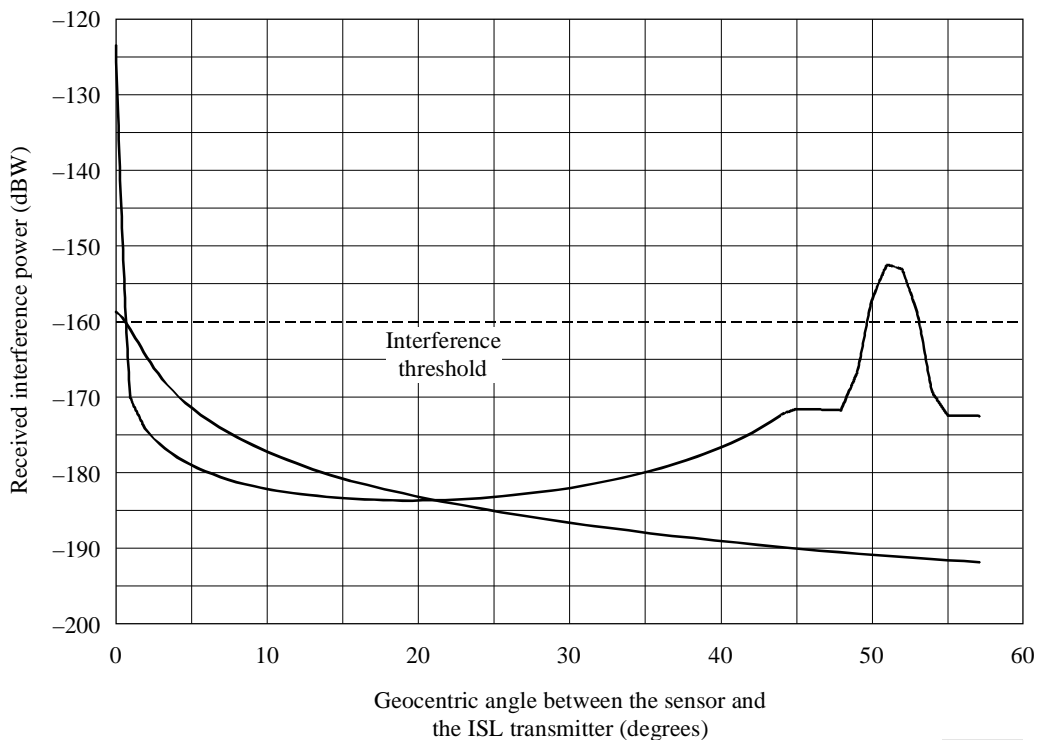


1416-03

FIGURE 4

**Interference power - Calibration mode**



Geocentric angle between the sensor and
the ISL transmitter (degrees)
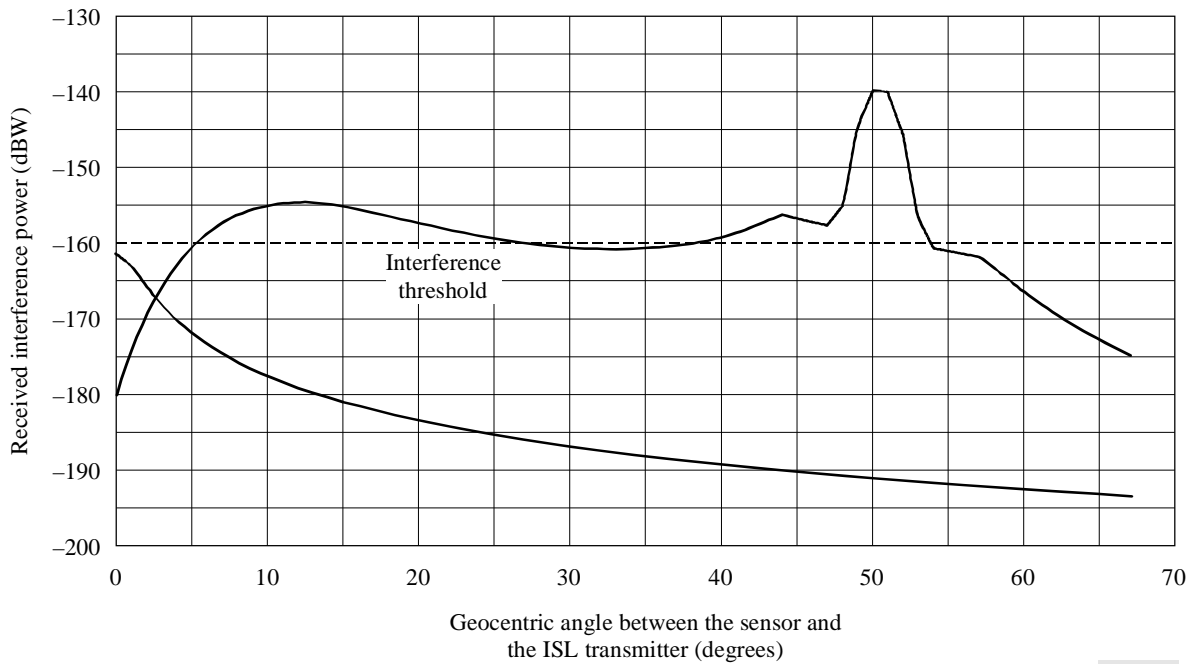
1416-04

Three lines are plotted on Figs. 3 and 4. The horizontal line at –160 dBW represents the interference threshold of the sensor. The lower curved line is a plot of the interference power received by the sensor assuming that both the sensor and ISL transmitter had 0 dBi gain omnidirectional antennas. The third line with peaks is a plot of interference power with directional gains for the sensor and ISL transmitter. The relative magnitudes of the interference curves show the effect of the high gain antennas. Observing from Fig. 3 the omnidirectional-gain-antenna curve only exceeds the threshold when the ISL transmitter is close to the sensor near 0°. The high gain antenna curve exceeds the interference threshold both when the ISL transmitter is near 0° and in the sensor antenna's main beam and when the ISL transmitter is nearer the horizon and its main beam illuminates the sensor. From Fig. 4 the interference level is above the threshold when the ISL transmitter is near the main beam of the sensor calibration antenna and again when the sensor is in the main beam of the ISL transmitter antenna.

In both Figures interference levels are high if the ISL transmitter gets near the main beam of the sensor antenna. Figure 5 illustrates the ranges over which the sensor antenna could be operating.

FIGURE 5

**Sensor angles and ranges for the scan and calibration modes**
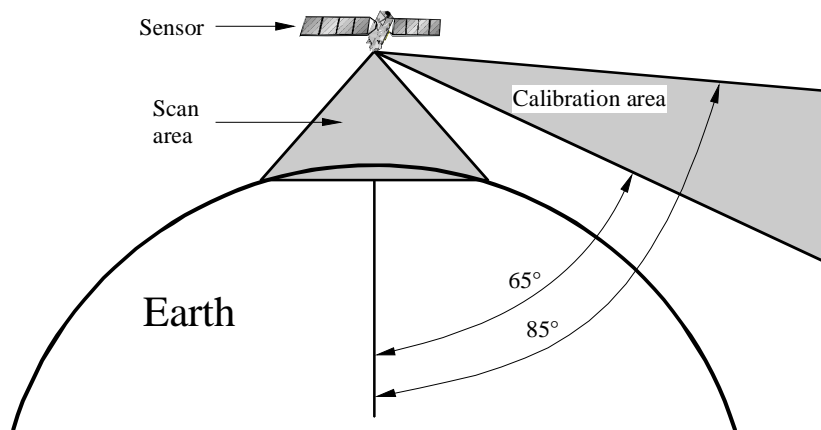


1416-05

Figure 5 can be applied to both the AMSU and push-broom sensors. The scan for the AMSU is the range over which the antenna sweeps during operation. For the push-broom sensor, multiple beams are continuously covering this area. The calibration area shown in the Figure is the range of angles that can be used by the AMSU sensor. In operation it will use only a single angle, nominally about 83°. The push-broom must use a separate antenna for cold calibration and is not as constrained as the AMSU. It can be pointed in any direction that will not include the Earth. But as a secondary consideration it must also avoid the sun. If a sun-synchronous orbit is used, as is assumed, it could point up to and beyond the horizontal. Also it could point along or oblique to the orbital plane.

Because excessive interference can occur when the ISL transmitter is in the sensor main beam, it occurs when it is in the shaded areas of Fig. 5. The scan mode therefore receives interference into the main beam of its antenna from constellations that orbit below the sensor. In contrast the calibration mode of the sensor is subject to interference into its main beam from satellite orbits both above and below its orbit. These interference orientations are illustrated in Figs. 6 and 7.

FIGURE 6

**Interference when the ISL transmitting satellite is in the
scanning beam of the sensor**



1416-06
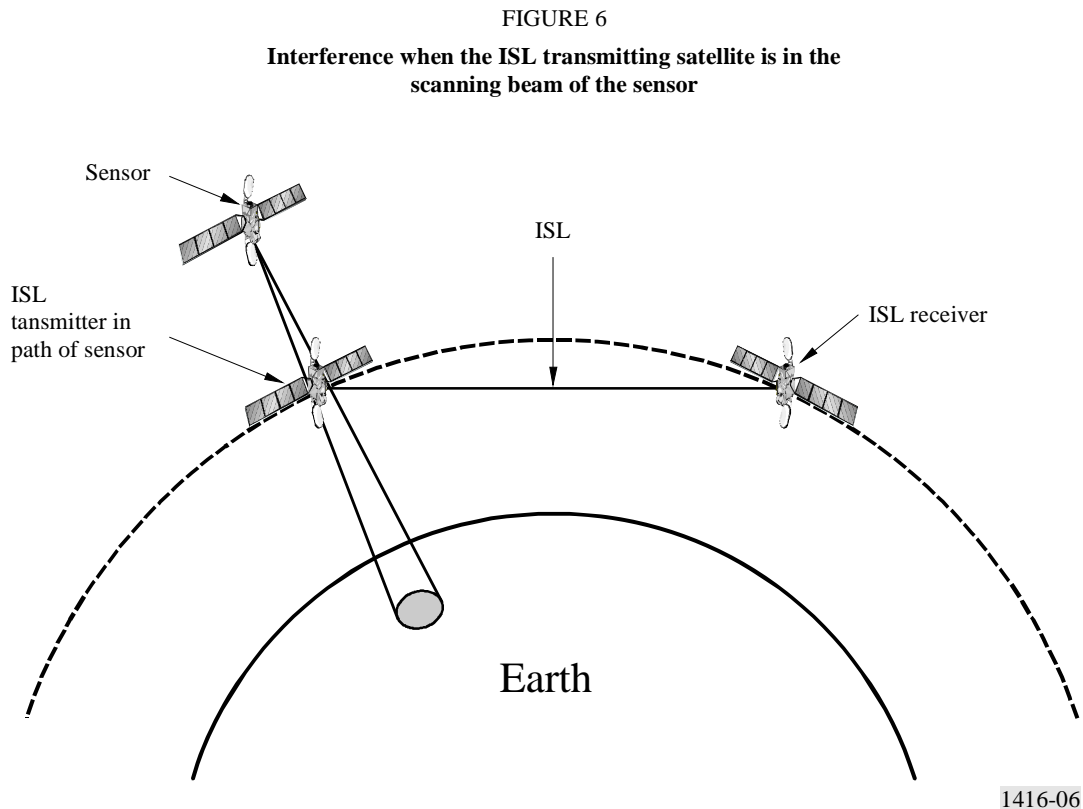
Interference also occurs as determined earlier when the main beam of the ISL transmitter intercepts the sensor. Figures 8 and 9 illustrate the intersection of the ISL main beam from constellations both below and above the sensor.

### 4.1.2 Temporal analysis

### 4.1.2.1 Low altitude analyses

Three areas of interference were identified:

– below the sensor in the scan mode where the main beam of the sensor couples with the ISL side lobe;

– to the side of the sensor in the calibration mode, when the sensor calibration antenna couples to the side lobe of the ISL transmitter satellite; and

– where the ISL transmitter main beam couples to the sensor's side lobe.

FIGURE 7

**Interference when ISL transmitter is in calibration antenna main beam**
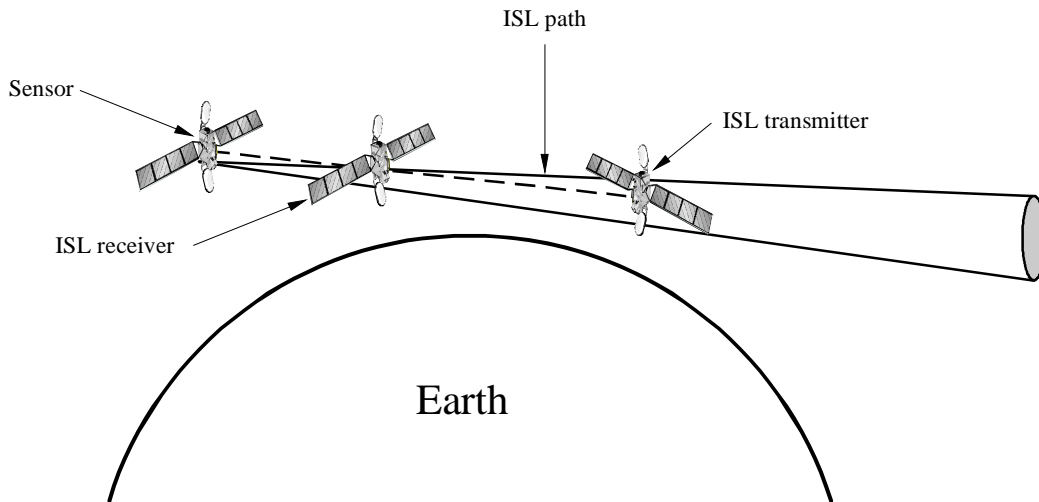


FIGURE 8

**Interference in calibration mode from ISL transmitter antenna main beam
or constellation orbiting below the sensor**
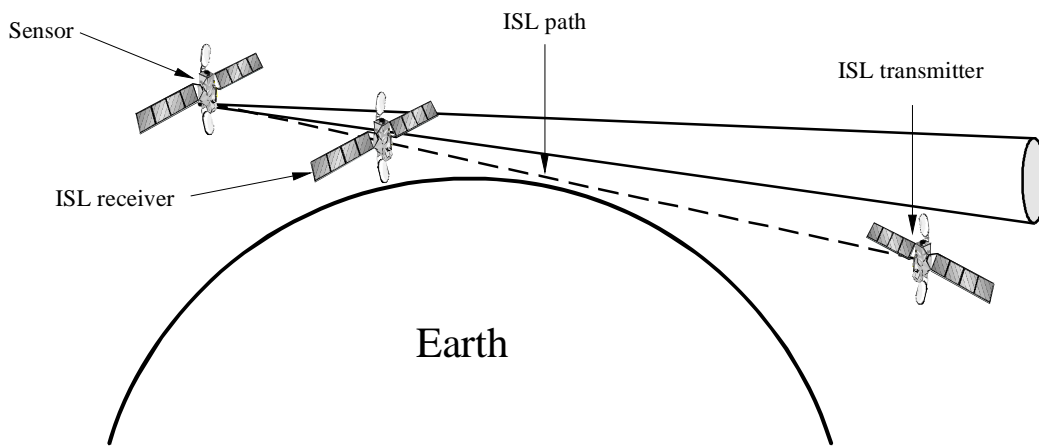


Results of this analysis (see Fig. 10), show that a maximum of eight satellites in the entire orbital sphere can share the 118 GHz band, and five satellites can share the 183 GHz band, if they are in an orbit near 300 km altitude. The number that can share drops to two satellites at around 500 km altitude, and to zero at 900 km altitude. The curve is a composite of the three probabilities for the three interference areas caused by main beam coupling to the sensor's scanning antenna, the sensor calibration antenna, and the ISL transmitter antenna. The dominant interference mechanism is ISL main beam transmission into the sensor side lobes. At 749 km altitude, interference into the sensor antenna during calibration dominates the composite curve.

FIGURE 9

**Interference in calibration mode from ISL transmitter antenna main beam
or constellation orbiting above the sensor**



1416-09
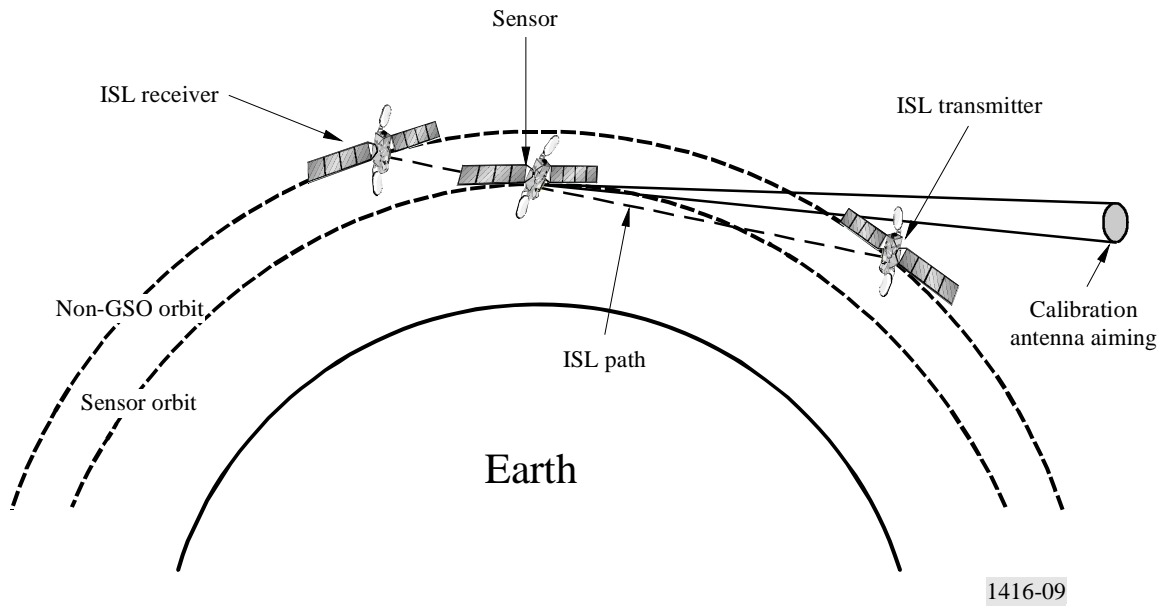
FIGURE 10

**Number of satellites in LEO constellation that meet 0.01% criterion**



1416-10
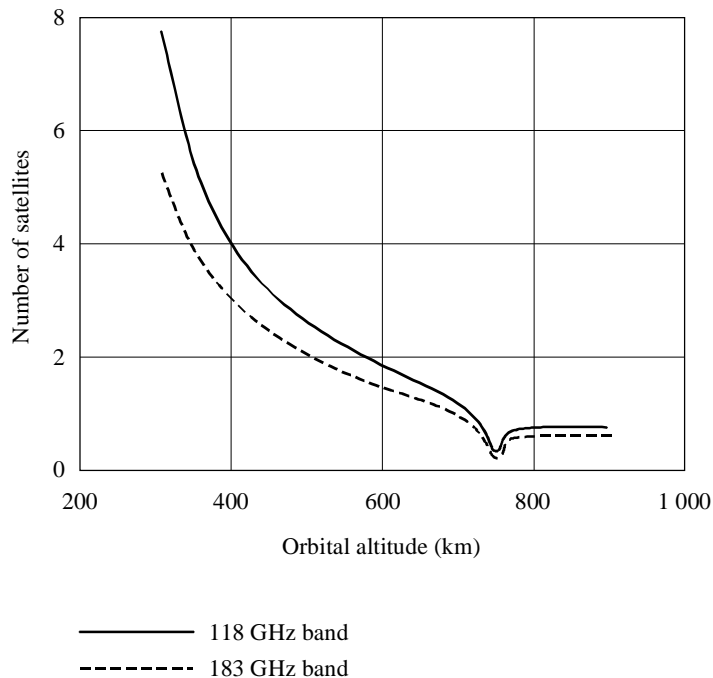
The calibration angle for the sensor influences the potential for sharing, as illustrated above. Generally, when interference can be received into the calibration antenna, only one satellite can share without violating the 0.01% criterion. As the calibration angle is changed from 65° to 85°, the maximum interference altitude moves upward. Table 6 shows the maximum-interference altitude for the range of calibration angles from 65° to 85° where the least number of satellites can share.

TABLE 6

**Minimum interference altitude to sensor antenna in calibration mode**

| Calibration angle (degrees) | Minimum interference altitude (km) |
|---|---|
| 65 | 308 |
| 70 | 555 |
| 75 | 749 |
| 80 | 888 |
| 85 | 971 |

### 4.1.3    Analysis of interference avoidance for ISLs

The ISL path lengths considered up to now produce the maximum amount of interference because they were the longest paths requiring the most transmitter power. Anything that reduces the satellite e.i.r.p. will reduce the interference levels. Two factors that affect the e.i.r.p. are the antenna gain and path length. If the ISL were designed with matching transmit and receive antennas, every decibel increase in the antenna gain results in a 2 dB increase in the ISL received signal power. To maintain the same received signal power, the ISL transmitter power can therefore be reduced to 2 dB. In other words, each decibel increase in antenna main beam gain results in a 1 dB reduction in main-beam e.i.r.p. and a reduction in side-lobe radiation. The required e.i.r.p. is also proportional to the square of the distance, so reduction of the link length reduces the e.i.r.p. and therefore the interference power received. There exists a maximum ISL path length for each altitude for which no unacceptable interference occurs.

Figures 11 and 12 show the maximum geocentric angle for ISLs that precludes unacceptable interference. These results were obtained by calculating the interference power at the sensor, and reducing the ISL path length until this power falls below the threshold of –163 dBW. ISL transmit and receive antenna gain is 45 dBi.

FIGURE 11

**Maximum geocentric angle for an inter-satellite system to avoid interference to the spaceborne sensors when a sensor is in the scanning mode at 850 km altitude**
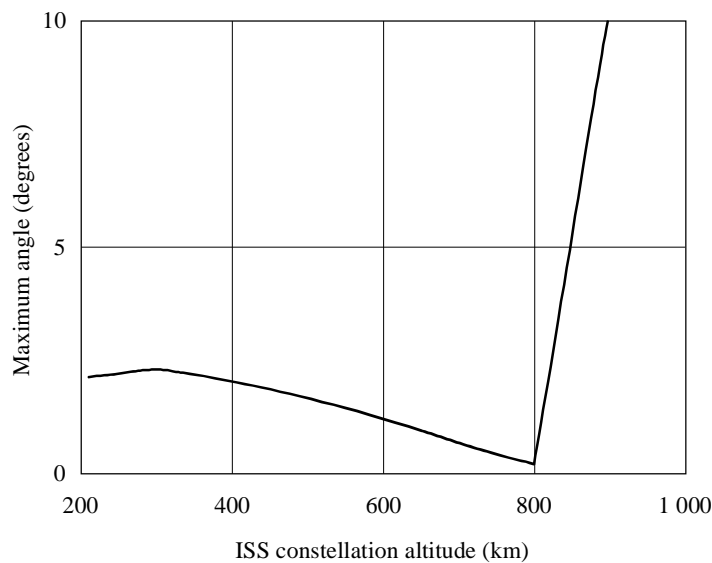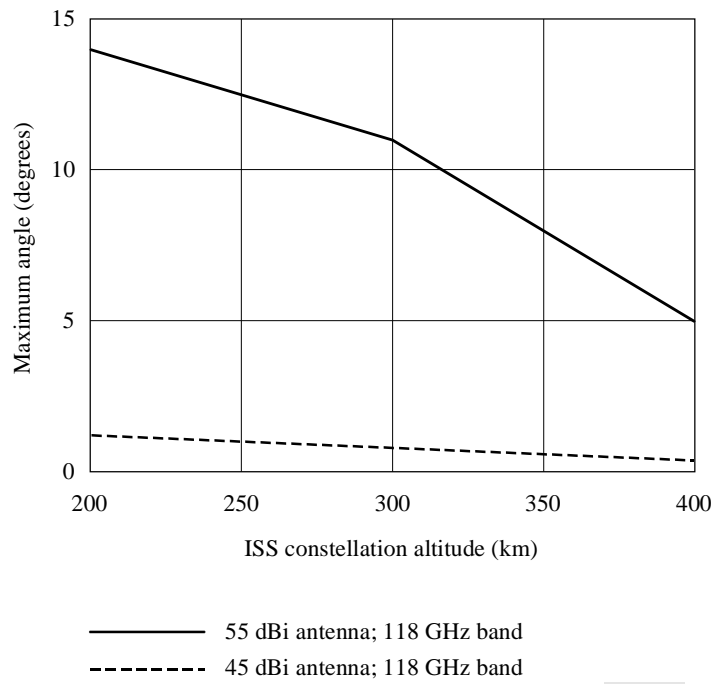


1416-11

Figure 11 depicts the case for the sensor at an altitude of 850 km in the scan mode with the ISL links below and slightly above it. The maximum geocentric angle is 2° or less for the scan mode until the ISL constellation is above the sensor's altitude. The maximum angle approaches zero when the altitudes of the ISL constellation and the sensor satellite are equal. In the calibration mode, shown in Fig. 12, the maximum angle is less than 1°. Therefore the calibration mode is more susceptible to interference.

FIGURE 12

**Maximum geocentric angle for an inter-satellite system to avoid interference to the spaceborne sensors when a sensor is in the calibration mode at 83° and 850 km altitude**
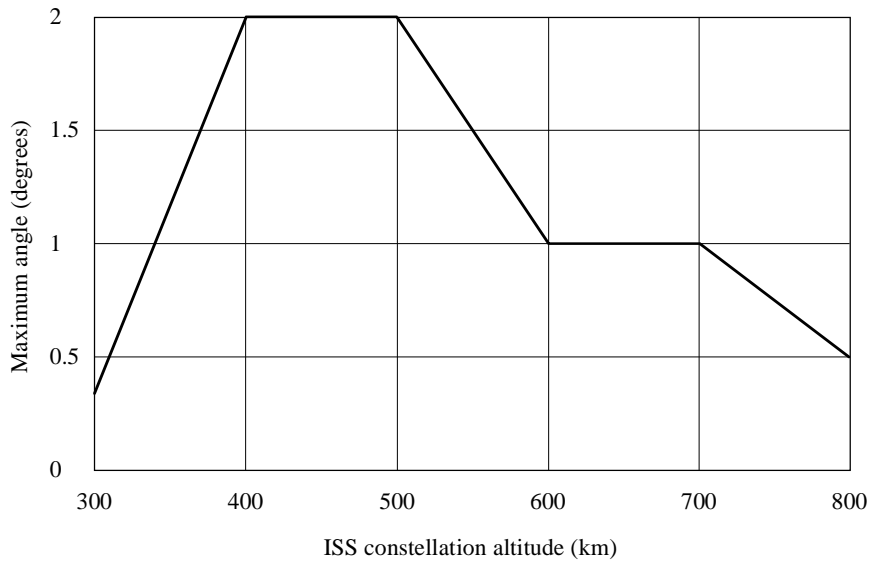


1416-12

The range of usable orbits for the sensors is 500 to 1 000 km. From Fig. 11 it can be observed that sharing is not feasible with ISLs at the same altitude but the sharing possibilities increase as the ISL transmitter orbit becomes lower than the sensor. Since the sensor can be anywhere from 500 to 1 000 km ISLs cannot occupy this orbital range. The sharing possibilities would be below 500 km for a sensor at 500 km and above 1 000 km with the sensor at that altitude. Figures 13 and 14 show the angle restrictions when the sensor is at 500 km for the scan and calibration modes, respectively. Figures 15 and 16 similarly show the angle restrictions for the sensor at 1 000 km altitude with ISLs above it. In these Figures two antenna gains are investigated for the ISL. Plots are provided for both a 45 dBi and 55 dBi antenna on the ISL.

Increasing the antenna gain for the ISL increases the link angles that avoid interference. First, this is because less ISL transmitter e.i.r.p. is required. Secondly, the ISL transmitter antenna has a narrower beam, which decreases emissions off the main lobe.

For the case when the ISL is above the sensor at 1 000 km, the antenna gain seems to have little effect in the scan mode (Fig. 15) and the geocentric angle limit of the ISL is less restrictive. The antenna gain of the ISL has more effect in the calibration mode (Fig. 16). The 45 dBi antenna is still quite restricted while the 55 dBi antenna is not. Figures 14 and 16 show the increased sharing achievable with higher gain ISL antennas.
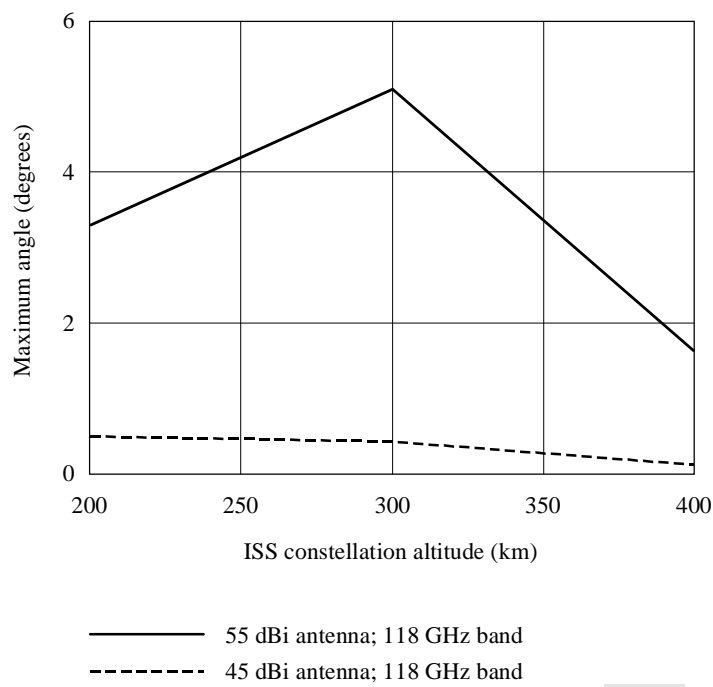
FIGURE 13

**Maximum geocentric angle for an inter-satellite system to avoid interference to the spaceborne sensors when a sensor is in the scanning mode at 500 km altitude**
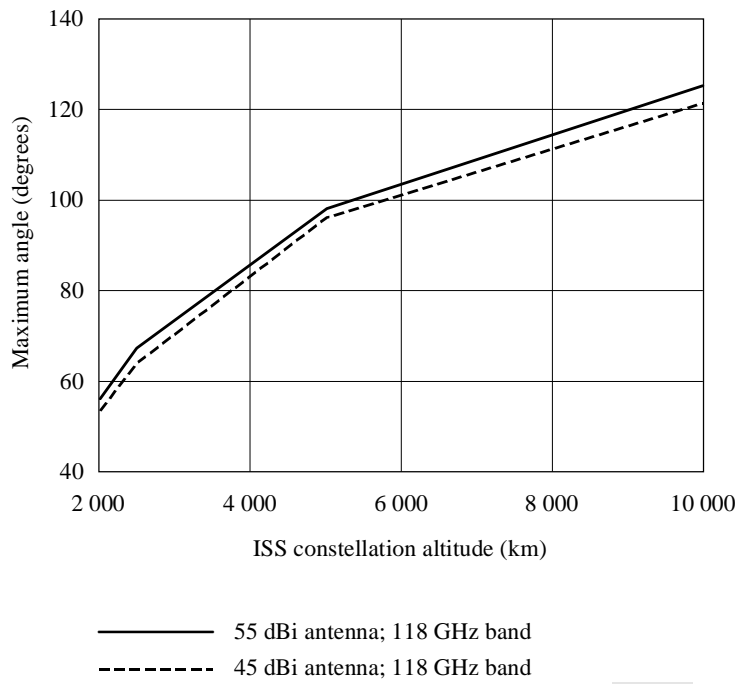


1416-13

FIGURE 14

**Maximum geocentric angle for an inter-satellite system to avoid interference to the spacecraft sensors when a sensor is in the calibration mode at 83° and 500 km altitude**
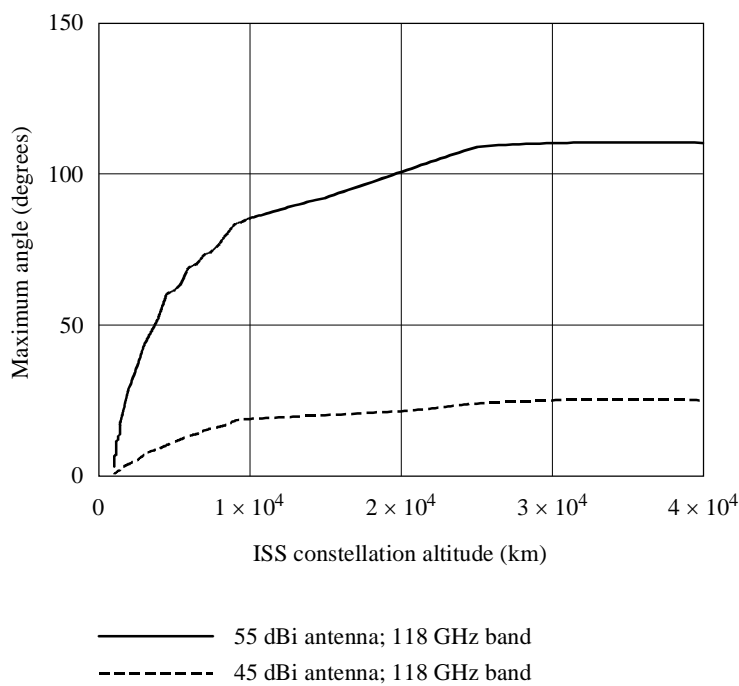


1416-14

FIGURE 15

**Maximum geocentric angle for an inter-satellite system to avoid interference to the spaceborne sensors when a sensor is in the scanning mode at 1 000 km altitude**



1416-15

FIGURE 16

**Maximum geocentric angle for an inter-satellite system to avoid interference to the spaceborne sensors when a sensor is in the calibration mode at 83° and 1 000 km altitude**



1416-16

**4.1.4    Restrictions on sensor calibration angle and antenna gain to facilitate sharing**

The sensor antenna calibration proved to be the most constraining mode for restricting sharing with the ISS. The sensor calibration antenna gain and angle were fixed at 45 dBi and 83° for the analysis. Just as a different antenna gain reduced the sharing restrictions on the ISLs, adjustments of antenna gain and calibration angle might improve the sharing possibilities. However, with implementation of a different calibration antenna on future sensors, the gain is likely to decrease rather than increase. Tables 7 and 8 present the results of an investigation into the restrictions caused by sensor antenna gains and orientation.

Table 7 presents the results of an investigation to determine how close the transmitter and receiver used on the ISL should be to avoid excessive interference. Altitudes both above and below the sensor are investigated. The sensor was set at 850 km and the calibration angle fixed at 90° from nadir. The less restrictive calibration angle could be deployed if separate antennas were used for calibration. The maximum geocentric angle is given in the Table 7 for combinations of ISL orbital altitude and calibration antenna gain.

TABLE  7

**Maximum ISL geocentric angle that fully protects passive
microwave sensors in an 850 km orbit**

| Non-GSO orbit height (km) | Calibration antenna gain | | | |
|---|---|---|---|---|
| | 45 dBi | 40 dBi | 35 dBi | 30 dBi |
| 300 | 2° | 5° | 10° | 20° (maximum distance)[1] |
| 400 | 2° | 4.4° | 8° | 21° |
| 500 | 1° | 3.3° | 5° | 13° |
| 600 | 1° | 1.9° | 3° | 8° |
| 700 | 0.5° | 1° | 2° | 3.8° |
| 800 | 0.2° | 0.2° | 0.5° | 0.9° |
| 1 500 | 2° | 4° | 7° | 12° |
| 2 000 | 4° | 7° | 12° | 18° |
| 2 500 | 7° | 11° | 14° | 25° |
| 3 000 | 8° | 13° | 20° | 30° |
| 5 000 | 13° | 21° | 31° | 45° |
| 10 000 | 17° | 27° | 40° | 59° |
| 15 000 | 21° | 33° | 49° | 67° |
| GSO | 134° | 143° | 149° | 153° |

[1]   The entry indicating (maximum distance) means that the link would pass through the atmosphere before the interference criteria were achieved.

Again from Table 7 it can be observed that the lower calibration antenna gains would increase the sharing possibilities. Also the closer the ISL orbit is to the sensor orbit, the more restrictive the angles become. Restrictions become even greater when considering that the analysis considered only an 850 km orbit and the sensors could be in an orbit from 500 to 1 000 km. However, the angles are not very restrictive for ISLs at the GSO considering that the maximum angle a GSO link can span without blockage form the Earth is 162.6°.

Table 7 illustrates the sensitivity of calibration antenna gain and pointing angle to interference from ISLs in orbits lower than the sensor. The minimum calibration angle that keeps the interference level below the threshold is presented for combinations of altitude and calibration antenna gain. The AMSU has an antenna gain of 45 dBi but the push-broom sensor could be using lower gains. In this example the sensor is in an 850 km orbit.

TABLE 8

**Minimum calibration angle from nadir to fully protect calibrating
microwave sensors from ISLs with the sensor in an 850 km orbit**

| Non-GSO orbit height (km) | Calibration antenna gain | | | |
|---|---|---|---|---|
| | 45 dBi | 40 dBi | 35 dBi | 30 dBi |
| 300 | 145° | 115° | 97° | 86° |
| 400 | 170° | 130° | 105° | 91° |
| 500 | 175° | 135° | 110° | 93° |
| 600 | >180° | 145° | 115° | 96° |
| 700 | >180° | 145° | 120° | 100° |
| 800 | >180° | 145° | 120° | 100° |

NOTE 1 – Entries showing >180° indicate that excessive interference cannot be avoided.

From Table 8 it can be observed that the lower the calibration antenna gain, the lower the calibration angle can be without receiving excessive interference. None of the angles determined in this investigation were as low as the range for the AMSU. This implies that protection cannot be achieved for sensors similar to the AMSU from lower ISLs orbits.

One clear observation in this analysis is that lower calibration angle gains increase sharing possibilities with ISLs. However, the calibration antenna must view only cold space and lower gain antennas would have broader antenna side-lobe patterns and expose the calibration antenna partially to the Earth, the atmosphere or the sun. Additionally a wider antenna view would expose the receiver to interference from multiple ISLs. Only a single link is considered here. Although 30 dBi may not be the smallest antenna usable for calibration, it has a 6.5° beamwidth and is likely to be near the limit.

**4.1.5     Limitations on ISLs in the GSO**

Some GSO systems can meet the interference criteria as noted from the wide angles shown in Table 7. In order for sharing to be considered feasible, limits must be placed on the GSO systems to protect the passive sensors. The worst scenario is coupling directly into the sensor's main beam during calibration. Therefore, setting a pfd limit based upon main beam coupling would protect the sensor. The interference threshold of –163 dBW per 200 MHz translates to a pfd of –145 dB(W/m$^2$) at 118 GHz and to –141 dB(W/m$^2$) at 183 GHz. Calculations are shown in Table 9.

TABLE 9

**Determination of pfd to protect passive sensors from emissions from ISLs in geostationary orbit**

| Item | 118 GHz band | 183 GHz band |
|---|---|---|
| Sensor interference threshold (dBW) | –163 | –163 |
| Antenna gain (dBi) | 45 | 45 |
| Effective aperture (dB/m$^2$) | –63 | –67 |
| Factor for multiple GSO systems (dB) | 3.0 | 3.0 |
| pfd threshold (dB(W/(m$^2$ · 200 MHz))) | –148 | –144 |

### 4.1.6    Compatibility summary on LEO sensors

Compatibility is determined by comparing the operational restrictions evaluated above with sample systems that are either planned or operational in this or other bands. These systems are described in § 2. The following conclusions can be drawn from the analysis and comparison to other systems.

–    ISL transmitters can produce interference over the sensor's threshold when near-main-beam antenna coupling occurs. Interference power levels can be below the threshold in other orientations.

–    Of the example ISL transmitters that exceed the threshold, fewer than eight can be in orbits below the sensor without exceeding the temporal criterion for sharing.

–    Although a lower calibration antenna gain does reduce the potential for interference to passive sensors in the calibration mode, the gain cannot be reduced sufficiently to permit ISLs with reasonably long range links distances as determined by comparing the calculated restrictions with typical systems planned or operating in other bands.

–    Restricting the angle off nadir where the sensor calibration antenna is aimed also reduces interference from ISLs at certain orbits, but the restrictions are not within the operating range of sensors already being deployed and may not be feasible.

–    Closer spacing of spacecraft with ISLs can reduce the potential for interference but the permissible maximum geocentric angles may not be practicable for communications satellite systems.

–    The push-broom sensor has fewer restrictions on its calibration antenna than the AMSU sensor, but the additional capability does not appear to significantly improve its immunity to interference from ISLs.

–    GSO ISLs can share with sensors provided their pfd at the sensor's orbit does not exceed certain limits.

The general conclusion of this section is that the restrictions either on the sensor or ISL parameters that would be needed to provide adequate protection may be too restrictive for typical systems that may be planned or implemented.

## 4.2    Interference to geostationary orbiting sensors

### 4.2.1    Identification of interference situations

Sensors in geostationary orbit will operate with a scanning type of antenna that would sweep the visible portion of the Earth to about $\pm 8°$ from the spacecraft's nadir. If this sensor uses cold space for calibration it could either point its scanning antenna away from the Earth similarly to the AMSU or have a separate antenna for calibration pointed at any convenient location. The cold calibration antenna must not only avoid the Earth but also the sun and preferably the moon. The AMSU sensor in sun-synchronous orbit can calibrate at the same location relative to the spacecraft and always avoid pointing toward the sun. If the geostationary satellite points anywhere within its orbital plane, it is likely to point at some time toward the sun or the moon and corrupt the cold measurement. It is therefore assumed that the geostationary satellite would point the cold calibration antenna in some direction that does not cause the antenna to aim near the sun, Earth or moon. Most isolation for the calibration antenna would occur if pointed either due north or south at 90° from the equatorial plane. This points the calibration antenna at least 67° from the ecliptic where the directional gain would be relatively low.

As noted, the calibration antenna would likely be aimed away from the Earth and away from the geostationary orbital plane. Since interference is predominantly due to near main beam coupling, the calibration antenna is unlikely to receive excessive interference. The interference modes that would likely effect the GSO satellite sensor would be:

1    The Earth facing antenna in the scan mode from the main beam of lower orbiting satellites.

2    The Earth facing antenna in the scan mode from side lobes of lower orbiting satellites.

3    The sensor in either mode from ISL links of satellites in the geostationary orbit.

Figure 17 illustrates the three possible modes.

FIGURE 17

**Interference modes to sensors in geostationary orbit**
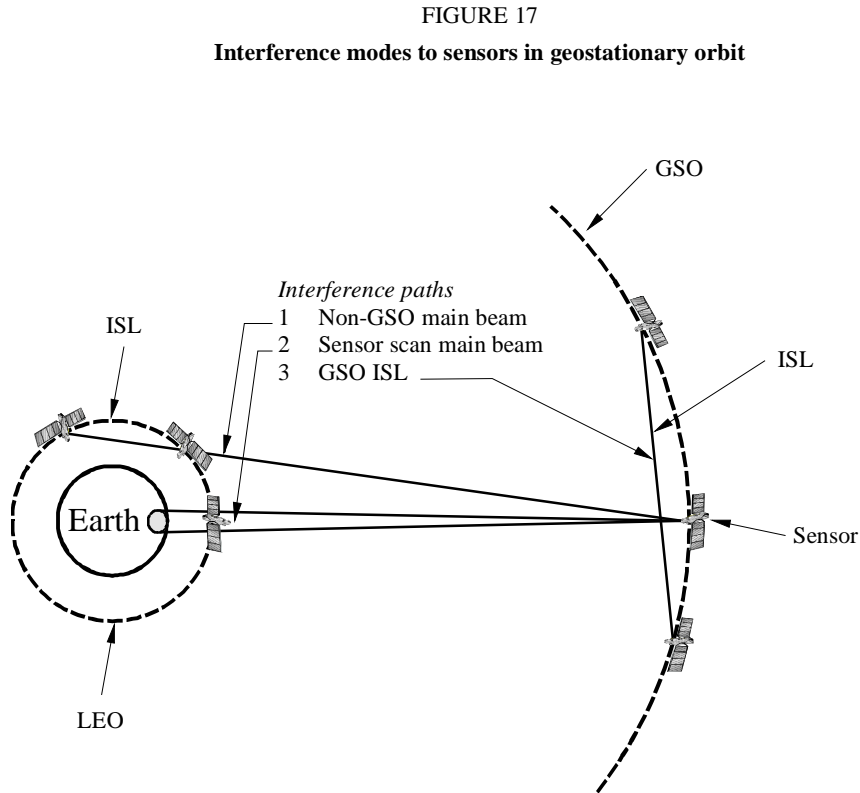


1416-17

## 4.2.2    Static analysis of interference from non-GSO ISLs

Prior analyses for the low orbiting sensor indicated that interference powers were the strongest when the main beam of either the sensor or non-GSO transmitter pointed directly at the other satellite. These alignments are illustrated as interference paths 1 and 2 in Fig. 17. These two paths will be investigated together by first determining the sensor's threshold sensitivity toward the non-GSO transmitter location.

The nine systems shown in Table 10 will be evaluated as if they were systems operating in these bands. The transmitter power for each link was determined by using equation (2) and angular separation from Table 10. A 45 dBi antenna was assumed for each link. For the interference path, the power plus full 45 dBi antenna gain was assumed to be radiated from a point 90° separation from the sensor sub-satellite point. For interference path 2 a backlobe gain was assumed to be –10 dBi with the non-GSO transmitter at an altitude above the sub-satellite point. The sensitivity of the sensor toward the interference path 1 was calculated assuming the sensor was scanning +8° in that direction. The sensor antenna gain is assumed to be 20 dBi (the directional sensitivity is –183 dBW). To the sub-satellite point the sensor is assumed to be pointed at nadir and the full 66 dBi gain of the sensor antenna adds to its sensitivity (–226 dBW).

Table 10 shows the results of these calculations and the comparison to the sensitivity of the GSO. The first four columns give parameters of these systems. The next four columns give the power level (dBW per 200 MHz) at the GSO for these systems. In the last two columns these power levels are compared to the threshold sensitivity levels of the sensor toward their direction.

TABLE 10

**Determination of compatibility between GSO sensor and non-GSO ISLs**

| System | Number of satellites | Degrees separation | Orbital altitude (km) | Power at GSO from side-lobe emissions (dBW) | | Power at GSO from main lobe emissions (dBW) | | Sharing with GSO sensor due to side-lobe emissions? | Sharing with GSO sensor due to main lobe emissions? |
|---|---|---|---|---|---|---|---|---|---|
| | | | | 118 GHz | 183 GHz | 118 GHz | 183 GHz | | |
| System A | 66 | 32.7 | 780 | –218.0 | –212.4 | –160.9 | –159.1 | No | No |
| System B | 12 | 90 | 10 350 | –205.2 | –188.6 | –151.4 | –149.7 | No | No |
| System C | 48 | 60 | 1 414 | –213.3 | –207.7 | –156.4 | –154.7 | No | No |
| System D | 32 | 45 | 775 | –215.6 | –210.1 | –158.6 | –156.8 | No | No |
| System E | 840 | 17.1 | 700 | –223.3 | –217.8 | –166.2 | –164.5 | No | No |
| System F | 48 | 45 | 950 | –215.5 | –209.9 | –158.5 | –156.7 | No | No |
| System G | 24 | 60 | 800 | –213.9 | –208.3 | –156.8 | –155.0 | No | No |
| System H | 10 | 72 | 500 | –213.3 | –207.7 | –156.2 | –154.4 | No | No |
| System I | 24 | 60 | 1 000 | –213.7 | –208.1 | –156.7 | –154.9 | No | No |

In all cases of the examined non-GSO systems, interference exceeded the sensor's allocated interference threshold.

### 4.2.3 Temporal analysis of non-GSO interference

It has already been established that a single ISL transmitter can transmit interfering levels of power when in the sensor's main beam even though the ISL antenna far side lobes are involved. Therefore any ISL that passes into the sensor's main beam can cause interference.

The proposed passive sensor has a footprint of $2\,000$ km$^2$ on the Earth and a similarly sized footprint at lower orbital altitudes. Assuming a nominal altitude of 800 km, the area ratio of the entire sphere to the footprint of the satellite is 0.0036%. If the satellites were evenly distributed, there would have to be 323 733 satellites for one to be in the sensor's field of view at all times. To reduce that to one satellite in the sensor's view for less than 0.01% of the time, there would have to be less than 33 satellites in LEO operating in any 200 MHz band.

### 4.2.4 Interference from other GSO ISLs

Interference from other GSO satellites is designated as interference path 3. In this case neither the main beam of the active satellite or the passive sensor point directly at each other unless the sensor is collocated with the intended receiver. The positional relationship between the satellites will not change with time for these satellites. Sharing is possible if the off-main-beam gain of the ISL transmitter is sufficiently low to prevent interfering signal levels at the sensor. This is controlled by the gain pattern of the ISL transmit antenna, the geocentric angle of the ISL link, and the geocentric angle between the sensor and ISL transmitter.

To determine if any ISL link might interfere with the sensor, links with antenna gains from 60 to 45 dBi were investigated. The geocentric angle was varied at angles up to 162.2° to determine where interference would occur. In the case of a 60 dBi antenna, no interference levels exceeded the threshold. The interference level only exceeded the threshold at wide spacing for the 55 dBi-, 50 dBi- and 45 dBi-gain antennas. Figure 18 shows the maximum spacing that avoids interference to the sensor over the threshold.

ISLs for systems in geostationary orbit can share with geostationary orbiting sensors provided the maximum geocentric angle relative to the antenna gain does not exceed the values plotted in Fig. 18.

FIGURE 18

**Maximum allowable geocentric angle for GSO ISLs**
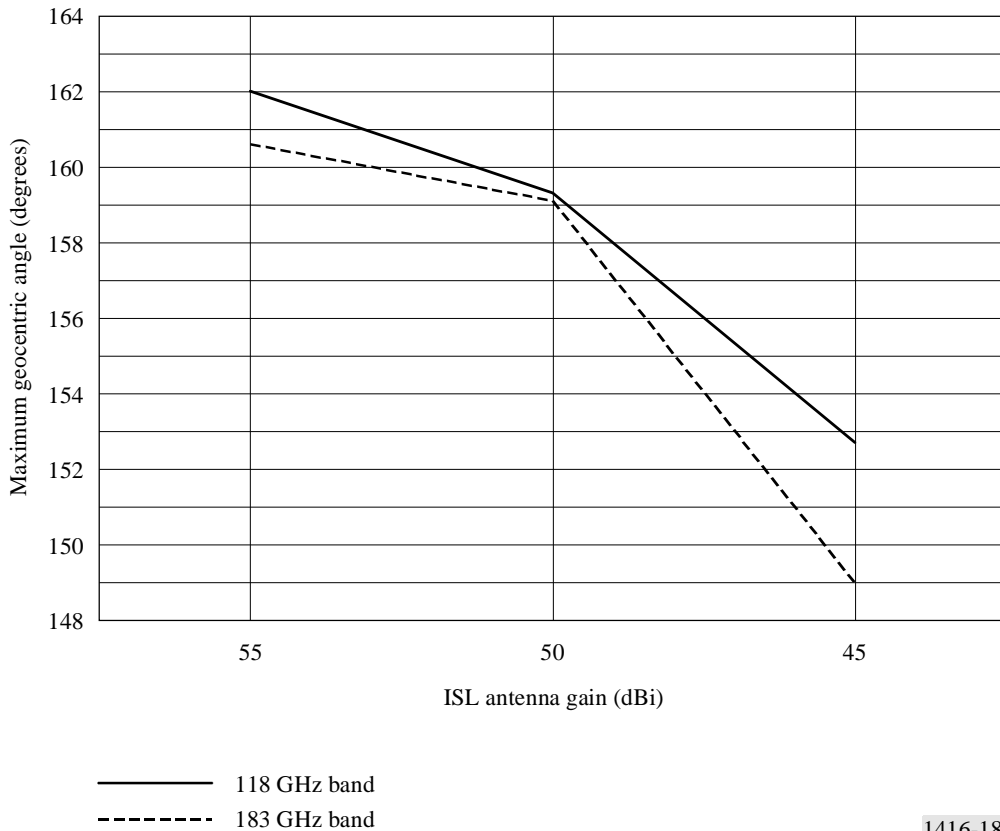


1416-18

### 4.2.5 Comparison and conclusions on sharing with geostationary orbiting sensors

– Geostationary orbiting sensors can receive levels of power over the interference threshold from LEO ISLs when near-main-beam antenna coupling occurs.

– All of the example LEO systems that were examined would cause interference to a geostationary orbiting sensor if deployed in these bands.

– LEO constellations with 33 or less ISLs in this band could operate without violating the temporal criterion for sharing.

– All but a few very long GSO ISLs can share with geostationary orbiting sensors without exceeding the interference threshold at any time. All example systems planned or operating in other bands could share if they were implemented in this band.

# 5       Conclusions

## 5.1       Sharing in the 116-126 GHz frequency band

Sharing with the ISS in the range from 116 to 126 GHz is not feasible except for ISLs between the GSO satellites. The analysis has shown that non-GSO ISLs that do not exceed the sensor's interference threshold are likely to be impractical in both path length and allowable number of circuits when compared with example systems planned or implemented in other bands. Inter-satellite systems at the geostationary orbit can share with the sensors provided their power at the sensor's orbital altitude of 1 000 km is restricted to:

$$-148 \text{ dB(W/(m}^2 \cdot 200 \text{ MHz))}$$

## 5.2       Sharing in the frequency bands between 174.5 and 190 GHz

Sharing with the ISS in the frequency bands between 174.5 and 190 GHz is similarly not feasible except for ISLs in the geostationary orbit. Inter-satellite systems at the geostationary orbit can share with the sensors provided their power at the sensor's orbital altitude of 1 000 km is restricted to:

$$-144 \text{ dB(W/(m}^2 \cdot 200 \text{ MHz))}$$

## 5.3       Restricting sensor techniques to facilitate sharing

It is unlikely that adequate protection for the passive sensors can be achieved by adjusting or restricting measurement techniques of the passive sensors.

———————————